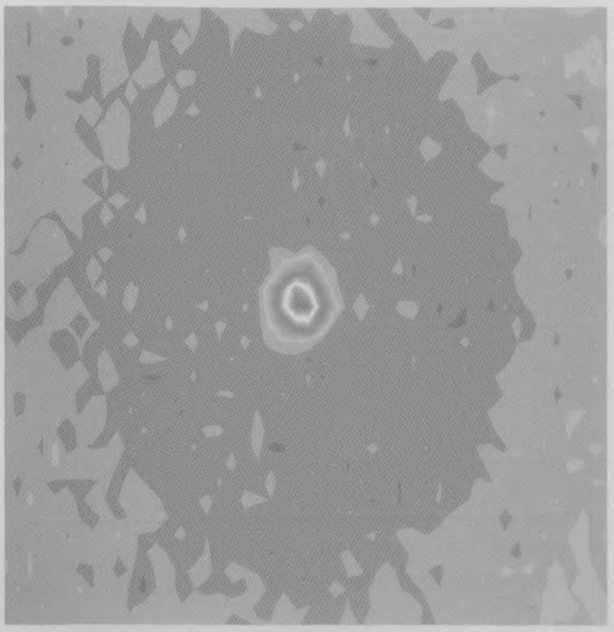

EBIT

Electron Beam Ion Trap

N-Division
Experimental Physics
Bi-Annual Report
1996 - 1997

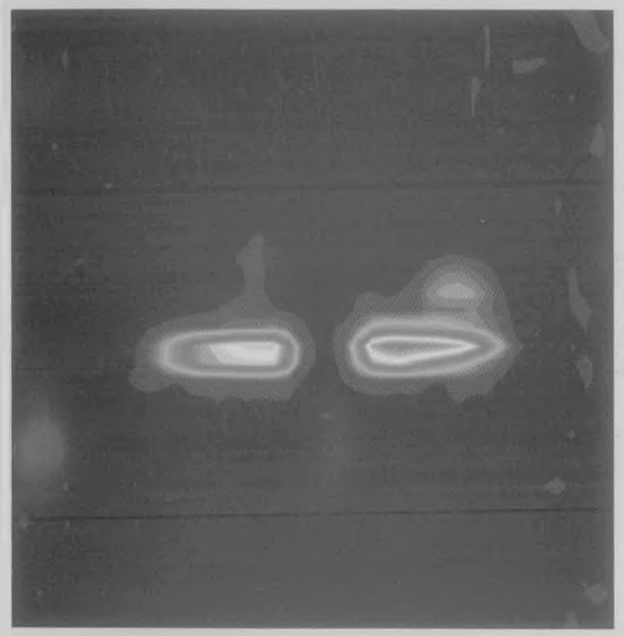

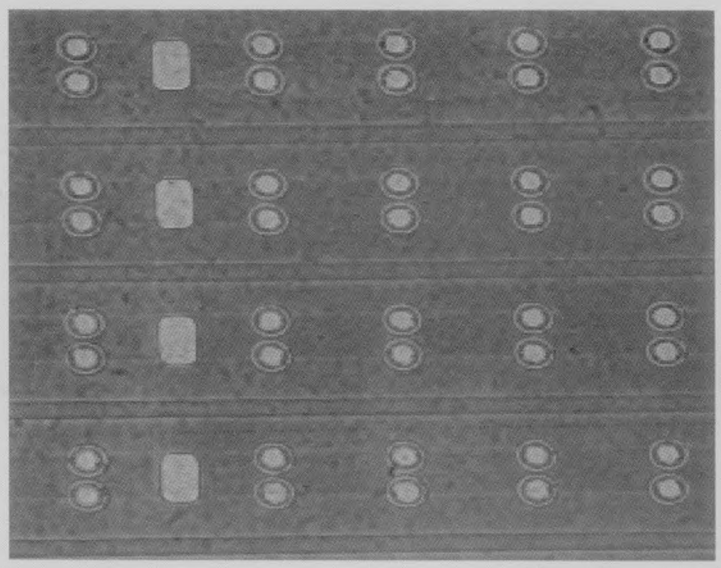

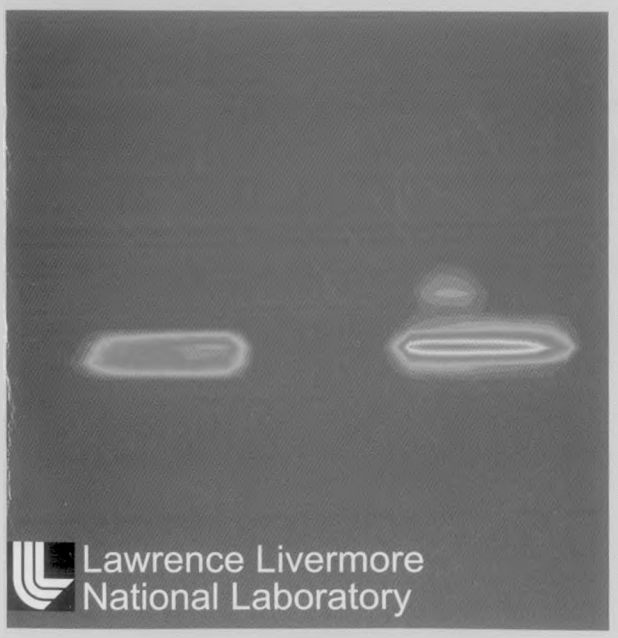

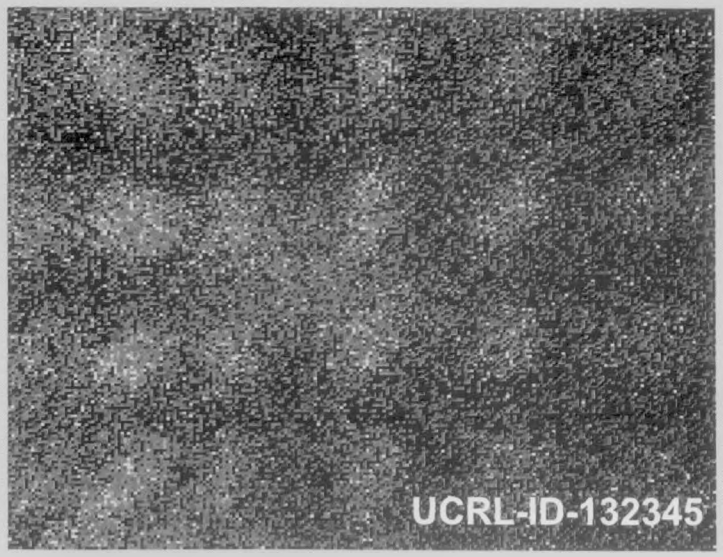

COVER

Left:
Three sideview CCD images of lasercooled Be^{+} and sympathetically cooled Be^{2+} and Xe^{44+}
Top: Be^{+} and Be^{2+} (hot)
Middle: Be^{+} and Be^{2+} (cold)
Bottom: Be^{+}, Be^{2+}, and Xe^{44+} (cold)

Right:
Top: Light microscope image of tungsten features on Silicon wafer
Bottom: HCI-SIMS microscope image of same tungsten feature (green areas) on silicon wafer

Work performed under the auspices of the U.S. Department of Energy by Lawrence Livermore National Laboratory under Contract W-7405-ENG-48.

EBIT

Electron Beam Ion Trap

N-Division

Experimental Physics

Bi-Annual Report
1996 / 1997

Edited by:
Dieter Schneider

For further information contact:
Physics & Space Technology Directorate
Lawrence Livermore National Laboratory
P.O. Box 808, L-414
Livermore, CA 94551-0808

Issued December 1998

EBIT 1996 / 1997 Bi-Annual Report

Table of Contents

INTRODUCTION 1

I. Atomic Structure Measurements and Radiative Transition Probabilities 3

Forbidden Line in Au^{57+} Seen at EBIT 4

EBIT Lifetime Measurement on a Forbidden Line in the Visible Spectrum 6

Measurements of Radiative Lifetimes in the Femtosecond Regime 8

The 1s Lamb Shift of Xe^{53+} 10

Re-examination of the Optical Gamma Ray Decay in ^{229}Th 12

Nuclear Magnetization Distribution Radii in H-like $^{185}Re^{74+}$ and $^{187}Re^{74+}$ Ions 14

Determination of Nuclear Properties from High-Resolution Spectra of Heavy Ions 16

A Quartz Quasimonolith for Absolute X-ray Wavelength Measurements 18

II. Spectral Diagnostics for High-Temperature Laboratory and Astrophysical Plasmas 21

Measurement, Line Identification, and Modeling of the L–Shell Fe XVII Spectrum Below 12 Å 22

Simulating a Single Electron Temperature Maxwellian Plasma using an Electron Beam Ion Trap 24

Laboratory Measurement of the 2p–3d Resonance to Intercombination Line Emission of Fe XVII 26

III. Electron-Ion Interactions Studies 29

Measurements of K-shell X-ray Spectra from Hydrogenic and Heliumlike Ions produced by Charge-Transfer Reactions 30

Laboratory Measurements of Resonant Contributions to Fe XXIV Line Emission 33

Dual Crystal Spectrometer Setup for Polarization Measurements of X-ray Lines from Beam-Excited Highly Charged Ions 36

Polarization-Dependent Spectra of X-ray Dielectronic Satellite Lines of Be-like Fe 38

IV. Ion / Surface Interaction Studies 43

Synergy of Electronic Excitations and Elastic Collision Spikes in Sputtering of Heavy Metal Oxides 44

Ablation of GaAs by Intense Ultrafast Electronic Excitation on a Nanometer Scale 49

Analysis of B-SiO_2 Films by Highly Charged Ion Based Time-of-Flight Secondary Ion Mass Spectrometry, Standard SIMS and Elastic Recoil Detection .. 53

Secondary Ion Coincidence in Highly Charged Ion Based Secondary Ion Mass Spectroscopy for Process Characterization 58

Dependence of Cluster Ion Emission from Uranium Oxide Surfaces on the Charge State of the Incident Slow Highly Charged Ion 62

Energy Loss of Slow, Highly Charged Ions in Solids 68

Charge State Dependent Energy Loss of Slow Heavy Ions in Solids 73

V. RETRAP and Ion Collisions 79

Performance of the Hyperbolic Traps in RETRAP 80

Laser Cooling of Be^+ in RETRAP 82

Separation of Lasercooled Be^+ and Be^{2+} in RETRAP 84

Molecular Dynamics Simulations of Cold Be+ and Be++ 86

Schemes to Capture Highly Charged Ions into a Be^+ Cloud 90

Capture of Xe^{44+} and Be^{2+} in the Same Trap 92

VI. Instrumental Development 95

An X-Ray Microscope Powered by Highly Charged Ions 96

Implementation of a Very High Resolution Vacuum Crystal Spectrometer on EBIT 99

Investigation of Electron Beam Structure as Affected by the Beam Current and Beam Energy 102

X-ray Analysis of the Magnetic Trapping Mode of an Electron Beam Ion Trap ... 104

X-ray Measurements of Electron Beam Compression in a Magnetic Field 107

A New Beamline for RETRAP and the Surface Chamber 110

X-ray Verification of Extracted Ion Charge State from Super EBIT..... 111

Charge Balance Versus Extraction Mode of EBIT..... 114

Fast Extraction Mode of EBIT..... 116

Evaporative Self-Cooling and High Brightness Ion Beams..... 118

Construction of a 6-Tesla Superconducting Magnet for an Intense EBIT..... 120

Appendix..... 123

A. Publications and Conference Contributions..... 124

1. Publications..... 124

2. Contributed Conference Papers..... 129

3. Conference Organization..... 134

B. Scientific Activities Centered Around EBIT..... 148

1. Visitors and Participating Guests..... 148

2. EBIT Seminar Series in N Division of LLNL..... 155

C. Education..... 156

D. Scientific Cooperations..... 157

E. Personnel..... 158

INTRODUCTION

The research of the EBIT (Electron Beam Ion Trap) program in N Division of the Physics and Space Technology Directorate at LLNL continues to contribute significantly to the understanding of physical processes with low energy highly charged ions in atomic physics, plasma physics, and material science. Low-energy highly charged ions (up to U^{92+}), provided by the EBIT facilities, provide a unique laboratory opportunity to study high field effects in atomic structures and dynamic interaction processes. The formation, existence, and structure of highly charged ions in astrophysical environments and laboratory plasmas make highly charged ions desirable for diagnosing various plasma conditions. The strong interaction of highly charged ions with matter and the response of solid surfaces make them a sensitive analysis tool and possibly a future capability for materials modifications at the atomic scale (nano technology). These physical applications require a good understanding and careful study of the dynamics of the interactions of the ions with complex systems.

The EBIT group hosted an international conference and a workshop on trapped charged particles. The various talks and discussions showed that physics research with trapped charged particles is a very active and attractive area of innovative research, and provides a basis for research efforts in new areas. It also became obvious that the EBIT/RETRAP project has unique capabilities to perform important new experiments with trapped very highly charged ions at rest, which are complementary to and competitive with research at heavy ion storage rings and other trapping facilities planned or in operation in Europe, Japan, and the United States.

Atomic structure research at EBIT provides ever better and more experimental complete benchmark data, supplying data needed to improve atomic theories. Research highlights through 1996 and 1997 include hyperfine structure measurements in H-like ions, QED studies, lifetime and polarization measurements on high-Z highly charged ions. Studies of the interaction of highly charged ions with solid surfaces and thin foil targets reveal new interaction phenomena. The measurements of high secondary ion sputter yields led to the development of a prototype electron/ion emission microscope, which allows simultaneous topographic and chemical composition analysis with high sensitivity and spatial resolution. The enabling technology to trap, confine, and cool hundreds of highly charged ions in a precision Penning trap has been established and first evidence for the formation of a strongly coupled highly charged ion plasma via a sympathetic laser/ion cooling scheme has been observed. The benefits to DOE programs for a continued long term EBIT program are evident. The program requires the application and development of state-of-the-art experimental techniques necessary for spectroscopy, ion confinement and manipulation with spin-off applications in other laboratory programs. Thus, it serves as an excellent training ground for young scientists who will later work on energy-related plasma research or similar areas. It promises new research results towards the growth of our understanding of basic physics phenomena in atomic, nuclear and plasma physics, such as solid phases, astrophysical plasma evolution, and quantum control. This research will also provide input for applications in areas like ion beam manipulation and control for materials research. The activities at EBIT have created great interest among scientists from other areas (e.g. biology and environmental sciences) with several new ideas and research directions emerging. External funding for the project has in part been provided by the DOE office of Basic Energy Science (Chemical Science Division) and by NASA.

Dieter H.G. Schneider

I. Atomic Structure Measurements and Radiative Transition Probabilities

Forbidden line in Au^{57+} seen at EBIT

E. Träbert[1], P. Beiersdorfer, S.B. Utter
Lawrence Livermore National Laboratory, University of California,
P.O. Box 808, Livermore, CA 94551, U.S.A.

High-resolution spectroscopy of light emitted from ions in a plasma can reveal many interesting details about the plasma environment, but the resonance lines of such ions move to the extreme-uv and the x-ray ranges even for moderate ion charges. Interferometric studies are largely constrained to the visible and near-ultraviolet ranges in which beam splitters are transparent. It is this technical condition that gives forbidden transitions in highly-charged ions a particular importance, because they may lie in the wanted (visible / near-uv) spectral range, but relate to low-lying, easily excited levels the emission from which serves as an indicator of particle density, temperature, gross motion, and microfields. However, as fine structure splittings usually increase with Z^4 (with Z the nuclear charge), the corresponding transitions in an isoelectric sequence vary grossly in wavelength. An exception is the transition $3d^4\ ^5D_2$ - $^5D_3$ in Ti-like ions (22 electrons), which varies remarkably little and remains in the visible or near-uv for a wide range of elements. After a computational search for such cases yielding this particular prediction [1], the line was first seen in the spectrum of an electron beam ion trap (EBIT) at NIST [2], where by now it has been observed with four elements [3], and then also at Oxford [4]. Theory has been improved since the original prediction, but improved numbers are available [5] only for the cases already covered by experiment.

We have extended the search for this line towards higher nuclear charges, using the LLNL SuperEBIT which is equipped with a metal vapor vacuum arc (MEVVA) ion source. A 1m normal-incidence spectrometer equipped with a CCD camera served for the dispersion and recording of spectra. It was tried to see the line of interest with W (Z=74), Au (Z=79) and U (Z=92), using various combinations of electrodes in MEVVA. Unfortunately, a developing water leak in SuperEBIT compromised the UHV conditions and hindered our reaching the very high charge states. Furthermore, at nuclear charges beyond Z=52, the level ordering in the Ti-like ions changes so that the wanted line becomes part of a branched decay, and the weaker branch at that for Z>62.

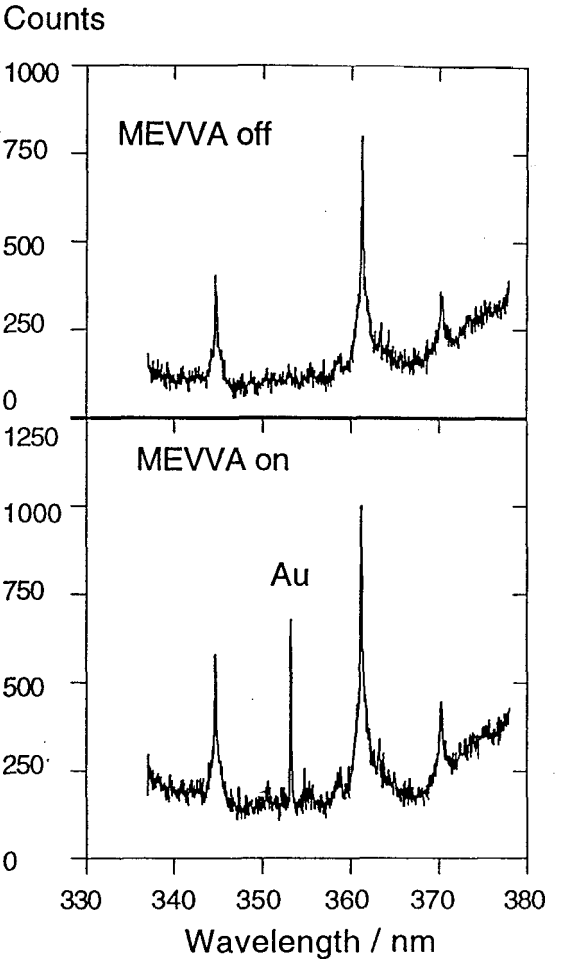

Figure 1: Spectra observed with and without firing the ion source with its Au electrode. The other lines, from the background gas in SuperEBIT, are unidentified..

[1] Permanent address: Experimentalphysik III, Ruhr-Universität Bochum, D-44780 Bochum, Germany

For W, which is notably difficult to sputter, the signal remained too weak to become useful. For U^{70+}, the predicted branching ratio is only 5%, and no trace was seen in the spectrum. However, our experiment on Au^{57+}, with a predicted branching ratio of 12%, yielded a clean line at (353.2±0.2) nm (Fig. 1). This observation extends the range of experimental data considerably (Fig. 2) and permits a reduction of the range of search for future experiments of this type. It remains to be seen, however, whether a semi-empirical scaling of the available calculations [1] or dedicated calculations will come closer to the experimental data, which for uranium we now expect near 325 nm, and near 363 nm for tungsten.

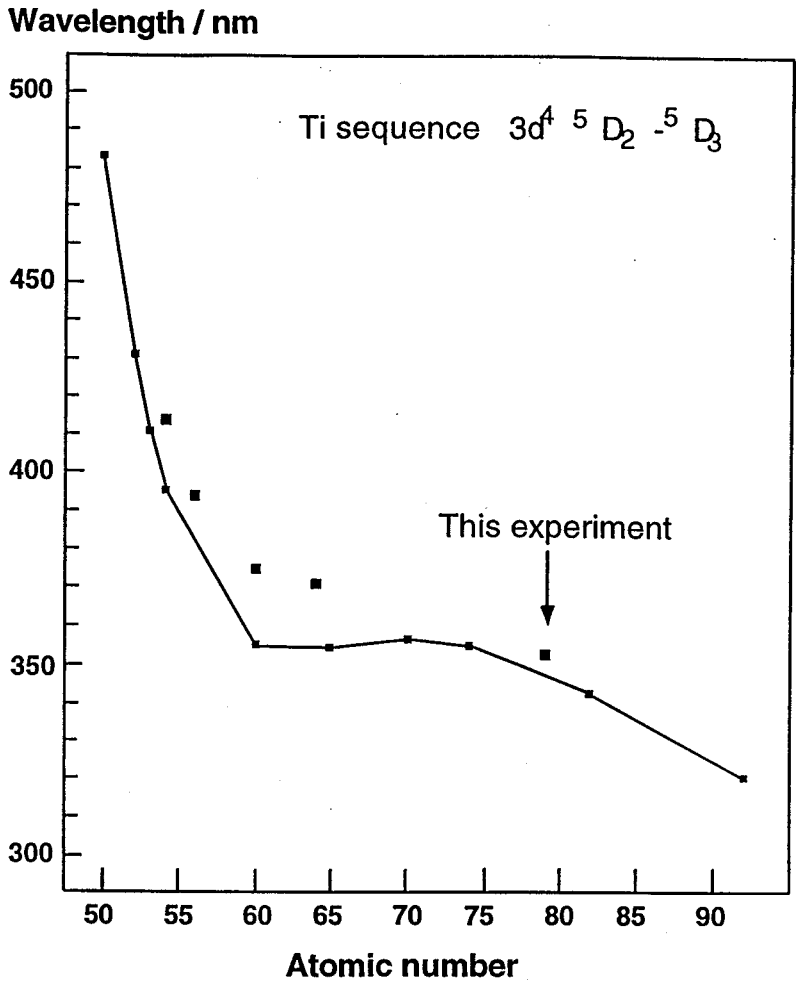

Figure 2: Isoelectronic trend of theoretical predictions [1] for the wavelength of a fine-structure transition in Ti-like ions, connected by an eye-guiding line, and experimental data from EBIT experiments.

References

[1] U. Feldman *et al.*, J. Opt. Soc. Am. B8, 3 (1991).
[2] C.A. Morgan *et al.*, Phys. Rev. Lett.74, 1716 (1995).
[3] F.G. Serpa *et al.*, Phys. Rev. A 53, 2220 (1996).
[4] D.J. Bieber et al., Phys. Scr. T73, 64 (1997).
[5] D.R. Beck, Phys. Rev. A 56, 2428 (1997).

E.T. appreciates travel support granted by the Humboldt Foundation, Germany. The work at Lawrence Livermore National Laboratory was performed under the auspices of the Department of Energy under Contract No. W-7405-Eng-48.

EBIT lifetime measurement on a forbidden line in the visible spectrum

E. Träbert[1], P. Beiersdorfer, S.B. Utter, and J.R. Crespo López-Urrutia
Lawrence Livermore National Laboratory, University of California,
P.O. Box 808, Livermore, CA 94551, U.S.A.

Slow radiative decays of few-electron atomic systems with level lifetimes in the range of *ms* to *s* are of interest both in fundamental atomic structure studies and in astrophysical and fusion test plasmas. The observation and study of such decays in the laboratory requires advanced trapping techniques in order to see the radiative transitions which compete with collisional quenching. Our study aimed at decay measurements of a particularly bright line from a forbidden transition, $3s^2\ 3p^2\ ^3P_1 - ^3P_2$ in the Si-like ion Kr^{22+}. The line has been observed in the TEXT tokamak, at an (air) wavelength of 384.09 nm [1], as well as at the NIST electron beam ion trap (EBIT) [2], where there also was a first lifetime measurement (τ = 5.7±0.5 ms) [3]. We undertook a fresh measurement in order to learn about systematic errors and to exploit the LLNL SuperEBIT's special features: Contrary to other EBITs, SuperEBIT can run also at very low electron energies in the trap region, by independent adjustment of the drift tube voltage. Atoms are stepwise ionized by electron impact in the intense electron beam which is guided and compressed by a strong (3 T) magnetic field. Under appropriate vacuum conditions, the charge state reached on any element is simply determined by the ionization potential of that ion species. With SuperEBIT, this gives good control over charge state distributions even for ions not in their highest possible charge states.

For the lifetime measurement, the magnetic trapping mode [4] was employed, that is alternating ionization/excitation (electron beam *on*) and detection (electron beam *off*) phases, with a 16 Hz cycle. In this mode the ions are still confined radially by the magnetic field and longitudinally by the trap electrodes; the disappearance of the attractive and space-charge compensating electron beam results in a sudden expansion step of the ion cloud. This step is as fast as the switching of the electron beam current and does not affect the decay curves at later times. In order to apply good light collection and reach sufficient distance of the detector from the strong magnetic stray fields, a Steinheil (glass) prism spectrograph was employed and fitted with a large (10 cm diameter, f/4) collection lens (achromat), resulting in a total collection solid angle of 0.003 sr. A CCD camera was used to find the proper optical alignment of this light collection and imaging system. Then the CCD camera was replaced by a single channel detector (photomultiplier) for the lifetime measurements. The low-dark rate (5 counts per second) photomultiplier tube (1/2" diameter, end-on cathode, Hamamatsu type R2557) permitted detection with more than 2.5% quantum efficiency from 300 to 580 nm. Data were collected over 50 ms intervals and sorted by the time of event after the electron beam was switched off.

Decay curves were recorded at various electron beam energies, from 1.4 keV (well above the 1.0 keV ionization energy of Kr^{22+}) to 648eV (just above the production threshold of Kr^{18+}). Even without gas injection, a signal with a time constant of about 0.8 ms was seen, which is slower than the about 50 µs switching time of the electron gun. A component of this time constant was corrected for in the decay curves taken with gas injection. Below the production threshold for Kr^{22+}, a dominant time constant of order 2 ms was seen which we ascribe to the branched M1 decay in Ar-like Kr^{18+} [5], which (at 402.5 nm) was marginally in the field of view of the attached attached (without an exit slit) to the prism spectrograph. At the higher excitation energies the observed signal is dominated by the wanted line in Kr^{22+}, but it will be contaminated by the other two contributions.

---

[1] Permanent address: Experimentalphysik III, Ruhr-Universität Bochum, D-44780 Bochum, Germany

Decay constants were determined for the individual runs, by least-squares fits of one or two exponentials plus a constant background to each of the observed decay curves. The error estimates were derived from the least-squares fit, augmented by estimates of error due to the spectral blend. The weighted averages yielding a mean value for the lifetime of (6.3±0.3) ms, or a transition probability of (160±8) s^{-1} for the $3s^23p^2$ $^3P_1$ - $^3P_2$ level of Kr^{22+}. The lifetime result overlaps with that obtained at NIST. However, due to better signal yield, our data have reached a smaller uncertainty of only 5%, and our result is closer to the range of the theoretical predictions. The two theoretical lifetime numbers available, 6.46 ms [6] and 5.83 ms [7], both require semiempirical adjustment for the transition energy. After such a correction, they are at 6.78 ms and 6.69 ms, respectively, which is outside our error estimate. With such good light collection as used here, but better spectral filtering, we expect to be able to improve the experiment in the future.

References

[1] J.R. Roberts *et al.*, Phys. Rev. A 35, 2591 (1987).
[2] F.G. Serpa *et al.*, Phys. Rev. A 55, 1832 (1997).
[3] F.G. Serpa, J.D. Gillaspy, and E. Träbert, E., J. Phys. B (submitted).
[4] P. Beiersdorfer et al., Rev. Sci. Instrum. 67, 3818 (1996).
[5] J.R. Crespo López-Urrutia *et al.*, LLNL Annual Report 1995
[6] E. Biémont and G.E. Bromage, Mon. Not. R. Astron. Soc.205, 1085 (1983).
[7] K.-N. Huang, At. Data Nucl. Data Tables 32, 503 (1985).

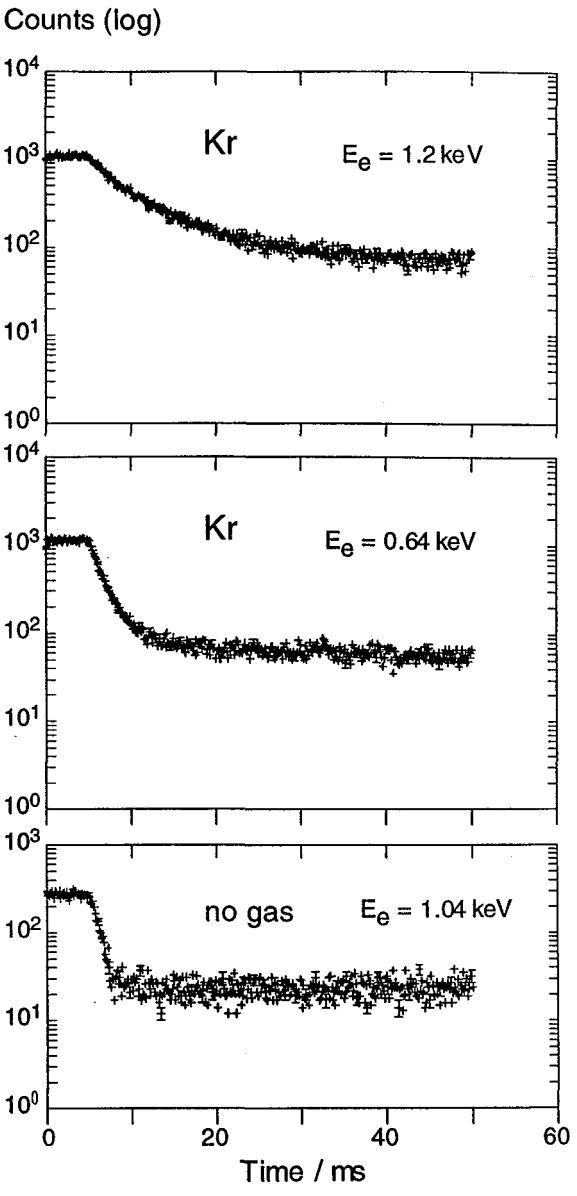

Figure 1: Decay curves observed with Kr ions at λ = 384 nm. The electron beam (energies E_e are indicated) is switched off at t=5 ms.

J. Steiger deserves thanks for the loan of the photomultiplier. E.T. appreciates the travel support granted by the Humboldt Foundation. The work at Lawrence Livermore National Laboratory was performed under the auspices of the Department of Energy under Contract No. W-7405-Eng-48.

Measurements of Radiative Lifetimes in the Femtosecond Regime

P. Beiersdorfer, A. L. Osterheld, V. Decaux, K. Widmann
Lawrence Livermore National Laboratory, Livermore, CA 94550

Radiative lifetimes less than a few femtoseconds are common among dipole-allowed resonance transitions in highly charged ions and are found, for example, among the K-shell transitions of heliumlike ions above argon (Z=18) and among the L-shell transitions of neonlike ions above krypton (Z=36). Dipole-allowed resonance transitions form the dominant lines in a given x-ray spectrum and play an important role in the density and temperature diagnostics of high-temperature plasmas, such as those found in inertial-confinement fusion, tokamaks, and astrophysical sources. Because fast transition rates correspond to large absorption oscillator strengths, resonance transitions dominate the Planck mean opacity of a high-temperatures plasma, and accurate knowledge of their radiative rates is important for plasma opacity and line transfer determinations. Predictions of the radiative rates of these transitions have not been subject to experimental scrutiny, as existing techniques for measuring fast transition rates fail to yield results for lifetimes shorter than a few picoseconds.

Employing ultra high resolution x-ray spectroscopy on the Livermore EBIT we performed the first measurement of the femtosecond radiative lifetime of a dipole-allowed resonance transition in a highly charged ion [1]. Our measurement was made possible by a systematic reduction of the ion thermal motion to a point where it was possible to observe the energy uncertainty associated with the radiative lifetime. The energy uncertainty ΔE of an excited state with lifetime Δt decaying to the ground state results in a lifetime-limited, Lorentzian-shaped "natural" line width given by Heisenberg's uncertainty principle

$$2\pi \, \Delta E \, \Delta t = h \, .$$

Direct observation of the natural line width has been precluded in other spectroscopic sources, such as tokamaks, laser-produced plasmas, heavy-ion accelerators, or the Sun, by source-specific line broadening mechanisms. These include density or opacity broadening, blending with satellite transitions, and broadening by the thermal or directional ion motion associated with the energy required to produce and excite x-ray transitions in highly charged ions. In EBIT we can control the source-induced line broadening. By lowering the electron beam current and the axial trapping potential we allow only very cold ions in the trap. With this technique we have reduced the ion temperature to values well below 100 eV [1-3].

Our investigations focused on the 2p-3d transition in neonlike Cs^{45+} situated at 4740 eV. The lifetime of its upper level is predicted by single configuration calculations to be 1.39 fs. By the uncertainty principle, this corresponds to a Lorentzian line width of 0.474 eV. The observed line width is shown in Fig. 1. Fitting the line with a Lorentzian trial function provides an excellent fit. The goodness of the fit is indicated by the reduced residuals also shown in Fig. 1 and defined as the difference between data and fit normalized to the square root of the fit value at each point. The residual contributions of thermal broadening on the line shape were accounted for by fitting the line with a Voigt profile, which represents a Lorentzian convolved with a Gaussian profile. For this, the temperature parameter for the Gaussian profile was taken from an independent measure of the ion temperature. A value of 0.398 eV averaged over all observations was obtained for the natural width of the line. From this we infer a radiative lifetime of the excited level of 1.65 fs with a combined statistical and systematic uncertainty of +0.24 fs and -0.05 fs. This is significantly larger than the 1.39 fs predicted by single-configuration calculations. However, the value is smaller than the value of 1.98 fs computed in a multi-configuration calculation that allows for configuration interaction by including all 36 excited levels with a vacancy in the n=2 shell and an excited electron in the n=3 shell. This

disagreement with theory shows that measurements are needed even for very fast electric dipole transitions in order to guide atomic calculations, especially when configuration interactions play a dominating role, as is the case for this transition.

We note that the lifetime we measured is more than three orders of magnitude faster than that accessible with existing measurement techniques. A variety of novel methods have been developed in recent years for the measurement of radiative transition probabilities of highly charged ions that are slower than those accessible with the original and highly successful beam-foil technique, e.g., the probing of excited levels by resonant recombination in storage rings, modulation of the electron-ion interaction energy, or the capture of excited ions into ion traps. The present method for the first time determines lifetimes that are considerably faster than the standard methods.

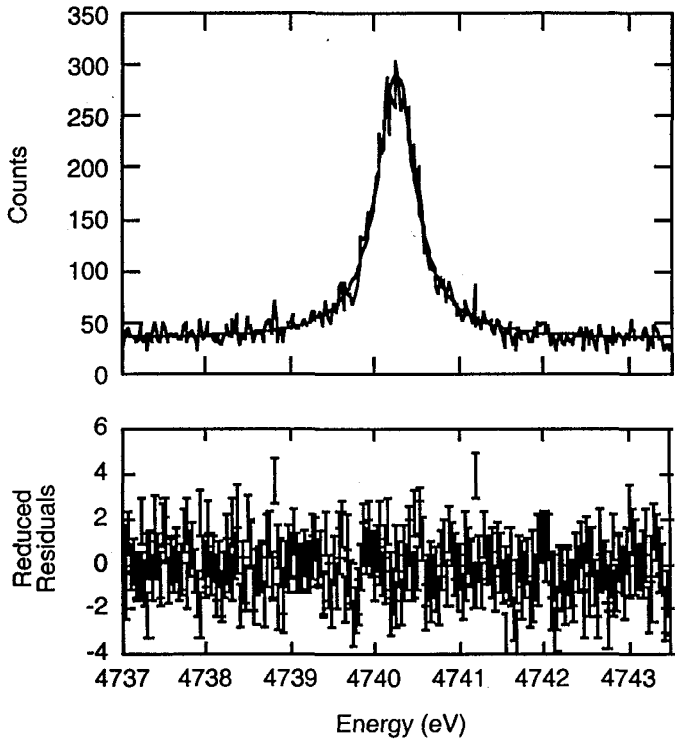

Fig. 1. Observed line shape of the 2p–3d transition. The result of a least-squares fit of a Lorentzian trial function is superimposed for comparison. The reduced residuals of the fit are shown below.

References:

[1] P. Beiersdorfer, A. L. Osterheld, V. Decaux, and K. Widmann, Physical Review Letters 77, 5353-5356 (1996).

[2] P. Beiersdorfer, in *Proceedings of the 17th International conference on X-Ray and Innershell Processes*, AIP Conf. Proc. No. 389, ed. by R. L. Johnson, H. Schmidt-Böcking, and B. F. Sonntag, (American Institute of Physics, New York, 1997), p. 121-135.

[3] P. Beiersdorfer, V. Decaux, S.R. Elliott, K. Widmann, K. Wong, Rev. Sci. Instruments 66, 303-305 (1995).

The 1s Lamb Shift of Xe^{53+}

P. Beiersdorfer, J. R. Crespo López-Urrutia, K. Widmann
Lawrence Livermore National Laboratory, Livermore, CA 94550

The wave function of the 1s electron overlaps with the nucleus more strongly than that of any other bound electron. Therefore, it is subject to the most intense electric fields nature can provide. Under these conditions quantum electrodynamical effects manifest themselves in significant shifts of the energy levels. Using the magnetic mode of the EBIT device [1] we have measured the energy shift induced by quantum electrodynamics in the $2p_{3/2} \rightarrow 1s_{1/2}$ (Lyman-α) transition in the one-electron ion Xe^{53+}.

Measurements of the transition energy of the Lyman-α transition in hydrogenic Xe^{53+} have been performed before by using ions produced in a heavy-ion accelerator [2]. These measurements were performed by exciting a beam of highly charged xenon ions in a thin carbon foil. Because ions produced in an accelerator move at relativistic speeds corrections for the Doppler shift of the observed lines must be made. Because ions in EBIT are trapped, our measurements of the xenon lines were performed without the need to account for Doppler shift corrections.

A close-up of the K-shell spectrum of xenon recorded in the magnetic trapping mode is shown in Fig. 1. The Lyman-α transition in hydrogenic Xe^{53+} is the highest energy transition among the K-shell lines and well resolved from the K-shell transitions in heliumlike Xe^{52+} . We determined its energy by recording a set of reference lines consisting of the innershell K-shell lines in the neutral elements Rb, Mo, Ag, Ba, and Tb excited by x-ray fluorescence in an ^{241}Am source. The energies of these calibration lines are well known. The energy of the $2p_{3/2} \rightarrow 1s_{1/2}$ transition determined with this calibration is $31{,}276 \pm 12$ eV. The result compares favorably with the value of $31{,}278 \pm 10$ eV measured by Briand et al. [2] and with the calculated value of 31,284 eV [3], as summarized in Table I. The calculated Lamb shift contribution to the $2p_{3/2} \rightarrow 1s_{1/2}$ transition energy is 46.4 eV. Our measurement thus tests this contribution to within 26 percent.

Table 1. Comparison of calculated and measured energies (in eV) of the $2p_{3/2} \rightarrow 1s_{1/2}$ transition in hydrogenic Xe^{53+}.

Measurement EBIT [1]	Measurement Accelerator [2]	Theory [3]
31 276 ± 12	31 278± 10	31 284

The accuracy of the present measurement is limited by statistical considerations, and higher-accuracy determinations appear possible in the future provided longer exposures are obtained.

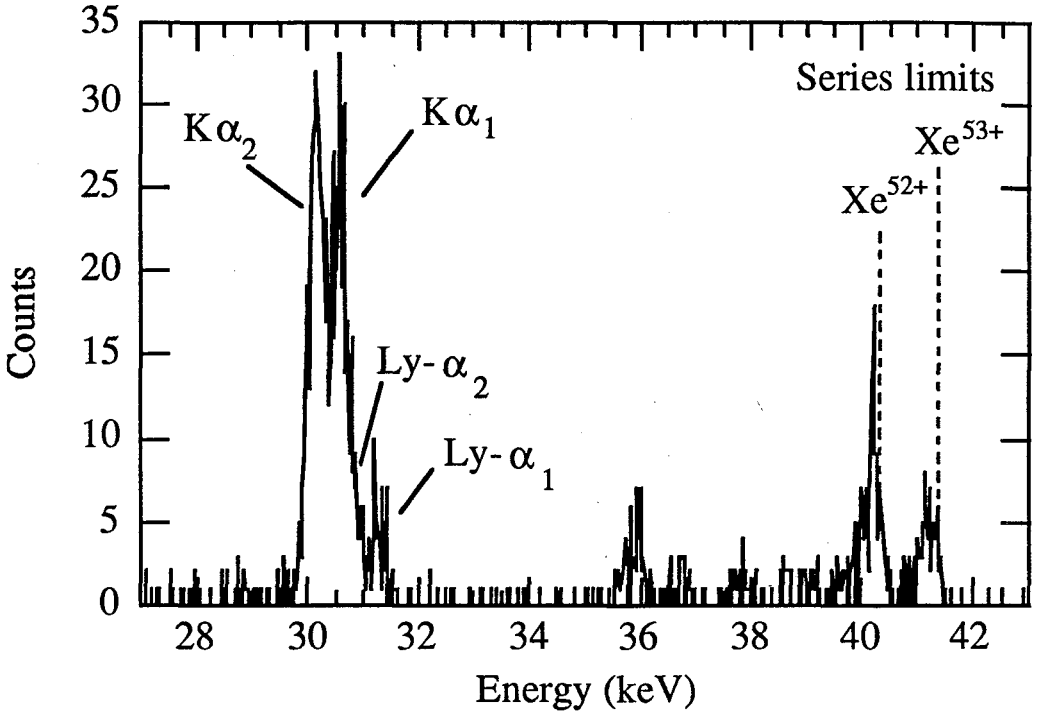

Fig. 1. Close-up of the xenon K-shell spectrum recorded in the magnetic trapping mode. The high-voltage supply to the electron gun was turned off during the measurements. The $2p_{3/2} \rightarrow 1s_{1/2}$ transition and $2p_{1/2} \rightarrow 1s_{1/2}$ transition in hydrogenic Xe^{53+} are marked Ly-α_1 and Ly-α_2, respectively. Kα_1 and Kα_2 refer to transitions of the type $2p_{3/2} \rightarrow 1s_{1/2}$ and $2p_{3/2} \rightarrow 1s_{1/2}$ in heliumlike Xe^{52+}.

References:

[1] P. Beiersdorfer, L. Schweikhard, J. Crespo López-Urrutia, and K. Widmann Rev. of Scientific Instruments 67, 3818-3826 (1996).

[2] J. P. Briand et al., Europhys. Lett. **9**, 225 (1989).

[3] W. R. Johnson and G. Soff, At. Data Nucl. Data Tables **33**, 405 (1985).

Re-examination of the Optical Gamma Ray Decay in ^{229}Th

P. Beiersdorfer[1], S. B. Utter[1], A. Barnes[1], J. R. Crespo López-Urrutia[1]
J. Becker[1], M. Weiss[1], R. Lougheed[2]
[1]*Department of Physics and Space Technology, Lawrence Livermore National Laboratory*
[2]*Department of Chemistry, Lawrence Livermore National Laboratory*

Interactions between the nucleus and atomic electrons have attracted considerable attention because of the potential of stimulating nuclear transitions by laser excitation of atomic electrons. In the inelastic bridge mechanism, for example, nuclear deexcitation is coupled to atomic excitation [1–3]. In particular, a gamma ray given off by the nucleus couples to an atomic electron, which is elevated to an excited state, thereby reducing the energy of the final gamma ray. The mechanism suggests that the inverse may be possible, i.e., that atomic deexcitation may induce nuclear excitations [4]. Nuclear excitation energies, however, are generally much larger than atomic excitation energies. The identification of cases where the energies are equal are, therefore, of highest importance.

Precision measurements of high-energy gamma rays from ^{229}Th produced in the α decay of ^{233}U have suggested a low-lying level with energy only a few eV above the ground state. The inferred energy is a mere 3.5 eV [5], which is lower than any other known excited nuclear level. Recently, a Letter was published by Irwin and Kim reporting the detection of photon emission resulting from the deexcitation of the ^{229}Th isomer [6]. The energy of the observed photons was determined to be 3.5 ± 1.0 eV, in agreement with predictions and well within the realm of present-day laser capabilities. Moreover, one of two samples of ^{233}U studied showed a second photon peak near 2.4 eV. The observation of this peak was consistent with predictions that the inelastic bridge mechanism could cause excitation of the thorium atom from the $6d_{3/2}$ ground level to the $7p_{1/2}$ excited level. The paper suggested that ^{229}Th provides a perfect isotope for future studies of low-energy nuclear-atomic interactions.

The Lawrence Livermore National Laboratory has an array of unique capabilities for ascertaining the important results purportedly found by Irwin and Kim [6]. These include state-of-the-art spectrometers and detectors in routine use by the EBIT spectroscopy group and a unique nuclear chemistry facility for preparing pure samples of ^{233}U. Using these capabilities we studied the optical emission of a 2-μC sample of ^{233}U with various optical instruments.

Our studies of ^{233}U decaying to ^{229}Th confirmed Irwin and Kim's [6] observation of light emission. However, we showed that the light is caused by α-particle induced fluorescence of air. In the absence of air, no light emission was discernable. This is illustrated in Fig. 1. In other words, no light was found that was attributable to the deexcitation of the predicted low-lying ^{229}Th isomer. Since the observation by Irwin and Kim was conducted in air [7], our results suggest that their observation is not that of a nuclear gamma ray, but that of the well known [?] air fluorescence. The ^{229}Th system, therefore, does not appear to be the good testbed for nuclear-atomic interactions it was thought to be.

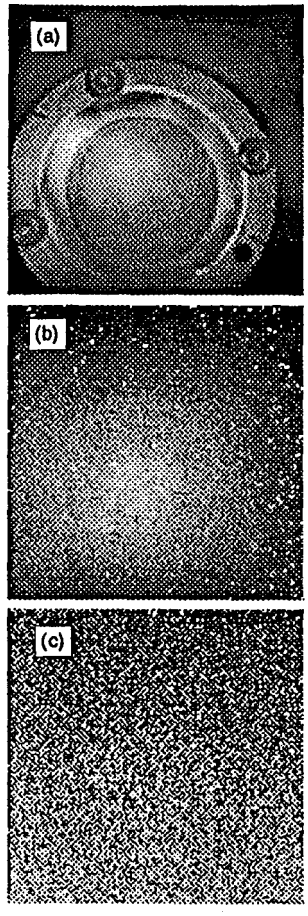

FIG. 1. Images of the ^{233}U sample: (a) visible light image showing the 2-cm-diameter sample on a 2.5-cm-diameter Pt disk held by a mounting ring; (b) image of the photon emission generated by the sample in air; (c) image of the photon emission generated by the sample in vacuum. The exposure time in (b) and (c) was 30 min each.

---

[1] V. F. Strizhov and E. V. Tkalya, Sov. Phys. JETP **72**, 387 (1991).
[2] D. Kekez, ALjubičić, K. Pisk, and B. A. Logan, Phys. Rev. Lett. **55**, 1366 (1985).
[3] D. Kekez, ALjubičić, K. Pisk, and B. A. Logan, Phys. Rev. C **34**, 1446 (1986).
[4] E. V. Tkalya, V. O. Varlamov, V. V. Lomonosov, and S. A. Nikulin, Phys. Scr. **53**, 296 (1996).
[5] R. G. Helmer and C. W. Reich, Phys. Rev. C **49**, 1845 (1994).
[6] G. M. Irwin and K. H. Kim, Phys. Rev. Lett. **79**, 990 (1997).
[7] G. M. Irwin, private communication (1998).
[8] G. Davidson and R. O'Neil, J. Chem. Phys. **41**, 3946 (1964).

Nuclear Magnetization Distribution Radii in H-like $^{185}Re^{74+}$ and $^{187}Re^{74+}$ Ions

J.R. Crespo López-Urrutia, P. Beiersdorfer, K. Widmann
Lawrence Livermore National Laboratory, Livermore, CA 94550
B.B. Birkett
University of California at Berkeley, Berkeley, CA 94720
A.-M. Mårtensson-Pendrill, M.G.H. Gustavsson
Göteborg University and Chalmers University of Technology, Göteborg, Sweden 412 96

Of all the electrons of an atom, only s electrons have enough overlap with the atomic nucleus so that their energies can tell of nuclear effects. In many-electron ions, in contrast, the electron-electron interactions play a pertinent role so that that it is difficult to disentangle the higher-order contributions to atomic structure. The best atomic system to explore properties of the nucleus therefore is one with only one electron, but with a high nuclear charge Z, because many interesting phenomena scale with powers of Z. We chose one-electron ions of Rhenium (Z=75) for a study of nuclear effects on the single electron, which in turn would yield information on the nucleus.

The highly charged ions were produced in an electron beam ion trap (SuperEBIT), and the observation was by photon emission on the F=3 to F=2 hyperfine transitions in the ground states of the isotopes $^{185}Re^{74+}$ and $^{187}Re^{74+}$. Re ions in low charge states were injected into SuperEBIT from a metal vapor vacuum arc (MEVVA) ion source prepared with natural Re (isotope abundances of 37% and 63%, respectively). A prism spectrograph (for high throughput) equipped with a cryogenically cooled CCD camera (for multi-channel detection at high detection efficiency and low intrinsic noise, and thus capable of long integration times) was set up and, after additional filtering against long-wavelength stray light from the hot electron gun, detected light at the rate of a few tens of photons per hour. The transitions of interest were found at (456.05±0.3) nm and (451.69±0.3) nm, respectively, after twenty days of observation (Fig. 1).

In order to interpret these findings, theory is needed. It has to take into account, among other factors, quantum electrodynamics (QED), the nuclear charge distribution, and the nuclear magnetization distribution. After considering the first two of these, the remaining discrepancy between theory and experimental data indicated that the nuclear magnetization radii of both isotopes are clearly larger, by factors 1.40(6) and 1.43(6), respectively, than the nuclear charge distribution radii [1]. Such a large difference was not expected from previous theoretical analyses.

If the QED contribution, the nuclear charge distribution and the magnetic moments are accurately known, this new technique provides a sensitive probe of the nuclear magnetization distribution that underlies the Bohr-Weisskopf effect.

References

[1] J.R. Crespo López-Urrutia, P. Beiersdorfer, K. Widmann, B.B. Birkett, A.-M. Mårtensson-Pendrill, M.G.H. Gustavsson, Phys. Rev. A 57, 879 (1998).

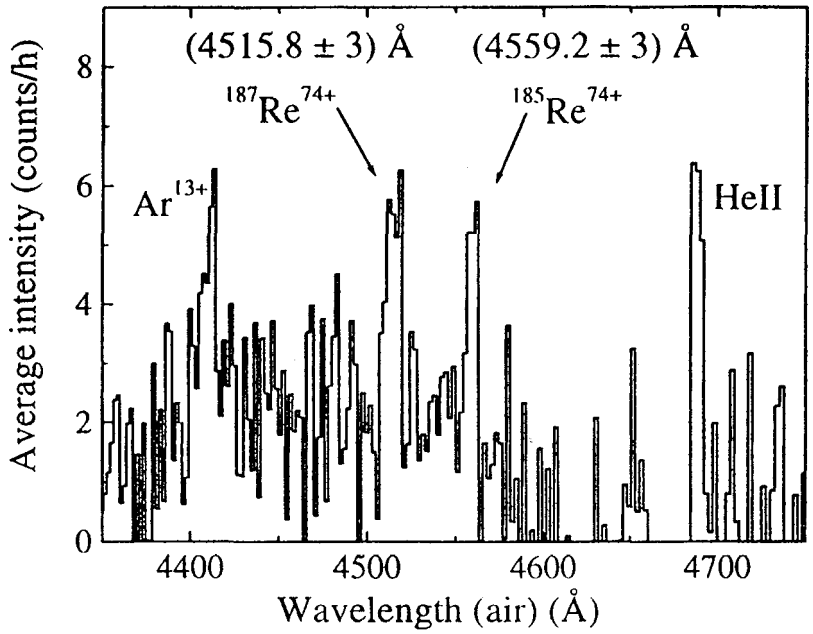

Figure 1: Spectrum showing the two lines from hyperfine structure transitions $F = 3 \rightarrow 2$ in the hydrogen-like ions Re^{74+} of the isotopes 185 and 187, as well as calibration lines of He^{+} and Ar^{13+}.

Determination of Nuclear Properties from High-Resolution Spectra of Heavy Ions

P. Beiersdorfer, J. R. Crespo López-Urrutia, K. Widmann
Lawrence Livermore National Laboratory, Livermore, CA 94550
S. R. Elliott
Department of Physics, University of Washington, Seattle, WA 98195

Properties, such as the nuclear magnetic moment, the nuclear charge radius, the nuclear neutron radius, and the distribution of the nuclear magnetic field, are fundamental to the understanding of matter and the structure of the nucleus. Some of these quantities, including the nuclear magnetic moment, have been measured and compiled by nuclear physicists since the beginning of the century. Others, especially the distribution of the nuclear magnetic field, have still not been mapped out.

The nuclear properties are not only important for the nucleus itself but they also manifest themselves in the atomic structure surrounding the nucleus. The wave functions of atomic electrons penetrate the nucleus and are affected by the nuclear properties. This interaction induces subtle shifts in the energy levels of the atomic electrons. The shifts are largest for those electrons that are closest to the core, i.e, innershell electrons. Moreover, this means that the shifts are largest for heavy elements, because electrons move closer to the core with increasing atomic number.

With the advent of high-resolution spectroscopy at the Livermore high-energy EBIT (SuperEBIT) it is now possible to observe the subtle shifts induced in the energy levels of innershell electrons by any of the nuclear properties mentioned above [1]. For example, the nuclear magnetic moment leads to a splitting of the 1s level of hydrogenic homium, Ho^{65+}. The splitting is directly proportional to the value of the nuclear magnetic moment. We have measured this splitting by optical spectroscopy to 2.1646(6) eV [2]. From this value we can infer the nuclear magnetic moment, as illustrated in Table I. The value we infer is more accurate than values infered earlier [1]. In cases where the value of the nuclear magnetic moment is known very accurately, this method can be used to infer the distribution of the magnetic moment in the nucleus or the extent of the nuclear neutron readius, as shown in [3].

Table 1. Comparison of the nuclear magnetic moment inferred from the EBIT measurement and those cited in the literature. Values are given in nuclear magnetron units. The uncertainty of the EBIT value includes only the experimental uncertainty.

Browne [4]	Peker [5]	EBIT result
4.1730 (270)	4.1320 (50)	4.1267 (11)

By measuring the energy shifts of 2s-2p transitions from different isotopes, we can infer differences in the nuclear proton radius for the different isotopes. This is illustrated in our measurements of the 2s-2p transitions in U^{86+} through U^{89+} for the three isotopes ^{233}U, ^{235}U, and ^{238}U [1,6,7]. From these energy level measurements we deduce $\delta\langle r^2\rangle^{235,238}$ is $-0.457 \pm$

0.042 fm^2 and $\delta\langle r^2\rangle^{235,238}$ is –0.250 ± 0.032 fm^2 for the isotopic variation in the nuclear charge radius. These values are more accurate than those from measurements involving muonic atoms or the value derived from a measurement of the K-shell x-rays, as shown in Fig. 1. By combining our values with those from optical measurements of neutral uranium isotopes we can interpolate among all isotopes between 233 and 238 and obtain even smaller error limits. In fact, we find $\delta\langle r^2\rangle^{233,238}$ is -0.416 ± 0.028 fm^2 and $\delta\langle r^2\rangle^{235,238}$ is –0.268 ± 0.017 fm^2.

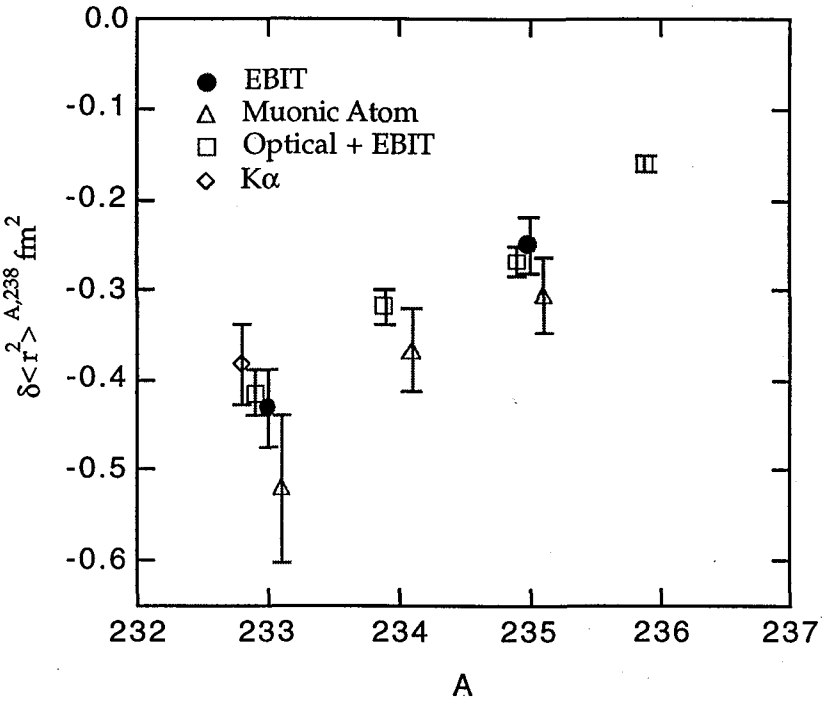

Fig. 1. Comparison of the EBIT measurements of $\delta\langle r^2\rangle^{A,238}$ with those from muonic atoms and K-shell x-rays. The optical data were normalized using the EBIT results

Our results illustrate the high accuracy achieved with spectroscopic techniques. This high spectroscopic accuracy opens nuclear properties for investigation. The results are more accurate than those obtained with standard techniques used in nuclear physics.

References:

[1] P. Beiersdorfer, S. R. Elliott, J. R. Crespo López-Urrutia, and K. Widmann, Nuclear Physics A 626, 357c-364c (1997).

[2] J. R. Crespo López-Urrutia, P. Beiersdorfer, D. W. Savin, and K. Widmann Physical Review Letters 77 826-829 (1996).

[3] J. R. Crespo López-Urrutia, P. Beiersdorfer, K. Widmann, B. B. Birkett, A.-M. Mårtensson-Pendrill, and M. G. H. Gustavsson, Physical Review A 57, 879-887 (1998).

[4] E. Browne et al., in *Table of Isotopes,* ed. by C. M. Lederer and V. S. Shirley, Wiley, New York, 1978, 7th ed.

[5] L. K. Peker, Nucl. Data Sheets 50, 137 (1987).

[6] S. R. Elliott, P. Beiersdorfer, M. H. Chen, Phys. Rev. Letters 76 1031-1034 (1996).

[7] S. R. Elliott, P. Beiersdorfer, M. H. Chen, V. Decaux, and D. A. Knapp, Physical Review C 57, 583-589 (1998).

A Quartz Quasimonolith for Absolute X-ray Wavelength Measurements

D. Klöpfel[1], G. Hölzer[1], P. Beiersdörfer[2], and E. Förster[1]

[1]*Max-Planck Arbeitsgruppe "Röntgenoptik" an der Friedrich-Schiller-Universität Jena, Max-Wien-Platz 1, D-07743 Jena, Germany*

[2]*Department of Physics and Space Technology, Lawrence Livermore National Laboratory, Livermore, CA 94550, USA*

Wavelength measurements on EBIT have generally been made relative to hydrogenic or heliumlike reference lines. Absolute wavelength measurements have not been possible on EBIT because of the difficulties in assuring that calibration lines from reference sources fill the optics the same way as the lines to be measured.

Using a novel approach we now made absolute wavelength measurements. The method we used relied on employing the reflections from two parallel crystal surfaces. The arrangement employed was a qusimonolithic crystal with absolutely calibrated lattice spacing [1].

A monolithic setup for measurement of x-ray wavelengths without the knowledge of a reference line was proposed and manufactured by Förster *et al.* [2] in 1983 and used in plasma diagnostics [3]. The crystal monolith (cf. Fig. 1) consists of two parallel crystal plates, which create the effect of two offset spectra in a single exposure. The absolute wavelength λ can be determined from the separation A of the two images of the spectral line registered on a single detector surface, if the distance between the reflecting crystal plates L and the lattice spacing d of the crystal are known in SI units.

For the detector perpendicular to the incoming x-ray beam, e.g. electronic detector in an Θ - 2Θ spectrometric setup, it follows from the Bragg equation:

$$\lambda = 2d\left(\sqrt{1-\left(\frac{A}{2L}\right)^2} - \delta(\lambda)\frac{1}{\sqrt{1-\left(\frac{A}{2L}\right)^2}}\right) \tag{1}$$

The correction factor $\delta(\lambda)$ takes into account the deviation of the x-ray refraction index in the crystal from unity. It is typically of the order from 10^{-4} to 10^{-3}.

For the quasimonolithic setup used on EBIT two quartz plates (surface orientation $10\bar{1}0$) with the dimensions $40\times20\times2.5$ mm^3 were mounted onto each side of a quartz glass spacer. The quartz plates were fixed to the spacer by optical contact with a horizontal displacement of 15 mm to allow a larger variation of the angle of incidence. The accuracy of the wavelength measurements was determined by the precision obtained in determining the monolith

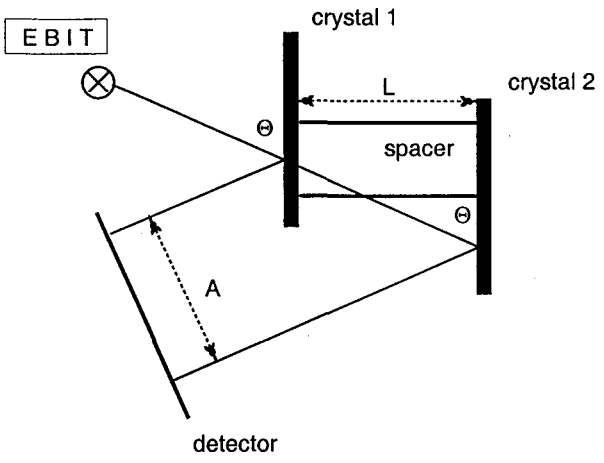

Figure 1: Schematic of the quasimonolithic setup.

parameters L and d, and indirectly by the parallelity of the lattice planes of both crystal plates (misorientation angle α). The lattice spacing of the quartz crystals were determined in SI units using an absolutely calibrated wavelength standard [4]. A measurement accuracy of L within 1 μm and of d within 0.5 fm (see Table I) was obtained. This, in principle, allows a wavelength determination with an accuracy of one part per million.

The quasimonolithic device was implemented on EBIT to measure the $(2s_{1/2}2p^6 3p_{1/2})_{J=1} \rightarrow (2s^2 2p^6)_{J=0}$ transition in neonlike Ge^{22+}. The wavelength is close to the measured value of $2d = 0.8505912(10)$ nm for the quartz plates of the quasimonolith and the corresponding Bragg angle is thus near to 82°. The resulting spectrum is shown in Fig. 2. The two images of the Ge^{22+} line shifted in relation to one another due to the diffraction at the two crystal plates of the monolith are clearly seen in the figure. The displacement A of the lines was determined by fitting each image with a Voigt profile (Fig. 2). The error involved with the evaluation of the distances between the peaks thus typically contributes the most to the overall uncertainty. The wavelength was calculated according to Eqn. 1 taking into account necessary corrections for refraction and temperature. We determine a wavelength of 0.8423 nm for the Ge line. The uncertainty of the measurement is ± 0.0012 nm with a 68% confidence limit, or a relative accuracy of 1.5×10^{-3}. While this is much less than the accuracy achievable based on the accuracy of the crystal parameters listed in Table I it demonstrates the utility of the method for absolute spectroscopic measurements.

The present uncertainty is completely dominated by the uncertainty with which the separation of the two images could be determined. Clearly, longer counting times in the future will make this a competitive method for wavelength measurements, especially in the case where no sutiable calibration lines can be generated *in situ* that are near the lines to be measured.

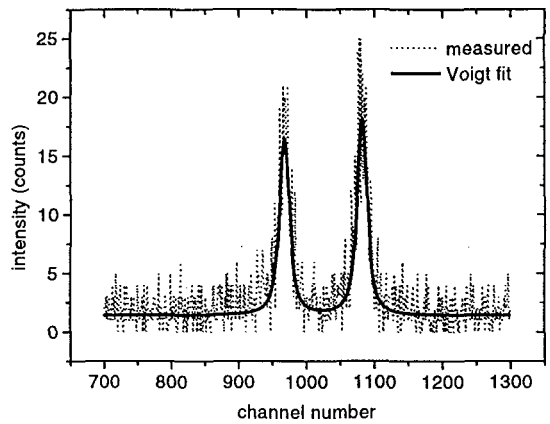

Figure 2: Spectrum of the $(2s_{1/2}2p^6 3p_{1/2})_{J=1} \rightarrow (2s^2 2p^6)_{J=0}$ transition in neonlike Ge^{22+} measured with the quartz quasimonolith and best fit using Voigt profiles. The detector was calibrated in an independent measurement, using an linear approximation one channel corresponds to 0.0807 mm.

Table 1: Summary of the crystal parameters determined at 293.0 K. Uncertainties reflect 95% confidence limits.

Quantity	*measured Value*	*Uncertainty*
L	32494	± 1 μm
α	$0.3'$	$\pm 20''$
d	0.4252956	$\pm 5 \times 10^{-7}$ nm

References

[1] D. Klöpfel, G. Hölzer, E. Förster, and P. Beiersorfer, Rev. Sci. Instrum. **68**, 3669 (1997).

[2] E. Förster, K. Goetz, S. Großwig, K. Schäfer, W. D. Zimmer and K. Sander, Preprint FSU Jena N/83/38, (1983).

[3] A. V. Rodé, A. M. Maksimchuk, G. V. Sklizkov, A. Ridgeley, C. Danson, N. Rizvi, R. Bann, E. Förster, K. Goetz and I. Uschmann, Journal of X-Ray Science and Technology **2**, 149 (1990).

[4] M. Fritsch, Thesis FSU Jena (1996)

II. Spectral Diagnostics for High-Temperature Laboratory and Astrophysical Plasmas

Measurement, Line Identification, and Modeling of the L–Shell Fe XVII Spectrum below 12 Å

G.V. Brown[1,3], P. Beiersdorfer[1] D. A. Liedahl,[1] S. M. Kahn,[2] and K. Widmann[1]
[1]Department of Physics and Space Technology, Lawrence Livermore National Laboratory, Livermore, CA 94551, USA
[2]Department of Astrophysics, Columbia University, New York, NY 10027 USA
[3]Department of Physics, Auburn University, Al 36849 USA

Fe XVII has shown strong emission in a number of astrophysical sources such as solar active regions, X–ray binaries, supernova remnants, and stellar coronae. The utility of the Fe XVII line emission as a diagnostic, however, depends critically on the accuracy of the atomic models used to interpret spectra. Atomic models, such as MEKA, MEKAL, and the Raymond and Smith code, rely heavily on large lists of wavelength and intensity data such as the compilation by Doschek and Cowan [1]. At present, these compilations are based on Solar observations, laboratory measurements, and calculations. While these compilations contain reliable data for the stronger $3 \rightarrow 2$, and to some extent the $4 \rightarrow 2$ Fe XVII line emission, the data for the $n \rightarrow 2$ transitions, where $n \geq 5$, which fall in the 1.0–1.2 keV range, are less reliable, and in most cases, not existent because they often blend with lines from higher charge states of iron and other ions, and are generally weak. While this may not seem very important, this missing data makes it impossible to accurately fit astrophysical data. For example, fits to data recently obtained by *ASCA* from Capella [2], and M87 [3] all show deficits in the flux in the 1.0–1.5 keV range.

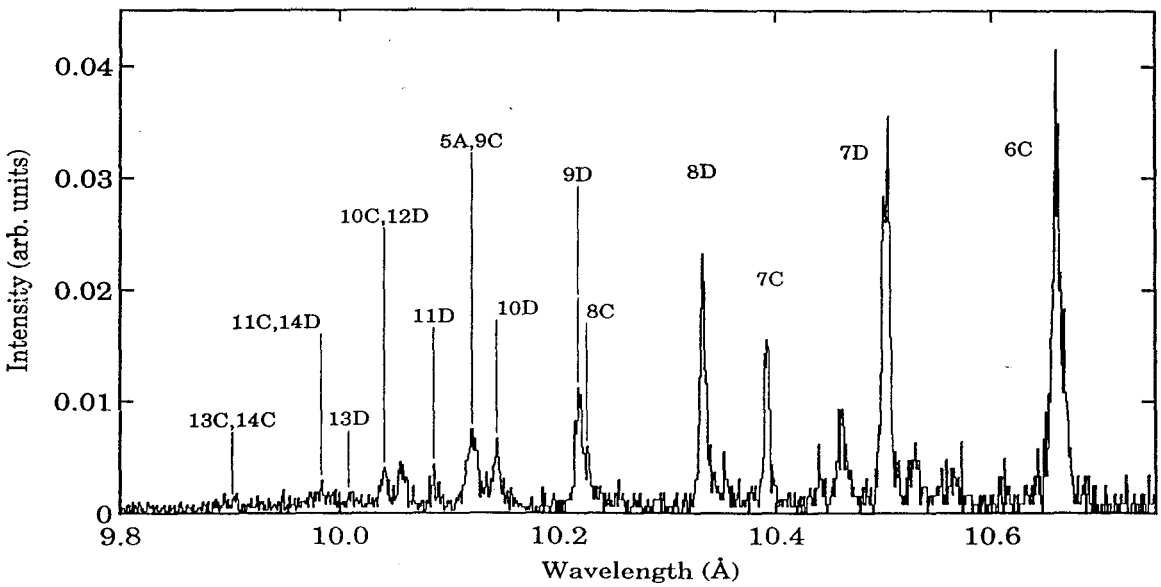

Figure 1: Spectrum of the high–n transitions in Fe XVII

Using the Electron Beam Ion Trap (EBIT) we have made a detailed measurement, and line identification of the Fe XVII L–shell emission spectrum between 9.8 and 11.5 Å [4].

We identify and accurately determined wavelengths for transitions from higher shells up to n=11. An example spectra is shown in figure 1. The total amount of flux contained in all the transitions nC and nD where $n \geq 5$, and np $\rightarrow$ 2s transitions with $n \geq 4$ relative to the line λ15.01 is 0.13 $^{+0.04}_{-0.03}$. This is a substantial fraction of the total emission unaccounted for by standard modeling codes.

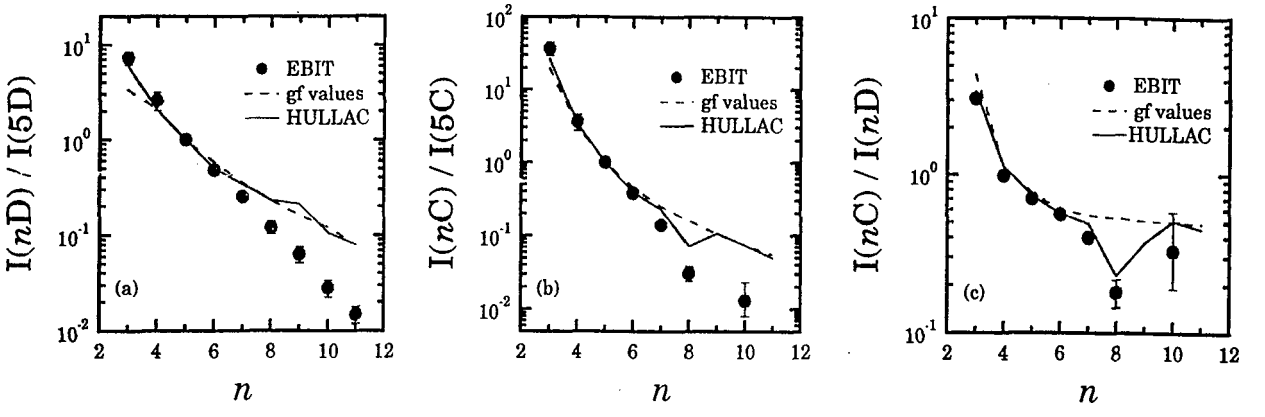

Figure 2: Relative intensity comparison with HULLAC and gf values

In Figure 2 we compare our measured intensity ratios to those predicted by the Hebrew University Lawrence Livermore Atomic Code (HULLAC) and gf values. Figure 2a compares ratios of the type $2p^5 nd_{5/2}\ ^3D_1 \rightarrow 2p^6\ ^1S_0$ (labeled nD) to $2p^5 5d_{5/2}\ ^3D_1 \rightarrow 2p^6\ ^1S_0$ (labeled 5D); figure 2b compares ratios of the type $2p^5 nd_{3/2}\ ^1P_1 \rightarrow 2p^6\ ^1S_0$ (labeled nC) to $2p^5 5d_{3/2}\ ^1P_1 \rightarrow 2p^6\ ^1S_0$ (labeled 5C); and figure 2c compares ratios of the type $2p^5 nd_{3/2}\ ^1P_1 \rightarrow 2p^6\ ^1S_0$ to $2p^5 nd_{5/2}\ ^3D_1 \rightarrow 2p^6\ ^1S_0$ (i.e. $I_{nC}/\ I_{nD}$). Figures 2a and 2b show that both HULLAC and the gf values agree well for n equal to 4, 5, and 6, however both decrease more slowly than the measured values for $n \geq 7$. For the ratio I(nC)/I(nD) both HULLAC and the gf values follow the data very closely with the exception of n = 8, where a dip caused by configuration interaction between states with nearly degenerate energy levels is seen. The dip is not reproduced by the gf values because that particular calculation does not include interaction between levels of different principal quantum number, n. Our measurements clearly show that models and calculations can only be made reliable if all relevant levels are included.

This work is supported by a NASA High Energy Astrophysics X-Ray Astronomy Research and Analysis grant NAGW-4185 (Columbia University) and work order W-19127 (Lawrence Livermore National Laboratory).

References

[1] Doschek, G. A., and Cowan, R.D. 1984, ApJS, 56, 67

[2] Brickhouse, N.S., et al. 1997, in prep

[3] Hwang, U., et al. 1997, ApJ,476,560

[4] Brown, G. V., Beiersdorfer, P., Liedahl, D. A., Kahn, S.M., and Widmann, K. 1998 ApJ, in press

Simulating a Single Electron Temperature Maxwellian Plasma using an Electron Beam Ion Trap

D. W. Savin, M.-F. Gu, and S. M. Kahn
Columbia Astrophysics Laboratory, Columbia University, New York, NY 10027.
P. Beiersdorfer, B. Beck, J. Crespo López-Urrutia, and K. Widmann
Lawrence Livermore National Laboratory, Livermore, CA 94550

In a collisionally dominated plasma, the ionization structure and line emission of a plasma is determined by electron collisions. These electrons are typically expected to have a Maxwell-Boltzmann energy distribution. We are attempting to use the Lawrence-Livermore electron beam ion trap (EBIT) to simulate a single electron density plasma with a Maxwell-Boltzmann electron energy distribution. Our aim is to produce the ionization balance appropriate for a Maxwellian plasma and to observe the resulting line emission. Achieving the ionization balance appropriate for a Maxwellian plasma is important because line emission from a given charge state is coupled to the one lower charge state by inner shell ionization and to the one higher charge state by dielectronic and radiative recombination.

EBIT uses a nearly monoenergetic beam of electrons to produce and trap ions. This results in a charge balance of trapped ions appropriate for the given electron beam energy. To simulate a Maxwell-Boltzmann electron energy distribution, it is necessary to sweep the electron beam energy in time in such a way that the time-averaged electron energy distribution matches a Maxwell-Boltzmann energy distribution. If the electron beam density in EBIT is kept constant while the electron energy is swept in time, then the trapping properties of EBIT remain constant while the electron energy is varied. This results in an electron-ion overlap in the trap that is independent of the instantaneous electron energy. This is necessary to insure that all electron-ion collision processes for a given charge state have the same geometric overlap factor, just as they would in a true Maxwellian plasma. Maintaining a constant electron density also insures that EBIT line emission from density sensitive transitions will approach the line emission from a true, single density Maxwellian plasma. In this way we aim to produce a plasma with an ionization structure and line emission profile approaching that of an astronomical plasma.

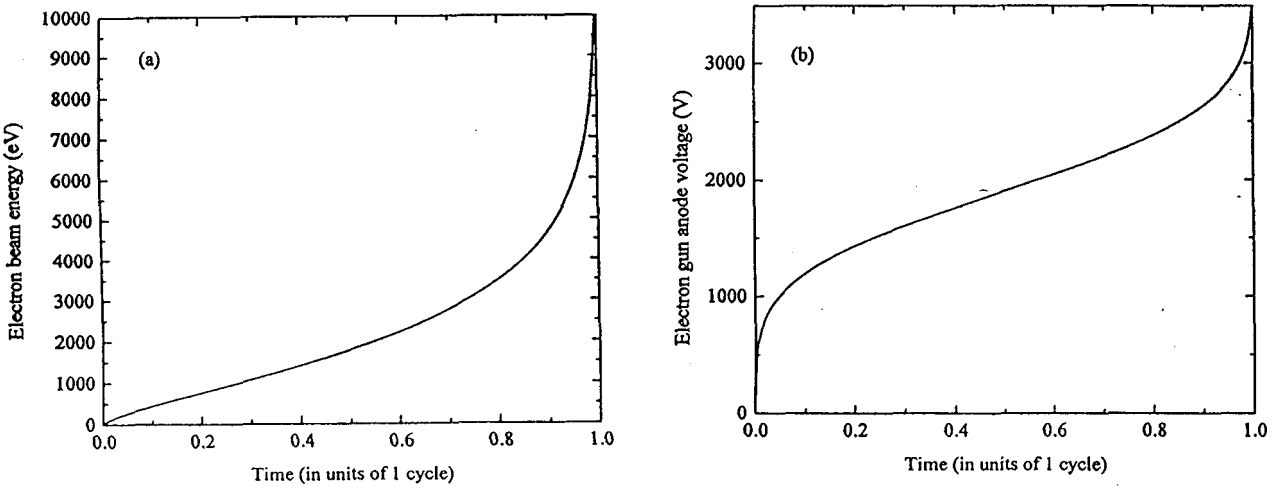

Figure 1: (a) The electron beam energy timing pattern for producing a quasi-Maxwellian plasma at a temperature of 1.5 keV. (b) The electron gun anode voltage pattern required for the producing a constant density 1.5 keV quasi-Maxwellian plasma.

We have recently demonstrated that the concept of producing quasi-Maxwellian plasmas can be implimented in EBIT by sweeping in time both the electron beam energy and electron gun anode voltage. Because the electron beam current varies as $n_e E^{1/2}$, we must also sweep the anode (extraction) voltage of the electron gun in EBIT synchronously with the beam energy, so as to vary the current in such a way as to keep the electron density nearly constant. To produce quasi-Maxwellian plasmas in EBIT for a range of electron temperatures, we have used electron beam voltage and electron gun anode voltage timing patterns similar to those shown in Fig. 1. Initial results have demonstrated that the concept of producing quasi-Maxwellian plasmas can be implemented in EBIT by sweeping in time both the electron beam energy and the electron gun anode voltage. For our initial tests, we injected iron into EBIT and observed the resulting X-rays using a solid-state Si(Li) detector. A representative spectrum for emission from a quasi-Maxwellian plasma of 1.5 keV is shown in Fig. 2.

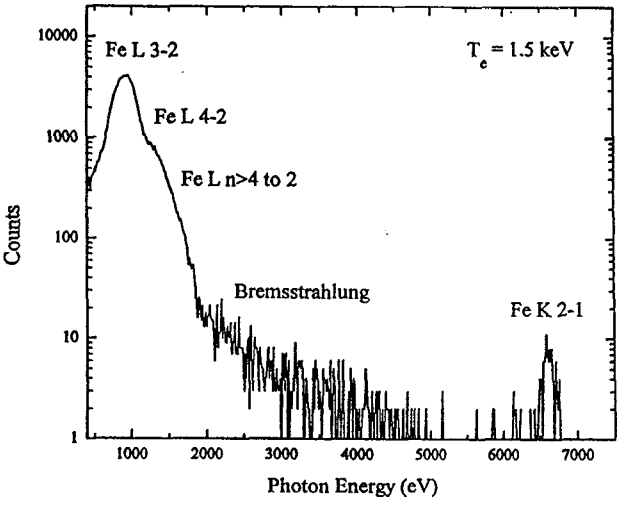

Figure 2: Iron X-ray emission from EBIT for quasi-Maxwellian conditions at 1.5 keV. Iron L-shell $3 \rightarrow 2$, $4 \rightarrow 2$, and $n > 4 \rightarrow 2$ line emission as well as iron K-shell $2 \rightarrow 1$ line emission and the bremsstrahlung continuum are all observed in the collected spectrum.

A number of technical and experimental issues need now to be addressed in order to assess the effects they may have (if any) on the accuracy of the simulated Maxwellian. These issues include the effects on the charge balance of charge transfer off of background neutrals, and any effects due to the truncation of lowest and highest beam energies that are accessible. Work is under way to address these issues.

This work was performed under the auspices of the U.S. Department of Energy by the Lawrence Livermore National Laboratory under contract number W-7405-ENG-48 and supported by the NASA High Energy Astrophysics X-Ray Astronomy Research and Analysis grant NAGW-4185.

Laboratory measurement of the 2p–3d resonance to intercombination line emission of Fe XVII

G.V. Brown[1,3], P. Beiersdorfer[1], D. A. Liedahl,[1] S. M. Kahn,[2] and K. Widmann[1]
[1]Department of Physics and Space Technology, Lawrence Livermore National Laboratory, Livermore, CA 94551, USA
[2]Department of Astrophysics, Columbia University, New York, NY 10027 USA
[3]Department of Physics, Auburn University, Al 36849 USA

The ratio of the intensity of the 2p–3d $^1P_1$ resonance and $^3D_1$ intercombination lines of neon–like Fe XVII situated at 15.01 and 15.26 Å, respectively, has been measured on the Sun to be between 2.2 and 2.7, while the ratio predicted by theoretical models range between 2.9 and 4.7. To account for the differences between the calculated ratio and those measured on the Sun, several authors have invoked resonance scattering of the flux in λ15.01 [1,2,3]. Basing the amount of scattering on a comparison of the solar value of I(λ15.01)/I(λ15.26) with the calculated value, which assumes λ15.01 is optically thin, and noting that the solar ratio is less than the calculated ratio, several authors have inferred physical parameters of the solar corona, such as density [2,3], relative iron abundance, and column density along the line of sight [3]. However, the reliability of inferred physical parameter is tainted by the large variation in the atomic calculations.

In order to to provide a baseline value for assessing the effect of resonance scattering of λ15.01, we have used the Electron Beam Ion Trap to determine the intensity ratio of the λ15.01 to λ15.26 line under precisely controlled conditions [4]. We measure a value of 3.04 ± 0.12 for this ratio at a monoenergetic beam energy of 1150 ± 30 eV (see fig. 1). Our measurement was carried out in a regime where electron impact excitation followed by radiative cascades is the only line formation process. The ratio was also measured at several different beam energies between 850 eV and 1300 eV as well using two different crystals, RAP and KAP.

The fact that most solar ratios are significantly lower than our measurement of the ratio, where no scattering occurs, lends support to the possibility of resonance scattering. In order to correctly infer any physical parameter in the solar corona using this ratio a correct optically thin value, i.e., a value where no resonant scattering occurs, is crucial as the following shows. Using the method described in Waljeski et al., as well as their emission measure ($2.3 \times 10^{29} cm^{-5}$), we infer a column density of $6.2^{+1.5}_{-2.2} \times 10^{19} cm^{-2}$, an electron density of $3.7^{+2.0}_{-0.7} \times 10^{9} cm^{-3}$, and an active region path length of $1.7^{+0.4}_{-0.7} \times 10^{10} cm$ from their solar ratio of 1.90 ± 0.21. Compared to the values given by Waljeski, our column density is a factor of 1.7 lower, making our density a factor of 1.7 higher, and our path length nearly a factor of three less. Our path length is in much better agreement with the path length derived from Waljeski's broad band image which is believed to be more reliable. The calculated ratio given by Waljeski et al. is 3.8, a difference of about 20% from our value of 3.04 ± 0.12. Hence, this 20% difference in the line ratio may cause a factor of nearly two difference in density and a factor of three difference in path length. These differences are summarized in table 1. New measurements are now planned to consider the effects of satellite contributions to the lines as well as the effect of resonance excitation.

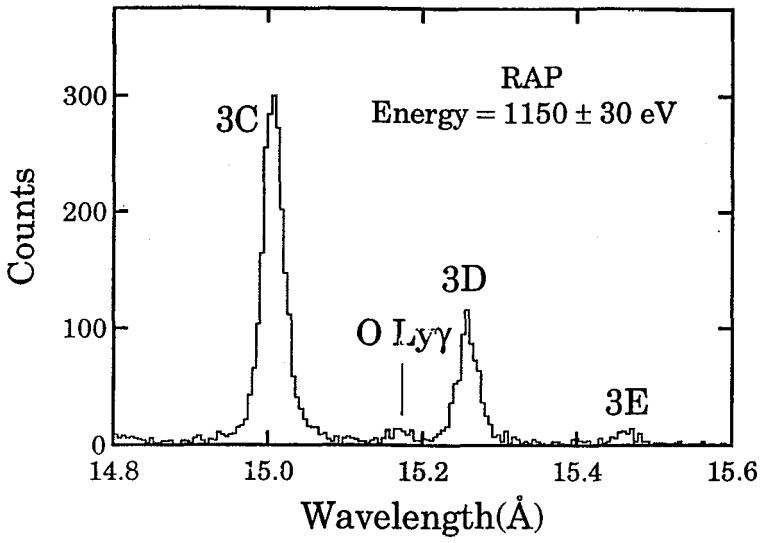

Figure 1: Spectrum of 15.01 Å (3C) resonance line and 15.26 Å (3D) intercombination line taken with RAP crystal at a beam energy of 1150 ± 30 eV.

	EBIT	Waljeski et al. 1994
$R_{opt.thin}$	3.04±0.12	3.80
$\tau(R_{Solar}=1.90\pm0.21)$	$2.5\ ^{+0.6}_{-0.9}$	$4.24^{+1.3}_{-1.0}$
$\int n_e dl$	$6.2^{+1.5}_{-2.2} \times 10^{19} cm^{-2}$	$1.05 \times 10^{20} cm^{-2}$
n_e	$3.7^{+2.0}_{-0.7} \times 10^{9} cm^{-3}$	$2.2^{+0.8}_{-0.4} \times 10^{9} cm^{-3}$
dl	$1.7^{+0.4}_{-0.7} \times 10^{10} cm$	$4.7^{+0.9}_{-1.8} \times 10^{10} cm$

Table 1: Values of various physical parameters inferred from the ratio (R) of λ15.01/λ15.26 for the optically thin case measured at EBIT and compared to calculations by Waljeski et al. 1994.

This work is suppported by a NASA High Energy Astrophysics X-Ray Astronomy Research and Analysis grant NAGW-4185 (Columbia University) and work order W-19127 (Lawrence Livermore National Laboratory).

References

[1] Rugge, H. R., and Mckenzie, D. L. 1985, ApJ, 297, 338

[2] Schmelz, J. T., Saba, J. L. R., and Strong, K. T. 1992, ApJ, 398, L115

[3] Waljeski, K., Moses, D., Dere, K. P., Saba, J. L. R., Web, D. F., and Zarro, D. M. 1994, ApJ, 429, 909-923

[4] Brown, G. V., Beiersdorfer, P., Liedahl, D. A., Kahn, S. M., and Widmann, K. 1998, ApJ, in press

III. Electron-Ion Interaction Studies

Measurements of K-shell X-ray Spectra from Hydrogenic and Heliumlike Ions produced by Charge-Transfer Reactions

P. Beiersdorfer[1], L. Schweikhard[2], K. Widmann[1]

[1] *Lawrence Livermore National Laboratory, Livermore, CA 94551, USA*
[2] *Institut für Physik, Johannes Gutenberg-Universität, D-55099 Mainz, FRG*

Using Fourier transform ion cyclotron mass spectrometry we have shown in recent studies that the ions produced in SuperEBIT remained trapped for several seconds after the electron beam was turned off.[1,2] In the absence of the electron beam, the ions are confined radially by the strong magnetic field produced by two superconducting coils in a Helmholtz configuration and axially in the potential applied to the end electrodes of the trap. We have now begun to make use of the ions trapped in this so-called magnetic trapping mode for collision studies with neutral atoms introduced into the trap.

The interaction between the highly charged ions and neutral atoms is studied by monitoring the x-ray emission resulting from charge transfer reactions.[3] A spectrum of the K-shell emission of highly charged xenon ions produced in the interaction of Xe^{53+} and Xe^{54+} ions with a continuous stream of neutral xenon is shown in Fig. 1(a). The x-ray emission from the xenon ions results because an electron captured from a neutral atom preferentially populates a level with large principal quantum number and x rays are emitted in subsequent radiative cascade processes.

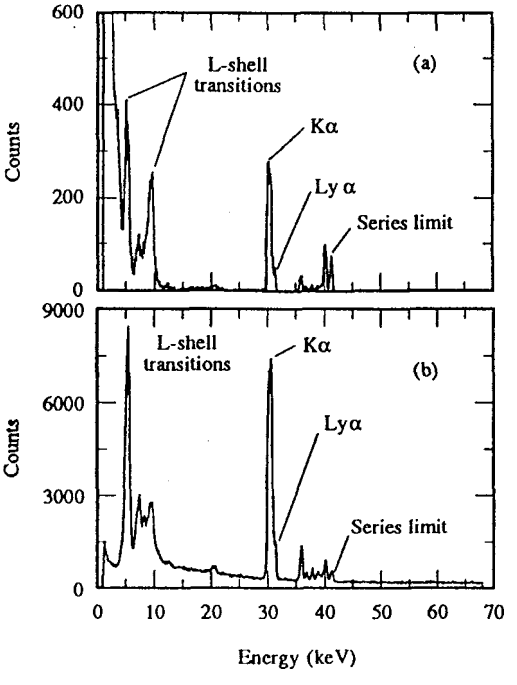

Figure 1: Xenon x-ray emission excited (a) by charge exchange reactions of Xe^{53+} and Xe^{54+} with neutral xenon and (b) by electron-impact excitation with a 158.3-keV electron beam.

The charge-transfer excited spectrum differs markedly from that produced by electron-impact excitation shown in Fig. 1(b). First, transitions from high-n levels near the series limit are enhanced. Second, there is no bremsstrahlung background, as the the spectrum is recorded in the absence of an electron beam. Third, xenon ions with charge less than 53+ cannot contribute to the spectrum, because ions with lower charge have no innershell vacancy that can be filled by electron capture. By contrast, electron-impact-induced inner-shell excitation can produce K-shell emission lines from lower charge states in Fig. 1(b). A corresponding set of spectra is given in Fig. 2 for highly charged krypton ions showing the same behavior as that for xenon.

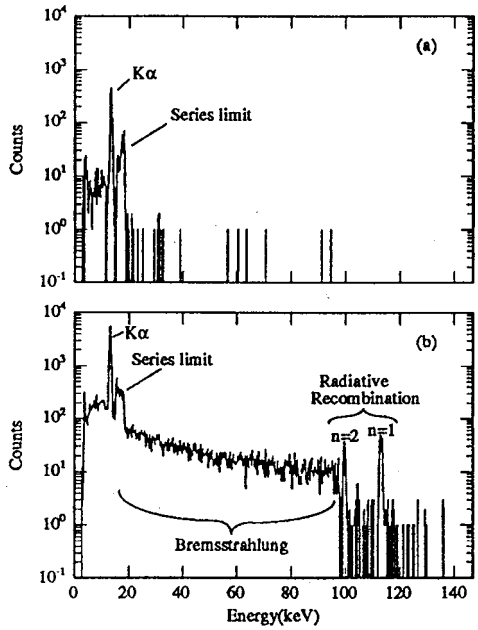

Figure 2: Krypton x-ray emission excited (a) by charge exchange reactions of Kr^{35+} and Kr^{36+} with neutral krypton and (b) by electron-impact excitation with a 95-keV electron beam.

Similar to spectra collected with use of a gas-jet target on the ESR heavy-ion storage ring,[4] the observed spectra allow the determination of x-ray transition energies and of the QED contributions. However, because the EBIT spectra were determined with ions at rest, no Doppler shift corrections needed to be made. A close up of the xenon K-shell spectrum is shown in Fig. 3. The $2p_{3/2} \rightarrow 1s_{1/2}$ Lyman-α_1 transition in hydrogenic Xe^{53+} is well resolved and unblended, allowing a direct measurement of its energy. We find an energy of $31,276 \pm 12$ eV. The total Lamb shift affecting this transition is about 40 eV. The accuracy of the measurement is thus within 30% of the Lamb shift.

The use of charge-transfer reactions to study the K-shell spectra of highly charged ions represents a new EBIT-based technique for measuring the Lamb shift. The accuracy in the Xe^{53+} measurement was limited by the counting statistics. Future measurements will undoubtedly produce result with much higher accuracy.

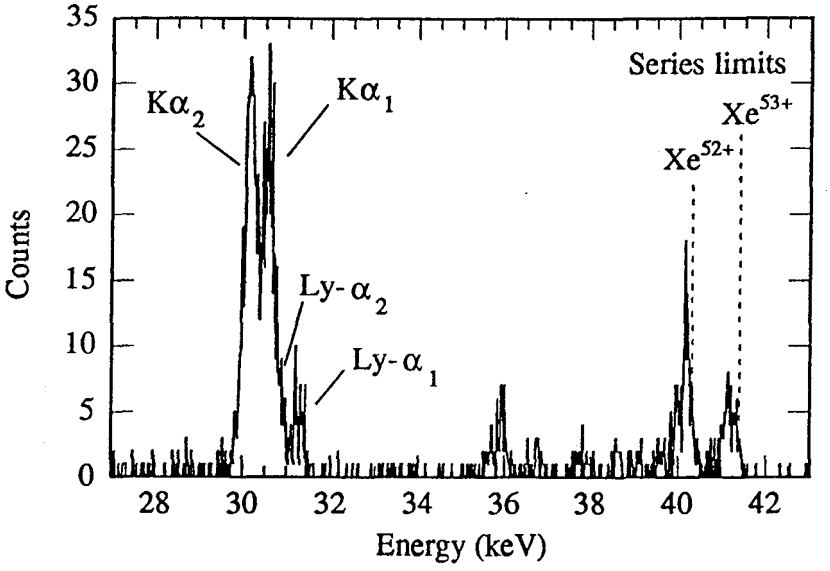

Figure 3: Close-up of the xenon K-shell spectrum recorded in the magnetic trapping mode. The $1s_{1/2}$-$2p_{3/2}$ and $1s_{1/2}$-$2p_{1/2}$ transitions in hydrogenlike Xe^{53+} are marked Ly-α_1 and Ly-α_2, respectively. Kα_1 and Kα_2 refer to transitions of the type $1s_{1/2}$-$2p_{3/2}$ and $1s_{1/2}$-$2p_{1/2}$ in heliumlike Xe^{52+}. Unlabeled features are caused by transitions from levels with principal quantum number $n \geq 3$. The ionization potentials of Xe^{52+} and Xe^{53+} are indicated and represent the high-n series limit of the K-shell transitions in the respective ion.

References

[1]P. Beiersdorfer, B. Beck, R. E. Marrs, S. R. Elliott, and L. Schweikhard, Rapid Commun. Mass Spectrom. **8**, 141 (1994).

[2]P. Beiersdorfer, B. Beck, St. Becker, and L. Schweikhard, Int. J. Mass Spectrom. Ion Proc. **157/158**, 149 (1996).

[3]P. Beiersdorfer, L. Schweikhard, J. Crespo López-Urrutia, and K. Widmann, Rev. Sci. Instrum. **67**, 3818 (1996).

[4]Th. Stöhlker, C. Kozhuharov, P.H. Mokler, A. Warczak, F. Bosch, H. Geissel, R. Moshammer, C. Scheidenberger, J. Eichler, A. Ichihara, T. Shirai, Z. Stachura, P. Rymuza, Phys. Rev. A **51**, 2098 (1995).

This work was supported in part by a NATO Collaborative Reserach Grant CRG-930125.

Laboratory Measurements of Resonant Contributions to Fe XXIV Line Emission

M. F. Gu[1], P. Beiersdorfer[2], G. V. Brown[2], S. M. Kahn[1],
D. A. Liedahl[2], K. J. Reed[2] and D. W. Savin[1]

[1] *Columbia Astrophysics Laboratory, Columbia University, New York, NY 10027*
[2] *Lawrence Livermore National Laboratory, Livermore, CA 94550*

Recent *Advanced Satellite For Cosmology and Astrophysics* (*ASCA*) observations of the Centaurus cluster of galaxies [1] exhibit discrepancies with the relative line intensities of various Fe XXIII and XXIV *L*-shell emission lines predicted by standard plasma codes. This discrepancy is seen with all standard emission codes and is attributed to problems with the atomic physics used in the emission codes. New distorted wave (DW) calculations of Fe XXIII and Fe XXIV electron impact excitation (EIE) rate coefficients [2] appear to provide better agreement with the *ASCA* observations. Using the EBIT, Savin *et al.* [3] measured the relative line emission of several Fe XXIV $3 \rightarrow 2$ and $4 \rightarrow 2$ lines and found good agreement with the calculations of Liedahl *et al.* These measurements, however, were carried out at electron energies significantly greater than the excitation threshold energies of the lines observed. The calculations remain to be experimentally verified for energies at which resonant processes may be important and for energies near threshold where DW calculations may overpredict the EIE cross section.

A number of X-ray astronomy satellites are scheduled for launch in the next few years. The *Advanced X-ray Astrophysics Facility* (*AXAF*) is scheduled for launch in 1998, and the *X-Ray Multi-mirror Mission* (*XMM*) and *Astro-E* in 1999. These satellites will carry spectrometers with resolving powers in the Fe *L*-shell emission region over an order of magnitude greater than the spectrometers aboard *ASCA*. Interpreting *AXAF, XMM, Astro-E* spectra will require atomic data at an accuracy significantly greater than the data presently used in the standard emission codes.

To address some of the existing and upcoming needs of X-ray astrophysics, we have continued our studies of Fe XXIV line emission. We measured the Fe XXIV $3 \rightarrow 2$ line emission at energies around threshold, using EBIT to examine the resonance contributions to the line emissivity. Here we present relative cross sections, at electron energies between 700 and 1500 eV, for producing line emission at wavelength $\lambda = 11.18$Å of the Fe XXIV $3d_{5/2} \rightarrow 2p_{3/2}$ transition.

Various processes can contribute to line emission observed from a collisional plasma. Direct excitation (DE) is the most important one at energies above the EIE threshold. Below threshold, Dielectronic recombination (DR) produces high n satellites which cannot be resolved from the EIE line. Resonant excitation (RE) can populate the same levels as DE via dielectronic capture followed by autoionization to the level of interest. We have measured the following processes:

- DE
  $Fe^{23+}(2s) + e^- \rightarrow Fe^{23+}(3d_{5/2}) + e^- \rightarrow Fe^{23+}(2p_{3/2}) + h\nu_1 + e^-$
- RE
  $Fe^{23+}(2s) + e^- \rightarrow Fe^{22+}(4l'nl'') \rightarrow Fe^{23+}(3d_{5/2}) + e^- \rightarrow Fe^{23+}(2p_{3/2}) + h\nu_1 + e^-$

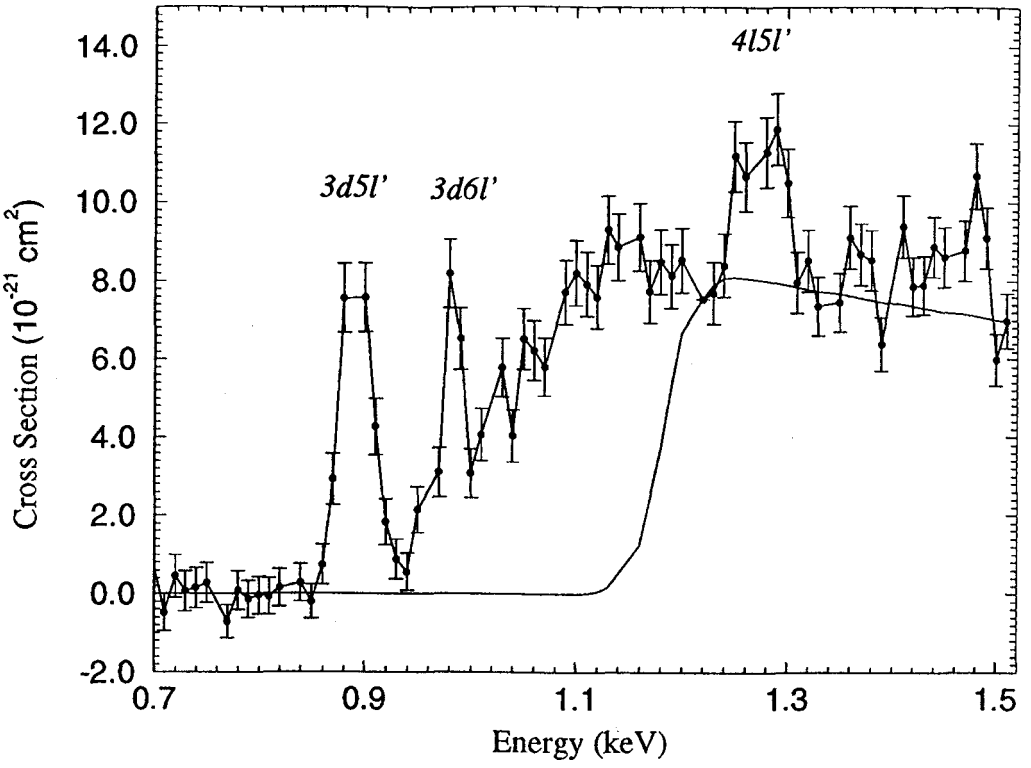

Figure 1: Normalized cross sections for producing line emission at $\lambda = 11.18$Å.

- DR
  $Fe^{23+}(2s) + e^- \rightarrow Fe^{22+}(3d_{5/2}nl') \rightarrow Fe^{22+}(2p_{3/2}nl') + h\nu_2 + e^-$

Quantum mechanically, there is no way to distinguish between DE and RE, and we measure the coherent sum of the two processes.

After injecting iron into EBIT, the electron beam energy is kept at 4 keV for 200 ms. Then every 10 ms the beam energy is swept between 700 and 1500 eV using a sawtooth pattern 2 ms in length. The intensity of a particular line is $I \propto \int d\mathbf{r} n_e(\mathbf{r}) n_q(\mathbf{r}) \sigma v$, where $n_e(\mathbf{r})$ is the electron density, $n_q(\mathbf{r})$ is the ion density, σ is the cross section for producing the observed line emission and v is the electron velocity. During the sweeping of the beam energy, the charge balance changes insignificantly because the ionization and recombination time scales at these energies are $\geq$ 100 ms. We maintain a nearly constant $n_e(\mathbf{r})$ by varying the anode voltage of the electron gun. We record the intensity of line emission at $\lambda = 11.18$Å as a function of beam energy using a flat crystal spectrometer. Because $\int d\mathbf{r} n_e(\mathbf{r}) n_q(\mathbf{r})$ is kept constant versus E, we can derive cross sections for producing these lines by normalizing our measurements to theory.

Figure 1 shows the normalized cross section for producing $\lambda = 11.18$Å line emission. The error bars on the data points show the 1σ statistical uncertainties. The normalization point is presented without error bar. The $3l5l'$ and $3l6l'$ DR resonances are well separated. All other DR resonances between 1.0 keV and the DE threshold are unresolved and appear as a continuous increase in the cross sections. The RE resonance at a beam energy of about 1.25 keV is produced by dielectronic capture into the Fe XXIV $4l5l'$ level followed by autoionizing to the $3d_{5/2}$ level.

Using the relative cross sections obtained above, we calculate the rate coefficients of each process. The DE rate is calculated by using HULLAC [2] cross sections. For experimentally inferred rates, only line emission within the measured energy range is included. Figure 2 shows the experimentally

inferred rates for DR, DE plus RE, and the total rates. The total rate includes the experimentally inferred DR, DE plus RE, and the theoretical DE rates at energies outside of our measured range. The theoretical DE rates do not include the cascade contributions. At a temperature of 1.7 keV, near where Fe XXIV emissivity peaks, DR contributions amount to ~20% for the $\lambda = 11.18$Å line emission. RE enhances the rates by ~5%. However, the unmeasured RE contributions at higher energies can be expected to increase the rates further. Thus, plasma emission codes which do not include the effect of DR and RE on line emissivities can be expected to underestimate line intensity by at least ~ 25%.

This program is supported by a NASA High Energy Astrophysics X-Ray Astronomy Research and Analysis grant NAGW-4185 (Columbia University) and work order W-19127 (LLNL).

References

[1] Fabian, A. C., *et al.* 1994, ApJ, 436, L63

[2] Liedahl, D.A., *et al.* 1995, ApJ, 438, L115

[3] Savin, D.W., *et al.* 1996, ApJ, 470, L73

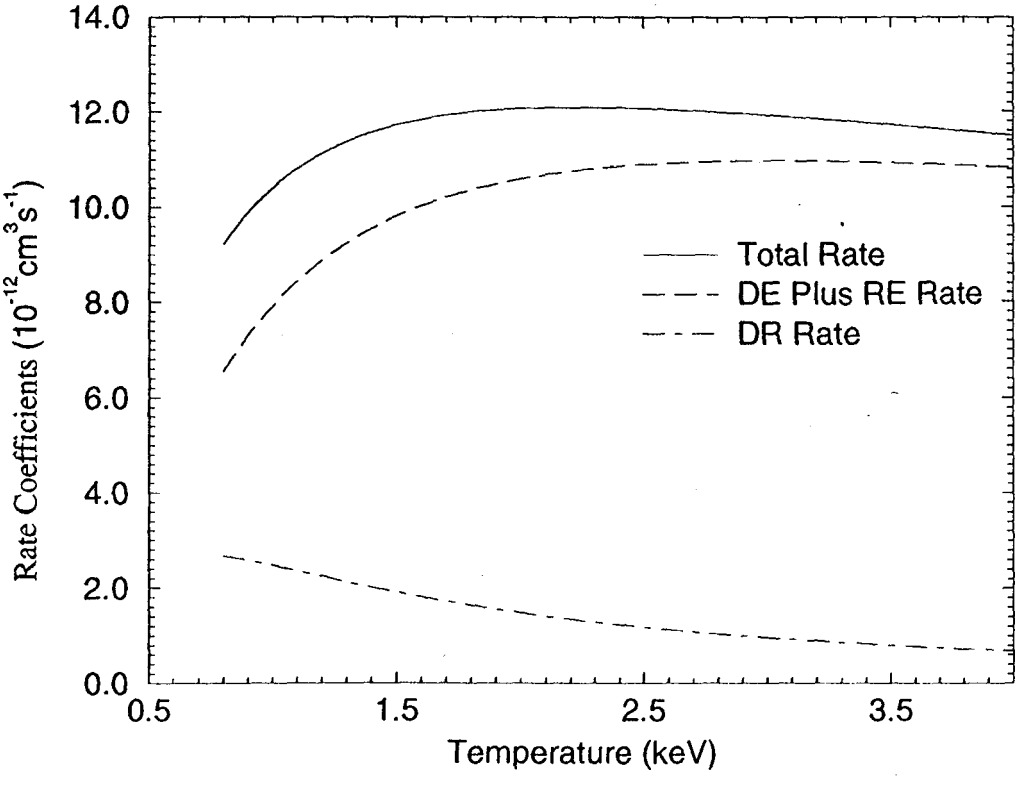

Figure 2: Rate coefficients for producing line emission at $\lambda = 11.18$Å.

Dual Crystal Spectrometer Setup for Polarization Measurements of X-ray Lines from Beam-Excited Highly Charged Ions

P. Beiersdorfer[1], K. Widmann[1], P. Neill[2]

[1]*Lawrence Livermore National Laboratory, Livermore, CA 94550*
[2]*Department of Physics, University of Nevada, Reno, NV 89557*

X-ray line polarization is maximized in electron beam x-ray sources, such as an electron beam ion trap, where highly charged ions are excited by a monoenergetic electron beam. Such sources are, therefore, ideal for testing theory and developing plasma-polarization spectrometers. Using an EBIT, measurements of the polarization of the x-ray line emission from highly charged heliumlike ions have been reported for Sc^{19+} and Fe^{24+} [1,2]. These measurements have used a single crystal spectrometer. In successive measurements, the entire spectrometer was either rotated by 90° [1] or the analyzing crystal was exchanged [2]. Because source conditions may change during the measurement sequence, it is of advantage to utilize two spectrometers that observe the emitting ions simultaneously. This is especially important when lines from different ionization stages need to be cross normalized. Such a dual crystal spectrometer setup has now been implemented on EBIT [3].

The new dual spectrometer was set up to measure the polarization of the K-shell line emission of heliumlike Fe^{24+}. The first spectrometer used a LiF(220) crystal with lattice spacing d=1.424 Å operating at a nominal Bragg angle of 41°. The second used a Si(220) crystal with lattice spacing d=1.920 Å operating at a nominal Bragg angle of 29°. The two spectrometers concurrently recorded spectra in a plane of dispersion perpendicular to the beam direction.

The reflection properties of x-ray crystals depend on the Bragg angle θ. For ideal crystals, the ratio of reflection for polarization components polarized perpendicular and parallel to the beam direction is given by

$$R_{perp}/R_{para} = \cos(2\theta).$$

The first spectrometer thereby recorded an almost pure polarization state where the radiation is linearly polarized parallel to the electron beam direction. The second spectrometer recorded a mixture of polarization states.

Typical spectra observed with the two spectrometers are shown in Fig. 1. The intensity of the triplet lines clearly changes its magnitude relative to that of the singlet line. This immediately indicates that the triplet lines have different polarization properties than the singlet line. A detailed analysis of the two spectra allows us to determine the actual degrees of linear polarization of each line. Good agreement with theory was found, as indicated in the comparison with theoretical spectra that take the polarization effects into account (cf. Fig. 1).

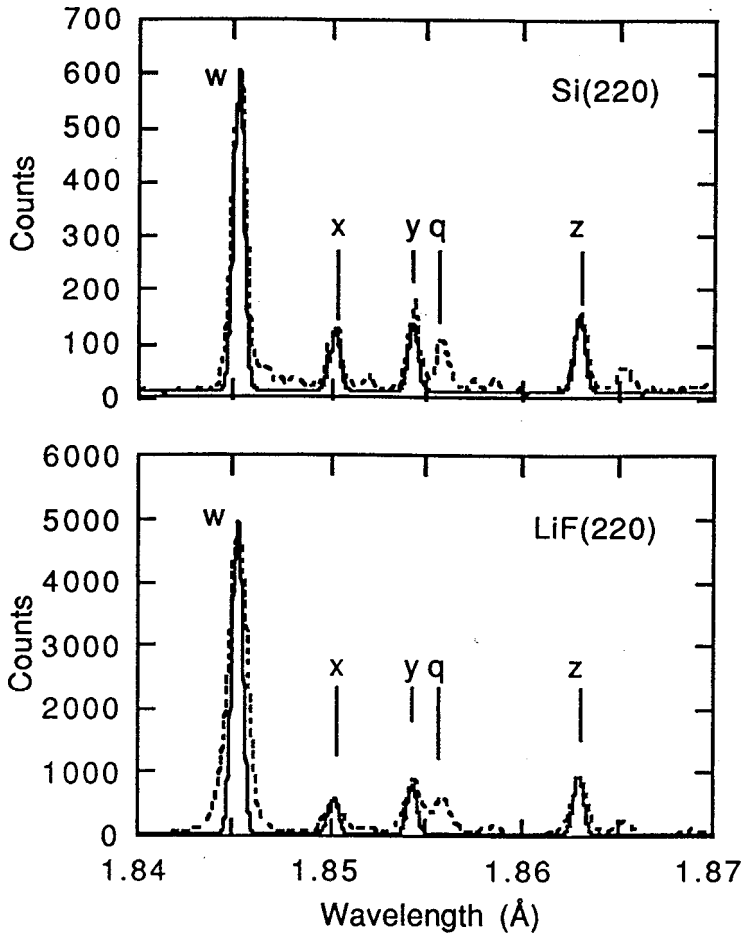

Fig. 1. Crystal-spectrometer spectra of lines w, x, y and z in heliumlike Fe^{24+} excited by a 6850-eV electron beam: (a) spectrum obtained with a Si(220) crystal at a Bragg angle of 41°; (b) spectrum obtained with a LiF(220) crystal at a Bragg angle of 29°. Unlabeled features are from transitions in Fe^{22+} and Fe^{23+} formed by innershell excitation. The predicted spectral intensities (solid lines) are superimposed for comparison.

References:

[1] P. Beiersdorfer, D. A. Vogel, K. J. Reed, V. Decaux, J. H. Scofield, K. Widmann, G. Hölzer, E. Förster, O. Wehrhan, D. W. Savin, and L. Schweikhard, Phys. Rev. A **53**, 3974 (1996).

[2] J. R. Henderson, P. Beiersdorfer, C. L. Bennett, S. Chantrenne, D. A. Knapp R. E. Marrs, M. B. Schneider, K. L. Wong, G. A. Doscheck J. F. Seely, C. M. Brown, R. E. LaVilla, J. Dubau, and M. A. Levine, Phys. Rev. Lett. **65**, 705 (1990).

[3] P. Beiersdorfer, J. Crespo López-Urrutia, V. Decaux, K. Widmann, and P. Neill, Rev. Sci. Instrum. **68**, 1073 (1997).

Polarization-Dependent Spectra of X-ray Dielectronic Satellite Lines of Be-like Fe

A.S. Shlyaptseva, R.C. Mancini, and P. Neill
Department of Physics
University of Nevada, Reno, NV 89557-0058

P. Beiersdorfer, J.R. Crespo López-Urrutia, and K. Widmann
Lawrence Livermore National Laboratory, Livermore, CA 94550

X-ray line spectroscopy is an important tool for the diagnosis of space and laboratory plasmas. Most of the spectroscopic diagnostics developed for plasmas have been based on properties of line intensity distributions and line profiles. However, for the case of non-equilibrium plasmas whose electron distribution functions can show different degrees of anisotropy, and even the presence of electron beams, the polarization of X-ray line emission can be particularly useful for spectroscopic diagnostic applications. During the last few years electron kinetics simulations of laser-produced plasmas driven by ultrashort (subpicosecond), high-intensity laser pulses have been done using Particle-In-Cell (PIC) codes [1-3], Fokker-Planck [4], and Vlasov models [5]. These studies show anisotropic, electron distribution functions for the plasma and the presence of beams of energetic electrons that can carry a substantial amount of the total energy deposited by the laser. Also, the production and characterization of energetic electrons play a critical role in the recently proposed Fast Ignitor concept where suprathermal electrons produced by ultrahigh intensity lasers ignite a fuel capsule originally compressed in a conventional laser-driven implosion [6]. New spectroscopic diagnostics leading to the characterization of beams of electrons in plasmas are needed in these areas. Electron beams represent an anisotropic excitation mechanism that results in the emission of partially polarized X-ray lines. In this connection, X-ray line polarization spectroscopy can help to diagnose electron beams in plasmas and to bridge the gap between electron kinetics simulations and experimental measurements. Few theoretical and experimental studies have been done on X-ray line polarization. The EBIT facility offers an excellent opportunity to observe polarization effects in X-ray line emission in experiments performed under well controlled conditions. In turn, these measurements can be used to make detailed comparisons with theoretical calculations before applying them to the analysis of polarized spectra from complicated systems like plasmas [7].

We have theoretically and experimentally studied the polarization properties of spectral features formed by the overlapping and blending of dielectronic satellite lines. This is different from previous investigations on X-ray line polarization, which have focused on the study of the degree of polarization or angular distribution of X-ray emission of single, well-resolved lines. The calculation of polarization-dependent spectra represents a suitable way to study the polarization properties of complex spectra. We have calculated polarization-dependent spectra of dielectronic satellite lines of Be-like Fe and compared them with experimental spectra observed at EBIT. To this end, dielectronic satellite spectra were simultaneously recorded with two crystal spectrometers, which acted as polarizers by selectively reflecting polarization states associated with directions parallel and perpendicular to the electron beam axis. The dielectronic satellite spectrum is significantly polarized and, in general, the two polarization-dependent spectra have different intensity distributions. The details of these spectra also depend strongly on the energy of the electron beam.

Theoretical results for polarization-dependent spectra of dielectronic satellite lines in Be-like Fe are presented on Fig. 1 calculated for three different energies of the electron beam. Since we compare synthetic polarization-dependent spectra with experimental spectra recorded at EBIT, theoretical results were calculated assuming electron beam characteristics, and line profiles suitable for the experimental conditions and instruments used at EBIT. The spectra displayed in Fig. 1 illustrate the main properties of the

theoretical results: (1) the dependence of the spectra on the electron beam energy E_b, and (2) the polarization properties of the spectra. In general, lines with different degrees of polarization blend to give rise to peaks and the polarization properties of these spectral features can be traced back to those of their constituent lines. Three traces are shown in Fig. 1, which represent the intensity distributions associated with the parallel polarization state, perpendicular polarization state, and their sum, i.e. the total intensity at 90°. This way of presenting the results clearly shows the relative contributions of parallel and perpendicular polarization states to the total intensity distribution, and it highlights those peaks (i.e. spectral features) which have significant polarization. The larger the difference between the intensity distributions associated with parallel and perpendicular polarization states the larger, the polarization of the peak. Peaks where the two traces are identical are unpolarized.

Fig. 2 illustrates a comparison between theoretical and experimental spectra for an electron beam energy of 4.762 *keV*. The top panel of Fig. 2 shows the spectrum obtained with LiF(220) crystal, which represents emission from an almost-pure parallel polarization state. The bottom panel shows the spectrum obtained with LiF(200) crystal. It represents emission from a mixture of both polarization states. Several comparisons were done for other electron beam energies. As the value of E_b increases, different electron capture resonances can be excited and the spectral line emission changes. The agreement between theoretical and experimental spectra is overall very good. The agreement extends from a good reproduction of the energy dependence of the line emission, the line position, and the relative line intensities to the polarization-induced differences between the spectra from the two crystal spectrometers. This good agreement demonstrates that modeling of beam-excited, polarization-dependent spectra can be accomplished with confidence [7].

Very important for developing polarization diagnostics is the good agreement between theoretical predictions and data for lines that are sensitive markers for polarized line emission. These include the pair of features labeled 1 and 2 and the pair labeled 5 and 6. The polarization sensitivity arises from the fact that these pairs are made up of lines with nearly opposite polarization properties. Peak 2 is comprised of two lines with positive polarization, while peak 1 contains five lines that on average are negatively polarized. Similarly, peak 5 consists of an unpolarized line, while peak 6 contains two lines that on average are strongly negatively polarized. The present work represents a test of the theoretical capability to model the polarization properties of complicated spectra excited by a low-density electron beam, and sets a reference framework for developing polarization-based spectroscopic diagnostics relevant to more complicated systems such as plasmas.

This work was supported by NSF OSR-9353227 and DOE-EPSCOR grants, and LLNL contract B336460. Work at LLNL was performed under the auspices of DOE under contract No. W-7405-ENG-48 and supported in part by the Office of Basic Energy Sciences, Chemical Sciences Division.

REFERENCES

[1] Wilks, W.L. Kruer, M. Tabak and A.B. Langdon, Phys. Rev. Lett. **69**, 1383 (1992).
[2] Gibbon, Phys. Rev. Lett. **73**, 664 (1994).
[3] Pukhov and J. Meyer-ter-Vehn, Phys. Rev. Lett. **76**, 3975 (1996)
[4] Matte, J.C. Kieffer, S. Ethier, M. Chaker and O. Peyrusse, Phys. Rev. Lett. **72**, 1208 (1994).
[5] Ruhl, J. Opt. Soc. Am. B **13**, 388 (1996).
[6] Tabak, J. Hammer, M.E. Glinsky, W.L. Kruer, S.C. Wilks, J. Woodworth, E.M. Campbell, M.D. Perry and R.J. Mason, Phys. Plasmas **1**,1626 (1994).
[7] Shlyaptseva, R.C. Mancini, P. Neill, P. Beiersdorfer, J.R. Crespo Lopez-Urrutia and K. Widmann, Phys. Rev. A **57**, 888 (1998).

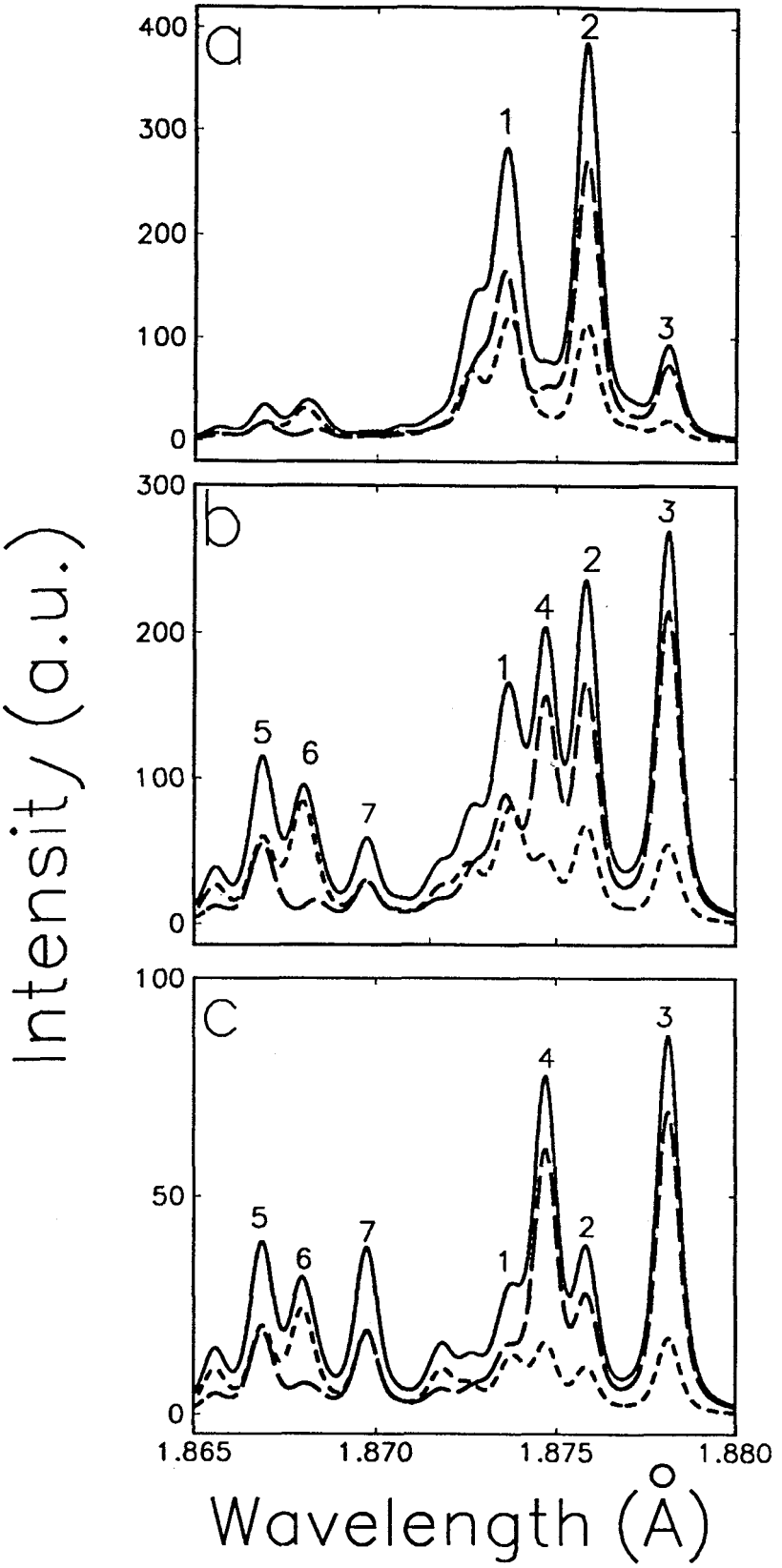

FIG. 1. Theoretical polarization-dependent spectrum of Be-like Fe calculated for three different energies of the electron beam: a) E_b=*4.734 keV*, b) E_b=*4.762 keV*, c) E_b=*4.775 keV*.
(- - -): intensity associated with parallel polarization state,
(.....): intensity associated with perpendicular polarization state,
(___): total intensity.

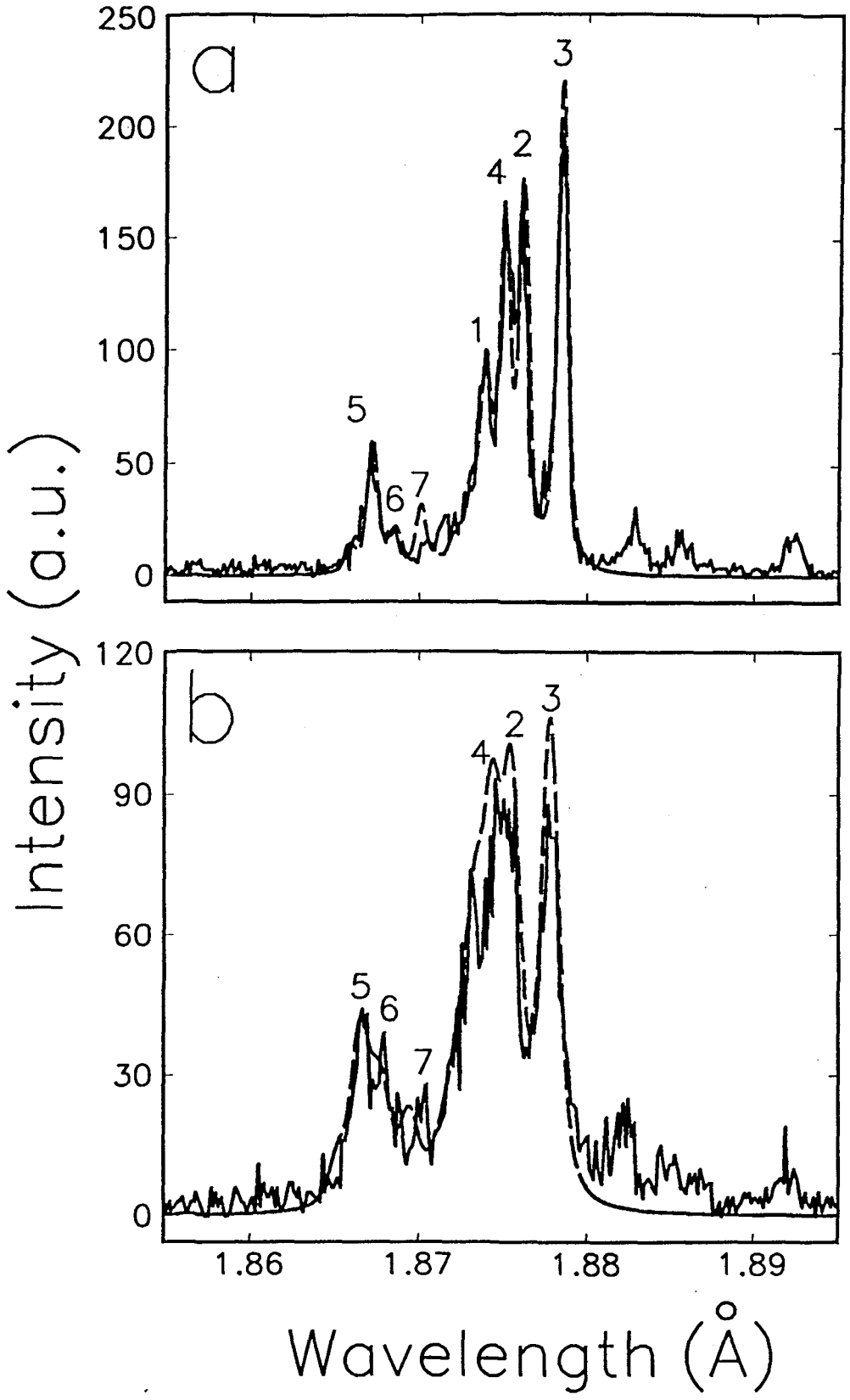

FIG. 2. Comparison of experimental spectrum (____) and theoretical spectrum of Be-like Fe (- - -) calculated at the electron beam energy E_b=4.762 *keV* associated with: a) almost pure, parallel polarization state, b) mixture of polarization states.

IV. Ion / Surface Interaction Studies

Synergy of electronic excitations and elastic collision spikes in sputtering of heavy metal oxides

T. Schenkel, A. V. Barnes, A. V. Hamza, D. H. Schneider J. C. Banks, and B. L. Doyle

Sputtering and secondary ion emission from solids interacting with energetic particles are active research fields of great fundamental and applied interest. Momentum transfer to target atoms can be accomplished through elastic collisions or electronic processes. Linear collision cascade theory [1] has been used most successfully in describing the sputtering of metals by ions of keV energies. Enhancements due to elastic collision spikes are observed when both projectile and target consist of very high Z materials [2]. At energies of several hundred keV, close to the nuclear stopping maximum, sputtering yields increase due to non-linear effects as most atoms in the spike volume are set into motion. Controversial discussions have evolved on the nature of sputtering mechanisms in the interaction of slow, highly charged ions with solids [3-8]. Defect mediated sputtering has been demonstrated for some alkali halides and SiO_2 [3] bombarded by slow Ar^{q+} ($q \leq 14$) and Xe^{q+} ($q \leq 27$). Sputtering through collective excitation mechanisms such as Coulomb explosions accompanied by shock waves was inferred from observations of high yields of atomic and cluster ions for very high projectile charge states ($q > 30$) [4, 5, 8]. Up to now total sputter yields of materials were known only for impact of ions with charge states $q \leq 27$ (for Xe).

We report on the first measurements of total sputtering and secondary ion yields from uranium oxide interacting with slow, highly charged, heavy ions with charge states up to 70+. Here, a new ion-solid interaction regime, where projectile charge and momentum are both critical, is observed. In this regime, electronic excitation by neutralization of highly charged ions and elastic collision spikes combine to produce a synergistic enhancement of secondary particle emission.

We used the catcher target technique [6] to determine total sputtering yields. Secondary ion yields were measured by time-of-flight secondary ion mass spectrometry (TOF-SIMS) [4, 8]. Highly charged ions (HCI) were extracted from the electron beam ion trap (EBIT) at Lawrence Livermore National Laboratory. The experimental setup for ion extraction and TOF-SIMS has previously been described [4, 8]. Polycrystalline uranium (^{238}U) targets were prepared by electropolishing followed by oxidation in air for several hours for native oxide formation. The oxide thickness was estimated from known oxidation rates [9] to be several hundred nanometers. Targets were cleaned after insertion into vacuum by low energy ion sputtering. For total sputter yield measurements, projectiles impinged on the targets at an incident angle of 30° relative to normal. SiO_2 (150 nm thick thermal oxide on Si) catcher targets were placed in parallel to the sputter target at a distance of 6 mm. Secondary neutrals and ions emitted from uranium oxide during exposure were collected on the catcher target. Typical highly charged ion fluxes were $\sim 10^5$ ions/s for Au and $\sim 10^6$ ions/s for Xe-ions. Accurate determination of the HCI flux is crucial for our experiment. The flux was determined by single ion pulse counting of projectiles impinging on a microchannel plate detector (MCP). Bias voltages and discrimination levels in counting electronics were carefully set to assure constant detection

efficiencies for ions of all charge states and impact energies [10]. The MCP used for direct detection of HCIs was calibrated by single ion counting in a Daly detector arrangement. The strong burst of secondary electrons emitted by individual HCIs incident on solid targets allows for detection of HCIs with 100% efficiency [4, 8]. The efficiency of the MCP for direct detection of HCIs was 0.61 +/-0.02. Doses ranged from 2×10^{10} (Au^{63+}) to 3×10^{11} (Xe^{27+}). Accumulation times were several days. Resulting surface coverages of ^{238}U on the catchers were $\sim10^{11}$ atoms/cm^2. We used the heavy ion backscattering (HIBS) system at Sandia National Laboratory to determine uranium coverages *ex situ* [11]. The HIBS sensitivity for detection of uranium on otherwise clean silicon is $<10^9$ atoms/cm^2. Additionally, catcher targets could be analyzed *in situ* by highly charged ion based TOF-SIMS [4]. Sputter yields were calculated from surface coverages of uranium on the catchers, the ion dose, the view factor [12] and the sticking probability of uranium atoms on the catcher surface. The later was assumed to be >0.9, similar to values found for uranium sticking on Al_2O_3 [6].

Total ablation rates (open squares) are shown together with positive secondary ion and cluster ion yields as a function of incident ion charge, q, in Fig. 1. For total yield measurements, incident ions were $Xe^{27, 44+}$, $Au^{62, 63+}$ and Th^{70+} at impact velocities of $0.3\times v_{Bohr}$. The relative error in the total yield data is ~15% resulting from uncertainties in HIBS results, ion dose measurements and relative variations of view factors. Also shown are sputtering yields of uranium oxide for singly charged xenon and thorium ions at $0.3\times v_{Bohr}$ as calculated by TRIM [13]. Sputtering yields of uranium oxide increase slightly with q for highly charged xenon ions. The increase by more than a factor of two when highly charged Au and Th ions interact with the target can result both from electronic sputtering at higher q and from increased momentum transfer due to the formation of elastic collision spikes in the target.

For measurements of secondary ion production, incident ions were Xe^{17-52+} (open triangles) and Au^{36-69+} (solid triangles). Here, the impact velocity was kept constant at $0.2\times v_{Bohr}$. The error in secondary ion production rates is statistical and amounts to <5% of the rate value. The values reported here are secondary ion counts detected per incident projectile. For determination of total secondary ion yields the detection efficiency of the spectrometer, η, must be known. Considering the detection efficiency for secondary ions in the MCP [14] and the geometry with annular detector, we estimate η to be ~0.1-0.15. $(UO_x)_n^+$-yields, n=1, 2, 3, increase strongly with q. At q=44 and 52, the higher potential energy of the xenon ions ($E_{pot}[Xe^{52+}]$ = 121 keV; m=136 u) dominate for n=1 over the higher momentum brought into the target by the gold ions ($E_{pot}[Au^{52+}]$ = 57.6 keV; m=197 u). This ratio is reversed for the emission of cluster ions, n=2, 3, were the influence of momentum dominates and cluster yields are higher for Au than for Xe projectiles. We attribute this to the development of elastic collision spikes in the target when bombarded with gold ions with energies of several hundred keV, near the nuclear stopping maximum [1, 2]. Xenon ions are too light to form strong elastic collision spikes in uranium oxide.

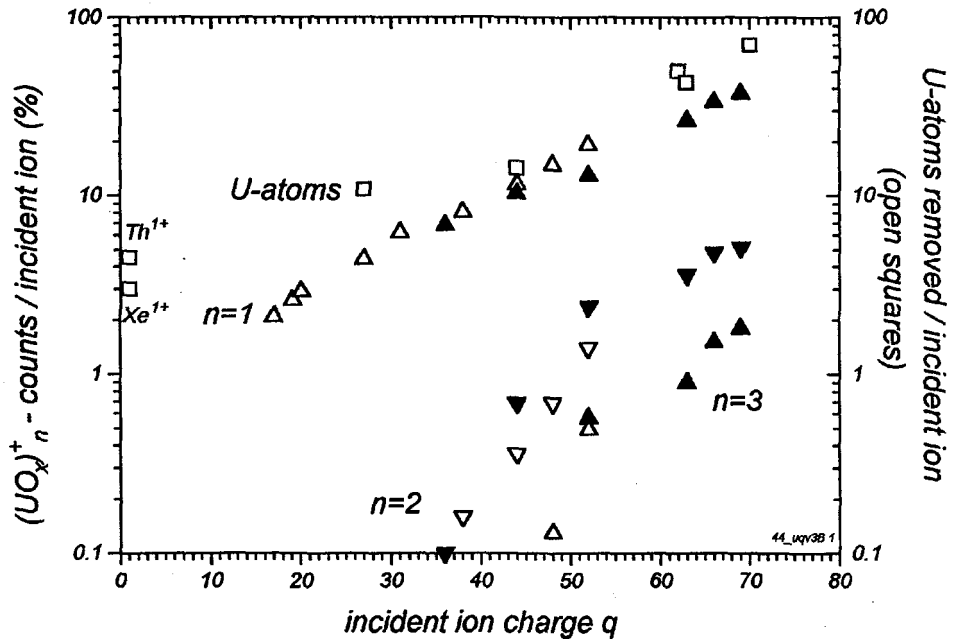

Fig. 1 Total sputtering yield of U-atoms (open squares), $(UO_x)^+_n$, n=1,2,3, secondary ion production from uranium oxide.

A characteristic signature of elastic collision spikes is the dependence of secondary neutral particle and ion emission on projectile energy. We have measured secondary ion yields as a function of kinetic energy for Xe^{27+}, Xe^{44+}, Au^{63+} and Au^{69+} (Fig. 2). Ion yields vary only very weakly for xenon projectiles when the impact energy is increased from 20 to 500 keV. The yield dependence for Au^{63+} displays some structure with a weak maximum. The data for Au^{69+} show a pronounced maximum at ~220 keV. This energy value coincides with observations in elastic collision spike sputtering [2] were the maximum sputter yield is achieved at energies slightly below the projectile energy corresponding to the nuclear stopping power maximum. The later is reached at an energy of ~600 keV for singly charged gold ions in uranium oxide [13]. The finding of a more pronounced maximum in secondary ion emission for a more highly charged projectile demonstrates the critical interplay of projectile momentum and charge. For Au^{63+} (E_{pot}=122.3 keV), the combination of high charge and momentum yields a weak but significant increase in secondary ion emission at elastic collision spike energies. For Au^{69+} (E_{pot}=168.6 keV) the additional electronic excitation energy creates a condition above critical in both charge and momentum and electronic sputtering through charge neutralization and elastic collision spikes combine synergistically. Increasing or decreasing the impact energy decreases momentum transfer below critical values for spike formation and yields drop similarly as observed in pure elastic spike sputtering. While conditions for elastic collision spikes are lost, electronic excitation through charge neutralization keeps secondary emission levels high.

Our results demonstrate the interplay of momentum transfer and electronic excitation in sputtering and secondary ion production from uranium oxide interacting with

highly charged ions. For the component of electronic excitations, potential sputtering through decay of self trapped excitons (STE) was demonstrated for LiF and SiO_2 bombarded by slow Ar^{q+} ($q \leq 14$) and Xe^{q+} ($q \leq 27$) [3]. Interestingly, strong potential sputtering with a pronounced dependence on charge does not always occur when STE can be produced in a material, as shown in Ref. 6 for CsI and Ar^{q+} ($4 \leq q \leq 11$). To our knowledge, formation of STE has not been reported for uranium oxides. A collective model of electronic sputtering is the Coulomb explosion model [15, 16].

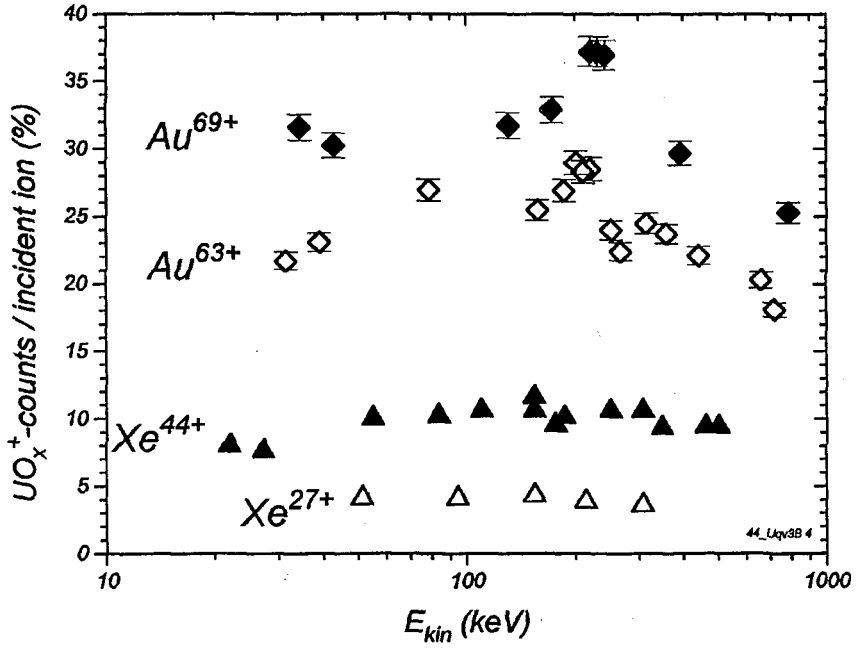

Fig. 2: Energy dependence of secondary ion production from uranium oxide at impact of Au^{69+}, Au^{63+}, Xe^{44+} and Xe^{27+}.

The authors gratefully acknowledge the excellent technical support at the LLNL EBIT facility provided by D. Nelson and K. Visbeck.

References:

[1] P. Sigmund, in *Inelastic Ion-Surface Collisions*, N. H. Tolk, J. C. Tully, W. Heiland, C. W. White (eds.) (Academic Press, New York, 1977), p. 128

[2] H. L. Bay, H. H. Anderson, W. O. Hofer, O. Nielsen, Nucl. Instrum. and Methods Phys. Res. **132,** 301 (1976); P. Sigmund, Appl. Phys. Lett. **25,** 169 (1974); ibid. **27,** 521 (1975)

[3] T. Neidhart, F. Pichler, F. Aumayr, HP. Winter, M. Schmidt, P. Varga, Phys. Rev. Lett. **74** 5280 (1995); ibid, Nucl. Instrum. and Methods Phys. Res., Sect. B **98,** 465 (1995); M. Sporn, G. Libiseller, T. Neidhard, M. Schmid, F. Aumayr, HP. Winter, P. Varga, M. Grether, D. Niemann, N. Stolterfoht, Phys. Rev. Lett. **79,** 945 (1997); P. Varga, et al., Phys. Scr. **T73,** 307 (1997)

[4] T. Schenkel, et al, Nucl. Instrum. and Methods Phys. Res., Sect. B **125,** 153 (1997); T. Schenkel, et al., Materials Science Forum **248-249,** 413 (1997)

[5] T. Schenkel, et al., Phys. Rev. Lett. **78,** 2481 (1997)

[6] D. L. Weathers, T. A. Tombrello, M. H. Prior, R. G. Stokstad, R. E. Tribble, Nucl. Instrum. and Methods Phys. Res., Sect. B **42,** 307 (1989); K. G. Liebbrecht, J. E. Griffith, R. A. Weller, T. A. Tombrello, Radiat. Eff. **49,** 195 (1980)

[7] S. T. de Zwart, T. Fried, D. O. Boerma, R. Hoekstra, A. G. Drentje, A. L. Boers, Surf. Sci. **177,** L939 (1986)

[8] D. H. Schneider, M. A. Briere, Phys. Scr. **53,** 228 (1996), and references therein

[9] G. W. McGillivray, D. A. Geeson, R. C. Greenwood, J. Nucl. Mat. **208,** 81 (1994)

[10] M. P. Stockli, D. Fry, Rev. Sci. Instrum. **68,** 3053 (1997)

[11] J. A. Knapp, D. K. Brice, J. C. Banks, Nucl. Instrum. and Methods Phys. Res., Sect. B **108,** 324 (1996)

[12] A. J. Chapman, Heat Transfer (Macmillan, New York, 1974), 3rd ed.

[13] J. Biersack, Nucl. Instrum. and Methods Phys. Res., Sect. B **27,** 21 (1987)

[14] J. Oberheide, P. Wilhelms, M. Zimmer, Meas. Sci. Technol. **8,** 351 (1997)

[15] I. S. Bitensky, E. S. Parilis, J. Phys., **50 C2,** 227 (1989), and references therein

[16] Cheng, H. P., J. D. Gillaspy, Phys. Rev. B, 55, 2628, 1997.

Ablation of GaAs by intense ultrafast electronic excitation on a nanometer scale

T. Schenkel, A. V. Hamza, A. V. Barnes, D. H. Schneider, J. C. Banks and B. L. Doyle

The interaction of slow ($v < v_{Bohr}$), highly charged ions (SHCI) with surfaces is an active field of research [1, 2] with applications in materials analysis [3] and modification [4-7]. Individual SHCI deposit tens to hundreds of keV of potential energy into a surface near volume. Charge state equilibration times are in the order of few femtoseconds [8]. Insulators and very thin (~10 nm) semimetallic conductors react to this massive local electronic excitation by emission of large numbers of neutral particles [5, 9] and secondary ions [1, 3]. For bulk semiconductors, no increase of ablation rates was observed for Si interacting with Ar^{q+}, $q \leq 9+$ [10]. Reports for GaAs are controversial. Using Ar^{q+}, $q \leq 9+$, Varga et al. [5] found no increase of the sputtering yield with charge. The null result was interpreted in the context of a model of defect mediated potential sputtering. For the same projectiles, Mochiji et al. [7] did observe a charge dependent sputter yield increase and results were interpreted using a Coulomb explosion model [11]. The ionization probability for secondary ions was not determined in either of these two studies. In this letter we report on measurements of charge state dependencies of total sputtering and secondary ion yields from GaAs interacting with slow, very highly charged ions up to Th^{70+}.

Highly charged ions were extracted from the Electron Beam Ion Trap (EBIT) at Lawrence Livermore National Laboratory [1]. The experimental setup has previously been described [1, 3]. Undoped GaAs (100) targets were cleaned *in situ* by repeated cycles of low energy Xe-ion sputtering and annealing at ~600° K. Low energy electron diffraction was used to establish a protocol for sputter-cleaning and annealing. Surface conditions were monitored by highly charged ion based time-of-flight secondary ion mass spectrometry (TOF-SIMS) [3]. The pressure in the target chamber was kept below 10^{-9} torr. Samples were cleaned and annealed before each exposure with SHCI. We used the catcher target technique for measurements of total ablation rates [13]. SHCI impinged on the GaAs targets with an incident angle of 30°. Silicon dioxide catchers were placed in parallel to the sputter target at a distance of 6 mm and secondary neutrals and ions emitted from the target during exposure to SHCI were collected on the catcher. SHCI fluxes ranged from ~10^5 Th^{70+}/s to 3.5×10^6 Xe^{27+}/s. The MCP used for direct detection of HCIs was calibrated by single ion counting in a Daly detector arrangement. The strong burst of secondary electrons emitted by individual HCIs ($q \geq 27$) incident on solid targets allows for their detection with 100% efficiency [3]. The efficiency of the MCP for direct detection of HCIs at the bias and discriminator settings used in this study was 0.52 +/-0.02. Doses of 2×10^{10} (Th^{70+}) and 3×10^{11} (Xe^{27+}) were accumulated over several days. Coverages of ~10^{11}-10^{12} Ga and As atoms per cm^2 on catchers were determined quantitatively by heavy ion backscattering (HIBS) at Sandia National Laboratory [15]. Ablation rates were calculated from surface coverages of Ga and As on the catchers, the ion dose, view factor and sticking probability of Ga and As atoms on the catcher surface. Secondary ion yields were measured by TOF-SIMS [3].

Total ablation rates are shown in Fig. 1 as a function of projectile charge state, q. Projectiles were Xe^{27+}, Xe^{44+}, Th^{56+} and Th^{70+} with impact velocities of $0.3 \times v_{Bohr}$. The shown relative errors in total yield data are dominated by uncertainties in HIBS results obtained at low surface coverages. Absolute uncertainties, including uncertainties in sticking probabilities and the view factor, are estimated to be +/-75%. The data at q=1+ give estimates of collisional sputter yields of GaAs for singly charged xenon and thorium projectiles as calculated by the TRIM code [16]. The sputtering yield increases from the collisional limit of ~12 atoms/Th^{1+} to 1410 +/- 210 atoms/Th^{70+}. This total yield is, to our knowledge, the highest sputtering yield observed so far for any bulk non-insulator.

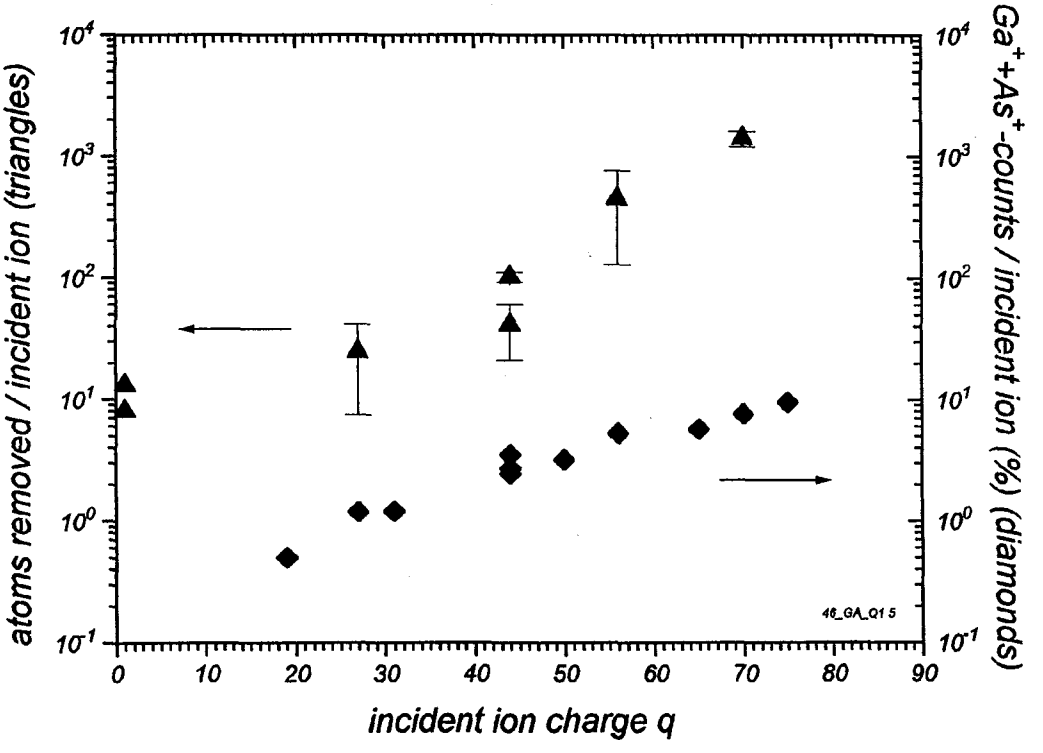

Fig. 1.: Total sputtering yields (triangles) and positive secondary ion yields (diamonds) from GaAs (100) as a function of projectile charge state, q.

Fig. 1 also shows the dependency of secondary ion yields on q. The reported values are the number of positive secondary ions detected per incident ion. Projectiles were Xe^{19+} ($v=0.18\ v_{Bohr}$), Xe^{27+} ($v=0.29\ v_{Bohr}$), Xe^{31+} ($v=0.23\ v_{Bohr}$), Xe^{44+} ($v=0.28\ v_{Bohr}$), Xe^{50+} ($v=0.3\ v_{Bohr}$), Th^{56+} ($v=0.28\ v_{Bohr}$), Th^{65+} ($v=0.26\ v_{Bohr}$), Th^{70+} ($v=0.27\ v_{Bohr}$) and Th^{75+} ($v=0.28\ v_{Bohr}$). The detection efficiency of the time-of-flight spectrometer with annular microchannel plate detector, η, of ~0.1-0.15 is not included. The error in secondary ion yields is typically <10%. Spectra were dominated by Ga^+-ions and small amounts of As^+ [17]. Positive secondary ion yields increase as a function of q, but the increase is much weaker than for total yields. The number of secondary ions detected per projectile is orders of magnitude smaller than previously observed for oxide targets [3]. No significant amounts of secondary cluster ions were detected from GaAs, contrary to

results from SiO_2 [3, 18] and UO_2. Positive secondary ion yields exhibited no prominent dependency on the kinetic energy of projectiles. Yields varied by less than 6% when changing the kinetic energy of Th^{70+}-ions between 196 keV ($v=0.18\ v_{Bohr}$) and 525 KeV ($v=0.3\ v_{Bohr}$).

A model of sputtering induced by SHCI has to describe mechanisms for the conversion of projectile potential energy into kinetic energy of ablated material. One such model is the defect mediated sputtering model [5]. Localized defects (self trapped excitons, STE) are formed in response to valence band excitations in some special materials such as alkali halides and SiO_2. Sputtering of mostly neutral atoms follows the diffusion of defects to the surface. The absence of a charge state dependent increase of sputtering yields as a function of ion charge in materials were no STE are known to be formed, like GaAs (100) [12, 19] and MgO, was used as strong evidence for the validity of this model. Our results show that the defect mediated sputtering model describes only one aspect of sputtering by SHCI.

A complementary sputtering model is the Coulomb explosion model [11, 20]. Electron emission in the course of the relaxation of SHCI is thought to form a highly ionized charge domain in insulators and poor conductors. If charge neutrality can not be re-established by target electrons on the time scale of lattice vibrations , ~0.5-1 ps, then electrostatic repulsion of ionized target atoms will force the rapid expansion of material in the charge domain. The emitted material will consist of ions and neutrals. A fraction of the initially ionized material will be neutralized by target electrons. Total sputtering yields are expected to increase with the charge or, respectively, the potential energy of projectiles. Also, the fraction of positive secondary ions is predicted to increase with q [11]. The rapid target expansion in a Coulomb explosion can cause the formation of a shock wave. Large clusters, charged and neutral, are emitted from an area of low electronic excitation when the shock wave intersects the target surface. An increase of both total sputtering yields and the ionization probability with q, as well as high yields of positive secondary ions and charged clusters are observations consistent with this Coulomb explosion model for the interaction of SHCI with oxides such as UO_2 and SiO_2 [3, 9, 18]. For GaAs however, the ionization probability decreases with q and yields of charged clusters are $<10^{-3}$ counts per Th^{70+}, showing no evidence for the presence of shock waves. We conclude that neither defect mediated sputtering models nor the Coulomb explosion model apply for describing ablation mechanisms of semiconductors interacting with SHCI.

A third model considers the structural stability of covalent solids under conditions of intense electronic excitation [21]. Evidence for structural instabilities induced by femtosecond laser pulses was recently presented for GaAs (100) [22]. Structural instabilities are non-thermal and arise directly from destabilization of atomic bonds by high density electronic excitations. Non-thermal structural changes are induced in covalent solids, when ~10% of valence electrons are promoted from bonding states in the valence band to anti-bonding states in the conduction band. Each electron-hole excitation causes a repulsive force between atoms. In GaAs, the resulting pressure is predicted to displace atoms by ~0.1 nm within only ~200 fs [21]. In contrast, heat exchange to the lattice requires many ps. A critical laser fluence to induce such a phase transition in GaAs is ~0.8 kJ/m^2 [22] or ~5 KeV/nm^2. Potential energies of SHCI used in this study range from 10

keV (Xe^{27+}), 51.3 keV (Xe^{44+}) and 67.8 keV (Th^{56+}) to 152.6 keV (Th^{70+}), nominally exceeding this critical fluence greatly.

The authors gratefully acknowledge the excellent technical support at the LLNL EBIT facility provided by D. Nelson and K. Visbeck.

References:

[1] D. H. Schneider, M. A. Briere, Phys. Scr. **53**, 228 (1996)
[2] A. Arnau et al., Surf. Sci. Rep. **229,** 1(1997)
[3] T. Schenkel, A. V. Barnes, M. A. Briere, A. V. Hamza, A. Schach von Wittenau, D, H. Schneider, Nucl. Instrum. and Methods Phys. Res., Sect. B **125,** 153 (1997); ibid., Materials Science Forum **248-249,** 413 (1997)
[4] D. Schneider, et al., Surf. Sci., **294** 403 (1993); D. C. Parks, M. P. Stockli, E. W. Bell, L. P. Ratkliff, R. W. Schmieder, F. G. Serpa, J. D. Gillaspy, Nucl. Instrum. and Methods Phys. Res., Sect. B **134,** 46 (1998)
[5] M. Sporn, G. Libiseller, T. Neidhard, M. Schmid, F. Aumayr, HP. Winter, P. Varga, M. Grether, D. Niemann, N. Stolterfoht, Phys. Rev. Lett. **79,** 945 (1997); P. Varga, et al., Phys. Scr. **T73,** 307 (1997)
[6] K. Suzuki, N. Itabashi, Pure and Appl. Chem. **68**, 1011 (1996)
[7] K. Mochiji, N. Itabashi, S. Yamamoto, H. Shimizu, S. Ohtani, Y. Kato, H. Tanuma, K. Okuno, N. Kobayashi, Surf. Sci. **357-358**, 673 (1996); ibid, Jpn. J. Appl. Phys. **34**, 6861 (1995)
[8] T. Schenkel, M. A. Briere, A. V. Barnes, A. V. Hamza, K. Bethge, H. Schmidt-Böcking, D. Schneider, Phys. Rev. Lett. **79,** 2030 (1997); ibid., Phys. Rev. Lett. **78,** 2481 (1997)
[10] S. T. de Zwart, T. Fried, D. O. Boerma, R. Hoekstra, A. G. Drentje, A. L. Boers, Surf. Sci. **177,** L939 (1986)
[11] I. S. Bitensky, E. S. Parilis, J. Phys., **50 C2,** 227 (1989); I. S. Bitensky, E. Parilis, S. Della-Negra, Y. Le Beyee, Nucl. Instrum. and Methods Phys. Res., Sect. B **72,** 380 (1992)
[13] H. H. Anderson, H. L. Bay, in R. Behrisch (ed.) *Sputtering by Particle Bombardment I* (Springer, Berlin, 1981), p. 159
[15] J. A. Knapp, D. K. Brice, J. C. Banks, Nucl. Instrum. and Methods Phys. Res., Sect. B **108,** 324 (1996)
[16] J. P. Biersack, Nucl. Instr. and Meth. Phys. Res., Sect. B **27**, 21 (1987)
[17] R. Matthäus, R. Moshammer, G. v. Hayn, K. Wien, S. Della-Negra, Y. Le Beyec, Int. J. Mass Spectr. and Ion Proc. **126**, 45 (1993)
[18] T. Schenkel, A. V. Barnes, A. V. Hamza, D. Schneider, European Physical Journal, D, in press; T. Schenkel, Ph. D. thesis, Goethe Universität, Frankfurt/M, 1997
[19] O. Pankratov, M. Scheffler, Phys. Rev. Lett. **75**, 701 (1995)
[20] H. P. Cheng, J. D. Gillaspy, Phys. Rev. B **55**, 2628 (1997)
[21] P. Stampfli, Nucl. Instr. and Meth. Phys. Res., Sect. B **107**, 138 (1996); P. Stampfli, K. H. Bennemann, Appl. Phys. A **60**, 191 (1996)
[22] L. Huang, J. P. Callan, E. N. Glezer, E. Mazur, Phys. Rev. Lett. **80**, 185 (1998)

Analysis of B-SiO_2 films by highly charged ion based time-of-flight secondary ion mass spectrometry, standard SIMS and elastic recoil detection

T. Schenkel, A. V. Hamza, A. V. Barnes , D. H. Schneider, D. S. Walsh and B. L. Doyle

Quantitative analysis of surfaces and thin films is a crucial problem in materials research. Quantitative accuracy, sensitivity and depth resolution of secondary ion mass spectrometry (SIMS) have been optimized continuously over the last decades. In dynamic SIMS, limits in quantitative accuracy due to changing secondary ion production probabilities as a function of chemical environment ("matrix effects") have been addressed by preparation of constant ionization environments, e. g. through use of oxygen ion beams and flooding of samples with oxygen during depth profiling [1, 2]. It has been shown that monitoring of MCs^+ molecular ions during Cs^+ bombardment is largely unaffected by changing matrixes [3]. Use of lasers for resonant [4] or non-resonant [5] post-ionization of secondary neutrals marks another route to quantitative compositional analysis. Useful yields, i. e. the number of secondary ions detected per sputtered target atom, are typically in the order of 10^{-2} [4, 6, 7] and can be as low as 10^{-6}. Accurate quantification often has to rely on the use of calibration standards or make use of cross-calibration with independent analytical techniques [8].

Recently, strong electronic sputtering effects were reported for impact of slow (~1 keV/u) highly charged ions, like Xe^{44+} and Au^{69+}, on thin insulating films and semi-metallic foils [9, 10]. Atomic and molecular secondary ion yields were found to be increased by over two orders of magnitude for highly charged as compared to singly charged ions at the same kinetic energy [9]. In the case of Au^{69+} on B-SiO_2 (50 nm on Si), at average more than 3 secondary ions were detected per incident highly charged ion. In this article we report on the first application of highly charged ion induced electronic sputtering for quantitative materials analysis.

Highly charged ions were extracted from the LLNL Electron Beam Ion Trap (EBIT) [11]. The setup for highly charged ion based time-of-flight secondary ion mass spectrometry (TOF-SIMS) has previously been described in detail [9]. In short, secondary electrons or protons, emitted at impact of individual ions, are used to start time-of-flight cycles. Start efficiencies were 100% for electron starts and typically >50% for proton starts. Negative or positive secondary ions are detected in a micro channelplate detector and are accepted as stops in a multi-stop time analyzer [ORTEC 9308]. Secondary ions are accelerated by a target bias of +/- 3 kV. The flight path has a length of only 10 cm. The resulting mass resolution was limited to $m/\Delta m=100$. Targets consisted of 50 nm thick B-SiO_2 films deposited on silicon substrates by standard plasma enhanced chemical vapor deposition (PE-CVD). For depth profiling, targets were eroded by conventional low energy ion sputtering (3 keV Ar^{1+}, at normal impact, rastered over 1 cm^2) and highly charged ions were used to analyze targets after subsequent sputtering cycles. Sputter depths were calculated from the Ar-sputter ion dose using literature values for sputter yields [12]. Resulting depth scales were consistent with determinations of the point of

interface crossing to the Si substrate by monitoring of characteristic molecular ions, like SiO_3^-. At the highly charged ion beam intensities of 10^3 - 10^4 ions per second that were used for TOF-SIMS, this corresponds to static conditions where only insignificant amounts of target material are removed.

B-SiO_2 targets were analyzed by elastic recoil detection (ERD) [13] at Sandia National Laboratory using a beam of 24 MeV Si^{5+} in order to independently determine the absolute boron concentrations. A CAMECA 4f magnetic sector instrument was used for standard SIMS measurements. Primary ions were O^- at an effective kinetic energy of 17 keV. The angle of incidence was ~25°. The beam spot diameter was ~20 μm, rastered over an area of ~100 μm × 100 μm.

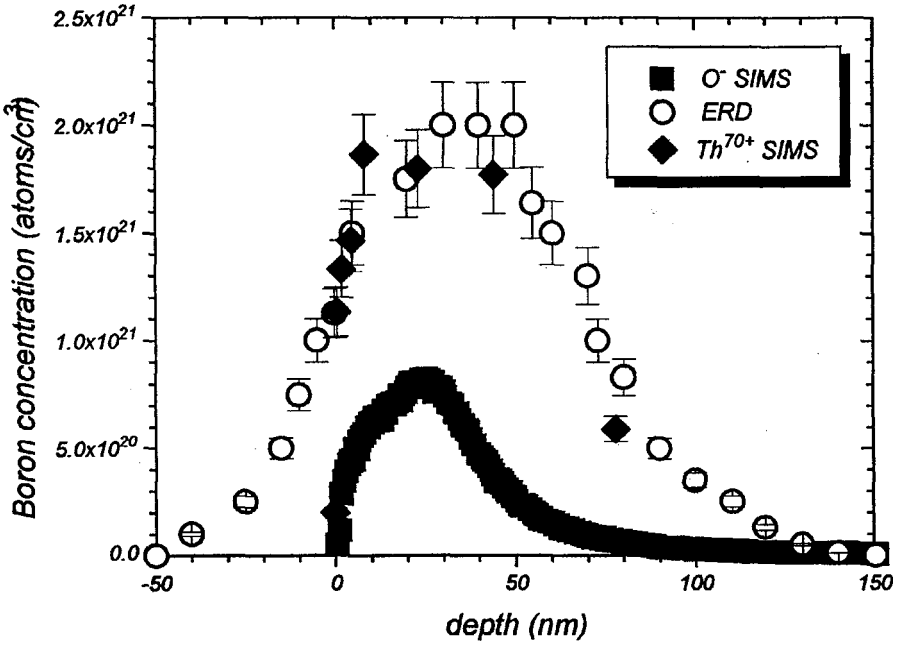

Fig. 1: Boron concentration in the B-SiO_2/Si films as determined by highly charged ion based TOF-SIMS (◆), elastic recoil detection (○) and standard SIMS (■).

Fig. 1 shows resulting boron depth profiles from highly charged ion based TOF-SIMS, ERD and standard SIMS. The peak concentration of boron in the films as determined by ERD was 2×10^{21} atoms/cm^3. Probe beams for highly charged ion based TOF-SIMS were Xe^{44+} (first two data points) and Th^{70+} at kinetic energies of 1.3 and 1.2 keV/u, respectively, and at normal incidence. The probe beam was switched in order to take advantage of increased secondary ion yields as a function of primary ion charge [9]. For determination of boron concentrations from positive secondary ion spectra, the number of counts in the $^{11}B^+$ and $^{10}B^+$ peak areas was divided by the integrated positive secondary ion counts from the matrix after background subtraction. The average fractional boron content in the broad maximum of the distribution was 2.8 at. %. At a given atomic density of the SiO_2 matrix of $\sim6.6\times10^{22}$ atoms/cm^3 we find that results from ERD (fractional boron content: at. 3 %) and TOF-SIMS (boron concentration: 1.8×10^{21}

atoms/cm^3) agree within the uncertainty of the measurements of +/-10%. In standard SIMS, $^{11}B^+$ and $^{30}Si^+$ ions were recorded as a function of sputtering time. Boron concentrations were calculated directly from measured $^{11}B^+$ to $^{30}Si^+$ count ratios without correction for different ionization probabilities of boron and silicon and assuming an atomic density of the SiO_2 matrix of 6.6×10^{22} atoms/cm^3. The value of the boron peak concentration was thus determined to be only 0.8×10^{21} atoms/cm^3. Standard SIMS underestimates the true concentration by over a factor of ~2.5. Quantitatively accurate concentrations can be derived from standard SIMS data using calibrated standards or cross calibration with independent analytical techniques [8].

Slow, highly charged ions impose conditions of extreme target ionization upon impact on a nanometer sized surface area. Over one hundred electrons are emitted from thin SiO_2 films at impact of individual Th^{70+} [9]. The target lattice reacts to the intense Coulomb stress by emission of high amounts of charged [9] and neutral [14] secondary particles. Positive secondary ion spectra are dominated by singly positively charged atomic ions [9]. We interpret the good agreement of boron concentration measurements by ERD and highly charged in based TOF-SIMS as resulting from strong de-coupling of positive secondary ion production probabilities from elemental ionization potentials under conditions of electronic sputtering induced by highly charged ions [15]. In standard SIMS, production of atomic secondary ions is dominated by elemental ionization potentials, P^+, and the chemical environment of the matrix. Ionization probabilities have been quantified in studies of relative sensitivity factors (RSF) [15]. Ionization potentials of Si (8.15 eV) and B (8.23 eV) are very similar and the RSF for boron in a silicon or SiO_2 matrix under oxygen bombardment has been found to be 6.5×10^{22} (cm^{-3}), indicating that detection of positive secondary ions allows for accurate determination of actual concentrations of boron in these matrixes. RSF factors are determined by use of implantation standards with impurity concentrations typically much lower than the atomic percent range present in the samples used in this study. Our results show that RSF factors in standard SIMS are affected by very high impurity concentrations, where the influence of the impurity on the chemical structure of the matrix is not negligible as it is for fractional impurity concentrations <0.1 %. From our measurements the RSF for the detection of boron in SiO_2 at concentrations in the atomic percent range follows to be 1.6×10^{23} (cm^{-3}) for SIMS using O^- primary ions. For highly charged ion based SIMS the RSF is 6.6×10^{22} (cm^{-3}).

Accurate quantitative analysis of near surface dopant concentrations in the atomic percent range is of significant technological relevance as these distributions are present in the low energy (<5 keV) implants used for ultra shallow junction formation.

The matrix stoichiometry of the B-SiO_2 films was confirmed to be 2:1 by Rutherford Backscattering. This ratio was not reproduced in the ratio of oxygen to silicon positive secondary ion yields in highly charged ion based SIMS, which was found to be only 0.8 (+/- 0.05). We note that the comparably large difference in ionization potentials between oxygen (13.6 eV) and silicon results in secondary ion yield variations by several orders of magnitude under standard SIMS conditions [16]. The deviation in oxygen and silicon ion yields from the true stoichiometry can be attributed in part to secondary ion formation at the fringe of the highly charged ion impact area, where the ionization density

is gradually decreasing and the influence of ionization potentials begins to dominate ionization probabilities.

Both positive and negative secondary ion yields were found to decrease strongly with decreasing oxide thickness after consecutive Ar-sputtering cycles (Fig. 2). This effect is in accordance with ion yield measurements from silicon oxides of different thicknesses [14, 18]. Electron transport from the silicon substrate to the highly ionized surface region can quench a fraction of the Coulomb stress and reduce the magnitude of secondary particle emission in electronic sputtering events. A fit to an exponential dependency on oxide thickness, Δx, yields an estimate of a materials parameter β (nm^{-1}):

(1) $$Y^{+/-} = Y_0 \exp(-\beta \cdot \Delta x) + Y_{Si}$$

($Y^{+/-}$, positive or negative secondary ion yield; Y_0, ion yield from thick oxide; Y_{Si}, ion yield from silicon substrate). β reflects the quenching of the induced Coulomb stress at the surface by substrate electrons. Values are found to be larger for negative cluster ions ($\beta_- \approx 0.2\ nm^{-1}$) then for positive atomic ions ($\beta_+ \approx 0.08\ nm^{-1}$). This observation indicates different quenching characteristics of primary and secondary (i. e. shock waves [8, 14]) Coulomb explosion effects, the detailed understanding of which is subject of ongoing studies.

We thank Dr. D. L. Phinney (LLNL) for the performance of the standard SIMS measurements.

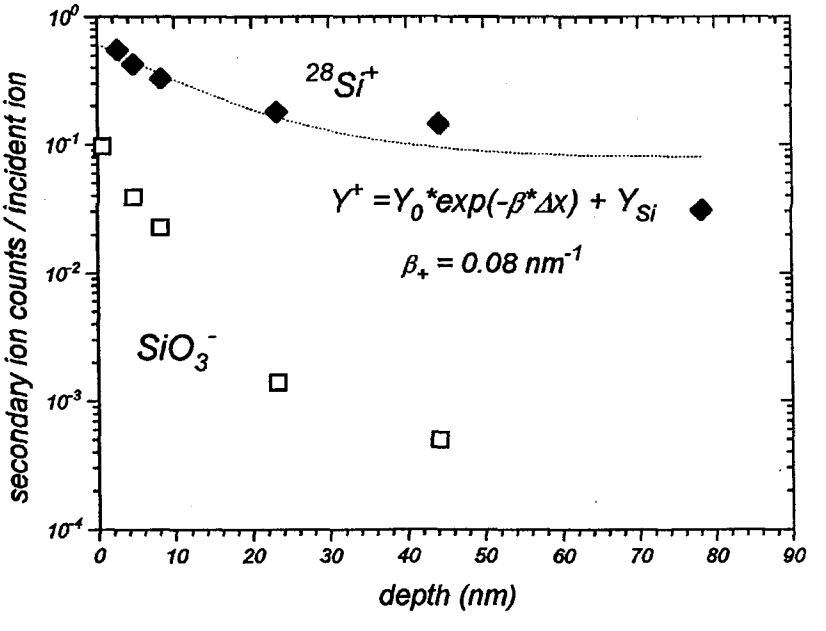

Fig. 2: SiO_3^- (❑) and $^{28}Si^+$ (◆) yields from a B-SiO_2/Si film as a function of sample depth. The fit is a least square fit to an exponential dependency of the $^{28}Si^+$-yield on oxide thickness. The initial oxide thickness, as determined by RBS, was 50 nm.

References:

[1] K. Wittmaack in *Inelastic Ion Solid Collisions*, N. H. Tolk, J. C. Tully, W. Heiland, C. W. White (eds.) (Academic Press, N. Y. 1977), P. 153

[2] for a recent discussion see L. A. Heimbrook, F. A. Baiocchi, T. C. Bitter, M. Geva, H. S. Luftman, S. Nalahara, J. Vac. Sci. Technol. B **14** 202 (1996); J. W. Erickson, R. Brigham, ibid., 353

[3] M. Haag, H. Gnaser, H. Oechsner, Fresenius J. Anal. Chemistry **353** 565 (1995)

[4] H. F. Arlinghaus, C. F. Joyner, J. Vac. Sc. Technol. B **14** 294 (1996)

[5] C. He, J. N. Basler, C. H. Becker, Nature **385** 797 (1997)

[6] J. L. Hunter, S. F. Corcoran, J. Vac. Sc. Technol. A**8** 2323 (1990)

[7] A. Schnieders, R. Möllers, M. Terhorst, H.-G. Cramer, E. Niehuis, A. Benninghoven, J. Vac. Sc. Technol. B **14** 2712 (1996)

[8] see for example: P. K. Chu, S. L. Grube, Anal. Chem. **57**, 1071 (1985)

[9] T. Schenkel, M. A. Briere, H. Schmidt-Böcking, K. Bethge, D. Schneider, Phys. Rev. Lett. **78** (1997) 2481; T. Schenkel, A. V. Barnes, M. A. Briere, A. Hamza, A. Schach von Wittenau, D. H. Schneider, Nucl. Instr. and Meth. B **125** 153 (1997); T. Schenkel, M. A. Briere, A. Schach von Wittenau, D. Schneider, Proceedings of the 43rd ASMS Conference, May 1995, Atlanta, P. 1336; T. Schenkel, M. A. Briere, H. Schmidt-Böcking, K. Bethge, D. Schneider, Materials Science Forum Vols. **248-249** (1997) 413

[10] D. H. Schneider, M. A. Briere, Physica Scripta **53** (1996) 228; G. Schiwietz, M. Briere, D. Schneider, J. McDonald, C. Cunningham, Nucl. Instr. and Meth. B **100** (1995) 47

[11] D. Schneider, et al., Phys. Rev. **A 42** (1990) 3889

[12] Y. Yamamura, H. Tawara, At. Data and Nucl. Data Tables **62** (1996) 149; G. Betz, G. K. Wehner in *Sputtering by Particle Bombardment II*, R. Behrisch (ed.) (Springer, Berlin, 1983), P. 11

[13] J. A. Knapp, J. C. Barbour, B. L. Doyle, J. Vac. Sc. Technol. A **10** (1992) 2685

[14] M, Sporn, G. Libiseller, T. Neidhart, M. Schmid, F. Aumayr, HP. Winter, P. Varga, M. Grether, D. Niemann, N. Stolterfoht, Phys. Rev. Lett. **79** 945 (1997); T. Schenkel, et al., to be published

[15] T. Schenkel, Ph. D. thesis, J. W. Goethe Universität, Frankfurt, Germany, 1997

[16] S. W. Novak, R. G. Wilson, J. Appl. Phys. **69** (1991) 463; ibid., 466

[17] I. S. Bitensky, E. S. Parilis, Nucl. Instr. and Meth. B **21** 26 (1987); R. E. Johnson, B. U. R. Sundqvist, A. Hedin, D. Fenyö, Phys. Rev. B **40** 49 (1989)

[18] M. A. Briere, T. Schenkel, D. H. Schneider, EBIT Annual report 1994, LLNL, UCRL-ID-121572, P. 38, unpublished

Secondary Ion Coincidence in Highly Charged Ion Based Secondary Ion Mass Spectroscopy for Process Characterization

Alex V. Hamza, Thomas Schenkel, Alan V. Barnes, and Dieter H. Schneider

In their pioneering work Schweikert and co-workers [1] demonstrated the use of coincidence counting in time-of-flight mass spectrometry. Time-of-flight is itself a coincidence counting technique where secondary ion stops are detected in coincidence with some start signal. In their work, Schweikert and co-workers added an additional coincidence requirement to the time-of-flight, the requirement that a particular secondary ion be present. In order for this second coincident requirement to provide any additional information, the secondary ion yield per primary event must be order one or greater, so that for a single start it is possible to detect secondary ions in coincidence with the required secondary ion. In addition the primary particles should address only a small region of the sample surface so that sample components can be spatially distinguished from one another.

Schweikert and co-workers used ^{252}Cf fission fragments as a primary source. The fission fragments have mass in the range of 95 to160 amu with kinetic energies of 60-120 MeV and charge states of 18-22+. The fission fragments excited a surface area of approximately 10-20 nm. The mass, energy and charge of the primary ions can not be controlled in the fission fragment case. Riggi has demonstrated the coincidence counting technique for fast heavy ion primary beams [2] where the mass and velocity can be varied. In the present work, we have used a beam of slow, highly charged ions extracted form an electron beam ion trap, where the charge, energy and mass of the primary beam can be varied independently.

The interaction of slow, highly charged ions with surfaces results in the emission of a large number of secondary ions per primary ion which increases with the charge of the incident ion [3]. For example, Au^{69+} impinging on 50nm thick SiO_2 layer on a Si wafer induces a positive secondary ion yield per primary ion of 20 [3]. The surface area addressed by each highly charged ion can be estimated from the size of blister observed for single ion impacts on mica surfaces [4]. The diameter of the blisters increases from 10 nm to 40 nm with incident charge from 35+ to 70+. Thus, highly charged ion excitation is very well suited to coincidence time-of-flight secondary ion mass spectrometry.

Highly charged ions were extracted from the electron beam ion trap (EBIT) at Lawrence Livemore National Laboratory [5]. A bending magnet in the beamline between the EBIT and the UHV scattering chamber (base pressure $<3x10^{-8}$ Pa) is used to select the mass-to-charge ratio of the incident ion beam. Time-of-flight secondary ion mass spectrometry (TOF-SIMS) was performed to measure secondary yields. The system is described in references [6] and [3]. Briefly, fluxes of <1000 ions per second were used and each TOF-SIMS cycle was triggered by secondary particles emitted from the target at impact of an individual HCI under normal incidence. Typical accumulation times for TOF-SIMS spectra are ~10 minutes. The flight path for secondary ions is ~10 cm from the surface to the annular detector. High yields of electrons and protons were used as start pulses for the time-of-flight for negative and positive secondary ions, respectively.

Start efficiencies were 100% for electron starts and between10 and 80% for proton starts. Start signals and secondary ion stop signals were detected by the same annular microchannel plate detector. The microchannel plate detection efficiency for secondary ions is estimated from the solid angle subtended and the active area to be ~10 to 15%. TOF-SIMS spectra are recorded with a multi-stop multichannel scaler (Ortec picosecond timing analyzer, model 9308). For coincidence measurements the events are collected in list mode, i.e. the time of each start and its associated stops are recorded in a list. The data is then filtered for particular coincidence ions. A event, a start pulse and its associated stop pulses, is accepted if the coincidence ion is present, i. e. a stop pulse is detected in a particular time window, and otherwise the event is discarded.

The sample was a patterned, thermally grown SiO_2/Si test wafer that was placed in a plasma chemical vapor deposition reactor for selective tungsten deposition. The SiO_2 layer is one micron thick. 1, 2 and 5 μm diameter via holes as well as 5-200 μm wide lines and other structures were present on the test wafer. Just prior to deposition the wafers were dipped in diluted 100:1 HF to eliminate the native oxide. Selective tungsten deposition occurred via the reaction of WF_6 with Si_2H_6 at wafer temperature of 150 C according to the procedure reported in reference [7]. ~ 150 to 400 nm of α-tungsten was deposited. After deposition and cooling to room temperature the wafer was removed from the plasma reactor. The wafer was stored in air many months before being placed to the UHV scattering chamber. No *in-situ* cleaning of the sample was performed.

Figure 1 shows a portion of the positive time-of-flight secondary ion mass spectrum for a Th^{75+} primary beam with 262.5 keV kinetic energy. Summing all of the collected events gives the spectrum labeled "full spectrum." Coincidence mass spectra selecting only events which have the secondary ion SiO^+ or WO^+, respectively, are also shown. The tungsten surface had become oxidized from months of storage in air; the most probably observed tungsten features were WO_x^+ secondary ions. As can been seen the Si_2O_x series is highly correlated to the SiO^+ secondary ion and the Si_2F_x series is highly correlated to the WO^+ secondary ion. The degree of correlation can be quantitatively determined from

$$Q(A^+, B^+) = P(A^+, B^+)/ [P(A^+)P(B^+)] \qquad (1)$$

where $P(A^+)$ is the probability of observing a given secondary ion, A^+, and $P(A^+,B^+)$ is the probability of observing B^+ in coincidence with A^+ [1]. Experimentally, the probability of observing a given secondary ion is defined by the number of counts in the secondary ion peak divided by the number of primary ions striking the sample (or the number of start pulses). If Q equals 1 the ions are independent of one another. If Q is greater than 1 the ions are correlated; the emission of one ion occurs with the emission of the other. If Q is less than 1 the ions are anticorrelated; the emission of one ion precludes the emission of the other. For example the $Q(WO^+, Si_2F^+) = 1.86$ or the Si_2F^+ secondary ion is emitted with the WO^+ secondary ion. In contrast $Q(SiO^+, Si_2F^+) = 0.77$ or the emission of SiO^+, precludes the emission of Si_2F^+. Thus, it is 2.4 times more likely that the Si_2F^+ secondary ion feature came from within 40 nm of the deposited tungsten than from within 40 nm of the silicon dioxide area of the wafer. Similarly the correlation of the Si_2O^+ secondary ion can be addressed. $Q(SiO^+, Si_2O^+) = 1.98$ and $Q(WO^+, Si_2O^+) = 0.29$; it is 6.8 times more

likely that the Si_2O^+ secondary ion feature came from within 40 nm of the silicon dioxide area of the wafer than the deposited tungsten. Given that the tungsten is deposited from the reduction of WF_6 with disilane, the Si_2F_x secondary ion impurity series is a byproduct of the reduction that deposits with the tungsten.

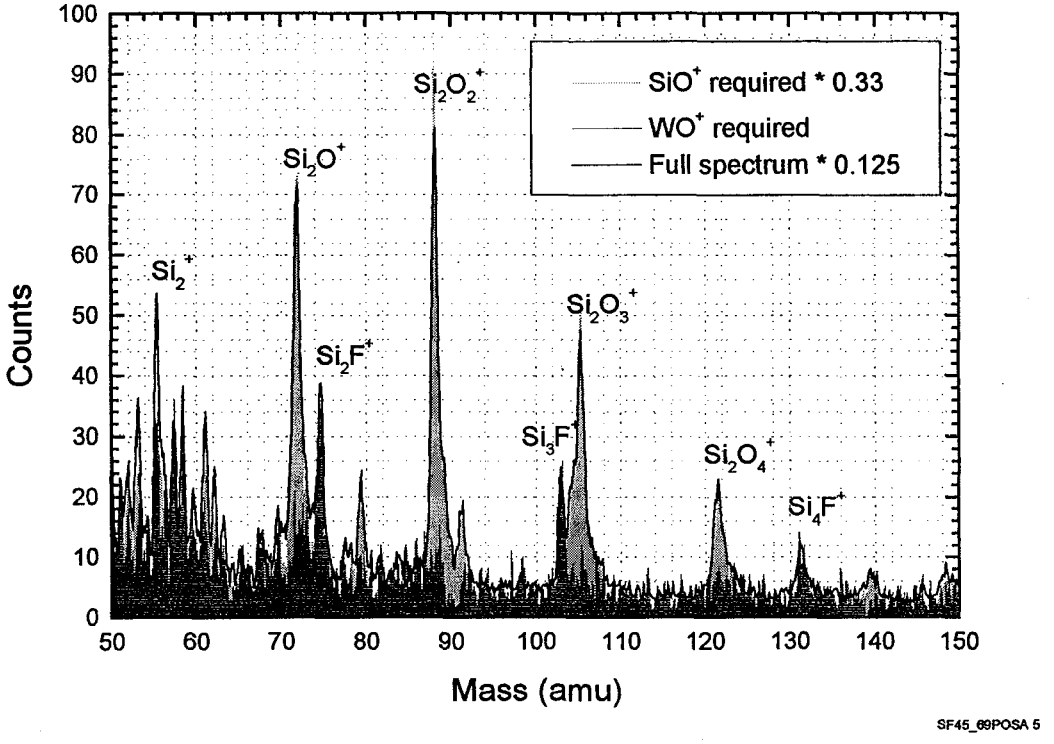

Figure 1. Coincidence counting time-of-flight positive secondary ion mass spectrum from $W/SiO_2/Si$ test wafer with a Th^{75+} primary beam with 262.5 keV incident energy. The black line is the full spectrum divided by 8. The SiO^+ coincidence spectrum divided by 3 is shown in light gray and the WO^+ coincidence spectrum is shown in gray. The spectra are scaled based on the relative number of events used to build each spectrum.

The coincidence counting technique shows the Si_2F_x impurity is localized on the deposited tungsten regions and can be assigned as a result of the WF_6 reduction step in the processing. In this example the tungsten features were rather large (greater than or equal to a micron) and other techniques could have been applied to determine the location of the Si_2F_x impurity, i.e. focused ion beam secondary ion mass spectrometry or scanning Auger electron microscopy. However, as the feature sizes get smaller the number of impurity atoms or molecules analyzed in the focus area of the ion beam becomes vanishing small. The coincidence technique can analyze many similar features simultaneously, thus, removing the restrictions due the number of impurities in one small feature. In addition the highly charged ion primary beam gives a higher ionization probability [8] and hence a higher useful yield, particularly for molecular species, for sensitive analysis of small features.

References

[1] M. A. Park, K. A. Gibson, L. Quinones, E. A. Schweikert, Science **248**, 988 (1990).
[2] F. Riggi, Nuclear Instruments and Methods in Physics Research **B 79**, 230 (1993).
[3] T. Schenkel, A. V. Barnes, M. A. Briere, A. Hamza, A. Schach von Wittenau, and D. H. Schneider, Nuclear Instruments and Methods in Physics Research **B 125**, 153 (1997).
[4] C. Rühlicke, M. A. Briere, and D. Schneider, Nuclear Instruments and Methods in Physics Research **B 99**, 528 (1995).
[5] D. Schneider, M. W. Clark, B. M. Penetrante, J. McDonald, D. DeWitt, and J. N. Bardsley, Physical Review A 44, 3119 (1991).
[6] D. Schneider and M. A. Briere, Physica Scripta **35**, 228 (1996).
[7] T. Ohba, T. Suzuki, T. Hara, Y. Furumura, and K. Wada, in Tungsten and Other Refractory Metals of VLSI Applications IV, Editors R. S. Blewer and C. M. McConica (Materials Research Society, Pittsburgh, PA 1989) pp.17-26.
[8] T. Schenkel, A. V. Barnes, A. V. Hamza, D. H. Schneider J. C. Banks, and B. L. Doyle, to be published.
[9] T. Schenkel, A. V. Barnes, A. V. Hamza, and D. H. Schneider, European Physical Journal D, in press.

Dependence of Cluster Ion Emission from Uranium Oxide Surfaces on the Charge State of the Incident Slow Highly Charged Ion

Alex V. Hamza, Thomas Schenkel, Alan V. Barnes, and Dieter H. Schneider

Clusters emission phenomenon are of scientific and technological interest because of the potential for clusters to form materials with new chemical and physical properties. In addition, studies of the cluster yields due to surface excitation will lead and have led to a better understanding of the excitation mechanism and sputtering process.

The most easily accessible experimental information on the cluster formation process is the cluster partial yield or the cluster size distribution. Two methods of obtaining this distribution have been used extensively; measurement of the charged cluster distribution and post-ionization of the neutral clusters with either electrons or photons beams. The first method suffers from the fact that the probability of cluster ionization increases with cluster size[1,2]. The second method suffers from the unknown fragmentation probability of the clusters in the post-ionization step [1,3]. In the case of metal clusters a rather large difference in the cluster distribution has been reported depending on the method used [2]. In the case of non-metallic clusters the ionization probability is relatively constant with cluster size, particularly if the n=1 cluster is not considered. The ionization potential for van der Waals, Ar_n and Kr_n, clusters is independent of cluster size, n, from 2 to 24 [4]. Even for metal atoms, small clusters may not exhibit metallic properties. One example of this is Hg_n clusters, where for $3<n<13$ the ionization potential is approximately constant; this effect is ascribed to nonmetallic behavior of these mercury clusters [5]. Wucher et al. [2] have shown via comparison of neutral metal cluster yields measured by laser post-ionization and ionized metal cluster yields that the ionization probability for clusters greater than n=5 is fairly constant, though oscillation of ion stabilities are observed.

Measurements of cluster ion yields at short times (much less than 1 μs) do not exhibit oscillations [6]. Mass spectra at late time (greater than 1 μs) are influenced by relative cluster ion stabilities [6]. In the measurements presented here the cluster ions are in the intermediate time regime of ~1 μs. We do not observe any effects due to ion stabilities for uranium oxide clusters (see below). However, the smoothed, intermediate-time cluster ion distribution is representative of the early time distribution. Since ion production occurs at short times, cluster ion stability is unimportant in the ion production process. Thus, the distribution of ionized non-metallic clusters for cluster size n>1 gives a relatively faithful picture of the relative neutral cluster distribution. We, therefore, report the ionized uranium oxide cluster yield as representative of the neutral cluster uranium oxide yield.

From the results presented below and previous work [1, 7-9] it is observed that a power law cluster yield distribution according to

$$Y(n) \propto n^{-\tau} \qquad (1)$$

is a general phenomenon. The observed value of τ varies between 2 and 15 depending upon sputtering conditions such as the incident kinetic energy, projectile charge, and angle of incidence of the projectile and on the material properties of the target surface. Wucher and co-workers [2, 9] have proposed and demonstrated for the case of silver clusters that the value of τ is correlated to the total sputtering yield of the sample in such a way that when the total sputter yield increases the value of τ decreases.

Only two published models predict a power law cluster yield distribution. The first is a shock wave initiated process of Parilis and Bitensky [10]. The assumption is that momentum is transferred to near-surface target molecules due to the propagation of a pressure pulse or shock wave, resulting in the emission of large clusters. The predicted exponent for the power law is $\tau \sim 2$. However, the exponent, τ, is fixed by the physics of the model and can not explain the variation with total sputter yield.

The second model that predicts a power law cluster yield distribution is the model by Urbassek [urbassek] which is applicable to sputtering by both singly and highly charged ions. In this "equilibrium " model, a highly energized region of the surface undergoes a liquid-gas phase transition upon expanding into vacuum. If the phase transition happens near the critical point (where interparticle binding is just balanced by the kinetic energy), fluctuations are high enough to produce high yields of large clusters. In this model the clusters are assumed to be in equilibrium with each other and monoatomic species. The cluster yield depends on the energy deposited into the near-surface volume, since to reach the critical point the kinetic energy of the target atoms have to be high, so that chemical bonding loses its importance and the system becomes fluid. Slow, highly charged ions can deposit a large amount of potential energy (100-300 keV per ion) into a small nanometer sized volume on very short, femtosecond, time scales [11, 12]. The equilibrium model predicts transitions from a exponential decay to power law decay as the phase transition occurs closer to the critical point. The dependence of the cluster yield Y(n) on the cluster size, n, is

$$Y(n) = Y_0 n^{-\tau} \exp[(-\Delta G n - 4\pi n^{2/3} r^2 \sigma)/kT] \qquad (2)$$

where ΔG is the difference of the Gibbs free energies of the liquid and gas phase, k is Boltzmann's constant, T is the temperature of the energized region, Y_0 is the sputter yield (a constant for a given projectile-target system), r is the cluster radius, σ is the surface tension and τ is the critical exponent. At equilibrium ΔG is zero and at the critical point the surface tension vanishes. Thus, the power law exponent at the critical point is τ, with τ between 2 and 2.5. It follows that predicted cluster size distributions at the critical point are very similar for the equilibrium and shock wave models.

Highly charged ions were extracted from the electron beam ion trap (EBIT) at Lawrence Livemore National Laboratory [13]. A bending magnet in the beamline between the EBIT and the UHV scattering chamber (base pressure $<3\times10^{-8}$ Pa) is used to select the mass-to-charge ratio of the incident ion beam. Time-of-flight secondary ion mass spectrometry (TOF-SIMS) was performed to measure cluster yields. The system is described in references [14] and [15]. Briefly, fluxes of <1000 ions per second were used and each TOF-SIMS cycle was triggered by secondary particles emitted from the target at impact of an individual HCI under normal incidence. High yields of electrons and protons

were used as start pulses for the time-of-flight for negative and positive secondary ions, respectively. Start efficiencies were 100% for electron starts and between10 and 80% for proton starts. Start signals and secondary ion stop signals were detected by the same annular microchannel plate detector. The microchannel plate detection efficiency for secondary ions is estimated from the solid angle subtended and the active area to be ~10 to 15%. TOF-SIMS spectra are recorded with a multi-stop multichannel scaler.

Polycrystalline uranium (^{238}U) targets were prepared by electropolishing followed by oxidation in air for several hours for native oxide formation. The oxide thickness was estimated from known oxidation rates [16] to be several hundred nanometers. Targets were cleaned after insertion into vacuum by low energy ion sputtering. The pressure in the target chamber was kept below 5×10^{-10} torr. Surface conditions were monitored closely by TOF-SIMS. Secondary ion spectra were reproducible over several sputter cleaning cycles.

The cluster ion yields and cluster ion distribution for highly charged ion sputtering have been measured for a uranium oxide target for Xe^{44+}, $Au^{63,66,69+}$ and Th^{75+} incident ions. A representative secondary ion mass spectra for Au^{69+} impinging on $^{238}UO_2$ is shown in figure 1.

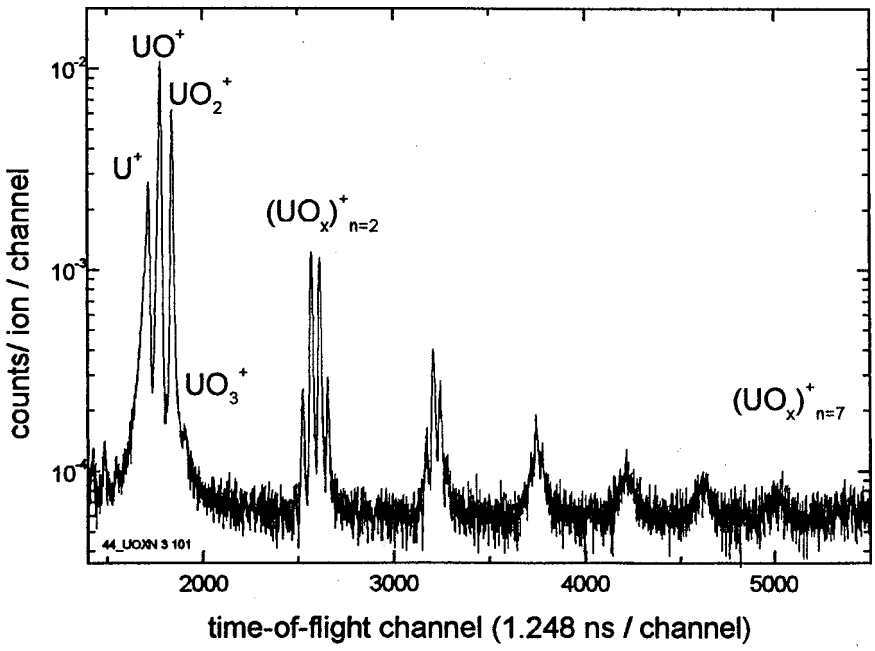

Figure 1. Highly charged ion based secondary ion mass spectrum from Au^{69+} impinging on $^{238}UO_2$. Uranium oxide clusters $(UO_x)_n$ are observed to n=7 in this example. A plot of the cluster yield (secondary cluster ions per primary ion) as a function of cluster size (n) is shown in figure 2 for Th^{75+} primary ions. The cluster partial yield exhibited a power law dependence on the cluster size with an exponent of -2.7. The cluster partial yields exhibited a power law dependence on the cluster size with exponents increasing from -4 to -2.4 with increasing primary ion charge from 44+ to 75+. Since the total sputter yield

increases with as the charge of the incident ion increases, it is instructive to plot the power law exponent versus total sputter yield.

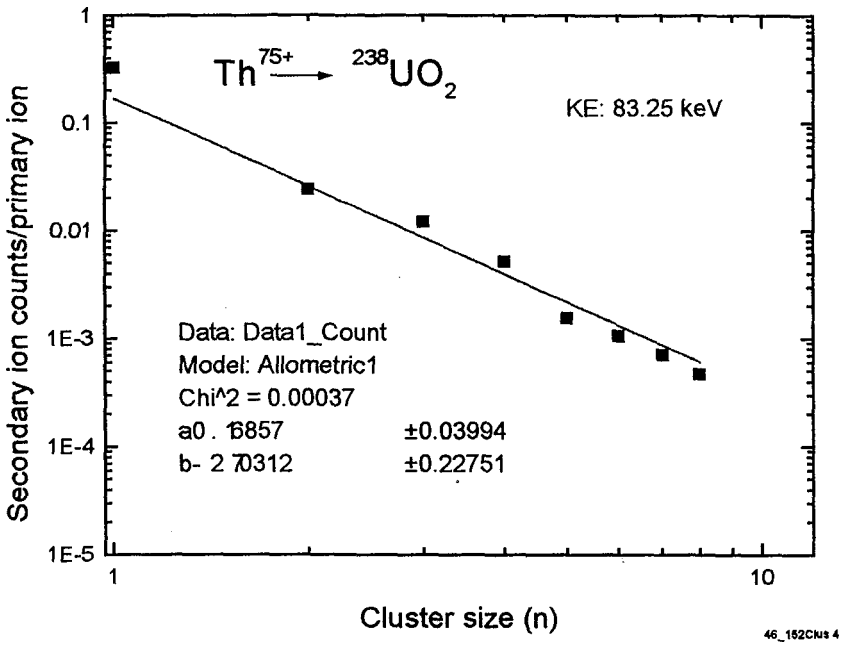

Figure 2. Plot of secondary cluster ion counts per incident Th^{75+} ion versus cluster size (n). The solid line is a power law fit to the data with exponent -2.7.

The power law exponent is correlated with the total sputter yield. Figure 3 shows the dependence of the power law exponent on the total sputter yield for slow, highly charged ions impinging on $^{238}UO_2$. As the total sputter yield increases the exponent increases, approaching the -2 limit of both the shock wave model and the equilibrium model. Also shown is the dependence of the power law exponent on total sputter yield for singly charged Ar ions impinging on Ag surfaces [wucher]. We believe it is fortuitous that for similar total sputter yields for UO_2 and Ag the power law exponent is the same. However, the trend is quite compelling that increased sputter yield give increased power law exponents. While it is tempting to ascribe the observation of power law behavior with critical point exponents to achieving critical point conditions this cannot unambiguously be claimed. However, if a critical point were reached the power law with critical exponent would be observed. These data suggest that as the deposited energy density increases, as occurs with increasing the charge state of the incident ion, critical behavior may be approached.

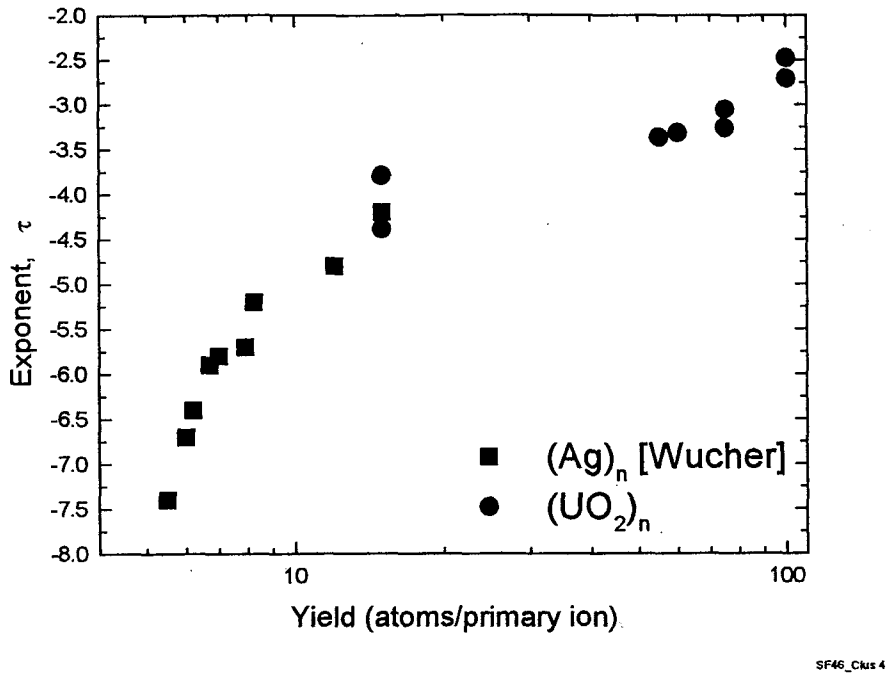

Figure 3. Plot of power law exponent versus total sputter yield for slow, highly charged ions impinging on $^{238}UO_2$ [present work] and Ar^+ ions impinging on Ag surfaces [wucher].

References

[1] S. R. Coon, W. F. Calaway, M. J. Pellin, and J. M. White, Surface Science **298**, 161 (1993).
[2] A. Wucher, M. Wahl, and H. Oechsner, Nuclear Instruments and Methods in Physics Research B **83**, 73 (1993).
[3] H. M. Urbassek, Radiation Effects and Defects in Solids, **109**, 293 (1989); H. M. Urbassek, Nuclear Instruments and Methods in Physic Research **B31**, 541 (1988).
[4] W. Kamke, J. de Vries, J. Krauss, E. Kaiser, B. Kamke, and I. V. Hertel, Zeitschrift für Physik **D 14**, 339 (1989).
[5] K. Rademann, B. Kaiser, U. Even, and F. Hensel, Physical Review Letters, 59, 2319 (1987).
[6] W. Ens, R. Beavis, and K. G. Standing, Phys. Rev. Lett. **50**, 27 (1983).
[7] Z. Ma, S. R. Coon, W. F. Calaway, M. J. Pellin, D. M. Gruen, and E. I. von Nagy-Felsobuki, Journal of Vacuum Science and Technology A 12, 2425 (1994).
[8] T. Schenkel, A. V. Barnes, A. V. Hamza, and D. H. Schneider, European Physical Journal D, in press.
[9] A. Wucher and M. Wahl, Nuclear Instruments and Methods in Physics Research B 115, 581 (1996).
[10] I. S. Bitensky, and E. S. Parilis, Nuclear Instruments and Methods B 21, 26 (1987).
[11] T. Schenkel, M. A. Briere, H. Schmidt-Böcking, K. Bethge, and D. H. Schneider, Physical Review Letters **78**, 2481 (1997).
[12] T. Schenkel, M. A. Briere, A. V. Barnes, A. Hamza, K. Bethge, H. Schmidt-Böcking, and D. H. Schneider Physical Review Letters **79**, 2030 (1997).
[13] D. Schneider, M. W. Clark, B. M. Penetrante, J. McDonald, D. DeWitt, and J. N. Bardsley, Physical Review A 44, 3119 (1991).
[14] D. Schneider and M. A. Briere, Physica Scripta **35**, 228 (1996).
[15] T. Schenkel, A. V. Barnes, M. A. Briere, A. Hamza, A. Schach von Wittenau, and D. H. Schneider, Nuclear Instruments and Methods in Physics Research B **125**, 153 (1997).
[16] G. W. McGillivray, D. A. Geeson, R. C. Greenwood, J. Nucl. Mat. **208,** 81 (1994)

Energy Loss of Slow, Highly Charged Ions in Solids

T. Schenkel, A. V. Hamza, A. V. Barnes and D. H. Schneider

Energetic ions traveling in solids lose kinetic energy in collisions with target electrons and nuclei [1]. Energy loss is a function of the projectile charge state in the solid [2]. Pre-charge-state equilibrium effects have been observed in the high energy regime (>0.5 MeV/u) where projectiles entering solids with charge states lower or higher than the mean equilibrium charge show increased or decreased stopping until charge state equilibrium is established [2, 3]. Stopping power increases in the first few atomic layers of solids have been reported also for N^+ and He^+ ions at relatively low kinetic energies (i. e. 300 keV) [4]. The interpretation of this effect in terms of "enhanced pre-equilibrium" stopping has been discussed controversially [5]. Pre-equilibrium effects on the stopping and ranges of slow, highly charged ions were investigated by implantation of Xe^{44+} (0.8-2.3 keV/u, v=0.18-0.3 v_{Bohr}) into thermal SiO_2 films on Si [6], but no effect of the ion charge on the range was observed. Analysis of the interaction potentials led to predictions of strong, pre-equilibrium nuclear stopping power increases for the interaction of very slow, highly charged ions with ionic insulators. Evidence for the latter was reported from a study using Ar^{16+} ($v \approx 0.3\ v_{Bohr}$) transmitted through thin CaF_2 films [7]. No charge effect on stopping was observed in measurements of the energy loss of Ar^{q+} (q=8, 12, 16+) at $v=0.75\ v_{Bohr}$ in thin carbon foils, indicating that charge-state-equilibrium was established upon penetration of the first monolayer of this semi-metallic target and within a de-excitation time of a fraction of 1 fs [8].

Highly charged ions at velocities below the Bohr-velocity have charge states very far from mean equilibrium charge states [9]. Relaxation of these ions into charge state equilibrium requires a finite, currently not well known, de-excitation time [10]. We report on observations of pre-equilibrium effects in measurements of the energy loss of slow, highly charged ions in thin carbon foils. We have studied energy loss as a function of projectile velocity for bare argon and neon-like xenon and gold ions in the velocity range from 6×10^5 - 11×10^5 m/s.

Slow, highly charged ions were extracted from the Electron Beam Ion Trap (EBIT) at Lawrence Livermore National Laboratory [12]. Projectiles reached the scattering chamber after momentum analysis in a 90° bending magnet. The ion beam was collimated after the magnet to a diameter of 1 mm. The target consisted of a thin carbon foil with a nominal thickness of 10 nm (2+/- 0.5 $\mu g/cm^2$) [13] and was tilted at 15°, resulting in an effective thickness of ~10.4 nm. The total ion dose used in this study was $<5\times10^8$. Repeated energy loss measurements under identical conditions showed no signs of foil modification in the course of the study. The experimental setup has previously been described in detail [7, 12]. Electrons emitted from the target upon impact of individual projectiles were detected by an annular microchannel plate detector (MCP) and provided start signals for the time-of-flight measurements. A bias of -100 V was applied to the target to provide for strong start pulses for all projectiles. Transmitted ions are detected after a flight path of 52.5 (+/-0.3) cm by a second MCP and provided time-of-flight stop signals. The solid angle of the detector was 15 msr. Selection of impact

parameters in transmission geometry can result in a preferential suppression of contribution to energy loss from small impact parameter collisions, where projectiles are scattered out of the detection angle. At a target thickness of ~50 atomic layers and at an estimated collision frequency of 0.5-1 collisions per atomic layer, this effect is partially compensated by multiple collisions [14]. Impact velocities were controlled by acceleration voltages. Including a small variation due to different image charge accelerations [15], the uncertainty in impact energy was 0.6%, or 3 keV at an impact energy of 454 keV. Energy loss in the foil resulted in flight time increases of 40-60 ns. The time resolution of the setup was ~1 ns.

Energy loss values were determined from energy loss distributions, dN/dE, after transformation of variables from measured flight time distributions, dN/dt [16]. Values reported here as average energy loss values, ΔE_{ave}, are approximations of the true, mean energy loss values [17] and were obtained after subtraction of a constant background. Signal to noise rations in TOF spectra were typically >300. The uncertainty in background determination limited contributions in the high loss tails that could be included in the determination of ΔE_{ave} values. Most probable energy loss values were found to be systematically lower than ΔE_{ave}. The energy loss is found to increase strongly as a function of initial projectile charge state [11] and, for Au^{69+}, as a function of impact energy. The charge dependent increase amounts to 46% (46 keV for Au^{33+} vs. 67.3 keV for Au^{69+}). ΔE_{ave} for Au^{33+} agrees reasonably well (i. e. within the large uncertainty in the value of the foil area density) with energy loss values estimated using the TRIM code [18] (see Fig. 1). The dependence of ΔE_{ave} on the impact velocity, v, is shown in Fig. 1 for Au^{69+}. The error bars reflect the relative errors in ΔE_{ave} resulting from an uncertainty of 0.6% in impact energy. For ions in charge state equilibrium in this velocity regime, contributions from elastic collisions are significant or dominant, but decrease with increasing impact velocity [18]. Inelastic energy loss of ions in solids has been found to increase proportional to the projectile velocity, $S_{el} \sim v^n$, with n=0.7-1 [18-20]. To allow for a comparison with the stopping of ions in charge state equilibrium, we use values for nuclear, S_n, and electronic stopping powers, S_{el}, as calculated by the TRIM code [18]. Resulting values, multiplied by the effective target thickness, are shown in Fig. 1 for slow gold ions in carbon. Stopping power values calculated using TRIM cannot expected to be very accurate in this velocity regime, but have been shown to reproduce the velocity dependencies of elastic and inelastic contributions to energy loss in conducting, monatomic solids correctly. The energy loss of Au^{69+} is found to increase strongly as a function of velocity. The increase is significantly steeper than the increase of S_{el} for ions in equilibrium alone. The sum of contributions from elastic and inelastic energy loss processes increases only very little (i. e. by < 10%) in the small velocity range probed in this study. Average energy loss values for Ar^{18+} are found to be nearly constant when the impact velocity is changed from 6.7×10^5 to 11×10^5 m/s. This can be attributed to a compensation of decreasing nuclear and increasing electronic contributions to energy loss processes [18, 20]. ΔE_{ave} for Xe^{44+} increases also, but the increase is weaker than that for Au^{69+}.

We interpret the strong increase in the stopping of Au^{69+} and Xe^{44+} with impact velocity as resulting from pre-equilibrium energy loss enhancements. This interpretation is consistent with recent first observations of charge state dependent energy loss increases of

slow, highly charged ions in solids [11]. Highly charged ions form hollow atoms above metallic and insulating surfaces [21]. At impact on a target, electrons in Rydberg states are peeled-off. Quasi-simultaneously a screening cloud of target electrons is build up around the projectile and a more compact hollow atom is formed inside the solid [22, 23]. Neutralization of the projectile charge by this screening cloud can require extreme degrees of target polarization, involving e. g. over ten carbon atoms to provide the charge required to neutralize a Au^{69+} projectile. De-excitation of hollow atoms in solids proceeds via Auger-cascades [23] and radiative transitions [21, 24]. Available estimates of total de-excitation times, τ_{eq}, range from less than 1 fs (Ar^{16+}) [8], to a few femtoseconds (bare argon, iron and krypton) [21] to an upper limit of 21 fs for ions up to Th^{65+} in carbon [10]. In the asymmetric combination of a heavy projectile ($Z_{projectile}$=79) incident on a light target (Z_{target}=6), direct filling of M-shell vacancies in gold projectiles by target electrons is strongly inhibited. Only projectile levels with principal quantum numbers n~6-10 can be populated directly. The charge distribution in the hollow atom is characterized by electrons in the initially filled K- and L-shells and by electrons in excited states. Intermediate levels with n=3-5 start out empty and are filled in the course of de-excitation.

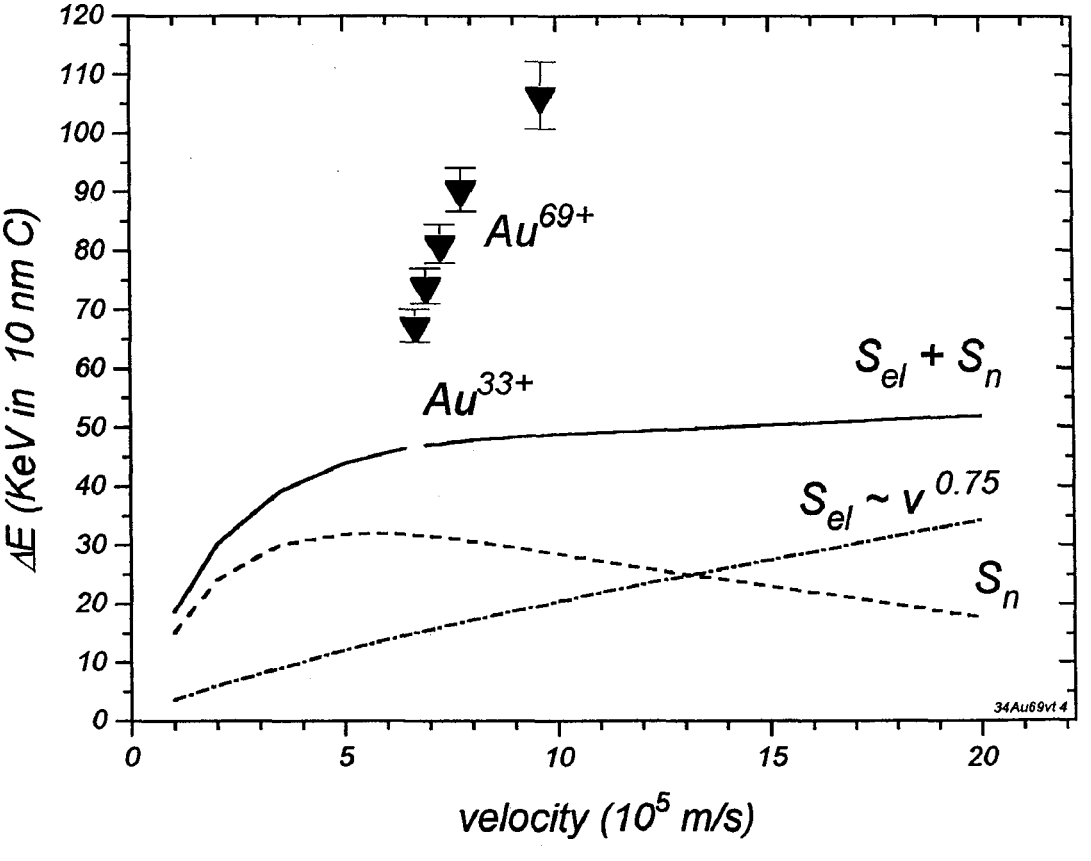

Fig. 1: Average energy loss, ΔE_{ave}, of Au^{69+} in a thin carbon foil as a function of projectile velocity. The lines are estimated energy loss values of gold ions in charge state equilibrium, calculated by TRIM [18]. •—•—: S_n, nuclear energy loss; ————: S_{el}, electronic energy loss; : sum of S_n and S_{el}.

Screening of the projectile nuclear charge is reduced at distances from the nucleus equal to the radii of these empty levels. Averaging over all impact parameters, this can be interpreted as an increased effective charge of hollow atoms. Scaling of the electronic stopping power with the square of an effective ion charge was proposed to estimate charge state dependent electronic stopping power increases for slow, highly charged ions [6, 8]. At atomic transition rates in the order of 10^{15}-10^{16} s^{-1} [21], screening of the nuclear charge and consequently also the interaction potential between projectile and target nuclei change on the time scale of individual collisions (~0.5 fs). Momentum transfer to target electrons and nuclei in collisions with impact parameters comparable to the radii of unoccupied levels in the transient hollow atom is increased over corresponding values for projectiles in equilibrium. Increasing the impact velocity of Au^{69+} allows for the de-exciting projectile to engage in more collisions before a dynamic charge state equilibrium is established. The pronounced velocity dependent energy loss increase is thus indicative of pre-equilibrium energy loss enhancements. Increasing the velocity further will extend de-excitation deeper into the target and will eventually allow projectiles to exit the foil highly excited and in mean charge states in excess of equilibrium charge states. From the charge state dependence of the energy loss [11] we have estimated the increase of pre-equilibrium over equilibrium stopping powers and the mean de-excitation time for Au^{69+} in carbon. Values ranged from a pre-equilibrium stopping increase of a factor of 5 during a de-excitation time of only 1 fs, to a stopping increase of a factor of 2 over 5 fs. For Ar^{18+} we found an upper limit for the pre-equilibrium stopping increase of a factor of 2 during a de-excitation time of 1 fs. The velocity dependencies of ΔE_{ave} are consistent with our earlier results. The pre-equilibrium effects of ion charge and velocity combined result in energy loss enhancements for Au^{69+} in thin carbon foils of over a factor of 2.

The authors gratefully acknowledge the excellent technical support at the LLNL EBIT facility provided by D. Nelson and K. Visbeck.

References:

[1] N. Bohr, Kgl. Danske Videnskab. Selskab. Mat.-fys. Medd. **18** (1948) No. 8

[2] J. Knipp, E. Teller, Phys. Rev. **59** (1941) 659; P. Sigmund, Phys. Rev. A **50** (1994) 3197, and references therein

[3] K. B. Winterbon, Nucl. Instr. and Meth. **144** (1977) 311; T. Kaneko, Y. Yamamura, Physics Letters **100A** (1984) 313

[4] P. Mertens, Th. Krist, Phys. Rev. B **25** (1982) 5591;

[5] J. P. Biersack, P. Mertens, in Proc. Conf. on Charge states and dynamic screening of swift ions in solids, ORNL, CONF-820131 (1983) P. 131; W. N. Lennard et al., same proceedings, P. 136; W. N. Lennard, D. Phillips, I. V. Mitchell, H. R. Andrews, D. Ward, Nucl. Instr. and Meth. B **2** (1984) 116; W. N. Lennard, Xia Yueyuan, H. Geissel, Nucl. Instr. and Meth. B **69** (1992) 89

[6] M. A. Briere, J. P. Biersack, 12th conference on Ion Beam Analysis, Hungary, July, 1993; ibid., EBIT Annual Report, 1993, LLNL, UCRL-ID-118274, P. 33; J. P. Biersack, Nucl. Instr. and Meth. B **80/81** (1993) 12

[7] M. A. Briere, T. Schenkel, P. Bauer, EBIT Annual Report, 1994, LLNL, UCRL-ID-121572, P. 43; M. A. Briere, T. Schenkel, P. Bauer, A. Arnau, D. Schneider, Physica Scripta, in press

[8] R. Herrmann, C. L. Cock, J. Ullrich, S. Hagmann, M. Stoeckli, H. Schmidt-Boecking, Phys. Rev. B **50** (1994) 1435

[9] K. Shima, N. Kuno, M. Yamanouchi, Phys. Rev. A **40** (1989) 3557

[10] T. Schenkel, M. A. Briere, H. Schmidt-Böcking, K. Bethge, D. Schneider, Phys. Rev. Lett. **78** (1997) 2481

[11] T. Schenkel, M. A. Briere, A. V. Barnes, A. V. Hamza, K. Bethge, H. Schmidt-Böcking, D. H. Schneider, submitted for publication

[12] D. H. Schneider, et al., Phys. Rev. **A 42** (1990) 3889; D. H. Schneider, M. A. Briere, Physica Scripta **53** (1996) 228

[13] Foils were produced by The Arizona Carbon Foil Company, Tucson, AZ

[14] W. N. Lennard, X. Yueyuan, H. Geissel, Nucl. Instr. and Meth. B **69** (1992) 89

[15] F. Aumayr, H. Kurz, D. Schneider, M. A. Briere, J. W. McDonald, C. E. Cunningham, HP. Winter, Phys. Rev. Lett. **71** (1993) 1943

[16] J. W. Rabalais (ed.) *Low energy Ion-Surface Interactions* (J. Wiley, New York, 1994), P. 62

[17] P. Sigmund, K. B. Winterbon, Nucl. Instr. and Meth. B **12** (1985) 1

[18] J. F. Ziegler, J. P. Biersack, U. Littmark, *The Stopping and Range of Ions in Solids*, V1, (Pergamon. New York, 1985)

[19] O. B. Firsov, Sov. Phys. JETP, **36** (1959) 1076,

[20] J. Lindhard, M. Scharff, Phys. Rev. **124** (1961) 128

[21] J. P. Briand, et al. Phys. Rev. Lett. **65** (1990) 159; ibid., Phys. Rev. A **53** (1996) 1, ibid., Phys. Rev. Lett. **77** (1996) 1452

[22] F. Aumayr, HP. Winter, Nucl. Instr. and Meth. B **90** (1994) 523; L. Folkerts, R. Morgenstern, Europhys. Lett. **13** (1990) 377; N. Stolterfoht, et al., Phys. Rev. **A 52** (1995) 445; A. Arnau, et al., Surf. Sci. Rep. **27** (1997) 113, and references therein

[23] R. Schuch, D. Schneider, D. A. Knapp, D. DeWitt, J. McDonald, M. H. Chen, M. W. Clark, R. E. Marrs, Phys. Rev. Lett. **70** (1993) 1073

Charge State Dependent Energy Loss of Slow Heavy Ions in Solids

T. Schenkel, M. A. Briere, A. V. Barnes, A. V. Hamza, K. Bethge,
H. Schmidt-Böcking and D. H. Schneider

Energetic ions traveling through solids lose kinetic energy in collisions with target electrons and nuclei [1]. Pre-equilibrium effects and charge state dependencies of energy loss processes of ions in solids have been investigated using beams of light ions [2] and heavy ions at energies ≥0.5 MeV/u [3, 4], and have been addressed in theoretical studies [5, 6]. We report on first observations of charge state dependent energy loss enhancements of slow, highly charged ions in solids.

The interaction of slow, highly charged ions with solids has been studied intensively over the last decade [7-18]. Neutralization of highly charged projectiles above metal surfaces has been described successfully in the framework of a "classical-over-the-barrier" model [7]. Having reached a critical distance from a surface, incoming ions begin to resonantly capture electrons into highly excited states, forming "hollow atoms" [10]. Electrons in states with radii in excess of a characteristic surface screening length are "peeled off" [7, 8] when the projectile reaches the surface. Quasi-simultaneously, a more compact screening cloud is formed around the projectile and a second, smaller, hollow atom is now formed inside the solid. Currently available estimates of mean de-excitation times, τ_{eq}, of highly charged ions in solids range from less then 0.1 fs (Ar^{16+} in carbon) [16], to a few femtoseconds (bare Ar- and Kr-ions in aluminum oxide) [10] and 20 fs (Ar^{17+} in carbon) [14]. An upper limit of $\tau_{eq} \leq 21$ fs has been determined from measurements of equilibrium charge state distributions of slow (2.1 keV/u) Th^{65+} after transmission through ~10 nm thick carbon foils [11].

Reduced screening of the nuclear charge of highly charged projectiles in insulators has been proposed [17, 18] to result in increased momentum transfer to target electrons and nuclei. A finite de-excitation time of highly charged ions should result in energy loss enhancements due to pre-charge-state-equilibrium contributions as compared to the energy loss of projectiles that reach a target in charge state equilibrium.

Other possible contributions to charge state dependent energy loss processes stem from the build-up of the screening cloud upon impact of highly charged projectiles on surfaces and from the energy balance in all charge-changing events during de-excitation.

In a study using Ar^{q+} (q=8, 12, 16) at $v=0.76\ v_{Bohr}$, Herrmann *et al.* found no effect of the initial charge state on projectile energy loss in a 31 nm thick carbon foil [16]. The authors concluded that projectiles reach charge state equilibrium upon penetration of the first monolayer of the target, too fast to enhance the stopping significantly through pre-equilibrium contributions to energy loss processes. Up to now, a dependency of the energy loss of slow ions in solids on the initial projectile charge state has not been observed.

We have measured the energy loss of slow ($v=0.3\ v_{Bohr}$), highly charged ions transmitted through thin carbon foils using time-of-flight spectrometry. The setup has previously been described in detail [18, 19]. Ions were extracted from the electron beam ion trap (EBIT) at Lawrence Livermore National Laboratory. The pressure in the target

chamber was kept below 2.7×10^{-8} Pa. Time-of-flight start signals were provided by secondary electrons emitted from the target at highly charged ion impact. Secondary electrons were detected by an annular micro-channelplate detector. A negative target bias of -100 V was applied to provide for strong start signals for all initial charge states. The target consisted of a ~10 nm thick (~2 +/- 0.5 $\mu g/cm^2$) carbon foil [20] with a diameter of 3 mm, mounted on a high transmission grid. The target was tilted at 15°, resulting in an effective thickness, Δx, of ~10.4 nm. The ion flux was typically $<10^3$ ions/s, and the foil was exposed to a dose $<5\times10^8$ ions. The energy loss of Xe^{44+}-ions was measured at the beginning and at the end of the study and no indications of foil modification were observed. Transmitted ions were detected by a second micro-channelplate detector after a flight path of 52.5 (+/- 0.3) cm, and provided time-of-flight stop signals. The solid angle of the detector was 15 msr. Impact parameter selection in transmission experiments results in the preferential suppression of contribution to measured energy loss values from collisions with small impact parameters in which projectiles are scattered out of the detection angle. At a target thickness of ~50 atomic layers and a collision frequency of ~0.5-1 collisions per layer, this effect is partially compensated by multiple collisions. Deceleration of positively charged, transmitted ions by the target bias resulted in a small energy reduction in the order of ~1% of the most probable energy loss of ions in the foil. The time resolution of the setup, including detectors and electronics, was about 1 ns. Energy loss in the foil increased ion flight times by ~40-60 ns, as compared to flight times at the initial ion velocity.

For the investigation of charge state effects on energy loss, we used a velocity of $v=0.3\ v_{Bohr}$ for all ion species and charge states. The initial kinetic energies, including relative errors, were 35.5 (+/- 0.2) keV, 92.3 (+/- 0.6) keV, 197.7 (+/-1), 312.4 (+/-2) keV and 454.4 (+/-3) keV for ^{16}O-, ^{40}Ar-, ^{86}Kr-, ^{136}Xe- and ^{197}Au-ions.

Energy-loss distributions of transmitted projectiles are shown in Fig. 1 for Au^{69+} and Au^{33+}. Signal to noise ratios in time-of-flight spectra were typically $>3\times10^2$. For determination of energy loss values, measured flight time distributions, dN/dt, were transformed into energy distributions, dN/dE, [22]. Values reported here as average energy losses, ΔE_{ave}, are approximations of the true mean energy loss values [22, 23], and were determined by averaging energy distributions, dN/dE, after subtraction of a constant background. The uncertainty in background determination imposed a limit on contributions from energy loss events in the high-loss tails that could be included in the determination of average energy loss values. Resulting values of ΔE_{ave} for Au^{33+} and Au^{69+} were 46.0 (+/- 3) keV and 67.3 (+/- 3) keV. Most probable energy loss values, ΔE_{peak}, were found to be systematically lower than ΔE_{ave} [23] (ΔE_{peak}= 39.1 keV and 55.7 keV for Au^{33+} and Au^{69+}, respectively). We note that, due to the relative narrowness of the flight-time distributions, calculations of energy loss values directly from average flight times yields values that deviate by less than 1% from values calculated after transformation of variables.

Fig. 2 shows ΔE_{ave} as a function of q for krypton, xenon and gold ions. For xenon- and gold-ions, ΔE_{ave} increases strongly with charge. The increase in ΔE_{ave} is 7.6 keV (+33%) as the charge state increases from Xe^{36+} to Xe^{49+}, and 21.3 keV (+46%) as the charge state increases from Au^{33+} to Au^{69+}. This charge state dependent energy loss

increase shows for the first time the presence of strong pre-equilibrium contributions to the energy loss of slow, heavy ions in conducting solids.

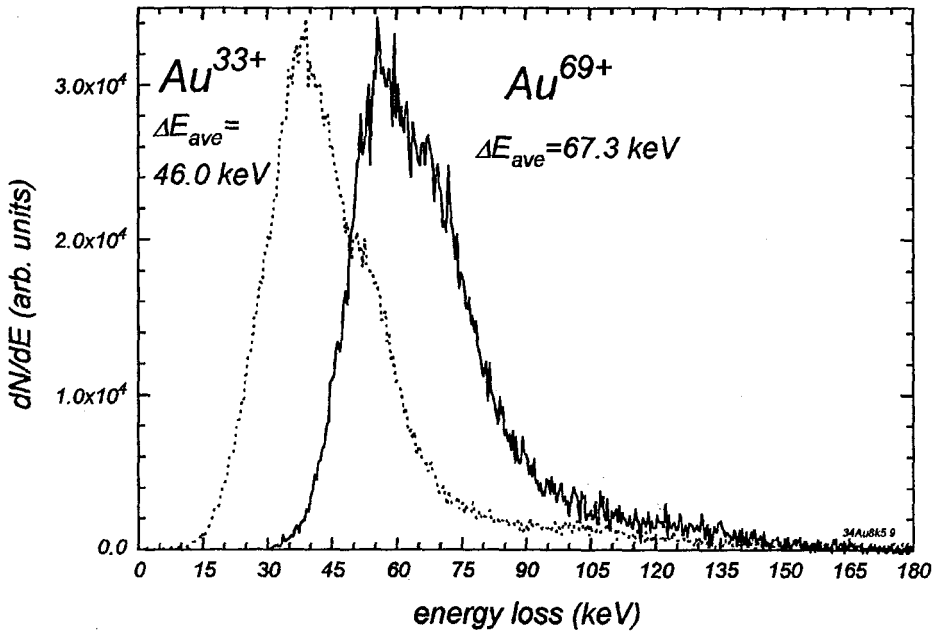

Fig. 1: Energy-loss distributions of Au^{33+} and Au^{69+} after transmission through a thin carbon foil ($\Delta x \approx 10.4$ nm). The initial energy was 454.4 (+/-3) keV.

The energy loss in the foil is the sum of contributions to stopping processes before, $(dE/dx)_{pre}$, and after, $(dE/dx)_{eq}$, charge-state equilibrium is reached. Both equilibration length, Δx_{pre}, and pre-equilibrium stopping power, $(dE/dx)_{pre}$, are a function of the projectile charge state, q. In an attempt to estimate charge-state dependencies, we assume a simple power law dependency of Δx_{pre} and $(dE/dx)_{pre}$ on q. This assumption is consistent with results from studies of secondary electron and ion emission from carbon surfaces as a function of projectile charge [11]. In a rough approximation that does not include the time dependency of q, we can then write for the energy loss in the foil:

$$(1)\ \Delta E(q) = \left.\frac{dE}{dx}\right|_{eq} \cdot [\Delta x - \Delta x_{pre}] + \left.\frac{dE}{dx}\right|_{pre} \cdot \Delta x_{pre} = \left.\frac{dE}{dx}\right|_{eq} \cdot [\Delta x - \alpha \cdot q^{n}] + \beta \cdot q^{n+m}$$

The average energy loss value for Au^{33+} agreed reasonably well with values calculated for gold ions in charge state equilibrium using the TRIM code [24]. Thus this value was taken to account for equilibrium energy loss contributions. With the constants α and β as free parameters, we used Eq.(1) to fit the gold-data in Fig. 2b) for n, m≤2. The shown fit was obtained for n=1 and m=2. Values for α and β from realistic fits allow for very tentative estimations of Δx_{pre} and $(dE/dx)_{pre}$. Resulting increases of pre-equilibrium over equilibrium stopping powers during de-excitation ranged from a factor 2 along an equilibration length of ~4 nm (τ_{eq}~6 fs), to a factor 5 with Δx_{pre}~1 nm (τ_{eq}~2 fs). The observed charge-state dependent energy loss enhancement can be interpreted as resulting from increased momentum transfer to target electrons and nuclei in collisions with impact parameters comparable to the radii of unoccupied levels in transient hollow atoms. The

interaction potential changes on the time scale of the collision time (~0.5 fs) due to rapid de-excitation of the projectile. In the absence of a critical number of inner shell vacancies, e. g. for ions like Kr^{33+}, de-excitation processes at and below the surface are too fast (τ_{eq}~ 1 fs, Δx_{pre}~ 0.7 nm) and pre-equilibrium stopping power increases are too weak ($dE/dx\big|_{pre} < 2 \cdot dE/dx\big|_{eq}$) to allow for strong contributions to energy loss processes before de-excitation is completed. Contributions to energy loss from the large (>q) number of charge changing events are expected to be significant, but can not be quantified on the base of our results.

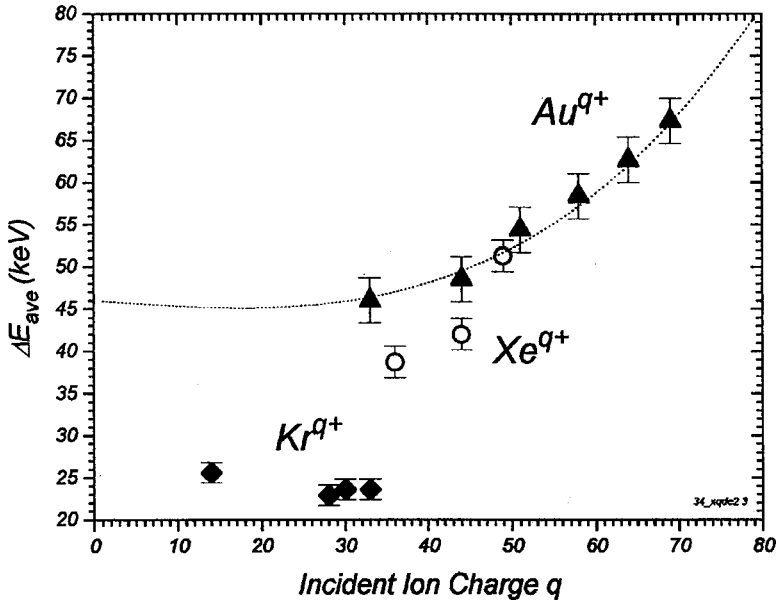

Fig. 2: Average energy loss of $Kr^{14, 28, 30, 33+}$, $Xe^{36, 44, 49+}$, and $Au^{33, 44, 51, 58, 64, 69+}$ in a thin carbon foil. The dotted line is a fit to the Au^{q+}-data using Eq. (1) with n=1, m=2 (α=0.0165, $\beta=8\times10^{-5}$).

The authors gratefully acknowledge the excellent technical support at the LLNL EBIT facility provided by D. Nelson and K. Visbeck.

References:

[1] H. A. Bethe, Ann. Phys. **5** (1930) 325; F. Bloch, Ann. Phys. **16** (1933) 285; N. Bohr, Kgl. Danske Videnskab. Selskab. Mat.-fys. Medd. **18**, No. 8 (1948); J. Lindhard, M. Scharff, Phys. Rev. **124** (1961); P. Sigmund, Phys. Rev. A **54** (1996) 3113, and references therein

[2] P. Mertens, Th. Kirts, Phys. Rev. B **25** (1982) 5591, W. N. Lennard, et al., Nucl. Instr. and Meth. B **2** (1984) 116

[3] H. Ogawa, et al., Nucl. Instr. and Meth. B **82** (1993) 80; C. M. Frey, et al., Nucl. Instr. and Meth. B **99** (1995) 205

[4] B. L. Doyle, D. K. Brice, Phys. Rev. A **24** (1981), 2232

[5] A. Arnau, et al., Nucl. Instr. and Meth. B **69** (1992) 102, and references therein

[6] P. Sigmund, Phys. Rev. **A 50** (1994) 3197, and references therein

[7] J. Burgdörfer, et al., Phys. Rev. A **44** (1991) 5674; J. Burgdörfer, F. W. Meyer, Phys. Rev. A **47** (1993) R20

[8] F. Aumayr, HP. Winter, Nucl. Instr. and Meth. B **90** (1994) 523

[9] D.H. Schneider, M. A. Briere, Physica Scripta, **53** (1996) 228, and references therein

[10] J. P. Briand, et al., Phys. Rev. Lett. **65** (1990) 159, J.-P. Briand, et al., Phys. Rev. A **53** (1996) 1, M. A. Briere, et al. Nucl. Instr. and Meth. B **90** (1994) 231

[11] T. Schenkel, et al., Phys. Rev. Lett. **78** (1997) 2481, ibid. Nucl. Instr. and Meth. B, in press

[12] R. Schuch, et al., Phys. Rev. Lett. **70** (1993) 1073

[13] L. Folkerts, R. Morgenstern, Europhys. Lett. **13** (1990) 377

[14] S. Winecki, et al., Phys. Rev. A **53** (1996) 4228

[15] R. Díez Muiño, et al., Phys. Rev. Lett. **76** (1996) 4636

[16] R. Herrmann, et al., Phys. Rev A **50** (1994) 1435

[17] J. Biersack, Nucl. Instr. and Meth. B **80/81** (1993) 12

[18] M. A. Briere, et al., Physica Scripta, in press

[19] D. H. Schneider, et al., Phys. Rev. A **44** (1991) 3119

[20] The Arizona Carbon Company, Inc., Tuscon, Arizona, AZ, 1996

[21] P. G. Bertrand, J. W. Rabalais in: *Low Energy Ion-Surface Interactions*, J. W. Rabalais (ed.) (Wiley, New York, 1994), P.62

[22] W. N. Lennard, et al., Nucl. Instr. and Meth. B **69** (1992) 89

[23] P. Sigmund, K. B. Winterbon, Nucl. Instr. Meth. B **12** (1985) 1

[24] J. F. Ziegler, J. P. Biersack, U. Littmark, The Stopping and Range of Ions in Solids (Pergamon, New York, 1985)

V. RETRAP and Ion Collisions

Performance of the Hyperbolic Traps in RETRAP

J. Steiger[1], B. R. Beck[1], L. Gruber[1], D. H. Schneider[1], D. A. Church[2], J. Holder[2]
[1]Lawrence Livermore National Laboratory
[2]Physics Dept., Texas A&M University

For experiments with cold, highly charged ions a set of two Penning traps with hyperbolic electrodes has been installed at EBIT (Fig. 1). In the following report the efficiency and performance of these traps is briefly described. The highly charged ions extracted from EBIT enter RETRAP's magnetic field with 7 kV·q of energy. This energy is too high for direct catching since the electrode potentials of the trap are limited to 600 V. Therefore the first step is to slow down the ions by ramping down the potential of the deceleration tube while the ion bunch or part of it resides inside. The slowed down ions are then caught by pulsing the catch electrode, typically to 200 V when the ions are inside the trapping volume. The trapping efficiency in a very simplistic model, ignoring all fringe fields is given by

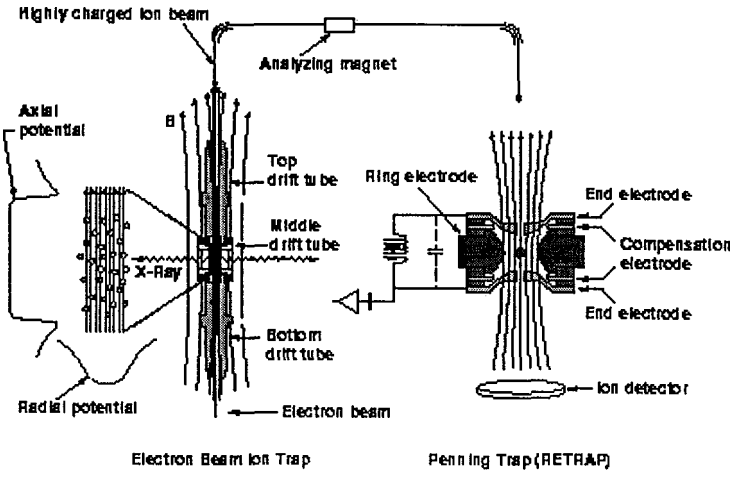

Fig. 1: Schematic of the EBIT/RETRAP system showing EBIT, where the highly charged ions are produced and extracted and one of the two, almost identical Penning traps in RETRAP. The tuned circuit for the nondestructive ion detection and a particle detector below the traps are also shown.

$$\eta = \frac{\Delta l}{\Delta t}\sqrt{\frac{m}{2}}\left(q(V_{ext} - V_{decel}) - E_{perp}\frac{B_{Trap}}{B_{decel}}\right)^{-\frac{1}{2}}$$

where Δl is the length of the trapping volume, Δt is the length of the ion bunch in time, m and q are the mass and charge of the ions, V_{ext} is EBIT's extraction potential, V_{decel} is the deceleration bias potential, E_{perp} is the perpendicular energy in the deceleration tube and B_{Trap} and B_{decel} are the magnetic flux densities in the trap and the deceleration tube, respectively. The last term in this equation is due to the conservation of the magnetic moment for the decelerated ions. This crude approximation sets an upper limit for the trapping efficiency to about 20%.

Experimentally, the number of trapped ions was measured by catching ions, holding them for a certain amount of time ($\approx$ 1 s) and dumping them on an open electron multiplier for counting. The number of dumped ions was maximized by tuning all optical beamline elements and keeping V_{decel} as high as possible. This procedure also minimizes the

amount of perpendicular energy which would lead to the capture of "high energy" ions (most of the energy residing in the cyclotron motion) and ultimately to an unwanted hot ion plasma. The measured efficiency was about 10%; up to 3000 ions could be caught out of 30000 extracted from EBIT.

The lifetime in the traps was measured with the help of the tuned circuits. The ions were confined for some time, and then the ring electrode potential was ramped over a certain range to probe the charge state distribution inside the trap (Fig. 2). The lifetime estimated from these kind of measurements was about 1000 s at the beginning of an experiment. It was noted however that the pressure increased over a period of about one week. The lifetime dropped considerably to less than 10 s. After a short warm-up (to roughly the temperature of liquid nitrogen) the long lifetimes were observed again. The reason for the increase of the pressure over such a short period of time is not completely understood. The constant flux of residual gas atoms and molecules from the beamline and through the ports of the ring electrode in the bottom trap offers a possible explanation. To block these fluxes, windows and shutters, in thermal contact with the He dewar of the magnet, have been installed. In a forthcoming experiment the effectiveness of these blocking devices will be tested.

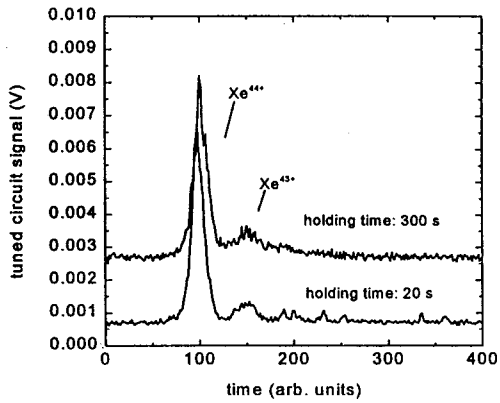

Fig.2: The charge state distribution inside the traps is measured with the tuned circuit detector by sweeping the ring electrode potential, thereby tuning ions with different mass to charge ratio on resonance with the tuned circuit. Even after a holding time of 300 s the charge state distribution has not changed, indicating a lifetime of more than 1000 s.

Laser Cooling of Be^+ in RETRAP

L.Gruber*, J.Steiger*, B.R.Beck*, D.Church‡, D. Schneider*
*Lawrence Livermore National Laboratory, Livermore, CA 94550
‡Physics Department, Texas A&M University, College Station, TX 77843-4242

The first two steps towards producing strongly coupled plasmas with highly charged ions is to laser cool Be^+ to low enough temperatures and to sympathetically cool a different ion species with the cold Be^+. Both steps have been shown in RETRAP and will be presented here.

The Laser system consists of an argon-ion laser pumped dye ring-laser with an internal $LiIO_3$ doubler crystal. The dye-laser has an output of about 5 mW at 313 nm. This light is transported a distance of over 15 m to the experiment where the beam is about 2.5 cm in diameter. A telescope allows us to produce a collimated beam of about 0.5 mm in diameter (see fig.1). A $\lambda/2$ waveplate rotates the polarization of the light interacting with the beryllium cloud perpendicular to the magnetic field. The laserbeam goes through two holes in the ring of the lower hyperbolical trap and hits a beamstop outside the vacuum. The scattered light from the trap center is observed at 90° with respect to the laser beam. A spatial filter is very effective in reducing the scattered light from the edges of the holes in the ring. In order to operate the photomultiplier tube it needs to be magnetically shielded.

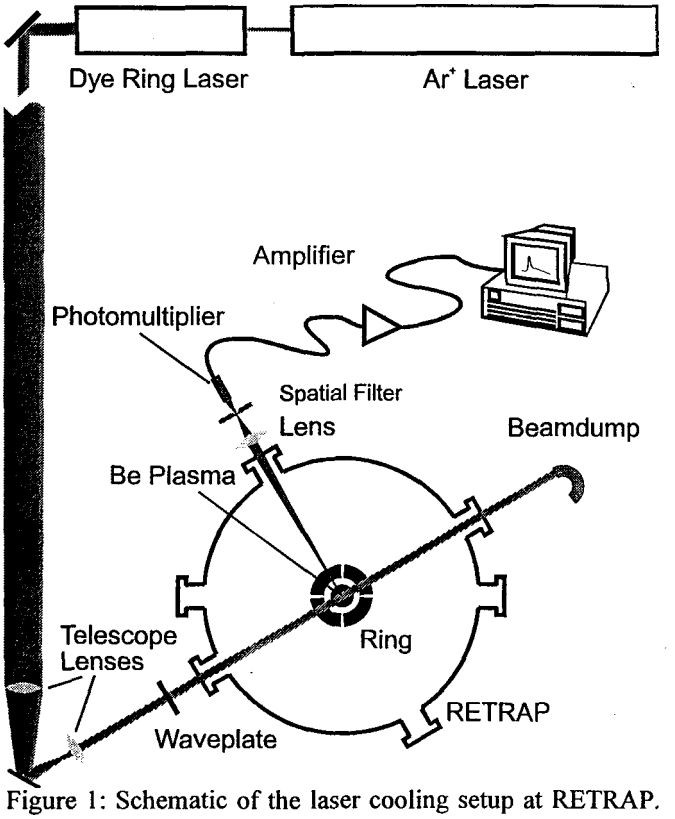

Figure 1: Schematic of the laser cooling setup at RETRAP. It shows a top view of RETRAP and the path of the coolin laser beam with the fluorescent light detection at 90°. The beam path between the dye laser and the first telescope lens is shown interrupted to indicate a long distance

Beryllium is loaded into the trap with a Metal Vapor Vacuum Arc (MeVVA). This ion source produces Be^+ and Be^{2+} and both types of ions are trapped simultaneously in RETRAP. In order to lasercool the ions efficiently they have to be precooled. This can be done with a tuned circuit attached to the endcap electrodes of the trap. This circuit has a quality factor of about 300-500. By adjusting the potential depth of the trap, the axial oscillation frequency of the ions can be tuned onto the resonance frequency of the tuned circuit increasing the signal induced by the ions in the circuit. The energy of the ions is dissipated by the resistor in the tuned circuit, leading to the resistive cooling of the ions. Fig. 2a shows the noise signal of the amplifier attached to the tuned circuit measured with a spectrum analyzer while Be^{2+} ions were on resonance. The flat part in the first 30 s is the final stage of the

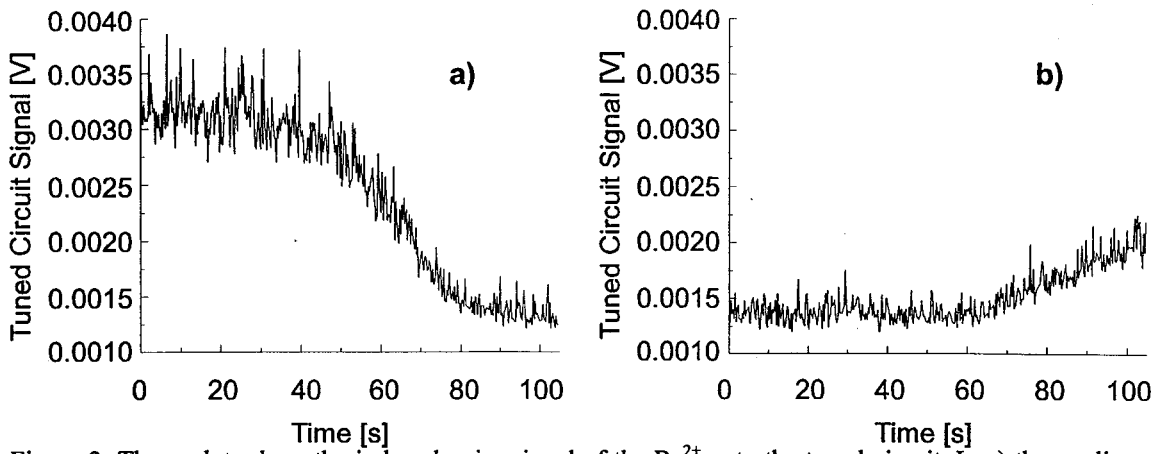

Figure 2: These plots show the induced noise signal of the Be^{2+} onto the tuned circuit. In a) the cooling laser is below the resonance frequency and is therefore cooling – resulting in a noise drop. In b) the cooling laser is slightly above the resonance and therefore heating the plasma. Note that the laser acts on the Be^{+} and here the signal of the Be^{2+} is observed. This indicates sympathetic cooling.

precooling and the sudden drop in the signal indicates the onset of the laser cooling. The signal drops within a few tens of seconds to the background level. Note that the lasercooling acts only on the Be^{+} but a drastic impact on the Be^{2+} signal is observed indicating sympathetic cooling is taking place in the trap. If the laser frequency is increased beyond the Be^{+} resonance, only ions moving into the same direction as the light can absorb photons. Therefore the momentum of the ions is increased and the plasma is heated. In fig.2b this effect can be seen.

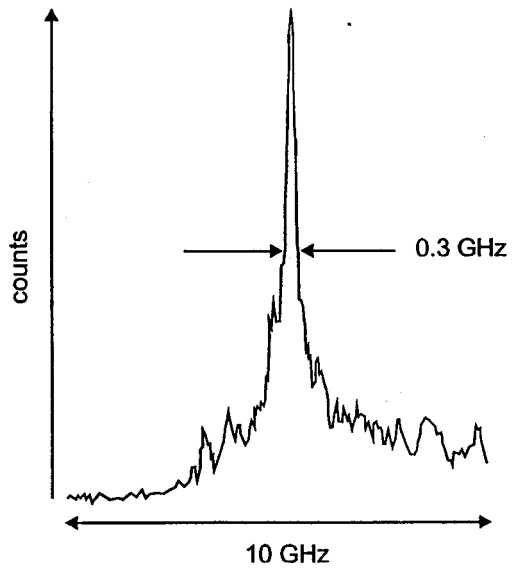

Figure 3: Fluorescence signal of the Be^{+} cloud in RETRAP detected with a photomultiplier at 90° with respect to the incoming beam. The cooling laser is scanned over the resonance from left to the right (i.e. sweeping from lower frequencies to higher frequencies). The temperature is estimated to be about 2 K.

An estimate of the minimum achieved temperature was made by scanning the cooling laser frequency from below resonance to above resonance. The resulting line shape (fig.3) is not expected to be Gaussian, because the laser is modifying the temperature of the plasma: below the resonance frequency the plasma is cooled to lower and lower temperatures (steepening of the wing) and above it is heated (flattening of the wing). The full width at half maximum of the line was used to estimate the upper limit of the lowest achieved temperature. In fig.3 the plasma was cooled to less than 2 K.

If Xe^{44+} can be cooled to such a temperature and we assume a density of about 10^{7} cm^{-3} then a Coulomb coupling constant of Γ=560 can be achieved. According to theoretical predictions, this value is large enough for the plasma to crystallize.

Separation of Laser Cooled Be^+ and Be^{2+} in RETRAP

L.Gruber*, J.Steiger*, B.R.Beck*, D.Church‡, D. Schneider*
*Lawrence Livermore National Laboratory, Livermore, CA 94550
‡Physics Department, Texas A&M University, College Station, TX 77843-4242

In a recent experiment in RETRAP Be^+ and Be^{2+} have been trapped simultaneously in a Penning trap. Theory predicts a centrifugal separation [1] for a plasma consisting of ions with different mass to charge ratios. Depending on the temperature of the plasma a partial or complete separation occurs. In a complete separation (low temperature), the species with the higher mass to charge ratio (Be^+) forms an annulus with constant density around the cloud of the other species (Be^{2+}) leaving a small gap between the two clouds. With rising temperature, the two clouds start to mix again and will end up as an ellipsoidal cloud.

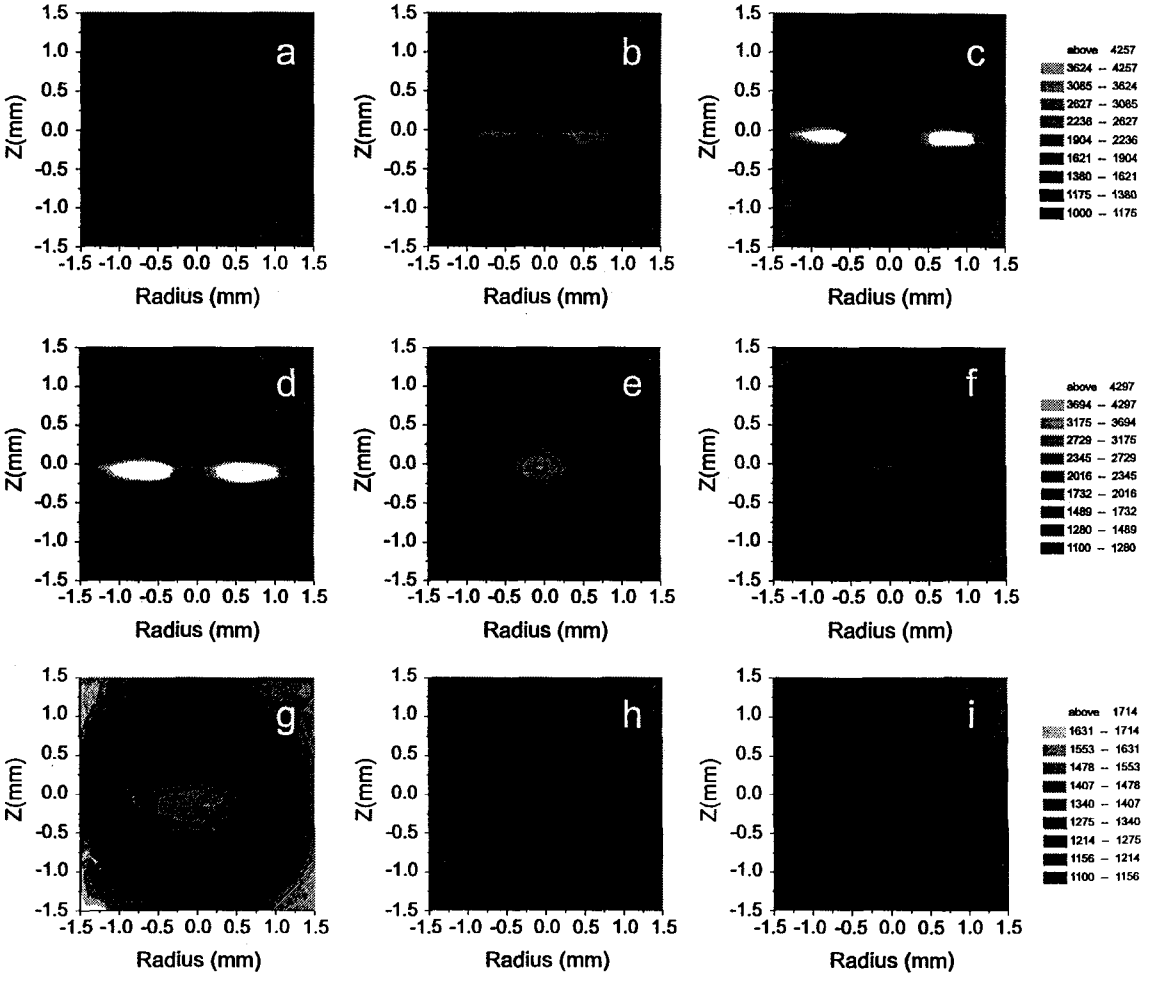

Figure 1: Side view images of a trapped Be^+ cloud being cooled (images a through c) and heated (images d through i) with a 313nm laser, taken with a cryogenically cooled CCD-camera. The intensity scale is logarithmic and the values of the different gray scales are indicated on the right hand side for all the images in the same row. The ion cloud in the trap consists of two species, Be^+ and Be^{2+}. For very low temperatures, these two species centrifugally separate. Only the Be^+ is visible as two spots (b through d) due to the annular shape of the cloud and the laser overlap (see fig.2).

For the observation of the Be^+ cloud, a cryogenically cooled CCD camera was mounted on the side of the trap observing the cloud perpendicular to the magnetic field. This 'side on' observation produces images of the projection of the fluorescing parts of the cloud onto the CCD chip (See fig.1). Images a through c were taken when the cooling laser was scanned over about 9 GHz from the red side towards the resonance frequency. For images d through i the laser frequency was already past the resonance frequency; therefore, the cloud was being heated. During the exposure of images e through i the laser was at a fixed frequency. Since in image e the cloud was cold (a maximum of fluorescence had been observed), the ions had a lower velocity therefore increasing the time they have the right velocity component in the beam direction allowing them to absorb and re-emit the laser-photons. By absorbing, they get additional momentum and the time they are able to absorb photons decreases. Therefore, the intensity in the following images decreases due to fewer scattering events.

When the ions are cold, the images show two distinct peaks. The reason for this shape is explained in fig.2. Since the diameter of the laserbeam is smaller than the inner diameter

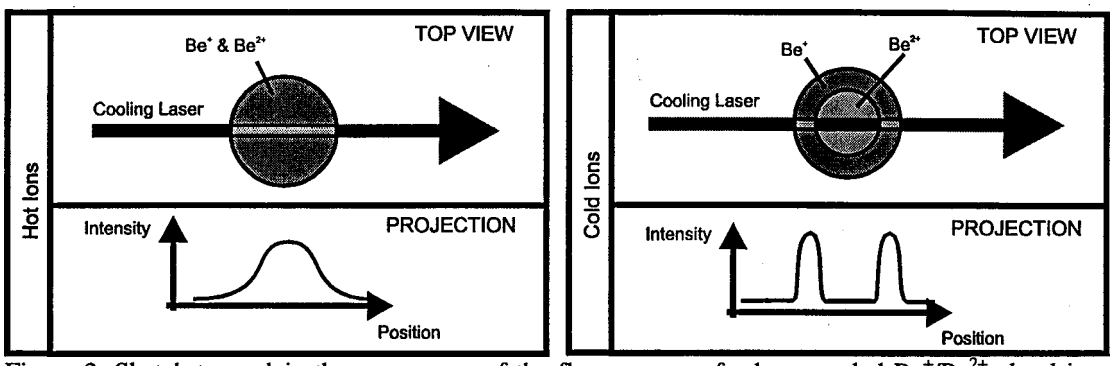

Figure 2: Sketch to explain the appearance of the fluorescence of a laser cooled Be^+/Be^{2+} cloud in a Penning trap. At higher temperatures, Be^+ and Be^{2+} are completely mixed and the cloud has a spheroidal shape. The overlap of the cloud with the laserbeam produces an oval shaped image on the CCD. When the ions are cold, the Be^+ forms an annulus around the Be^{2+} and therefore the overlap with the laserbeam gives rise to two radially elongated spots on the camera.

of the cold Be^+ annulus, the cloud fluoresces only in the two sections where it overlaps with the laser. As soon as the cloud is hot enough, the two ion species mix, the projection of the fluorescing volume is oval shaped (image e in fig.1) and the image of the cloud increases in the z direction since the cloud is expanding axially. In the last four images, the extent of the cloud in the z direction is constant. This is an indication that the laserbeam is not wider than the height of the cloud-image. Therefore, an estimate of the diameter of the laserbeam can be made. A cross section along the z-axis through the middle of the cloud gives a full width at half maximum of about 500 μm.

From image c in fig.1 the extent of the Be^+ annulus can be extracted. The estimate for the inner diameter is (900 ± 200) μm and the estimate for the outer diameter is (2300 ± 200) μm.

[1] O'Neil, T. M., *Phys. Fluids* **24**, 1447-1451 (1981)

MOLECULAR DYNAMICS SIMULATIONS OF COLD Be+ and Be++

Hugh DeWitt
Lawrence Livermore National Laboratory

In 1981 O'Neil[1] developed a theory of the behaviour of ions in a Penning trap with two different values of M/Z. When the ions are at equilibrium in the trap they will rotate with a constant frequency, and at high temperature they will stay mixed. At sufficiently low temperature, however, O'Neil showed that the ions with the smaller value of M/Z would move toward the center of the trap. The final equilibrium state would be cloud of one charge in the center of the trap surrounded by a ring of the cloud with the other charge. This centrifugal separation was first observed experimentally in 1986 by the NIST group in Boulder, Larson et al[2] who studied a mixture of Hg+ and Be+ ions. Since both Hg+ and Be+ have electronic transitions in the visible region that could be excited by lasers, both Hg+ and Be+ clouds could be seen. Separation of the Be+ ions to the center was observed at temperatures well below 1 K after laser cooling.

Recently the EBIT group has studied the mixture of Be+ and Be++ in the RETRAP experiments and verified that laser cooled Be+ could sympathetically cool the Be++. A ring of Be+ was observed at sufficient cooling, and the Be++ ions are a cloud in the center of the trap. Unfortunately there is no convenient resonance line for Be++ so this cloud of ions could not be observed directly.

Roy Pollock has written a molecular dynamics code to model ionic mixtures found in the EBIT RETRAP experiments, and numerically carry out the centrifugal separation described by the O'Neil[1] theory. The Hamiltonian of the trapped ions consists of i) kinetic energy with momentum **p** replaced by **p - (e/c)A** and **A** is the vector potential for a magnetic field along the z axis of the Penning trap, ii) the sum of the Coulomb interactions among all particles, and iii) a quadrupole term of the form $qQ(2z^2 - x^2 - y^2)$. This is the system described by the O'Neil theory and gives rise to the standard equations for trapping ions in harmonic potential. The modelling calculations were done with parameters for the code that fitted the actual experimental conditions of the RETRAP. The numbers of particles used is far less than the thousands of charges that can be trapped. The simulations are done with 64 Be+ ions and 64 Be++ ions. The experimenters believed that the combination of laser cooling and sympathetic cooling had brought the temperature of the ions down to below 2 K Several simulation runs with the code indicated that no centrifugal separation was possible

at 2 K or even 1 K. A clear separation of the Be++ ions to the center was first observed at T = .125 K. This is best illustrated in Fig. 1 with an x - y plot of the cloud with filled diamonds indicating Be++ and open circles indicating Be+. Even with a fairly long simulation, 2,000,000 time steps, the separation is not quite complete, but close. The x - z plot of Fig. 2 corresponds to the experimental pictures where only the Be+ ions can be seen with laser excitation.

To do these simulations the quadrupole field can be adjusted so that the resulting ion cloud can trapped in any spheroidal shape ranging from prolate to oblate. A large value of the quadrupole field results in a nearly pancake shape. An interesting and significant feature of the simulation as seen in the x - z plane is the formation of charged layers perpendicular to the magnetic field. These layers are a result of the high ion density when the ion cloud is squeezed into a thin oblate shape.

The centrifugal separation that is seen in the molecular dynamics simulation is clearly a result of different values of M/Z for the two ions, namely 9/1 for Be+ and 9/2 for Be++. If one uses in the simulation Z_1 =1 and Z_2 = 2, but the same value of M/Z, there is no separation.

1. T. M. O'Neil, Phys. Fluids 24, 1447 (Aug. 1981)

2. D.J. Larson, J.C. Bergquist, J.J. Bollinger, W.M. Itano, D.J. Wineland, Phys. Rev. Lett. 57, 70 (7 July 1986)

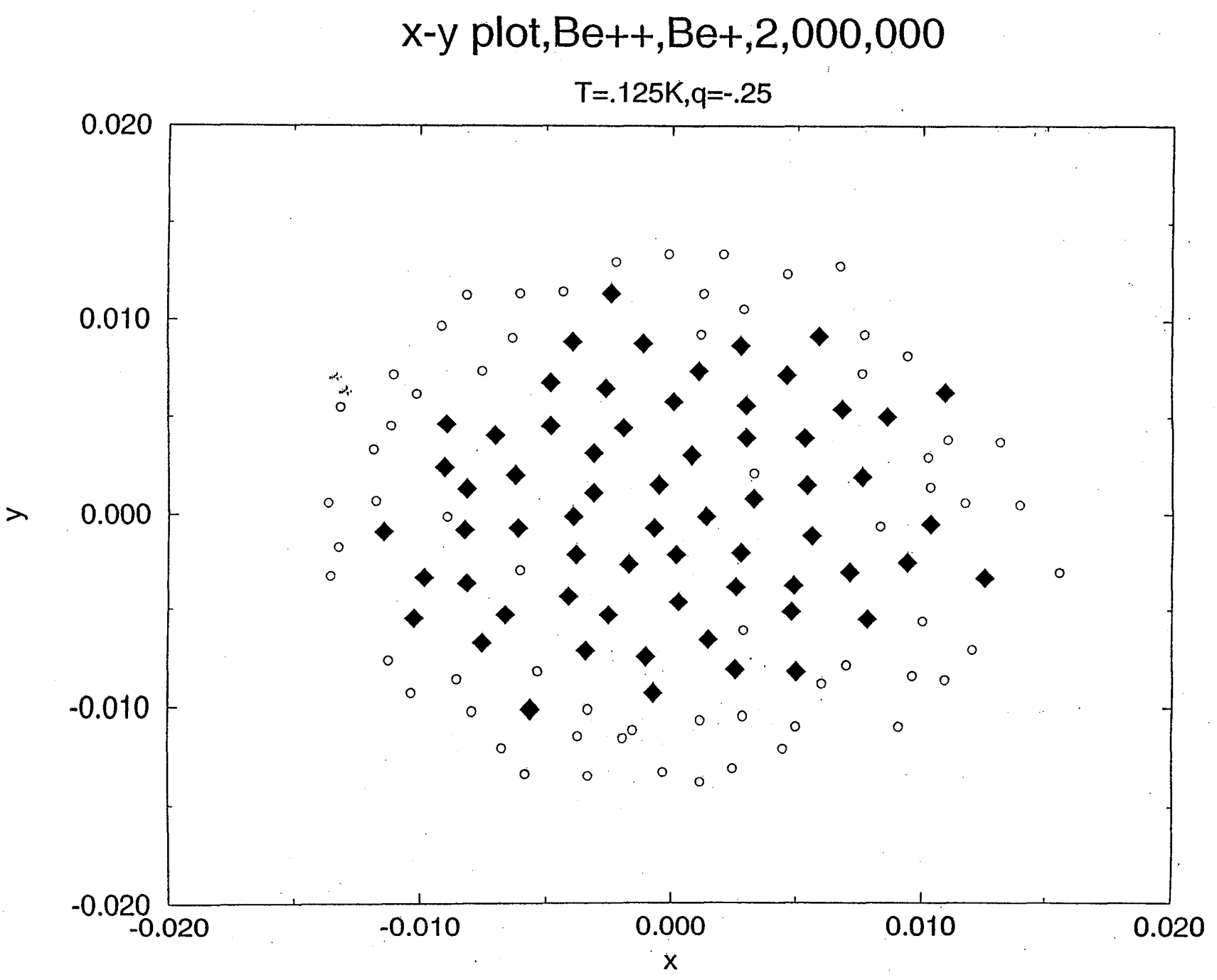
x-y plot,Be++,Be+,2,000,000
T=.125K,q=-.25
0.020
0.010
0.000
-0.010
-0.020
y
-0.020
-0.010
0.000
0.010
0.020
x

FIGURE 1

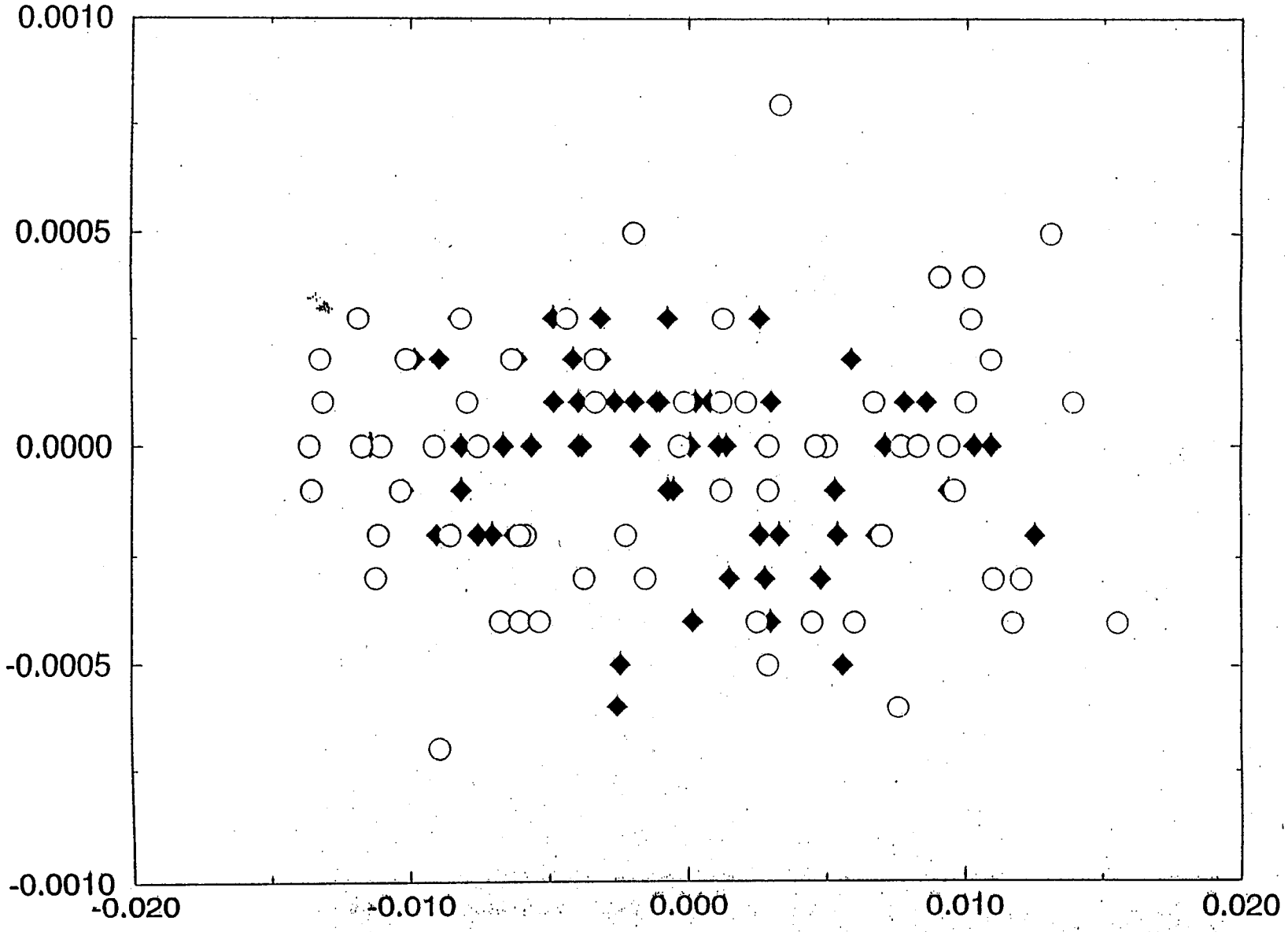
x-z plot ,Be++,Be+,2,000,000
T=.125 K,q=-.25
0.0010
0.0005
0.0000
-0.0005
-0.0010
-0.020
-0.010
0.000
0.010
0.020

FIGURE 2

Schemes to Capture Highly Charged Ions into a Be^+ Cloud

B.R. Beck, J. Steiger, L. Gruber, D. Schneider and D.A. Church*
Lawrence Livermore National Laboratory
*Texas A&M University

To cool highly charged ions (HCI) in RETRAP to low temperatures (< 5 K) may require the HCIs to be sympathetically cooled by another ion species that is cooled to the desired temperature. Be^+ ions are a good candidate for the other ion species since they can be laser cooled to low temperatures (< 5mK) and via Coulomb collisions, will cool the HCI. However, such a sympathetic cooling scheme requires the Be^+ ions and the HCIs to reside in the same trapping region. Furthermore, since more HCIs may be desired than a single fast extraction from EBIT yields, a capture scheme that allows stacking of several EBIT extractions would be preferred. Two schemes to capture MEVVA produced Be^+ ions and EBIT produced HCIs into the same trap have been proposed and are outlined in this paper.

An ideal capture scheme would have the following properties; 1) a transfer of the HCIs into the trapped Be^+ should not increase the phase space of the ions. 2) The temperature of the ions before the transfer should be low. This, in conjunction with 1, insures that the ion-ion collision time is as short as possible; because of the $T^{-2/3}$ dependence of the collision rate and because lower temperatures imply small axial excursion of the ions and hence higher densities. In addition, if the temperatures of the Be^+ ions and HCIs are too high, charge exchange between Be^+ and HCIs can occur (e.g., for Xe^{44+} this happens for $T_{Xe} \approx q \times 20$ eV when $T_{Be} << T_{Xe}$). 3) A sufficient number of the Be^+ ions should be captured so that the collision rate of the Be^+ ions with the HCIs is high enough so that cooling of the HCIs can occur before the next EBIT extraction pulse. EBIT extraction cycle should be around a second so that charge exchange of the HCIs with neutrals can be ignored during the stacking phase.

In both schemes presented here the Be^+ ions are captured into the bottom hyperbolic trap of RETRAP[1]. The Be^+ ions are first resistively cooled via a tuned circuit to a temperature where laser cooling of them becomes effective. The resistive cooling time is hundreds of seconds; whereas, the laser cooling time is much less than a second for cold (T < 10 K) Be^+ ions. With cold Be^+ ions the axial confinement potential well can be very shallow (much less than a volt in theory).

In the first capture scheme the Be^+ ions are cooled as described above, then a shallow potential well is created by biasing the ring electrode negative with respect to the endcaps. Next, HCIs are captured directly into the trap by pulsing down the capture electrode (see figure 1). This scheme has the advantage that it is very simple to implement. However, the HCIs are not pre-cooled before they are mixed with the Be^+ ions; thus, the collision rate may be too low. Furthermore, the Be^+ ions have to dissipate the energy of the HCIs, which may heat the Be^+ ions sufficiently so that the laser cooling becomes ineffective. Thus, the capture of the HCIs should be tuned so that they have low energies when trapped. In addition, the pulsing of the capture electrode to catch the HCIs may, because of proximity, excite the Be^+ ions, causing them to heat up.

In the second scheme, the shallow Be^+ potential well is biased several hundred volts above the bias of the top hyperbolic trap (see figure 2). The HCIs are then captured into the top hyperbolic trap. Next, the bias of the top hyperbolic trap is ramped above the bias of the bottom

hyperbolic trap on about a second time scale. As the potential on the top hyperbolic trap is slowly raised, HCIs, depending on their axial energy, will make it over the bias of the bottom hyperbolic trap and bounce within the two traps. Since a HCI's axial kinetic energy in the bottom trap is low, approximately the shallow potential well depth times q, for the first few passes through Be^+ ions, a collision of the HCI with a Be^+ ion has a good probability of trapping the HCI in the shallow potential well. This scheme requires that the HCI have little radial energy. If a HCI has lots of radial energy then the collision rate of the HCI with the Be^+ ions is determined by the radial energy and not the low axial energy of the HCI. Furthermore, a collision with a Be^+ ion will probably not trap the HCI, since some of the radial energy of the HCI may be converted into axial energy. The advantage of this scheme is that the HCI's axial energy is transferred to the power supply biasing the bottom trap and not to the Be^+ ions.

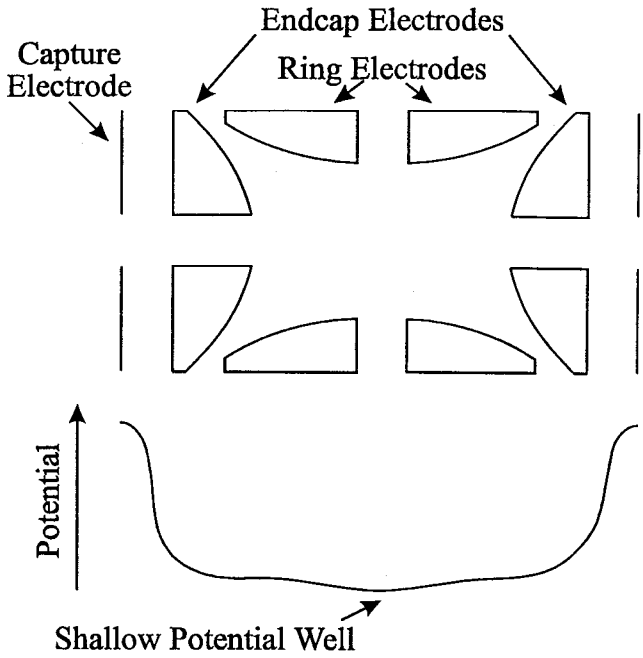

Figure 1) Schematic of RETRAP bottom hyperbolic trap and shallow potential well where Be^+ is confined.

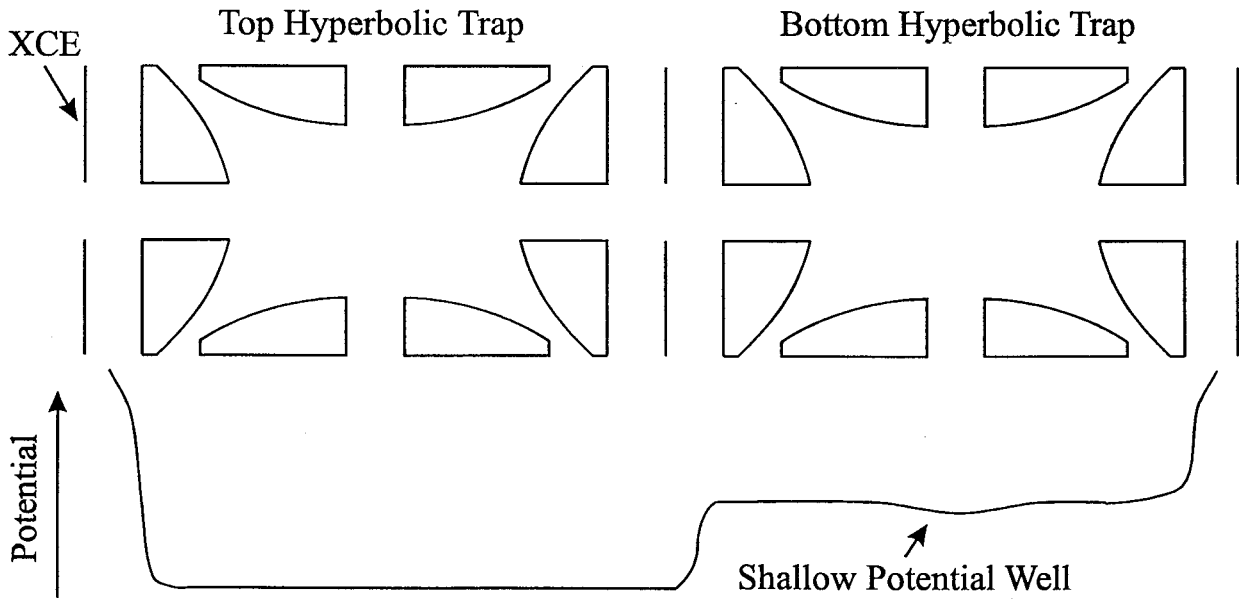

Figure 2) Schematic of both hyperbolic trap and potential with shallow well. XCE is the HCI capture electron.

1) A longer description of the new RETRAP trap is in: G. Weinberg, et al., "Electron Capture from H_2 to Highly-Charged Th and Xe Ions Trapped at Center-of-Mass Energies near 6 eV", accepted by Phys. Rev. A.

Capture of Xe^{44+} and Be^{2+} in the Same Trap

B.R. Beck, J. Steiger, L. Gruber, D. Schneider and D.A. Church*
Lawrence Livermore National Laboratory
*Texas A&M University

Laser cooled, singly charged ions have been trapped and cooled to very low temperatures (T < 5 mK), and crystal structures observed. Cooling highly charged ions (HCI) to low temperatures (T < 10 K) is more difficult since transitions in HCIs accessible by lasers are rare and have much lower cross-sections. Thus, sympathetic cooling of HCIs by laser cooled singly charged ions has been proposed to obtain cold HCIs. However, this scheme requires that the highly- and singly-charged ions be confined in the same trapping region. In this paper we show that highly charged ions of Xenon and Be^{2+} ions have been confined in the same trap. Furthermore, evidence showing sympathetic cooling of the highly charged ions of Xenon by the Beryllium ions is also presented.

Figure 1 shows the scheme used to capture the Xe^{44+} and Beryllium ions into the same trap. First, the Beryllium ions are captured into a hyperbolic trap by pulsing the capture electrode to ground and back. (The Beryllium ions are produce by a MEVVA, which produces both Be^{+} and Be^{2+} ions). The ring electrode potential is then ramped from 200V to -40V, trapping the Beryllium ions into the region of the ring electrode. The endcap potential was 500V. Next, a pulse of Xe^{44+} ions from EBIT is captured by again pulsing the capture electrode. A time t_D after the Xe^{44+} is captured, information about the trapped ions is determined by ramping the ions' axial oscillation frequencies sequentially through the tuned circuit resonance (see probing ramp in figure 1) while recording the tuned circuit signal. Figure 2 shows the tuned circuit signal where several highly charged states of Xenon are observed as well as Be^{2+}. Many charge states of Xenon are present because of charge exchange between the Xenon ions and a neutral background gas. The signal in figure 3 was recorded with the same trapping setup as that in figure 2, except that the MEVVA was not triggered. Hence, no Beryllium ions were produced, as indicated by the missing Be^{2+} signal. In figure 2 the Xenon charge states are resolved; whereas, they are not in figure 3. This is most likely due to the Xenon ions in figure 2 having a much lower temperature than the Xenon ions in figure 3. Signals (not shown) recorded for a mixture of Xenon and Beryllium ions taken with t_D = 1s show a Xenon signal similar to

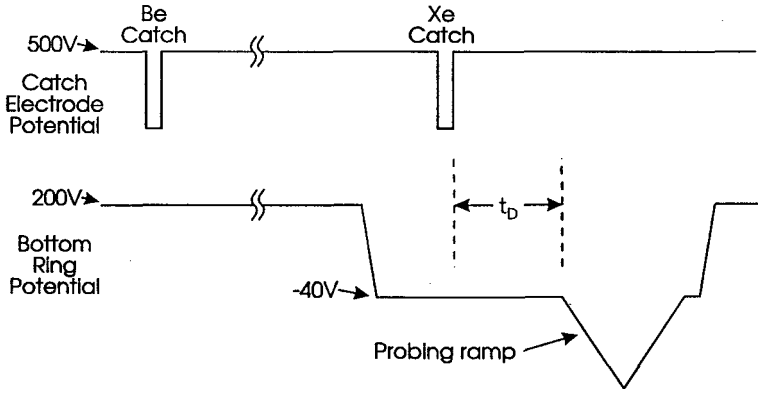

Figure 1) Schematic of catch and ring electrode potentials as a function of time.

that of figure 3. This data strongly indicates that the Xenon ions are being cooled by the Beryllium ions on a time scale of a few seconds.

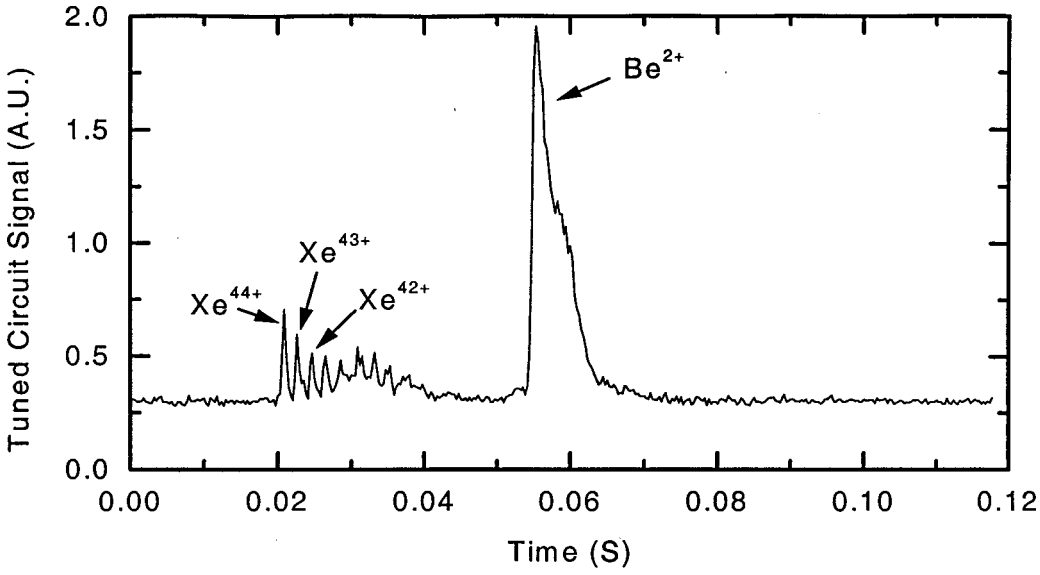

Figure 2) Tuned circuit signal with t_D = 10s, showing resolved signals of Xenon and Be^{2+} ions. The highest three charge states of Xenon are labeled.

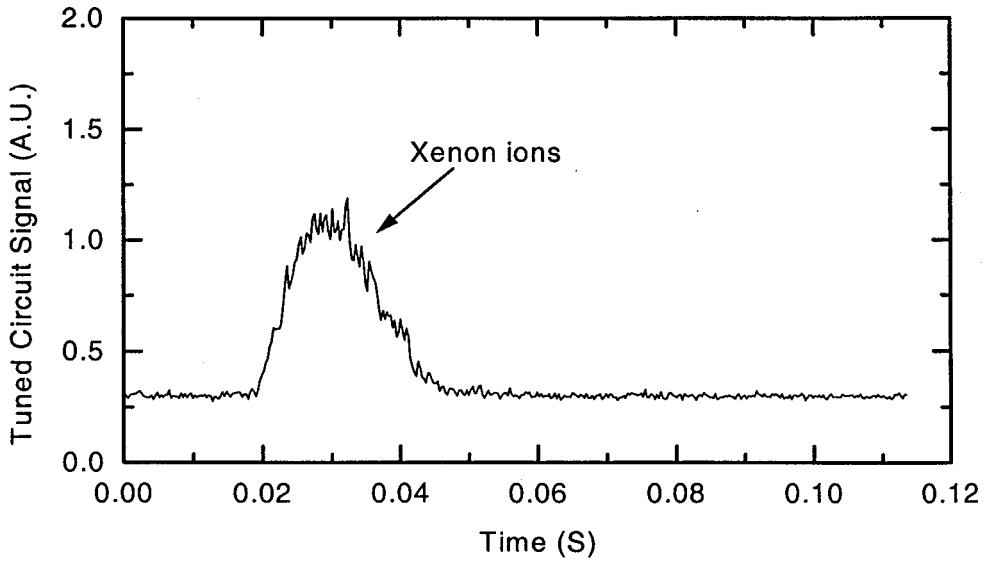

Figure 3) Tuned circuit signal with t_D = 1s, showing unresolved signals of Xenon ions. The MEVVA was not triggered for this data, hence there were no Beryllium ions trapped for this data set.

VI. Instrumental Development

An X-Ray Microscope Powered by Highly Charged Ions

R. E. Marrs, D. H. Schneider, and J. W. McDonald
Lawrence Livermore National Laboratory, Livermore, CA 94551

X-ray microscopy provides information unobtainable with visible-light microscopy due to the different absorption properties of x rays and the possibility of imaging smaller structures. As the capabilities of x-ray microscopes improve, they are becoming valuable tools in biology and materials science. Several different types of x-ray sources and techniques have been used to obtain microscopic images. In recent years synchrotron radiation has been used to obtain high quality x-ray images, and most synchrotron facilities have beam lines for x-ray microscopy. We are developing a "laboratory" x-ray microscope based on another type of x-ray source -- the radiation from slow highly charged ions as they radiatively deexcite at the surface of a target foil [1]. This novel x-ray source avoids several fundamental limitations of conventional x-ray sources, suggesting that it could eventually lead to an x-ray microscope with superior performance.

The key to the success of our x-ray microscope is the low emittance of the highly charged ion beams obtained from our EBIT. This allows the ions to be focused to very small spots. Several other properties of EBIT ions make them attractive for x-ray microscopy. The radiation yield during surface recombination is very high, up to 5% or more of the total ion energy depending on the ion species and incident energy. (In comparison, the radiation yield for electrons striking the anode of an x-ray tube is on the order of 10^{-3} - 10^{-4}, and anode heating is often a serious problem.) Unlike x-ray tubes, the recombination x-ray spectrum is bremsstrahlung-free and consists entirely of the characteristic line radiation of the incident ions. The x-ray energy can be selected by choosing an appropriate ion species. The range and scattering of slow highly charged ions is far less than that of electrons. In fact, radiative deexcitation occurs within a few nanometers of the target surface [2]; hence beam spreading does not limit the resolution.

The concept of our projection x-ray microscope is illustrated in Fig. 1. The magnification is given by $M = b/a$, where a is the distance from the x-ray source to the sample and b is the distance from the x-ray source to the CCD. The magnification is easily adjusted by varying the sample position. The resolution of the microscope is determined entirely by the size of the focused ion spot: 20 μm for the initial results described here.

An ion focusing column consisting of two einzel lenses was used to focus a beam of Ar^{18+} and Ar^{17+} ions onto a 125-μm-thick beryllium vacuum window that served as the x-ray production target. An electroformed nickel mesh with 70-μm wide lines on 500-μm centers was used to test the performance of the microscope. Argon K X rays in the energy range of 3 - 4 keV were produced from argon ions incident on the target at energies of 17q keV. The thickness of the nickel mesh was 4.7 μm, thick enough so that x-ray transmission through the mesh is small.

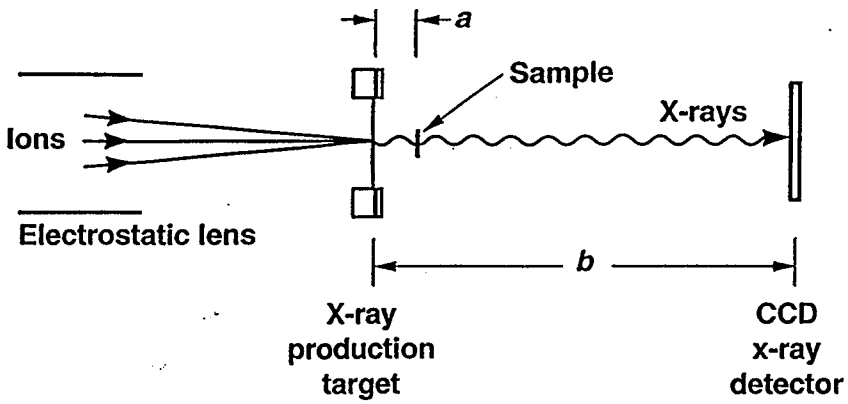

Fig. 1. Arrangement of the projection x-ray microscope using x rays from highly charged EBIT ions. A magnified radiograph of a sample is obtained by projection of its x-ray shadow onto a CCD camera.

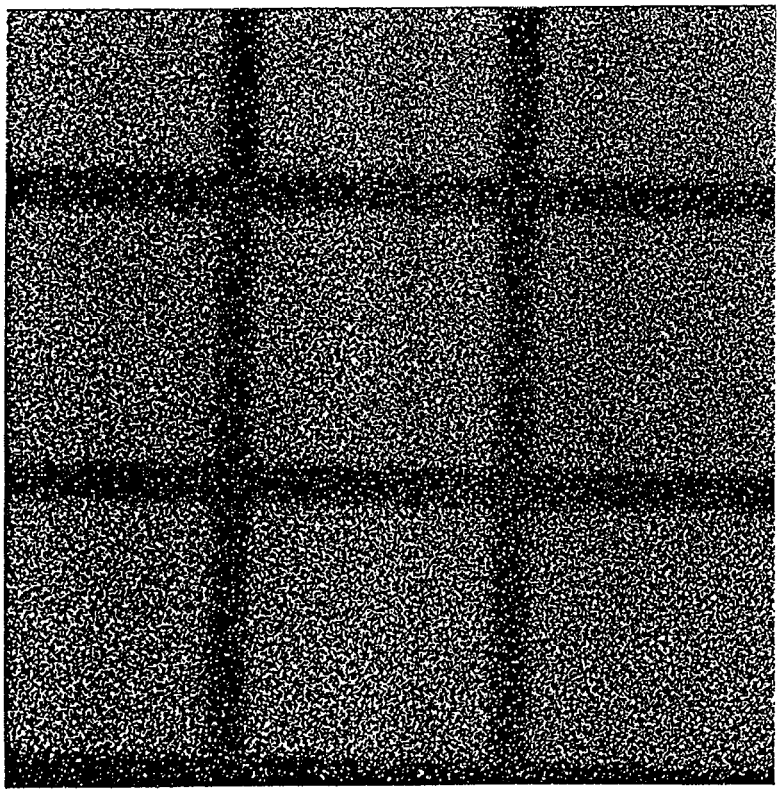

Fig. 2. Image of a nickel mesh with 3-keV x rays. The spacing of the mesh lines is 500 μm.

The microscope was set up directly above the EBIT in a vertical orientation. The nickel mesh was located 5 mm above the x-ray source, and the CCD was 50 mm above the x-ray source, giving a magnification of M = 10. An x-ray image of the nickel mesh from a two-hour exposure is shown in Fig. 2. The intensity of each pixel is the integral of the charge it collects from multiple x-ray events during the exposure time. The noise in the image is from x-ray photon statistics and could be reduced with a longer exposure time. The contribution of electronic noise from the CCD is negligible.

Inspection under a visible-light microscope confirmed that the profile of the nickel mesh lines was rectangular, so the blurring of the edges of the mesh lines in the x-ray image was used to obtain an estimate of the resolution of the x-ray microscope. Figure 3 shows a profile from one of the mesh lines of Fig. 2 obtained by averaging over 100 rows in the CCD image. Since the nickel-mesh sample was much closer to the x-ray source than the CCD, the resolution of the microscope is approximately equal to the width of the focused ion spot. If the focused ion spot has a Gaussian intensity profile with cylindrical symmetry, as expected, then each edge of a mesh line will have an error-function profile. The solid curve in Fig. 3 was calculated using a Gaussian beam profile with its width adjusted to fit the observed image. The resulting value for the diameter of the x-ray emitting spot is 20 μm FWHM. The resolution can be improved by tighter collimation of the incident ion beam.

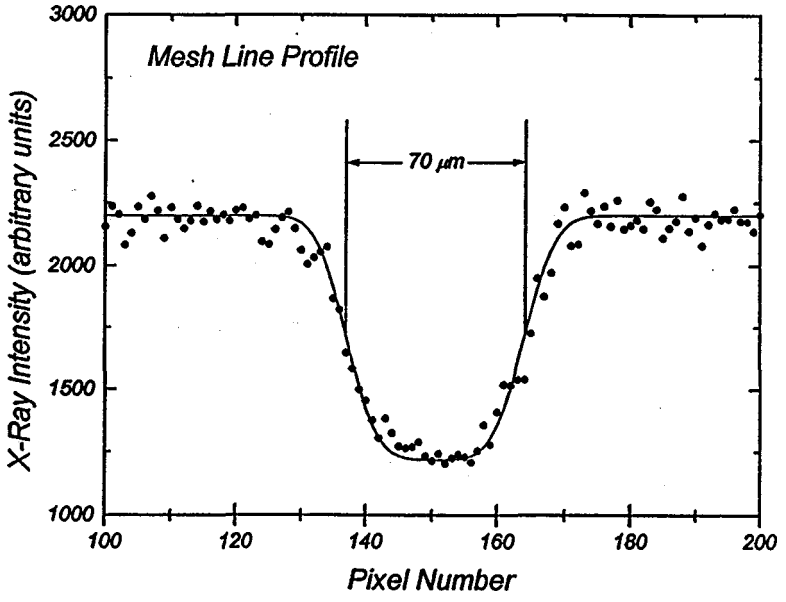

Fig. 3. Profile of one of the mesh lines in the image of Fig. 2. The solid curve is a fit with the x-ray source size adjusted to match the measured profile.

References

[1] R. E. Marrs, D. H. Schneider, and J. W. McDonald, Rev. Sci. Instrum. 69, 204 (1998).

[2] T. Schenkel, M. A. Briere, H. Schmidt-Böcking, K. Bethge, and D. H. Schneider, Phys. Rev. Lett. 78, 2481 (1997).

Implementation of a Very High Resolution Vacuum Crystal Spectrometer on EBIT

P. Beiersdorfer,[a] J. R. Crespo López-Urrutia,[a] E. Förster,[b]
J. Mahiri,[a,c] K. Widmann[a]
[a]*Department of Physics and Space Technology, Lawrence Livermore National Laboratory, Livermore, CA 94550, USA*
[b]*Max-Planck-Arbeitsgruppe Röntgenoptik, Friedrich-Schiller-Universität, D-07743 Jena, Germany*
[c]*Department of Physics, Morehouse College, Atlanta, GA 30314, USA*

Using very high-resolution spectrometers we showed that the temperature of the ions confined in an electron beam ion trap (EBIT) can be much lower than the energy of the electron beam used to produce and excited the ions. Temperatures as low as 60 eV was found for Cs^{45+} ions excited by 7.5-keV electrons [1]. The corresponding line widths are on the order of $\lambda/\Delta\lambda > 10{,}000$ so that very precise measurements can be made. The measurements were made using crystal spectrometers in the von Hámos geometry operating in a helium atmosphere [2]. These spectrometers were sensitive to x rays with wavelength less than 5 Å. In order to perform measurements with similar accuracy of low-Z ions which emit x radiation in the wavelength region above 5 Å, a very high resolution flat-crystal spectrometer was designed and built [3] that operates *in vacuo* . We have successfully implemented this spectrometer and obtained a resolving power that is more than an order of magnitude better than that of an existing [4] flat-crystal spectrometer. For the first time, very precise, high-resolution spectral measurements are now possible in the soft x-ray range above 5 Å.

The resolving power of a crystal spectrometer is given by $\lambda/\Delta\lambda = \tan\theta/\Delta\theta$, where $\Delta\theta$ represents the angular resolution of the instrument. An increase in the resolving power can be achieved in two ways, either by decreasing $\Delta\theta$ or by increasing $\tan\theta$. The angular resolution $\Delta\theta$ is a function of the spatial resolution of the detector, the source width, and the resolving power of the crystal, and generally is inversely proportional to the overall dimensions of the spectrometer. The resolving power of the spectrometer can thus be improved by increasing the overall dimensions of the instrument. The value of $\tan\theta$ can be increased by measuring at large Bragg angles. Especially desirable is to operate the spectrometer at Bragg angles approaching 90^o where $\tan\theta \rightarrow \infty$. In the design of our new high resolution flat-crystal spectrometer, we have implemented both options. We increased the overall dimensions of the spectrometer relative to that of an existing spectrometer [4] and modified the design to accomodate Bragg angles near 90^o.

Figure 1 shows a schematic of the new high-resolution flat-crystal spectrometer. The diffraction plane is oriented perpendicular to the electron beam. Easy alignment is achieved by rotating the crystal and position-sensitive detector around a common pivot point using a vacuum feed-through. The point of rotation is located at the far end of the entrance port, which makes it is possible to situate the detector at a Bragg angle as large as 85^o. Moving the point of rotation away from the entrance of the spectrometer also increases the distance between the EBIT source and the detector. In the present design, this distance is about 160 cm. A free-standing, 25-mm diameter foil is used to separate the spectrometer vacuum (5×10^{-6} torr) from the high vacuum of the EBIT vessel ($\sim 10^{-10}$ torr), and a by-pass pumpline (cf. Fig. 1) is employed during the evacuation of the

spectrometer to maintain nearly equal pressure on both sides of the foil. We use either a 1-μm polyimide foil or a 0.5-μm mylar foil. These foils are sufficiently thin to allow detection of x rays with energies as low as the carbon K-egde. The position-sensitive gas-filled detector has a spatial resolution of about 250 μm. Placing it 160 cm away from the EBIT source provides an angular resolution of $\Delta\theta = 1.6 \times 10^{-4}$ radians and corresponds to a nominal resolving power $\lambda/\Delta\lambda = 6400$ at a Bragg angle of 45°.

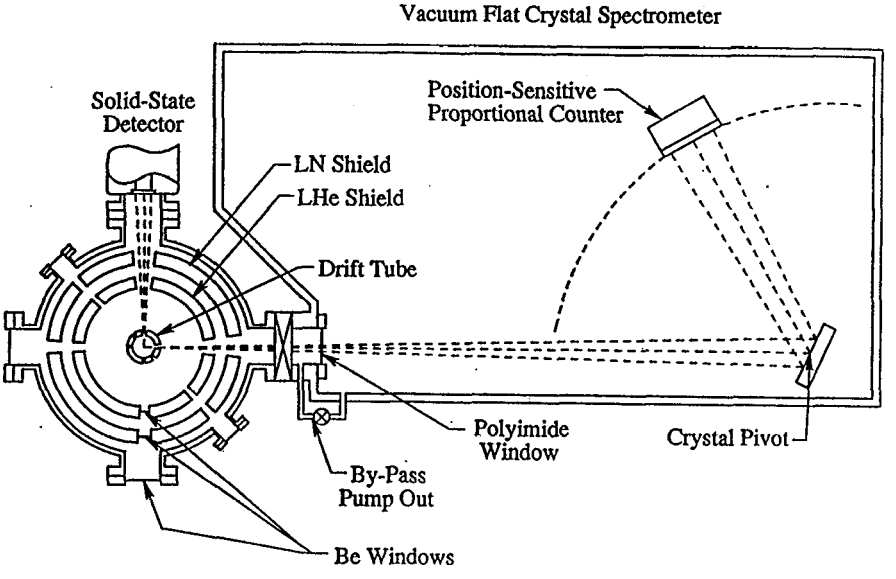

Fig. 1. Schematic layout of the new flat-crystal spectrometer on the EBIT facility. The electron beam direction is out of the page and represents a 60-μm-wide line source so that no entrance slit is needed. Crystal and detector rotate about a common pivot point at the opposite end of the entrance port. This permits setting the detector to Bragg angles as large as 85°.

To illustrate the performance of the new spectrometer a measurement of the $2p_{1/2}$, $2p_{3/2} \longrightarrow 1s_{1/2}$ (Ly-α_1 and Ly-α_2, respectively) transitions in hydrogenic Mg^{11+} was made. The transitions are situated at $\lambda =$ 8.42461 and 8.41920 Å, respectively. For the measurement we used a 2 x 4-cm^2 quartz(100) crystal with a lattice spacing 2d = 8.5099 Å. The spectrometer was adjusted to a nominal Bragg angle of 81.7° and the detector placed 25 cm away from the crystal. The distance between EBIT and the crystal was about 93 cm. The nominal resolving power at this Bragg angle thus was better than 30,000. The spectrum recorded with the new instrument is shown in Fig. 2. The two Ly-α lines are completely resolved. By contrast, we measured the same lines with the existing flat-crystal spectrometer. The resulting spectrum is also shown in Fig. 2. For this measurement we used a 2.5 x 5-cm^2 ammonium dihydrogen phosphate (ADP) crystal cut to the (101) plane with a lattice spacing 2d = 10.65 Å. The corresponding Bragg angle was 52°. In this measurement, the two Ly-α lines are not resolved, although a slight asymmetry can be noted. The comparison between the two spectra in Fig. 2 illustrates the dramatic differences in resolving powers. The two Lyman components are clearly resolved. In fact, the resolving power of the spectrometer is sufficiently high that from the observed linewidth we were able to infer a temperature of 246±20 eV for the Mg^{11+} ions.

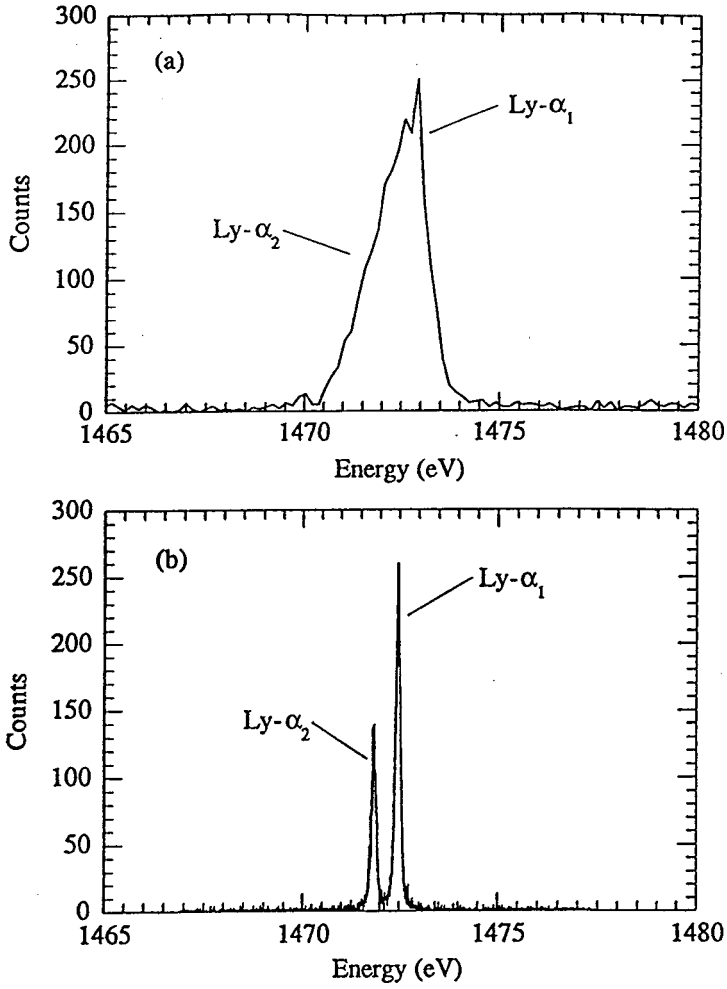

Fig. 2. Spectra of the $2p_{1/2}$,—> $1s_{1/2}$ Ly-α_1 and $2p_{3/2}$ —> $1s_{1/2}$ Ly-α_2 transitions in hydrogenic Mg^{11+}. The top spectrum was recorded with the existing EBIT flat-crystal spectrometer using an ADP (101) crystal at a Bragg angle of 52°. The bottom spectrum was recorded with the new EBIT flat-crystal spectrometer using a quartz (100) crystal at a Bragg angle of 82°.

References:

[1] P. Beiersdorfer, A. L. Osterheld, V. Decaux, and K. Widmann, Phys. Rev. Lett. 77, 5353 (1997).

[2] P. Beiersdorfer, R. E. Marrs, J. R. Henderson, D. A. Knapp, M. A. Levine, D. B. Platt, M. B. Schneider, D. A. Vogel, and K. L. Wong, Rev. Sci. Instrum. 61, 2338 (1990).

[3] P. Beiersdorfer, J. R. Crespo López-Urrutia, E. Förster, J. Mahiri, K. Widmann , Rev. Sci. Instrum. 68, 1077 (1997).

[4] P. Beiersdorfer and B. J. Wargelin, Rev. Sci. Instrum. 65, 13 (1994).

The work was supported by the NASA X-Ray Astronomy Research and Analysis Program under grant NAGW-4185 and in part by the Lawrence Livermore National Laboratory Collaborations Program for Historically Black Colleges and Universities.

Investigation of Electron Beam Structure as Affected by the Beam Current and Beam Energy

S. Utter, P. Beiersdorfer, J. Crespo López-Urrutia, K. Widmann
Department of Physics and Space Technology, Lawrence Livermore National Laboratory, Livermore, CA 94551

A. J. Smith
Department of Physics, Morehouse College, Atlanta, GA 30314

The width and position of the electron beam is a critical EBIT parameter. For a given current, a small width means higher electron density and, thus, faster ionization times and higher excitation rates. Because spectroscopic instrumentation both in the X-ray and optical regimes operates slitless and uses the beam as an effective slit [1,2], the beam width also represents one of the limiting parameters for the resolving power of our spectrometers. Along the same lines, a shift in the position of the beam is reflected in a corresponding shift in position of an observed spectral line. A study of the width and position of the electron beam is thus of critical importance.

We have made a study of the beam radius and position as a function of electron beam current, I_{beam}, and electron beam energy, E_{beam}. The measurements were performed using a permanent slit on one viewing port of Super-EBIT. The slit consists of two parallel, platinum plated cylinders separated by 8 μm. The distance between the electron beam and the slit is 1.81 cm [3]. The beam image was obtained by observing X-rays emitted by trapped ions with a position sensitive proportional counter set a distance of 102 cm from the slit, yielding a magnification of 56x. A typical beam image is shown in Fig. 1. The profile is fit best with a Lorentzian fit.

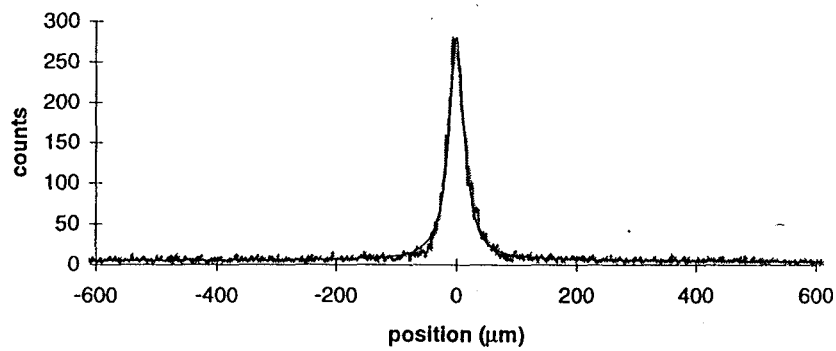

Fig. 1. Beam image as obtained with a position-sensitive proportional counter. The image is overlaid with a Lorentzian line profile.

The result of a measurement of the electron beam radius as a function of I_{beam} is shown in Fig. 2(a). For these measurements the E_{beam} = 136 keV. The measured 80% beam radius increased with current ranging from 27.1 ± 1.2 μm at a current of 90 mA to 32.3 ± 0.8 μm at a current of 230 mA. Fig. 2(b) shows the effect of I_{beam} on the line position. As can been seen, the position of the line center is steady, varying only on the order of one-half channel, or equivalently 1.1 μm during these measurements. This variation is fully compatible with statistics.

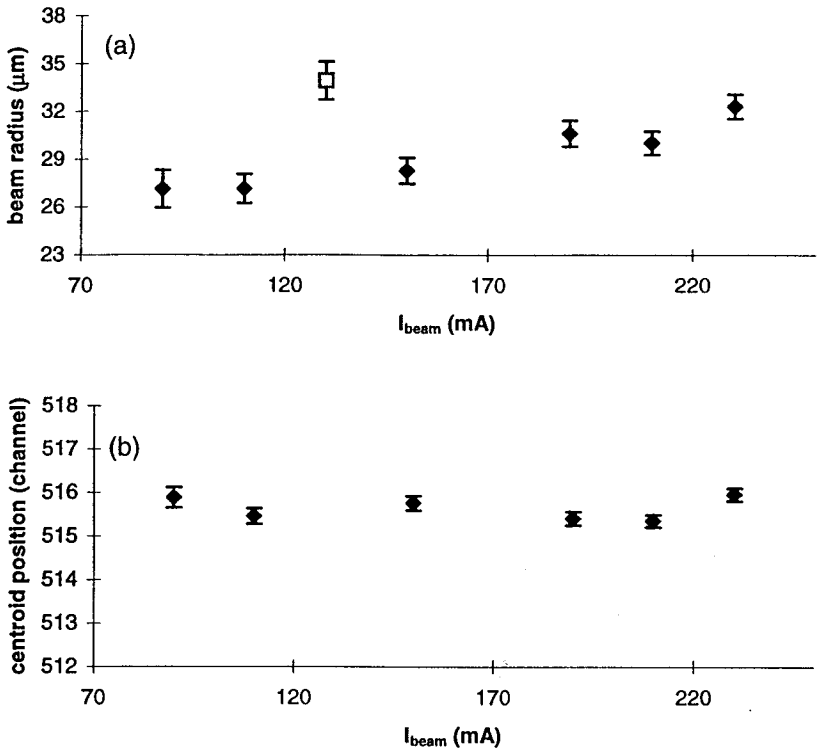

Fig. 2. (a) Plot of electron beam radius as a function of I_{beam}. The energy of the beam is 136 keV. The square represents the beam radius as determined in 1993 by Knapp *et al.* , Ref. [3]. (b) Plot of centroid line position as a function of I_{beam}. One channel corresponds to about 2.2 μm.

Similar measurements were made with I_{beam} held constant for various beam energies. Because the Super-EBIT device parameters are very sensitive to the E_{beam}, re-tuning, i.e., alignment of the electron beam along the trap, which may affect the electron beam structure, was required for each successive energy. For I_{beam} = 150 mA the energy was set to 166 keV, 145 keV, and 125 keV, successively. The noted trends are that the line position was steady, varying about 2.4 μm, which is again compatible with statistics. The line width increased with decreasing energy from around 50 μm at 125 keV to 30 μm at 166 keV.

References

[1] P. Beiersdorfer, R. E. Marrs, J. R. Henderson, D. A. Knapp, M. A. Levine, D. B. Platt, M. B. Schneider, D. A. Vogel, and K. L. Wong, Rev. Sci. Instrum. **61**, 2338 (1990).

[2] J. R. Crespo López-Urrutia, P. Beiersdorfer, D. W. Savin, and K. Widmann, Phys. Rev. Lett. **77**, 826 (1996).

[3] D. A. Knapp, R. E. Marrs, S. R. Elliot, E. W. Magee, and R. Zasadzinski, Nucl. Instrum. Methods Phys. Res., Sect. A **334**, 305 (1993).

This work was supported in part by the Lawrence Livermore National Laboratory Research Collaborations Program for Historically Black Colleges and Universities.

X-ray Analysis of the Magnetic Trapping Mode of an Electron Beam Ion Trap

P. Beiersdorfer[1], L. Schweikhard[2], K. Widmann[1]
[1]*Lawrence Livermore National Laboratory, Livermore, CA 94550*
[2]*Gutenberg Universität, D-55099 Mainz, Germany*

The properties of the EBIT facility as a trap have been analyzed both theoretically and experimentally in the context of ion confinement in the presence of an electron beam. In fact, the electrostatic fields of the electron beam are an integral part of the EBIT design to provide ion confinement in the radial direction. By contrast, the trapping properties in the absence of the electron beam, which in principle are irrelevant to the performance of the EBIT facility as a spectroscopic or ion source, have not been investigated. In the absence of the electron beam, ions should continue to be confined in the radial direction by the presence of a strong axial magnetic field (typically 3 T) used to compress the electron beam. Moreover, the ions are confined axially by the potential applied to the end electrodes of the cylindrical trap (typically 10–500 V), even under standard operating conditions. It should thus be possible to operate the EBIT facility as a trap facility after the electron beam is turned off. This mode of operation of an EBIT, which we refer to as the "magnetic trapping mode" and in which we operate the EBIT like a Penning trap was demonstrated in Fourier transform ion cyclotron resonance (FT-ICR) mass spectrometry studies [1-4]. It had been shown that the ions persist in the trap for a minimum of 1.5 seconds after the electron beam had been turned off. Moreover, these measurements showed that the composition of the ions trapped in the magnetic mode matches that just before the beam is turned off. Because ions were prepared *in situ* during the electron trapping mode there was no need to fill the trap externally. Losses associated with the transport of ions and filling a trap were thus avoided.

We have now also characterized the magnetic mode of operation with x-ray spectroscopic means [6] and demonstrated its utility for the spectroscopy of highly charged ions. In the absence of an electron beam, photons are produced solely by capture from ambient neutrals in the trap. Monitoring the resultant x rays emitted as a function of time after turning off the electron beam (cf. Fig. 1) enabled us to determine the ion storage times in the magnetic mode. Ion storage times up to 5 s were found (cf. Fig. 2) as the trap depth was varied. For highly charged xenon ions, we determined trapping times in excess of 20 s [6].

Novel types of spectroscopic measurements are enabled by use of the magnetic trapping mode. These include measurements of radiative decay rates of very long-lived metastable levels; measurements of the 1s ionization potentials of the recombining ions important for QED determinations; ion-neutral interactions at very low collision energies. The spectroscopic measurements enabled by the magnetic mode thus extend and complement those enabled by the electron trapping mode and thus greatly enhance the utility of the EBIT device for atomic physics measurements.

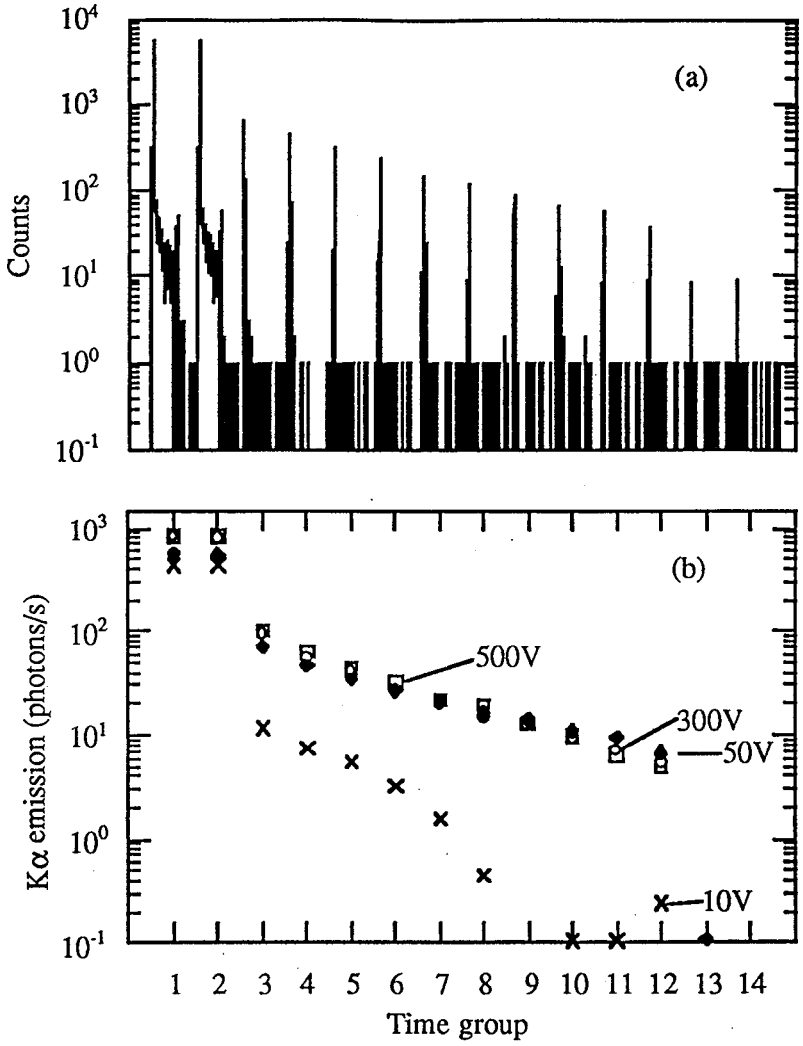

Fig. 1. Evolution of the x-ray emission of highly charged krypton as the trap was switched from electron to magnetic trapping: (a) time series of x-ray spectra recorded with a germanium detector; (b) intensity of the observed Kα emission for different values of the externally applied axial trapping potential. A series of 14 time groups per filling of the trap were recorded with a one second duration each. The trap is operated in the electron trapping mode in time groups 1 and 2, and in the magnetic trapping mode in time groups 3 through 12. The externally applied trapping potentials are off in time groups 13 and 14. Different values of the externally applied axial trap potential V_{ax} are indicated in (b): 10 V (crosses), 50 V (solid diamonds), 300 V (open circles), and 500 V (open squares).

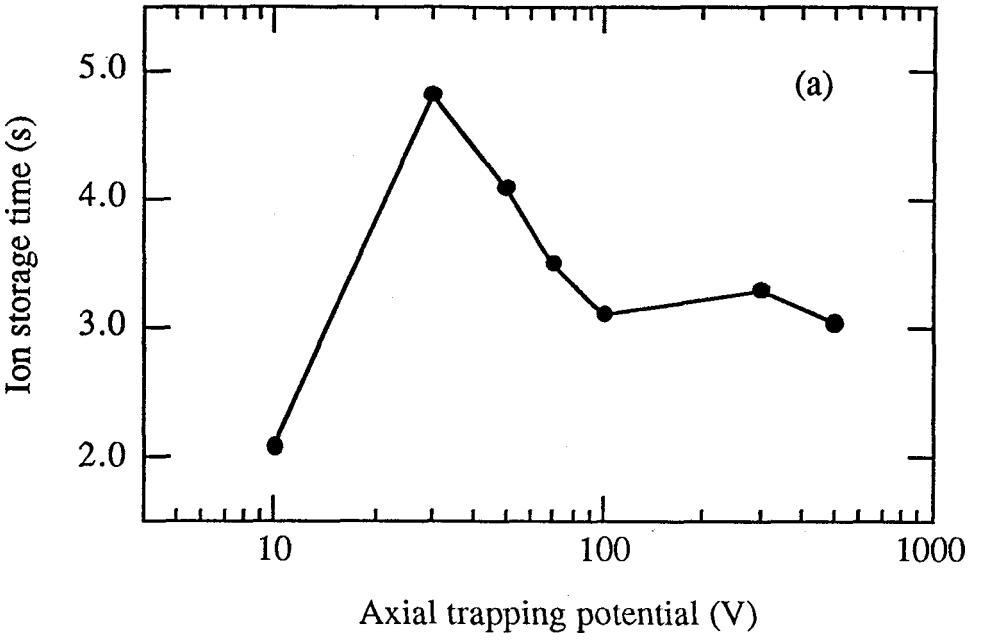

Fig. 2. Effect of the applied axial trapping potential (a) on the ion storage time in the magnetic trapping mode and (b) on the intensity of the Kα emission during the electron trapping mode (solid squares) and the magnetic trapping mode (solid circles).

References:

[1] P. Beiersdorfer, B. Beck, R. E. Marrs, S. R. Elliott, and L. Schweikhard, Rapid Commun. Mass Spectrom. **8**, 141 (1994)

[2] P. Beiersdorfer, St. Becker, B. Beck, S. Elliott, L. Schweikhard, and K. Widmann, Nucl. Instrum. Meth. in Phys. Research **B98**, 558 (1995)

[3] L. Schweikhard, J. Ziegler, P. Beiersdorfer, B. Beck, St. Becker, S. Elliott, Rev. Sci. Instrum. **66**, 448 (1995).

[4] P. Beiersdorfer, B. Beck, St. Becker, and L. Schweikhard, Intern. J. Mass Spectrom. Ion Proc. **157/158**, 149-161 (1996).

[5] P. Beiersdorfer, L. Schweikhard, J. Crespo López-Urrutia, and K. Widmann, Rev. of Scientific Instruments **67**, 3818-3826 (1996).

This work was supported by NATO Collaborative Research Grant CRG-930125.

X-Ray Measurements of Electron Beam Compression in a Magnetic Field

R. E. Marrs and A. Schach von Wittenau
Lawrence Livermore National Laboratory, Livermore, CA 94551

The propagation and confinement of electron beams in high axial magnetic fields is a basis for many different kinds of devices. Examples include klystrons, traveling wave tubes, and gyrotrons for the generation of microwave power, and electron coolers for particle storage rings. The highest magnetically confined electron beam current densities are found in the electron beam ion trap (EBIT), and the amount of electron beam compression in these devices is probably the most important parameter for determining their performance. Unfortunately, the measurement of the properties of magnetically compressed electron beams at very high intensity is difficult, and few results have been reported.

We have been using an x-ray imaging technique to measure the profile of magnetically compressed electron beams [1]. Our goal is a comprehensive understanding and analysis of the combined results from two different devices that together span a decade of magnetic field strength from 0.3 to 3.2 T. One of the devices, an electron gun test stand, uses a room-temperature magnet [1]. It has been used with two different EBIT-type electron guns at fields of 0.3 and 0.5 T. The other device is our original EBIT (since converted to Super EBIT). It was operated at fields of 1.6 and 3.2 T with our "standard" electron gun, and measurements of both compression and rotation of the electron beam were obtained [2]. In this report we summarize the beam compression measurements with both the EBIT and the test stand using the standard EBIT electron gun.

In our experiments, each beam electron follows a single particle trajectory determined by the applied magnetic fields and electrostatic potentials, the space charge of the beam, and the initial electron temperature at the cathode. Complete calculations of the electron beam envelope and the current distribution within it are not easy due to the multiple processes that affect the electron trajectories. For example, rippling of the beam envelope (i.e., oscillation of the beam radius) may occur at the transition between electrostatic and magnetic focusing at the exit of the electron gun. These ripples may or may not be damped out farther downstream by electron thermal motion.

The maximum electron beam compression that can be obtained in a magnetic field without space-charge neutralization by positive ions is known as Brillouin flow. It occurs when the space charge and centrifugal forces acting on each electron are exactly balanced by the $\mathbf{v} \times \mathbf{B}$ force of the magnetic field. Perfect Brillouin flow requires zero cathode magnetic field, laminar electron flow (i.e. no trajectory crossing and zero electron temperature), and electron optics that avoid rippling of the beam envelope. In our EBIT, the actual current density is about ten times less than the Brillouin limit due to the effect of finite electron temperature. A theory of magnetic beam compression that accounts for both finite electron temperature and cathode magnetic field has been developed by Herrmann [3]. We expect this theory to apply for the conditions of the present work.

Our standard EBIT electron gun operates at beam currents up to roughly 200 mA. The magnetic field on the cathode of the electron gun and its gradient at the exit of the electron gun are determined by the current in a bucking coil, a steel shim plate, and the fringing field of the main magnet. The gun was mounted on the EBIT and the test stand so that the fringing field (and its gradient) at the gun location is the same for both setups. With the electron-gun bucking coil turned off, a field of approximately 1 kG is produced at the cathode by the fringing field of the main magnet. In the present work the electron-gun bucking coil current was varied to obtain small ($\leq$ 100 gauss) cathode fields of either polarity in order to measure the effect of cathode field on beam compression.

The electron beam current profile in the peak magnetic field was measured by imaging x-ray emission with a narrow slit located close to the electron beam. The x-ray emission is produced by electron collisions with neutral gas atoms or ions trapped by the space charge of the electron beam. The slit was oriented parallel to the electron beam, and its width was much smaller than the beam diameter. A position sensitive proportional counter was used to detect the projected x-ray image. An example of the measured electron beam profiles for the EBIT is shown in Fig. 1. The upper profile, obtained at near-zero cathode field, corresponds to maximum beam compression. The broadening effect of a nonzero cathode field is clearly seen in the bottom profile.

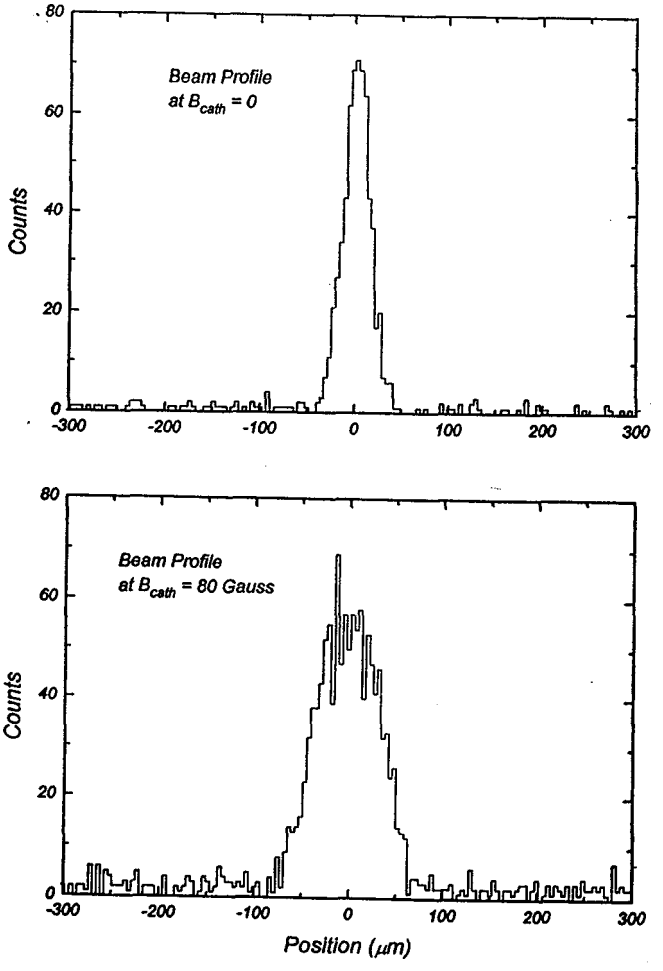

Fig. 1. Electron beam profiles observed at B_0 = 3.2 T for two different values of cathode magnetic field.

The measured beam radius (defined as the radius that encloses 80% of the current) for the EBIT operating at 3.2 T is compared to the Herrmann theory in Fig. 2. using an initial electron temperature equal to the cathode brightness temperature of 0.12 eV. The measured beam radius is approximately 75% of the Herrmann-theory prediction, a result that is probably explained in terms of the overlap of the electron and trapped-ion distributions. Further analysis of the measurements is in progress.

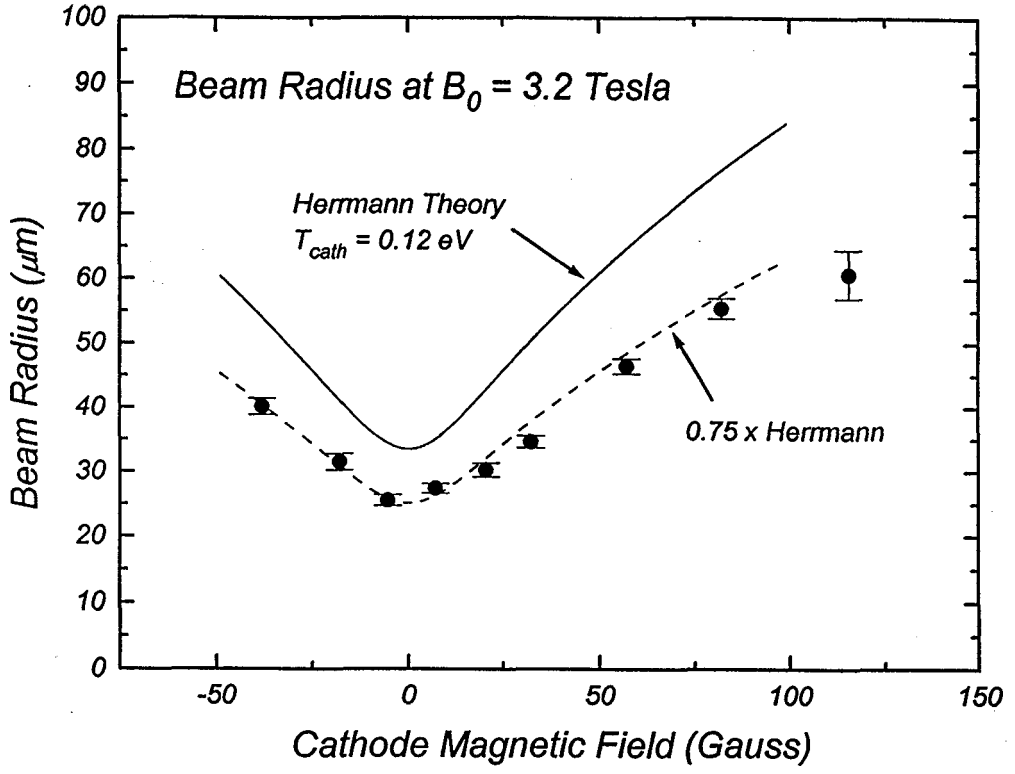

Fig. 2. The 80%-current electron beam radius as a function of cathode magnetic field for a 70-mA electron beam at 6.15 keV.

References

[1] EBIT 1995 Annual Report, pg. 95.
[2] R. E. Marrs and J. R. Henderson, unpublished.
[3] G. Herrmann, J. Appl. Phys., 29, 127 (1958)

A New Beamline for RETRAP and the Surface Chamber

J. Steiger, J. McDonald, L. Gruber, B. R. Beck, D. H. Schneider
Lawrence Livermore National Laboratory

For some solid state applications (exposures) and especially for RETRAP the number of ions which can be extracted from EBIT and transported to the experiments should be as high as possible. So far this number was not limited by the production of ions in EBIT but rather by the poor transport conditions in the beamline. The electrostatic cylindrical condensors used for bending the beam have focusing properties in only one direction with a focal point inside the bender. The result is a strongly divergent beam in one dimension. To overcome this difficulty a single quadrupole lens has been placed behind each bender (3 total) to get a beam with a more circular cross section. In addition the size of all lenses and steering elements has been enlarged to ensure that no ions are hitting these elements.

The beam profile was measured at the end of the RETRAP beamline by impinging the ions directly onto a CCD chip (Fig. 1). The beam had an elliptic cross section with main axes of 2.2 mm and 1.5 mm respectively.

EBIT can be operated as a source in two modes, continuously and pulsed where the pulse length can be varied from ~ms down to a few μs. The mode of operation depends on the application; for retrapping the highly charged ions are extracted in a short pulse containing as many ions as possible is feasible. Pulse lengths as short as 4 μs have been achieved by a fast ramp of EBIT's middle drift tube. The number of ions in such a pulse was determined by measuring the accumulated charge when the ions hit the first dynode of an open electron multiplier placed at the very end of the beamline. The dynode could be biased positively to prevent the escape of secondary electrons. As many as $4 \cdot 10^4$ Xe^{44+} ions have been observed in a 5 μs pulse, leading to a density of $8 \cdot 10^3$ ions/μs, a considerable improvement when compared to the density of 20 ions/μs achieved before the upgrade of beamline.

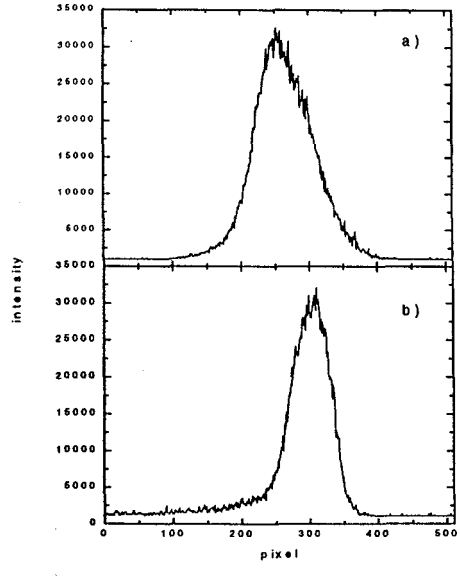

Fig. 1: Beam profile as seen by a CCD camera. The ions were directly hitting the CCD chip. Part a) of the figure shows a vertical cut through the center of the beam whereas b) shows a horizontal cut. The widths are 2.4 mm and 1.5 mm. The pixel size is $27 \cdot 27$ μm^2.

X-ray Verification of Extracted Ion Charge State from Super EBIT

J. W. McDonald, and D. H. G. Schneider
Lawrence Livermore National Laboratory, Livermore, CA 94550

J. P Briand, G. A. Machicoane , and V. Leroux
Laboratoire de Physique Atomique et Nucl'eair-Institut du Radium, Universite' Pierre et Marie Curie, Paris Cedex 05, France

As a highly charged ion approaches a solid surface electrons from the surface are captured into high-lying Rydberg states. Because of the short interaction distances and the velocity of the approaching ions there is insufficient time for electrons in these outer Rydberg states to decay into the inner shells before the ion impacts the surface. As a result the approaching ions, which can be fully neutralized, are left with inner shell vacancies. Ions or atoms in this condition are designated "Hollow" atoms and have been the focus of many investigations in the past few years.

"Hollow" atom studies by means of characteristic x-ray emission measurements have been performed at EBIT for a variety of ions. In order to study higher Z ions with higher charge states ions were extracted from Super-EBIT. These first measurements also served as a verification of the charge state of the extracted ions. In the experiment Xe^{q+} ($33 \leq q \leq 53$) ions were extracted from Super-EBIT, momentum analyzed and focused onto a SiO_2 target while the x rays were collected by a Ge(Li) detector. Figure 1 shows x ray emission following radiative deexciation of hollow atoms at energies consistent with the K-Shell vacancies of xenon. The absence of these K-Shell x rays in the next lower charge state verifies the identification of the extracted ion spectra presented in Figure 2.

The Xe^{53+} and Xe^{54+} ion beams were decelerated to less than a few 10 eV/q kinetic energies over metal and insulator surfaces. The hollow atoms formed and decaying above these surfaces have been observed in x ray spectroscopy with Ge(Li) detectors and have been separated from the ions which decay after surface contact. It has been found for impinging Xe^{53+} ions that, like for Ar ions, the emission of the x rays above the surface mainly occur at a time when the ion has lost all the captured electrons but one and is in a singly excited He-like state.

The extracted Xe^{53+} ion beam has been sent onto Au and SiO_2 targets at 8.5 keV/q initial kinetic energy. The x ray spectra have been compared to multiconfiguration Dirac Fock calculations. A detailed analysis of the energy and relative intensity of the Lyman $\alpha, \beta, \gamma, \delta, \varepsilon...$ lines leads to the following conclusions:

(i) below the surface the electrons are captured into the highest available states of a Xe ion inside a solid (i.e., the O, P,... shells)

(ii) these ions own much more than 35 excited electrons (the most excited atomic state observed to date)

(iii) the KL^x characteristic x ray satellite pattern is strongly peaked on the KL^2 line in agreement with the expected Z^{-4} law of variation of the K lifetime

(iv) similar spectra have been observed for the Au and SiO_2 targets

Similar measurements with U^{q+} ($82 \leq q \leq 90$) have been performed and L-Shell x ray emission was observed. Figure 3 shows x ray emission following radiative deexciation of hollow atoms at energies consistent with the L-Shell vacancies of uranium.

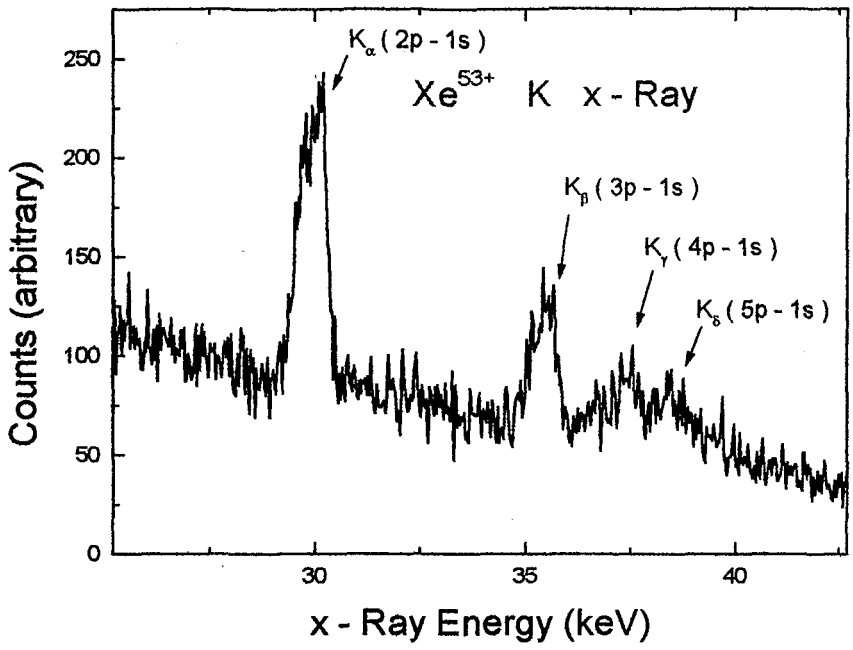

Figure 1. X-ray spectrum following Xe^{53+} impact on a native oxide covered Si wafer.

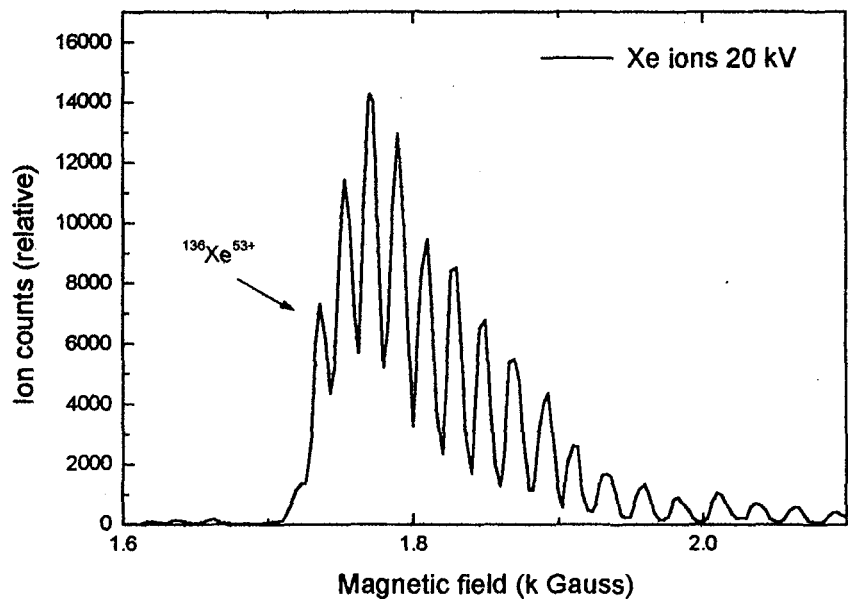

Figure 2. Super EBIT Extracted Xe^{q+} ($33 \leq q \leq 53$).

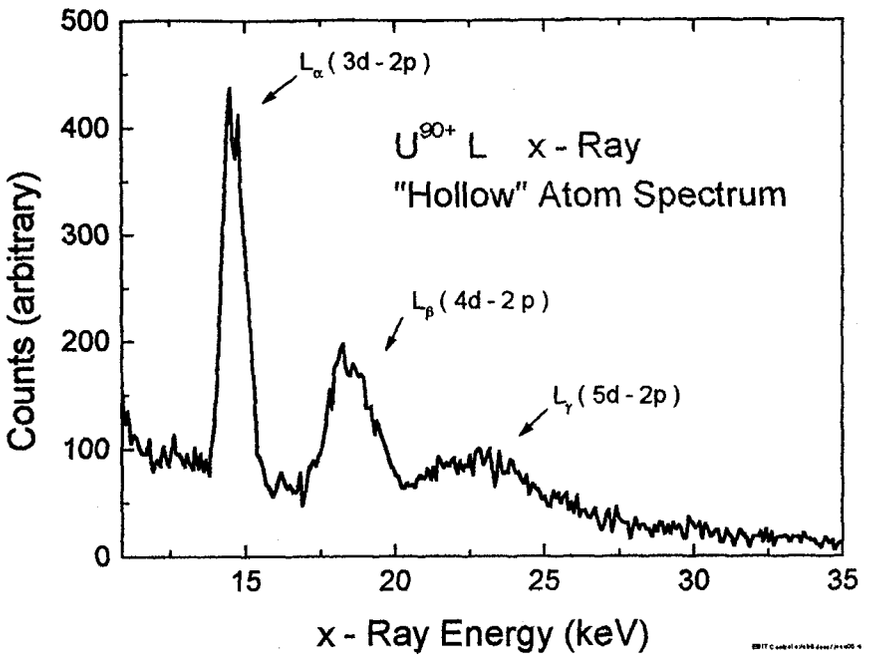

Figure 3. X-ray spectrum following U^{90+} impact on a native oxide covered Si wafer.

Charge Balance Versus Extraction Mode of EBIT

J. W. McDonald and D. H. G. Schneider
Lawrence Livermore National Laboratory, Livermore, CA 94550

The LLNL EBIT has been used to study the differences in charge state balance for highly-charged ions extracted in two modes. The extraction of highly-charged ions from EBIT has been described in detail[i]. During normal operation an axial trap is produced by three drift tubes, as is shown in Figure 1. Typical potentials applied to these drift tubes are 500, 250, and 350 for the bottom, middle, and top respectively. The two extraction modes described here are the leaky mode and slow extraction mode. In the leaky mode ions evaporate out of the trap formed by the potential of the three trap electrodes and the electron beam. In the slow extraction mode the potential of the middle drift tube is raised above that of the top drift tube and the trapped ions spill out of the trap at the potential of the top drift tube. See figure 1.

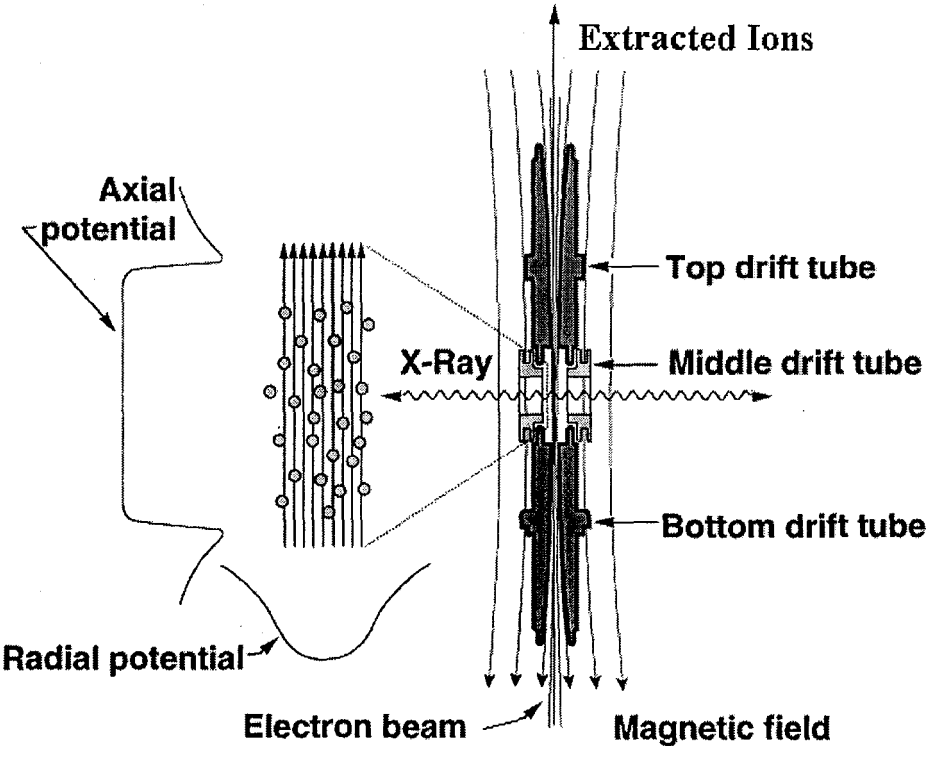

Figure 1. EBIT Drift Tubes and Potential Wells.

A comparison of the two extraction modes is shown in Figure 2. The ion counting circuit was gated to the ion extraction time in both modes. With the exception of the pulsing of the middle drift tube all EBIT system parameters were held constant during

the two measurements. The ions are trapped in the axial potential well with potential q e V where q is the ion charge state, e is the electron charge, and V is the axial or radial potential. Therefore the trapping efficiency is directly proportional to the charge of the trapped ion. As can be seen from the figure ions with lower charge states evaporate out of the trap in larger numbers than the ions with higher charge states. In the pulsed mode of extraction ions with higher charges that are trapped more efficiently are forced out of the trap resulting in a larger population of higher charged ions in the pulsed mode of extraction.

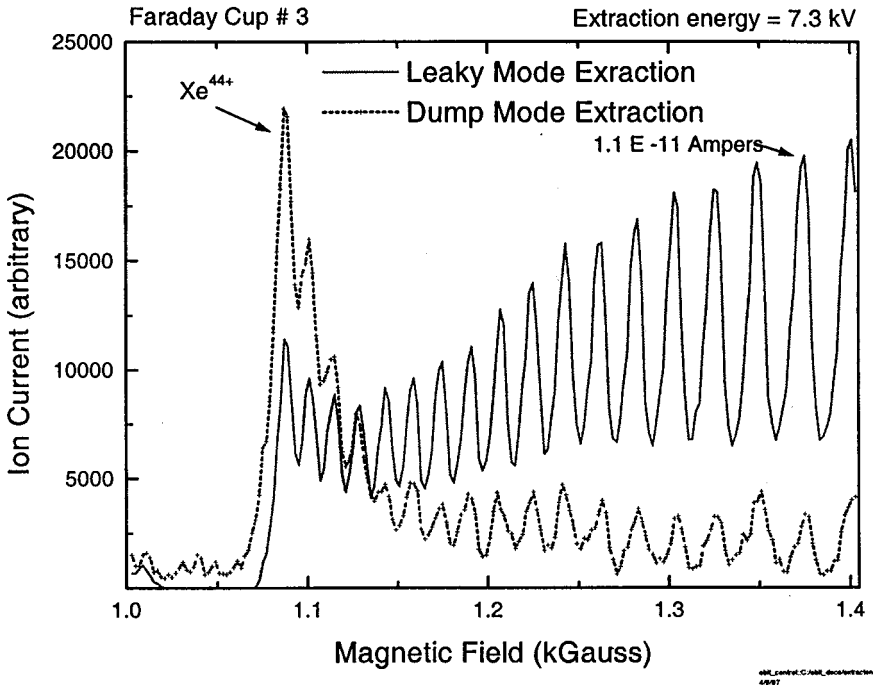

Figure 2. Extracted Ions from EBIT in the Pulsed and Leaky modes.

[i] D. Schneider, M. Clark, B. Pentrante, J. McDonald, D. Dewitt, N. Bardsley, Phys. Rev. A, **44** (1991) 3119

Fast Extraction Mode of EBIT

J. W. McDonald, J. Steiger, and D. H. G. Schneider
Lawrence Livermore National Laboratory, Livermore, CA 94550

The fast extraction mode is essential for the retrapping of ions in a secondary ion trap. The ions are decelerated from 7 keV/q to ≈ 200 eV/q by reducing the potential on a decelerating tube at the input of the trap, while the ions are in transit[i]. The trapping efficiency depends on how many ions are in the deceleration tube when the potential is lowered. The trapping efficiency also depends on the ion temperature and the transverse temperature in particular. It has been established that the momentum spread of the extracted ions can be reduced substantially by reducing the electron current without significant loss of ion intensity. Electron beam currents of 90 mA or less are used in the fast extraction mode. The extraction of highly-charged ions from EBIT has been described in detail[ii]. In the fast extraction mode the potential of the middle drift tube is pulsed above that of the top drift tube thereby forcing the trapped ions out of the trap. The middle drift tube can be raised in as little as 12 μsec producing ion pulse widths as short as 10 μsec.

A typical fast extraction mode measurement is shown in figure 1. The bottom waveform in this figure is obtained by connecting a Faraday cup directly to a one Meg. Ohm input of an oscilloscope. The rise time of the waveform is indicative of the pulse width of the ion signal and is 10 μsec here. The RC decay time of the ion pulse can be used to find the capacitance of the circuit $C = {}^{t}/_{R}$. The charge deposited is given by, $q = \frac{CV}{e\beta}$. For the case presented here of Xe^{44+} Figure 1 yields values of V = 2.75 E -3 Volts, RC_{time} = 2.875 E-3 sec. The input resistance of the oscilloscope is R = 10^6 Ohms. The constant β accounts for the multiplicity of electrons that are emitted for each highly-charged ion for the case of Xe^{44+} ions β = 200. This measurement yields 5500 Xe^{44+} ions in the 10 μsec pulse.

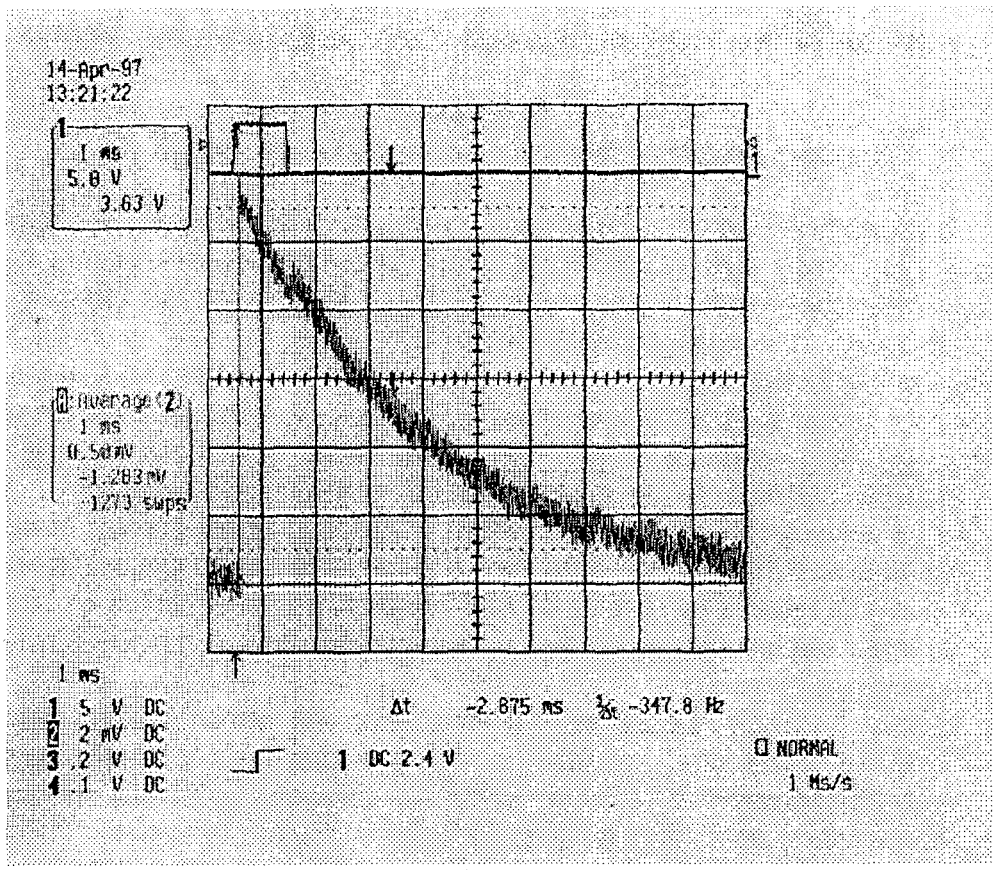

Figure 1. Measurement of Xe^{44+} ions in the fast extraction mode from EBIT II.

---

[i] D. Schneider, D. A. Church, G. Weinberg, J. Steiger, B. Beck, J. McDonald, E. Magee, and D. Knapp, Rev. Sci. Instrum. 65 (1994) 3472

[ii] D. Schneider, M. Clark, B. Pentrante, J. McDonald, D. Dewitt, N. Bardsley, Phys. Rev. A, **44** (1991) 3119

Evaporative Self-Cooling and High Brightness Ion Beams

R. E. Marrs
Lawrence Livermore National Laboratory, Livermore, CA 94551

Electron beam ion traps (EBIT) and sources (EBIS) are known for their ability to produce ions in very high charge states. Another remarkable, but seldom mentioned, property of these sources is the low emittance of the ion beams extracted from them. Low emittance makes it possible to focus low-energy beams of ions to small spots for microanalysis and other applications. For example, Ar^{18+} ions from an EBIT have been focused to a 20-μm diameter spot at an energy of $17q$ keV, where q is the ion charge[1]. The corresponding emittance is ~1 π mm mrad. If an even lower emittance can be obtained, it would enable new applications for very-highly-charged ions. We have performed a computer calculation of the effect of evaporative self-cooling of ions during extraction from an EBIT [2]. The results indicate that, under favorable conditions, the ion emittance can be reduced by roughly 30 fold compared to the uncooled emittance. The predicted effect can be used to construct a very high brightness source of highly charged ions.

Although the role of evaporative cooling in ion confinement in EBITs and EBISes is now well recognized [3,4], its effect on ion extraction has not been addressed. To understand the power of self-cooling during ion extraction, note that the equilibrium trapped-ion temperature for highly charged species is roughly 10% of the trap potential. Hence each ion escaping over the axial barrier removes an energy much larger than the average thermal energy of the trapped ions. The cooling power of each ion will be somewhat lower when the axial barrier is reduced to extract the trapped ions. However, our calculations predict that a reduction in the ion temperature of more than two orders of magnitude is possible if the axial barrier is ramped to zero slowly and other conditions are favorable. This is possible because of a fortunate ordering of the time scales for ion-ion energy exchange, electron-beam heating, and ion evaporative cooling. With properly chosen trapping conditions and a properly chosen potential-barrier waveform for ion extraction, it is possible for escaping ions to cool the remaining trapped ions within a time that is faster than the time for electron-beam reheating but much slower than the ion-ion collision rate. The predicted cooling effect does not occur without this ordering of time scales.

The physical processes that are important for evaporative self-cooling are: (1) ion confinement in the combined space charge potential of the electron beam and the trapped ions, (2) electron-beam heating of the ions, (3) work done on the ions by the space-charge potential, (4) energy exchange through ion-ion collisions, and (5) ion escape (evaporation) from the trap. These processes have been included in a time dependent calculation of the ion temperature and emittance.

The ion temperature, emittance, brightness, and other parameters were calculated for "slow" extraction from two types of EBIT devices: our existing low-energy EBIT operating with at typical beam of Ar^{18+} ions at 20 kV potential, and a high-intensity EBIT operating with a beam of Kr^{36+} ions at 80 kV potential. The 25-cm trap length and other parameters assumed for the high-intensity EBIT are similar to those of a device under

development at LLNL. The calculated emittance for these two cases is shown in Fig. 1 as a function of the fraction of ions extracted from the trap. The key result is the dramatic reduction in emittance for the last 20% or so of ions leaving the trap. This suggests that it may be possible to construct EBIT-type sources of very-highly-charged ions with an absolute brightness of order 2×10^{10} ions / mm^2 mrad^2 s, a value more than four orders of magnitude larger than that of existing highly-charged-ion sources.

It is natural to ask how far the ion temperature can be reduced with evaporative self-cooling. One effect that limits the evaporative cooling power is the very short mean free path of the ions at low temperature. (At low temperature the mean free path becomes much shorter than the 2-cm trap length of our EBIT.) This effect can be reduced with a well that has a sloping bottom (i.e., sawtooth shape), so that the ions fall to one end as their temperature and number decrease. We approximated this situation by repeating the Ar^{18+} calculation with a trap length that was proportional to the number of ions remaining in the trap. The calculated temperature for these conditions is plotted in Fig. 2. The calculation indicates that the ion temperature falls almost without limit, to the point where the ions may become strongly coupled. However, the lowest temperatures occur only for very low values of the axial well and for very short times just before the trap is inverted and the remaining ions are expelled.

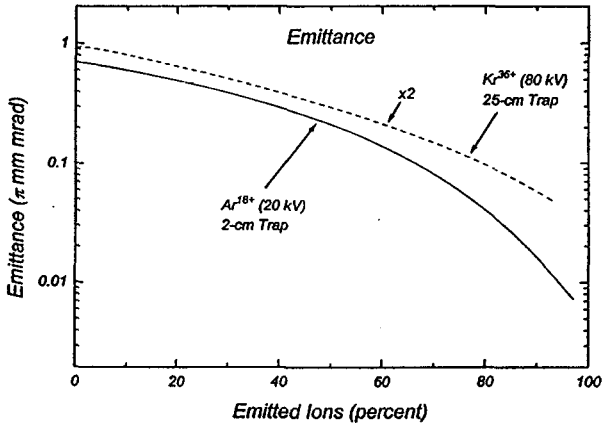

Fig. 1. Calculated absolute emittance for Ar^{18+} ions accelerated by a 20-kV potential and Kr^{36+} ions accelerated by a 80-kV potential.

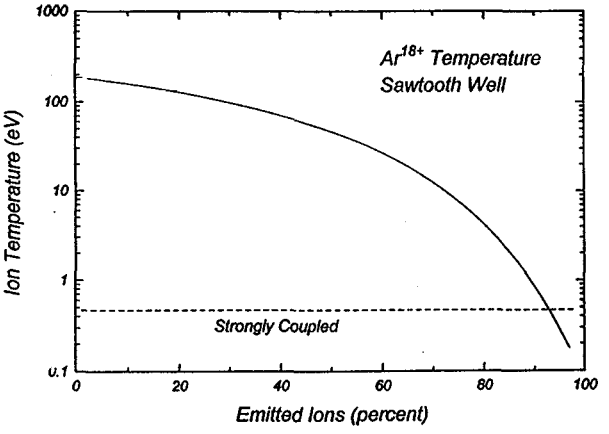

Fig. 2. Temperature of Ar^{18+} ions in a sawtooth well calculated as explained in the text. The ions are expected to become strongly coupled at temperatures below the broken line.

References

[1] R. E. Marrs, D. H. Schneider, and J. W. McDonald, Rev. Sci. Instrum. 69, 204 (1998).

[2] R. E. Marrs, submitted to Nucl. Instrum. Methods B.

[3] M. A. Levine, R. E. Marrs, J. R. Henderson, D. A. Knapp, and M. B. Schneider, Phys. Scr. T22, 157 (1988).

[4] B. M. Penetrante, J. N. Bardsley, D. DeWitt, M. Clark, and D. Schneider, Phys. Rev. A 43, 4861 (1991).

Construction of a 6-Tesla Superconducting Magnet for an Intense EBIT

M. A. Green[1], S. M. Dardin[1], R. E. Marrs[2], E. Magee[2], and S. K. Mukhergee[1]
[1]*Lawrence Berkeley National Laboratory, Berkeley, CA 94720*
[2]*Lawrence Livermore National Laboratory, Livermore, CA 94551*

For several years we have been working toward the completion of an Intense EBIT at LLNL [1]. This device is intended to have 100 times more x-ray emission per cm of beam length, and 1000 times more extracted ions than any existing EBIT. In addition, the maximum electron beam energy will be somewhat higher than that of our Super EBIT, resulting in a further increase in intensity for the highest charge states. The Intense EBIT will have a dramatic impact on nearly all of our on-going EBIT research programs. For example, the precision of EBIT transition energy measurements is presently count-rate limited, hence a 100-fold increase in count rate will provide a 10-fold improvement in precision. We also expect that the Intense EBIT will enable several exciting new research and development programs.

The design of the superconducting magnet for the Intense EBIT is a compromise between the conflicting requirements of a high and uniform magnetic field (needed for high electron beam density) and a large viewing angle (needed for x-ray measurements). The magnet is a four-coil solenoid with radial access at two elevations as shown in Fig. 1. The design field is 6 T, uniform to within 1% over a 28-cm length. The stored energy at the design current is approximately 180 kJ. There are eight radial holes of 41.3-mm diameter located in the central plane of the magnet. Four additional holes of 25.4-mm diameter are located near the bottom of the good-field region. The lower set of holes will provide additional radial access, and allow gas injection at a location removed from the

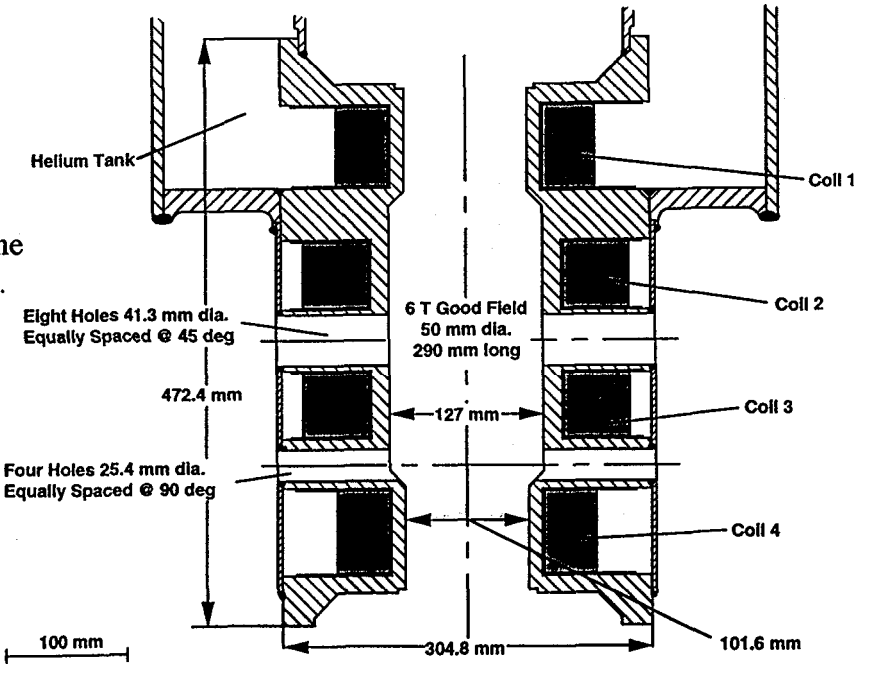

Fig. 1. Cross section of the 6-T Intense EBIT magnet.

trap center so that trapped ions and neutral gas can be separated. The inside cold bore of the solenoid is 127 mm in the central region, and 102 mm at the ends. This is significantly larger than the bore of our existing EBIT magnets and will allow the drift tube structure to operate at higher voltage. The helium vessel for the magnet and the dewar above the magnet are vacuum insulated with a liquid nitrogen shield and a gas cooled shield. The expected helium usage is roughly 0.5 liter per hour, an order of magnitude less than the helium consumption of our existing EBITs. The superconducting solenoid was wound using a round conductor made from Nb-Ti alloy that is nominally 46.5% titanium. The design critical current density for the superconductor is 3100 A/mm^2 at 4.2 K and 5 T. The four coils of the solenoid are wound on a bobbin made from 6061-T4 aluminum. The layers of conductor were wound over a layer-to-layer separator of 0.125-mm thick Nomex paper under a tension sufficient to compress the paper into the voids between the conductor. The completed coils were vacuum potted in epoxy. The coils are connected in series, and their inductive coupling to the aluminum bobbin contributes to the quench protection of the magnet. The new magnet will operate in persistent mode.

During winding the current center of the coils moved in the radial direction compared to the design because the compression of the Nomex paper was slightly different than expected. There are also small differences in the coils due to variations in the conductor diameter. However, none of these variations has a significant effect on the magnetic field. The magnetic field profile of the completed magnet was measured at room temperature. The results are compared to the calculated field profile in Fig. 2. The actual field profile is very close to the design, and within the design uniformity of roughly 1%.

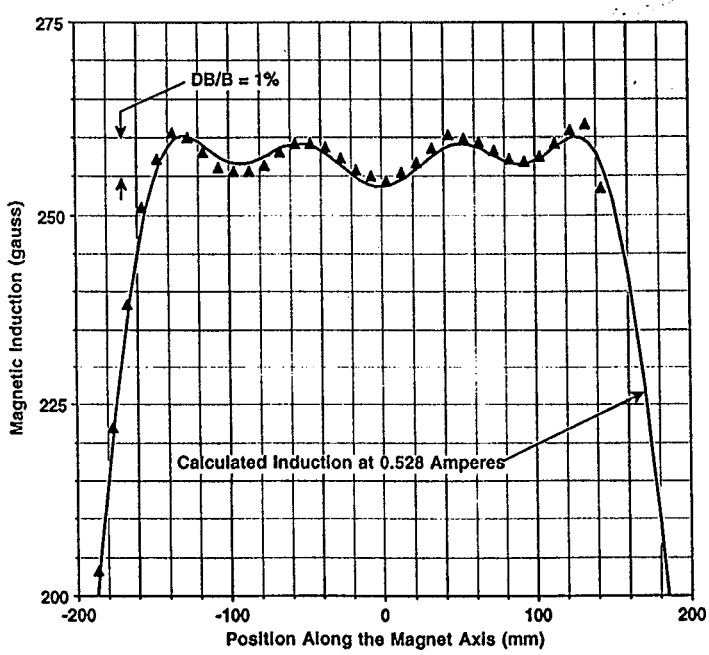

Fig. 2. Comparison of the calculated and measured magnetic field along the centerline of the magnet.

References

[1] EBIT 1995 Annual Report, pg. 90.

Appendix

A. Publications and Conference Contributions

1. Publications
2. Contributed Conference Papers
3. Conference Organization

B. Scientific Activities Centered Around EBIT

1. Visitors and Participating Guests
2. EBIT Seminar Series in N Division of LLNL

C. Education

D. Scientific Cooperations

E. Personnel

A. Publications and Conference Contributions

A-1 Publications in Refereed Journals in 1996 and 1997

Surface Physics

D. H. Schneider, M. A. Briere, "Investigations of the Interaction of Highest Charge State Ions with Surfaces", Phys. Scr. 53, 228 (1996).

D. Schneider, "EBIT as a Versatile Experimental Facility", Hyperfine Interactions 99, 47 (1996).

P. Briand, L. Debilly, J. Jin, H. Khemliche, M. Prior, Z. Xie, M. Nectoux, D. Schneider, "Interactions of Slow Ar(17,18)+ Ions with C-60: An Insight into Ion-Surface Interactions", Phys. Rev. A 53 R2925 (1996).

J. P. Briand, G. Giardino, G. Borsoni, M. Froment, M. Eddrief, C. Sebenne, S. Bardin, D. Schneider, J. Jin, H. Khemliche, and Z. Xie, "Decay of Hollow Atoms Above and Below a Surface", Phys. Rev. A 54, 4136 (1996).

J. P. Briand, B. d'Etat-Ban, D. Schneider, M. A. Briere, V. Decaux, J. W. McDonald, and S. Bardin, "Time for the empty L-Shell of a Hollow Atom to be Filled", Phys. Rev. A 53, 2194 (1996).

D. H. Schneider, "Atomic Physics", in McGraw Hill Yearbook of Science and Technology (McGraw Hill, New York, 1997), p. 26.

M. A. Briere, T. Schenkel, D. Schneider, "Super TOF Secondary Ion Mass Spectrometry using Very Highly Charged Primary Ions up to Th^{70+}", in Proceedings 10th. International Conference on Secondary ion Mass Spectrometry, SIMS X, A. Benninghoven, B. Hagenhoff, H. W. Werner (Wiley, Chichester, 1997), p. 227.

C. Ruehlicke, D. Schneider, R. DuBois, R. Balhorn, "Fragmentation of Biomolecules Using Slow Highly Charged Ions", in Applications of Accelerators in Research and Industry, AIP Conference Proceedings 392, (AIP, Woodbury, 1997), J. L. Duggan, I. L. Morgan (eds.), p. 519.

M. Reaves, Q. C. Kessel, E. Pollack, W. W. Smith, M. A. Briere, and D. H. Schneider, "Negative Ion Production in Small Angle Scattering of Highly Charged Ions from the (0001) Surface of Highly Oriented Pyrolytic Graphite", in Applications of Accelerators in Research and Industry, AIP Conference Proceedings 392, (AIP, Woodbury, 1997), J. L. Duggan, I. L. Morgan (eds.), p. 165.

T. Schenkel, A. V. Barnes, M. A. Briere, A. V. Hamza, A. Schach von Wittenau, D. Schneider, "Emission of Secondary Particles from Metals and Insulators at Impact of Slow Highly Charged Ions", Nucl. Instruments and Methods Phys. Res., Sect. B 125, 153 (1997).

T. Schenkel, M. A. Briere, H. Schmidt-Böcking, K. Bethge, D. Schneider, "Electronic Sputtering of Thin Conductors by Neutralization of Slow Highly Charged Ions", Phys. Rev. Lett. 78, 2481 (1997).

J. P. Briand, D. Schneider, S. Bardin, H. Khemliche, J. Jin, Z. Xie, and M. Prior, "X-ray Studies of the Interaction of N, O, and Ne Hydrogen like Ions Below Surfaces", Phys. Rev. A. 55, 3947 (1997).

T. Schenkel, A. V. Hamza, A. V. Barnes, D. H. Schneider, "Energy Loss of Slow, Highly Charged Ions in Solids", Phys. Rev. A 56, R1701 (1997).

T. Schenkel, M. A. Briere, H. Schmidt-Böcking, K. Bethge, D. Schneider, "Electronic Sputtering and Desorption Effects in TOF-SIMS Studies Using Slow Highly Charged Ions like Au^{69+}", Materials Science Forum, Vols. 248-249, 413 (1997).

T. Schenkel, M. A. Briere, A. V. Barnes, A. V. Hamza, K. Bethge, H. Schmidt-Böcking, D. Schneider, "Charge State Dependent Energy Loss of Slow Heavy Ions in Solids", Phys. Rev. Lett. 79, 2030 (1997).

M. A. Briere, T. Schenkel, D. H. Schneider, P. Bauer, A. Arnau, "Non-Equilibrium Energy Loss for Very Highly Charged Ions in Insulators", Phys. Scr.T73, 324 (1997).

R. E. Marrs, "Recent Results from the EBIT and Super-EBIT at Lawrence Livermore National Laboratory", Physica Scripta T73 354 (1997).

RETRAP

D. Schneider, "The EBIT as a Versatile Experimental Facility", Hyperfine Interactions 99, 47 (1996).

B. R. Beck, J. Steiger, G. Weinberg, D. A. Church, J. McDonald, D. Schneider, "Measurement of Charge Exchange Between Hz and Low-Energy Ions with Charge States $35 \leq q \leq 80$", Physical Review Letters 77, (1996) 1735~1738.

D. A. Church, J. Steiger, B. R. Beck, L. Gruber, G. Weinberg, J. McDonald, D. Schneider, "Collisions and Spectroscopy of Low-Energy Highly-Charged Ions Using an Ion Trap", Nucl. Instr. Meth. B 132, (1997) 335-343.

J. Steiger, D. A. Church, G. Weinberg, B. Beck, J. McDonald, D. Schneider, "Observation of Sequential Electron Capture to Individual Highly Charged Th^{79+} Ions", Hyperfine Interactions 108, (1997) 115-119.

D. Schneider, "New Research Initiatives at the Electron Beam Ion Trap (EBIT) Facilities", McGraw Hill, Yearbook of Science and Technology, (1997) p. 26.

D. A. Church, J. Steiger, G. Weinberg, B. R. Beck, J. McDonald, L. Gruber, D. Schneider, "Collisions and Spectroscopy of Low-Energy Highly-Charged Ions using an Ion-Trap", CP392, Application of Accelerator in Research and Industry, edited by J. L. Duggan, I. L. Morgan, AIP Press, New York, (1997).

X-ray Spectroscopy

P. Beiersdorfer, B. Beck, St. Becker, and L. Schweikhard, "FT-ICR Analysis of the Magnetic Trapping Mode of the Electron Beam Ion Trap", Int. Journal of Mass Spectrometry and Ion Processes, 157/158, 149-161 (1996).

R. DuBois, D. Schneider, "Report on the 14th International Seminar on Ion-Atom Collisions", (ISIAC XIV), Comment At. Mol. Phys., 32, 5 (1996) p. 317.

S. Bliman, R. Bruch, P. L. Altick, D. Schneider, M. H. Prior, "Double Electron Capture in Low-Energy Fe^{17+} +He Collisions", Phys. Rev. A, 53, 6, 4176 (1996).

P. Beiersdorfer, A. L. Osterheld, V. Decaux, and K. Widmann, "Observation of Lifetime-Limited X-Ray Line Widths in Cold Highly Charged Ions", Physical Review Letters, 77, 5353-5356 (1996).

P. Beiersdorfer, L. Schweikhard, J. R. Crespo López-Urrutia, and K. Widmann, "The Magnetic Mode of an EBIT – New Opportunities for Highly Charged Ion Research", Review of Scientific Instruments, 67, 3818-3826 (1996).

S. R. Elliott, P. Beiersdorfer, M. H. Chen, "Trapped-Ion Based Technique for Measuring the Nuclear Charge Radii of Highly Charged Radioactive Isotopes", Physical Review Letters, 76, 1031-1034 (1996).

D. W. Savin, P. Beiersdorfer, J. R. Crespo López-Urrutia, V. Decaux, E. M. Gullikson, S. M. Kahn, D. A. Liedahl, K. J. Reed, and K. Widmann, "Laboratory Measurements of Fe XXIV L-Shell Line Emission", Astrophysical Journal Letters, 470, L73-L76 (1996).

J. Nilsen, P. Beiersdorfer, K. Widmann; V. Decaux and S. R. Elliott, "Energies of Neonlike n=4 to n=2 Resonance Lines", Physica Scripta, 54, 183-187 (1996).

D. W. Savin, P. Beiersdorfer, G. V. Brown, J. R. Crespo López-Urrutia, V. Decaux, S. M. Kahn, D. A. Liedahl, K. J. Reed, and K. Widmann, "Laboratory Astrophysics measurements of n=n' to n=2 Line Emission in Fe^{16+} to Fe^{23+}", Atomic Processes in Plasmas, AIP Conf. Proceedings No. 381, ed. by A. L. Osterheld and W. H. Goldstein (AIP, NewYork 1996), 39-46.

J. R. Crespo López-Urrutia, P. Beiersdorfer , D. W. Savin, K. Widmann, "Direct Observation of the Spontaneous Emission of the Hyperfine Transition F=4 to F=3 in Ground State Hydrogenlike $^{165}Ho^{66+}$ in an Electron Beam Ion Trap", Physical Review Letters, 77, 826-829 (1996).

A. J. Smith, P. Beiersdorfer, V. Decaux, K. Widmann, K. J. Reed, and M. H. Chen, "Measurement of the Contributions of High-n Satellites to the Kß Lines of He-like Ar^{16+}", Physical Review A, 54, 462-466 (1996).

P. Beiersdorfer, D. A. Vogel, K. J. Reed, V. Decaux, J. Scofield, K. Widmann, G. Hölzer, E. Förster, O. Wehrhan, D. W. Savin, and L. Schweikhard, "Measurement and Interpretation of the Polarization of the X-Ray Line Emission of Heliumlike Fe xxv Excited by an Electron Beam", Physical Review A, 53, 3974-3981 (1996).

P. Beiersdorfer, S. R. Elliott, A. L. Osterheld, Th. Stöhlker, J. Autrey, G. V. Brown, A. J. Smith, and K. Widmann, "Search for 1s2s $^3S_1$-1s2p $^3P_2$ Decay in U^{90+}", Physical Review A, 53, 4000-4006 (1996).

L. Schweikhard, P. Beiersdorfer, W. Bell, G. Dietrich, S. Krückeberg, K. Lützenkirchen, B. Obst, and J. Ziegler, "Production and Investigation of Multiply Charged Metal Clustes in a Penning Trap", Hyperfine Interactions, 99, 97-104 (1996).

P. Beiersdorfer, G. Brown, J. R. Crespo López-Urrutia, V. Decaux, D. Savin, A. J. Smith, G. Stefanelli, K. Widmann, K. L. Wong, "Overview of the Current Spectroscopy Effort on the Livermore Electron Beam Ion Traps", Hyperfine Interactions, 99, 203-215 (1996).

K. Widmann, P. Beiersdorfer, V. Decaux, and M. Bitter, "Measurement of the Kα Transition Energies of Heliumlike Kr^{34+}", Physical Review A, 53, 2200-2205 (1996).

S. R. Elliott, P. Beiersdorfer, M. H. Chen, "Trapped-Ion Technique for Measuring the Nuclear Charge Radii of Highly Charged Radioactive Isotopes", Physical Review Letters (Feb. 1996) V76 N7: 1031-1034.

P. Beiersdorfer, S. R. Elliott, J. R. Crespo López-Urrutia, and K. Widmann, "Measurements of Nuclear Parameters of High-Z Isotopes Performed on an High-Energy Electron Beam Ion Trap", Nuclear Physics A, 626, 357c-364c (1997).

D. Klöpfel, G. Hölzer, E. Förster, and P. Beiersdorfer, "A Quartz Quasimonolith for Absolute X-Ray Wavelength Measurements", Review of Scientific Instruments 68, 3669-3675 (1997).

V. L. Jacobs, V. Decaux, and P. Beiersdorfer, "Kα Emission in Equilibrium and Non-Equilibrium Plasmas", Journal of Quantitative Spectroscopy and Radiative Transfer, 58, 645-659 (1997).

J. R. Crespo López-Urrutia, P. Beiersdorfer, D. W. Savin and K. Widmann, "Hyperfine Transitions in Ground State Hydrogen-like $^{165}Ho^{66+}$ and $^{185,187}Re^{74+}$", Application of Accelerators in Research and Industry, AIP Conf. Proc. No. 392, ed. by J. L. Duggan and I. L. Morgan (American Institute of Physics, New York, 1997), p. 87-88.

S. R. Elliott, P. Beiersdorfer, M. H. Chen, "Trapped-Ion Based Technique for Measuring the Nuclear Charge Radii of Highly Charged Radioactive Isotopes", Application of Accelerators in Research and Industry, AIP Conf. Proc. No. 392, ed. by J. L. Duggan and I. L. Morgan (American Institute of Physics, New York, 1997), p. 305-308.

V. Decaux, P. Beiersdorfer, S. M. Kahn, and V. L. Jacobs, "High-Resolution Measurement of the Kα Spectrum of Fe XXV to Fe XVIII: New Spectral Diagnostics of Non-Equilibrium Astrophysical Plasmas", Astrophysical Journal, 482, 1076-1084 (1997).

K. Widmann, P. Beiersdorfer, J. R. Crespo López-Urrutia, and S. Elliott, "Spectroscopy at the High-Energy Electron Beam Ion Trap (SuperEBIT)", Atomic Physics with Stored Highly Charged Ions II, ed. by R. Schuch, E. Lindroth, H.-J. Kluge (Balzer, Amsterdam, 1997), p. 73-86.

S. Krückeberg, P. Beiersdorfer, G. Dietrich, K. Lützenkirchen, L. Schweikhard, and C. Walther, "First Observation of Multiply Charged Vanadium Clusters in a Penning Trap", Rapid Communications of Mass Spectrometry, 11, 455-458 (1997).

I. Yu. Skobelev, A. Ya. Faenov, V. M. Dyakin, H. Fiedorowicz, A. Bartnik, M. Szczurek, P. Beiersdorfer, J. Nilsen, and A. Osterheld, "High-Resolution Measurement, Line Identification, and Spectral Modeling of the Kβ Spectrum of Heliumlike Argon Emitted by a Laser-Produced Plasma Using a Gas Puff Target", Physical Review E, 55, 3773-3776 (1997).

P. Beiersdorfer, J. R. Crespo López-Urrutia, V. Decaux, K. Widmann, and P. Neill, "Polarization Spectroscopy of X-Ray Transitions from Beam-Excited Highly Charged Ions", Review of Scientific Instruments, 68, 1073-1076 (1997).

P. Beiersdorfer, J. R. Crespo López-Urrutia, E. Förster, J. Mahiri, and K. Widmann, "Very High Resolution Soft X-Ray Spectrometer for an Electron Beam Ion Trap", Review of Scientific Instruments, 68, 1077-1079 (1997).

K. Widmann, P. Beiersdorfer, G. V. Brown, J. R. Crespo López-Urrutia, V. Decaux, and D. W. Savin, "A High Resolution Transmission-Type X-Ray Spectrometer Designed for Observation of the Kα Transitions of Highly Charged High-Z Ions", Review of Scientific Instruments, 68, 1087-1090 (1997).

P. Beiersdorfer, "High-Resolution X-Ray Spectra from Low-Temperature, Highly Charged Ions", Proceedings of the 17th International conference on X-Ray and Innershell Processes, AIP Conf. Proc. No. 389, ed. by R. L. Johnson, H. Schmidt-Böcking, and B. F. Sonntag, (American Institute of Physics, New York, 1997), p. 121-135.

A. S. Shlyaptseva, R. C. Mancini, P. Neill, and P. Beiersdorfer, "Polarization of X-Ray Li- and Be-Like Fe Satellite Lines Excited by an Electron Beam", Review of Scientific Instruments, 68, 1095-1098 (1997).

R. Bruch, V. Kantsyrev, G. Golovkina, A. Shlyaptseva, I. Golovkin, R. Phaneuf, D. Schneider, "Application of high-resolution, high-sensitivity spectrometry in the extreme ultraviolet wavelength range for diagnostics of single and double electron capture processes in He^{2+} +He and Ar^{8+} +He collisions", Review of Scientific Instruments, 68 (1), 1091 (1997).

R. Bliman, M. Cornille, A. Langereis, J. Nordgren, R. Bruch, R. Phaneuf, J. Swenson, D. Schneider, "Soft x-ray and Auger electron spectroscopy of single and double electron capture processes in slow Ne^{8+} +He collisions", Review of Scientific Instruments, 68 (1), 1080 (1997).

R. Bruch, U. I. Safronova, A. S. Shlyaptseva, J. Nielsen, D. Schneider, "Theoretical analysis of the doubly excited 3lnl' states of sodiumlike copper", Physica Scripta, 57, 334 (1997).

R. Bruch, V. Kantsyrev, R. Phaneuf, V. Golovkina, A. Shlyaptseva, I. Golovkin, "Application of New Spectroscopic Technique for the Study of Interaction of Multicharged Ions with Gaseous Targets in the Extreme Ultraviolet", Physica Scripta, T73, 397 (1997).

V. Kantsyrev, R. Bruch, R. Phaneuf, V. Golovkina, D. Schneider, V. Leroux, "Application of Glass-Capillary Converters to High Resolution EUV Spectrometry: First Results for Ion-Atom Collisions, CP392", Application of Accelerator in Research and Industry, edited by J. L. Duggan, I. L. Morgan, AIP Press, New York (1997).

A-2 Contributed Conference Papers

"EBIT and Super EBIT: A Source of Atomic Data for any Ion of any Element"
R.E. Marrs, P. Beiersdorfer, J. Crespo López-Urrutia, V. Decaux, S.R. Elliott, D.W. Savin, Th. Stoehlker, K. Widmann
10th APS Topical Conference on Atomic Processes in High Temperature Plasmas, San Francisco, CA, Jan. 14-18, 1996

"Forbidden Optical Lines in Highly Charged Ions"
Jose Crespo López-Urrutia, P. Beiersdorfer, K. Widmann, V. Decaux
10th APS Topical Conference on Atomic Processes in High Temperature Plasmas, San Francisco, CA, Jan. 14-18, 1996

"K-Shell Emission and Dielectronic Recombination Satellite Spectra of Heliumlike Magnesium"
G.S. Stefanelli, P. Beiersdorfer, V. Decaux, K. Widmann
10th APS Topical Conference on Atomic Processes in High Temperature Plasmas, San Francisco, CA, Jan. 14-18, 1996

"Kα Radiative Emission Processes in Equilibrium and Non-Equilibrium Plasmas"
V.L. Jacobs, V. Decaux, P. Beiersdorfer
10th APS Topical Conference on Atomic Processes in High Temperature Plasmas, San Francisco, CA, Jan. 14-18, 1996

"Fe XXIV n=3 → n=2 and n=4 → n=2 Line Emission Produced by Electron Impact Excitation"
D.W. Savin, S.M. Kahn, P. Beiersdorfer, D.A. Liedahl, K. Reed
10th APS Topical Conference on Atomic Processes in High Temperature Plasmas, San Francisco, CA, Jan. 14-18, 1996

"Observation and Interpretation of Polarized X-ray Line Emission from Heliumlike Fe XXV Excited by a Monoenergetic Electron Beam"
P. Beiersdorfer, V. Decaux, K. Reed, J. Scofield, D.A. Vogel, K. Widmann, D.W. Savin
10th APS Topical Conference on Atomic Processes in High Temperature Plasmas, San Francisco, CA, Jan. 14-18, 1996

"FeXXIV 3 → 2 and 4 → 2 Line Emission Produced by Electron Impact Excitation"
D. Savin, P. Beiersdorfer, J. Crespo López-Urrutia, V. Decaux, S. Kahn, D. Liedahl, K. Reed, K. Widmann
Meeting of the High-Energy Astrophysics Division of the American Astronomical Society, San Diego, CA, Apr. 29-May 3, 1996

"Survey and Identification of L-Shell Transitions from Fe XVII to Fe XXIV in the Wavelength Band 10-17Å"
P. Beiersdorfer, G. V. Brown, V. Decaux, S.M. Kahn, D. Liedahl, D.W. Savin, K. Widmann
Meeting of the High-Energy Astrophysics Division of the American Astronomical Society, San Diego, CA, Apr. 29-May 3, 1996

"A High-Resolution Transmission-Type X-ray Spectrometer for Observation of the Kα Transitions of Xe^{52+} and Xe^{53+}"
K. Widmann, P. Beiersdorfer, J. R. Crespo López-Urrutia
11th Topical Conference on High-Temperature Plasma Diagnostics, Monterey, CA, May 12-16, 1996

"Very High Resolution Soft X-ray Spectrometer for an Electron Beam Ion Trap"
P. Beiersdorfer, J. Crespo López-Urrutia, J. Mahiri, K. Widmann
11th Topical Conference on High-Temperature Plasma Diagnostics, Monterey, CA, May 12-16, 1996

"Polarization Spectroscopy of X-ray Transitions for Beam-Excited Highly Charged Ions"
P. Beiersdorfer, J. Crespo López-Urrutia, V. Decaux, W. Widmann, D. Savin
11th Topical Conference on High-Temperature Plasma Diagnostics, Monterey, CA, May 12-16, 1996

"Observation of the Hyperfine Transition of the 1s $^2S_{1/2}$ Ground State of H-like $^{165}Ho^{66+}$"
J. Crespo López-Urrutia, P. Beiersdorfer, D. Savin, D. Widmann
DAMOP96 Meeting of the American Physical Society, Ann Arbor, MI, May 15-18, 1996

"Measurements of Femtosecond Radiative Lifetimes in Highly Charged Ions"
P. Beiersdorfer, V. Decaux, K. Widmann
DAMOP96 Meeting of the American Physical Society, Ann Arbor, MI, May 15-18, 1996

"Lifetime-Limited, High-Resolution X-Ray Spectra from Low-Temperature, Highly Charged Ions"
P. Beiersdorfer
X-96, 17th International Conference on X-ray and Inner-Shell Processes, Hamburg, Germany, Sept. 9-13, 1996

"Measurements of Nuclear Parameters of High-Z Isotopes Performed on the Livermore High-Energy Electron Beam Ion Trap"
P. Beiersdorfer, S.R. Elliott, M.H. Chen, J. Crespo López-Urrutia, K. Widmann
3rd International Conference on Nuclear Physics at Storage Rings, Bernkastel-Kues, Germany, Sept. 30-Oct. 4, 1996

"Kα Emission in Equilibrium and Non-Equilibrium Plasmas"
V.L. Jacobs, V. Decaux, P. Beiersdorfer
7th International Workshop on Radiative Properties of Hot Dense Matter, Santa Barbara, CA, Nov. 4-8, 1996.

"Determination of the Ion Temperature from Spectrally Resolved Measurements of Hard X Rays"
K. Widmann, P. Beiersdorfer, J. Crespo López-Urrutia
37th Annual Meeting, APS Division of Plasma Physics, Denver, CO, November 11-15, 1996

"Dielectronic Satellite Contributions to the He-ß Line Profiles of Highly Charged Ions"
P. Beiersdorfer, K. Widmann, A.J. Smith
37th Annual Meeting, APS Division of Plasma Physics, Denver, CO, November 11-15, 1996

"Measurement of the Hyperfine Splitting in the $1s_{1/2}$-$2p_{3/2}$ X-Ray Transition in Bi^{80+}"
P. Beiersdorfer, A. Osterheld, J. Scofield, J. Crespo López-Urrutia, V. Decaux, K. Widmann
Division of Atomic, Molecular, and Optical Physics Meeting of the American Physical Society, Washington, DC, April 17-21, 1997

"Laboratory Measurement of the 2p-3d 15.01 Å Resonance to 15.26 Å Intercombination Line of Fe XVII"
G.V. Brown, P. Beiersdorfer, D.A. Liedahl, S.M. Kahn, V. Decaux, K. Widmann.
10th Cambridge Workshop on Cool Stars, Stellar Systems and the Sun, Cambridge, MA, July 15-19, 1997

"Laboratory Measurement, Line Identification, and Modeling of the L-Shell Fe XVII Spectrum Below 12 Å"
G.V. Brown, P. Beiersdorfer, D.A. Liedahl, S.M. Kahn, M.H. Chen, V. Decaux, K. Reed, K. Widmann, and E.J. Clothiaux.
10th Cambridge Workshop on Cool Stars, Stellar Systems and the Sun, Cambridge, MA, July 15-19, 1997

"A Trap for Collision Studies at Very Low Temperature (<10 K)"
L. Gruber, B. Beck, D. Church, J. McDonald, J. Steiger, G. Weinberg, D. Schneider
XX ICPEAC, Vienna, Austria, July 23-29, 1997

"Electronic Sputtering of Thin Conducting Foils by Neutralization of Slow Highly Charged Ions"
T. Schenkel, A. V. Hamza, A. V. Barnes, D. H. Schneider
XX ICPEAC, Vienna, Austria, July 23-29, 1997

"Pre-Charge Equilibrium Energy Loss Enhancement of Slow Very Highly Charged Ions in Solids"
T. Schenkel, A. V. Hamza, A. V. Barnes, D. H. Schneider, R. J. Fortner
XX ICPEAC, Vienna, Austria, July 23-29, 1997

"Emission of Secondary Electrons and Ions in the Interaction of Slow Highly Charged Ions with Solids"
T. Schenkel, A. V. Barnes, A. V. Hamza, D. H. Schneider
XX ICPEAC, Vienna, Austria, July 23-29, 1997

"Double Electron Capture Processes in 80 keV NE8+ + He Collisions Studied by Electron and Photon Spectroscopy"
A. Langereis, S. Bliman, M. Cornille, R. Bruch, R. Phaneuf, D. Schneider, J. Nordgren
XX ICPEAC, Vienna, Austria, July 23-29, 1997

"Measured Charge Exchange Between H_2 and Low-Energy Ions with Charge States $35 \leq q \leq 80$"
B. R. Beck, D. A. Church, L. Gruber, J. McDonald, J. Steiger, G. Weinberg, D. Schneider
XX ICPEAC, Vienna, Austria, July 23-29, 1997

"Fragmentation of Large Molecules Using Slow, Highly Charged Ions"
C. Ruehlicke, D. Schneider, R. DuBois, R. Balhorn
XX ICPEAC, Vienna, Austria, July 23-29, 1997

"Collision Studies of Cold Highly Charged Ions with Neutral Atoms"
P. Beiersdorfer, G.V. Brown, J. Crespo López-Urrutia, D. Schneider, L. Schweikhard, S. Utter, K. Widmann
XX International Conference on the Physics of Electronic and Atomic Collisions, Vienna, Austria, July 23-29, 1997

"Polarized Line Emission From Electron Beam Excited Highly Charged Ions"
P. Beiersdorfer, G.V. Brown, J. Crespo López-Urrutia, R. Manicini, P. Neill, K. Reed, A. Shlyaptseva, S. Utter, K. Widmann
XX International Conference on the Physics of Electronic and Atomic Collisions, Vienna, Austria, July 23-29, 1997

"A Trap to Produce Strongly Coupled Plasmas with Highly Charged Ions", L. Gruber, B. Beck, D. Church, J. McDonald, J. Steiger, D. Schneider
XX International Conference on the Physics of Electronic and Atomic Collisions, Vienna, Austria, July 23-29, 1997

"Interactions of Slow, Highly Charged Ions with Fullerness", D. Schneider, T. Schenkel, V. Barnes, A. Hamza
XX International Conference on the Physics of Electronic and Atomic Collisions, Vienna, Austria, July 23-29, 1997

"Light Emission from Surfaces Hit by Xe^{53+} and U86+ lows", J. R. Crespo López-Urrutia, J. McDonald, S. B. Utter, D. Schneider
XX International Conference on the Physics of Electronic and Atomic Collisions, Vienna, Austria, July 23-29, 1997

"Fragmentation of Proteins using Highly Charged Ions"
C. Ruehlicke, D. Schneider, R. DuBois, R. Balhorn
AIP Conference Proceedings, 392 (AIP, Woodbury, 1997)

"Measurement of Quantum Electrodynamical Corrections and Hyperfine Splittings in the $2s_{1/2}$-$2p_{3/2}$ X-Ray Transition in Bi^{80+}"
P. Beiersdorfer, A.L. Osterheld, J. Scofield, J. Crespo López-Urrutia, K. Widmann
3rd Euroconference on Atomic Physics With Stored Highly Charged Ions in Ferrara, Italy, Sept. 22-26, 1997

"The Hyperfine Structure of the Ground State Hydrogen-like $^{165}Ho^{66+}$ and $^{185,187}Re^{74+}$ Ions"
J. Crespo López-Urrutia, P. Beiersdorfer, K. Widmann, B. Birkett, D.W. Savin, A.M. Martensson-Pendrill
3rd Euroconference on Atomic Physics With Stored Highly Charged Ions in Ferrara, Italy, Sept. 22-26, 1997

"High-Resolution Measurements of the Kα Transition Energies of Trapped Heliumlike and Hydrogenlike Xenon"
K. Widmann, P. Beiersdorfer, G.V. Brown, J. Crespo López-Urrutia, S. Utter.
3rd Euroconference on Atomic Physics With Stored Highly Charged Ions in Ferrara, Italy, Sept. 22-26, 1997

"Laboratory Measurements Iron *L*-Shell Line Emission"
M. F. Gu, S. M. Kahn, D. W. Savin, P. Beiersdorfer, G. V. Brown, D. A. Liedahl
International Conference on Atomic and Molecular Data, Washington, DC, October 28-30, 1997

"Laboratory Measurements of Fe XXIV Line Emission for the X-Ray Observation of Clusters of Galaxies"
M. F. Gu, P. Beiersdorfer, G. V. Brown, S. M. Kahn, D. A. Liedahl, D. W. Savin
American Astronomy Society - High Energy Astrophysics Division Meeting, Estes Park, CO, November 4-7, 1997

"Calibration of the Standard Plasma Line Emission Codes for Upcoming X-ray Satellite Missions"
P. Beiersdorfer, G. V. Brown, M. F. Gu, S. M. Kahn, D. A. Liedahl, D. W. Savin, S. B. Utter
American Astronomy Society, High Energy Astrophysics Division Meeting, Estes Park, CO, November 4-7, 1997

"Laboratory Calibration of the nd $\longrightarrow$ 2p Resonance Line Emission from Fe XVII"
G. V. Brown, P. Beiersdorfer, D. A. Liedahl, S. M. Kahn, K. Widmann
American Astronomy Society, High Energy Astrophysics Division Meeting, Estes Park, CO, November 4-7, 1997

"High-resolution Measurements of the K-shell Radiation of Highly Charged Krypton"
K. Widmann, P. Beiersdorfer
Division of Plasma Physics, Meeting of The American Physical Society, Denver, CO, November 11-14, 1997

"Ion Temperature Measurements in an Electron Beam Ion Trap (EBIT)"
P. Beiersdorfer, V. Decaux, K. Widmann
Division of Plasma Physics, Meeting of The American Physical Society, Denver, CO, November 11-14, 1997

A-3 Conference Organization

During 1996 and 1997 a workshop and an international conference were organized by the LLNL EBIT Program, and took place in 1998.

Workshop on "Physics with Trapped Highly Charged Ions at the LLNL EBIT/RETRAP" Lawrence Livermore National Laboratory, Livermore, California February 27 - 28th, 1998

Summary

A small workshop organized by the EBIT program at LLNL was held on February 27-28, 1998. A total of 35 scientists attended. In addition to the invited speakers, a number of physicists from LLNL attended the workshop and participated in the discussions.

Throughout the workshop, the various talks and discussions showed that physics research with trapped particles is a very active and attractive area of current innovative research, and the basis for efforts in new areas. It also became obvious that the EBIT/RETRAP project has unique capabilities to perform important new experiments with trapped very highly charged ions at rest, which are complementary to and competitive with research at heavy ion storage rings and other trapping facilities planned or in operation in Europe, Japan and the US.

The beautiful results from the NIST group at Boulder using singly charged ions demonstrate that structure studies of crystallized ions in traps can be performed with $<10^5$ ions. Similar ion numbers are feasible with RETRAP. It was explicitly stated that RETRAP, with it's highly-charged ion capability, has clear advantages for the study of mixed, strongly-coupled ion plasmas, which should provide new insights in the understanding of crystallized highly-charged ion plasmas, phase separations, and temperature dependencies. These studies will have application to matter in neutron stars and white dwarf stars. They intrinsically require the continued development of techniques to crystallize ions and provide cold ion plasmas at temperatures above 4K. Such developments are also essential to multiply-charged ion use in new lithography-type techniques, where manipulation and control of very highly-charged ions from a high-brightness ion source is envisioned. This particular aspect could develop into a major research effort in conjunction with ongoing materials research at EBIT.

Laser spectroscopy on highly charged ions is in its infancy, but applying it to cold confined ions in RETRAP or EBIT has several advantages, e.g. optimum spatial overlap, Doppler-free spectroscopy, efficiency in collection of fluorescence, and long observation times in a controlled environment. This spectroscopy opens up not only a new dimension of precision for few-electron high-Z ionic systems, but it also enables measurements of atomic and nuclear parameters without the (often poorly understood) corrections and shielding of electrons in many-electron atoms, for example nuclear magnetic moments, nuclear size effects, and the distribution of nuclear magnetism. Even nuclear masses are measured to higher precision in ion traps. The Z-dependence on energy-level separations, lifetimes, and g-factors make possible important tests of atomic structure with very highly-charged ions, which are not feasible otherwise. Low-order QED effects with Z near 1 are calculable, but the individual terms of perturbation theory do not converge well, requiring the development of all-order calculations. When combined with relativity and nuclear effects, there are puzzles, such as the existing deviation of hyperfine transition rates from theory. It is expected that such puzzles will be directly addressed using RETRAP, and superior precision in many measurements obtained.

Besides beta-decay for nuclear studies, the large potential of ion trap technology for nuclear mass spectrometry has been demonstrated through the work done with ISOLTRAP at CERN and the storage ring at GSI. The EBIT/RETRAP scheme and the techniques developed at LLNL for capture, trapping, and cooling of highly-charged ions in a Penning trap, coupled with charge-capture measurements of ion charge-state lifetimes, can be applied in various combinations at accelerator and synchrotron facilities for atomic structure measurements, mass spectrometry, and collisions related to plasma processes at low and high temperatures. The ability to carry out plasma and ionic measurements under well-controlled conditions should be very important to plasma modeling, both for laboratory and astrophysical plasmas. It is well known that improved measurements of many atomic parameters are now required for sophisticated astrophysical models.

The benefits to LLNL of a continued long-term EBIT/RETRAP project seem clear. This project requires the application and development of state-of-the-art experimental techniques required in spectroscopy, ion confinement and manipulation. Thus it serves as an excellent training ground for young scientists who will later work on energy-related plasma research or similar areas. It promises new research results towards the growth of our understanding of basic physics phenomena in atomic, nuclear and plasma physics, such as solid phases, astrophysical plasma evolution, and quantum control. This research will also provide applications in areas like ion beam manipulation and control for materials research. It was clear from the workshop that EBIT/RETRAP research already has great interest for a wider community of scientists, with several new ideas and research directions emerging. Stimulated by the workshop and the research opportunities at the EBIT and RETRAP, several participants have expressed a strong interest in future collaborations. This interest is greatly appreciated by the EBIT program.

Agenda

Friday, February 27, 1998

9:00 a.m.	Welcome and facility introduction	D. Schneider
9:10 a.m.	Purpose of workshop	R. Fortner
9:20 a.m.	Recent results on RETRAP	J. Steiger
9:40 a.m.	Charge transfer	B. Beck
10:00 a.m.	Hyperfine structure and g-factors	D. Church (Texas A & M)
10:20 a.m.	Break	
10:40 a.m.	QED and g-factors	J. Sapirstein (Notre Dame)
11:00 a.m.	Hfs/laser spectroscopy	T. Kühl (GSI)
11:20 a.m.	Laser spectroscopy on Be-like Ti	J. Farley (UNLV)
12:00 p.m.	Lunch discussion	D. Church
2:00 p.m.	Trapped ion physics	J. Kluge (GSI)
2:20 p.m.	Coulomb clusters (experimental)	J. Bollinger (Boulder)
2:40 p.m.	Quantal studies of charge transfer	B. Zygelman (UNLV)
3:00 p.m.	Break	
3:20 p.m.	Astrophysics	H. DeWitt (LLNL)
3:40 p.m.	Nuclear physics	V. Nienov (LBNL)
4:00 p.m.	Surface physics aspects	N. Bardsley
4:20 p.m.	Discussion	J. Kluge
6:30 p.m.	Dinner / West Cafeteria	Summary

Saturday, February 28th

10:00 a.m.	Visit of the EBIT/RETRAP facility and working brunch

Workshop Attendees

External
David Church, Texas A&M University
John Bollinger, National Institute of Standards & Technology, Boulder
Sheldon Datz, Oak Ridge National Laboratory
Dan Dubin, University of California, San Diego
R. Dunford, Argonne National Laboratory
John W. Farley, University of Nevada, Las Vegas
H.-Jürgen Kluge, GSI-Darmstadt, Germany
Thomas Kühl, GSI-Darmstadt, Germany
Richard Marrus, University of California-Berkeley
V. Ninov, Lawrence Berkely National Laboratory
Jonathan Sapirstein, University of Notre Dame
Reinhold Schuch, Stockholm University, Sweden
Takako Kato, National Insititute for Fusion Science, Tokyo
Bernard Zygelman, University of Nevada, Las Vegas

LLNL Attendees
Alcock, Charles
Bardsley, Norman
Bauer, Rudolf
Becker, John
DeWitt, Hugh
Fortner, Richard
Hazi, Andrew
Holzrichter, John
Kreisler, Michael
Libby, Stephen
More, Richard
Pollock, Edwin
Weiss, Mort

International Conference on "Trapped Charged Particles and Fundamental Physics"
Asilomar Conference Center, Monterey, California
August 31 – September 4, 1998

Chairman: Dieter Schneider, LLNL
Co-Chairman: Daniel Dubin, UCSD

The scientific topics covered the following areas of physics:

- Precision spectroscopy
- Special topics and exotic applications
- Weak interaction studies
- Precision mass spectroscopy
- Storage ring physics
- Manipulation and measurement of low-energy trapped ions
- Plasma and collective behavior
- Frequency standards
- Coherent quantum control

Third and Final Announcement
July 6, 1998

International Conference
on
"Trapped Charged Particles and Fundamental Physics"

Asilomar Conference Center
Pacific Grove / Monterey, California, USA

August 31 - September 4, 1998

Website address: http://www.llnl.gov/llnl/06events/TCPFP98.HTML

Dear Colleague:

This is the third and final announcement on the "Trapped Charged Particles and Fundamental Physics" Conference being held August 31 through September 4, 1998, at the Asilomar Conference Center in Pacific Grove / Monterey, California.

A copy of the preliminary program is included with this announcement. When you arrive at the Asilomar Conference Center you will receive the final program and further information about special activities.

If you have not yet submitted your registration form, your housing request, or EBIT tour information, please visit our website and register now.

CONTRIBUTIONS
In the event that you have changed your plans regarding specific contributions, and/or desire to contribute a paper on your work, please advise us accordingly, including the topic you wish to address. A short abstract about your planned contribution would be appreciated.

POSTERS
Poster size is restricted to 4'x8'. Please advise us if you plan to submit a Poster so that we may include it in the Poster Sessions. All Posters will remain on display throughout the Conference.

PROCEEDINGS
We plan to publish contributed and invited papers (and posters as contributed papers) in a bound American Institute of Physics (AIP) volume. Camera-ready manuscripts should be made available to the conference organizers by the end of the conference. Papers based on invited talks should be a maximum of ten pages in length; papers based on contributed talks should be a maximum of five pages in length. Format is single column, on 8 1/2 by 11 inch plain white paper.
Detailed instructions and examples can be found on the AIP website:
http://www.aip.org/epub/compuscripts.info.html

LODGING AT ASILOMAR

A block of rooms has been reserved at Asilomar for the dates of August 30 through September 5, 1998. Room assignments are handled through our Conference Secretary via our website. Payments for lodging are made directly to Asilomar. Please note that Asilomar requires each attendee to pay for the entire six nights lodging at the dates shown below. The only exceptions will be those who contact our Conference Secretary before July 15, 1998, specifying a later arrival or earlier departure date. **Please see payment information at the end of this announcement.**

Check-in begins: 3:00 p.m. on Sunday, August 30, 1998
Check-out time: 12:00 Noon on Saturday, September 5, 1998

Please note that if you plan to arrive a day earlier or stay longer, you will need to contact Asilomar directly and make a separate reservation for the extra nights only, or make a reservation at one of the many nearby hotels. The number for Asilomar reservations is: (408) 372-8016.

ATTENDEES NOT LODGING AT ASILOMAR

For those not lodging at Asilomar, meal tickets may be purchased during the Conference directly from Asilomar at the following rates: Breakfast $6.11, Lunch $8.31, and Dinner $13.30. Asilomar will accept payments by cash, check, Visa, or MasterCard.

DIRECTIONS TO ASILOMAR

Asilomar Conference Center
800 Asilomar Boulevard
Pacific Grove, CA 93950
Telephone: (408) 372-8016 / FAX: (408) 372-7227

The Monterey peninsula is located on the California coast 120 miles south of San Francisco and 330 miles north of Los Angeles. Asilomar is located on the Pacific Ocean at the end of Highway 68 in Pacific Grove on the Monterey peninsula. Nearest airports are the San Francisco International Airport, San Jose International Airport, and Oakland International Airport. Traveler can arrange for a rental car, use bus transportation or take a commuter airline to the Monterey Airport (two hours by car, approximately four hours by bus).

If you are coming from the North or the South on Highway 1, take the Pacific Grove/Pebble Beach exit at Highway 68. Highway 68 will lead to Forest Avenue. Turn left at Sunset Avenue and right on Asilomar Boulevard which will lead to the Asilomar Gates.

From Monterey Peninsula Airport, take Olmstead Road out of the airport and turn right on Highway 68. Take Highway 68 to Highway 1 South and follow the directions above.

From Highway 101 coming from the San Francisco/San Jose area, take the Monterey Peninsula exit at Highway 156 to Highway 1 South and follow the directions above.

From Highway 101 coming from Los Angeles, take the Monterey Peninsula exit and follow signs to Highway 68, then follow the directions above.

REGISTRATION FEE

After May 31, 1998, the registration fee is $265.00 (U.S. dollars). This fee will cover the cost of proceedings and some of the special activities, such as the Welcome Reception at Asilomar, and Dinner at the Monterey Bay Aquarium.

Please see registration payment information at the end of this announcement.

SPECIAL ACTIVITIES

Sunday, August 30: 7:00-9:00 p.m. - Welcome Reception

Tuesday, September 1: Kayak Ride, Monterey Bay Cruise, Whale Watching Tour
Sign up sheets will be available at the Conference registration desk. Fees to be determined.

Wednesday, September 2: Dinner at the Monterey Bay Aquarium
(Fee for accompanying guest is: $50.00; please see payment information at the end of this announcement.)

Thursday, September 3: Barbecue Dinner and Concert at Asilomar
Attendees not lodging at Asilomar are welcome to attend by purchasing a dinner meal ticket at the Conference directly from Asilomar.

TOUR OF THE EBIT FACILITY AT LLNL

Deadline for registering to attend the tour is July 17, 1998

On Saturday, September 5, it will be possible for you to tour the EBIT facility at the Lawrence Livermore National Laboratory in Livermore, CA, which is approximately a two hour drive from Monterey. If you desire to join this tour, please visit our website now and submit the necessary information required to approve your entry into the Laboratory.

Times given are approximate:

9:00 a.m.	Bus departs the Asilomar Asilomar Conference Center for LLNL
11:30 a.m.	Arrive LLNL; receive badges
12:00 a.m.	Box Lunch
1:00 p.m.	EBIT facility tour
4:00 p.m.	Bus departs LLNL
6:00 p.m.	Bus arrives at the Asilomar

****

Candace Lewis, Conference Secretary (replacing Lynda Allen)
Lawrence Livermore National Laboratory
P.O. Box 808, L-414, Livermore, CA 94551, USA
Telephone: (925) 422-8018 / FAX: (925) 422-5940
E-mail: lewis24@llnl.gov

Dieter Schneider, Chairman
Lawrence Livermore National Laboratory
P.O. Box 808, L-414
Livermore, CA 94551, USA
Telephone: (925) 423-5940
FAX: (925) 422-5940
E-mail: schneider2@llnl.gov

Dan Dubin, Co-Chairman
University of California, San Diego
Physics Dept., B-019
San Diego, CA 92093, USA
Telephone: (619) 534-4174
FAX: (619) 534-0173
E-mail: dhdubin@ucsd.edu

FINAL PROGRAM

International Conference on "Trapped Charged Particles and Fundamental Physics"

Asilomar Conference Center
Pacific Grove / Monterey, California, USA

August 31 - September 4, 1998

SUNDAY, August 30, 1998

3:00 p.m.	Registration Begins	Administration Building
6:00 p.m.	*Dinner Served (Asilomar)*	*Crocker Dining Hall*
7:00 p.m.- 9:00 p.m.	Welcome Reception	Merrill Hall Auditorium

MONDAY, August 31, 1998

7:30 a.m.	*Breakfast Served (Asilomar)*	*Crocker Dining Hall*
9:00 a.m.	Welcome Dieter Schneider (LLNL)	Merrill Hall Auditorium
9:10 a.m.	Opening Remarks Richard Fortner (LLNL)	

SESSION #1: Precision Spectroscopy (Eva Lindroth, Chair)

9:20 a.m.	Jonathan Sapirstein (University of Notre Dame) "Relativistic and QED Effects in Few-Electron High Z Systems"
9:50 a.m.	Thomas Stöhlker (GSI Darmstadt) "Lamb Shift Experiments on High-Z Hydrogenlike Ions at the ESR Storage Ring"
10:10 a.m.	Ulrich Jentschura (National Institute of Standards and Technology) "Numerical Lamb Shift Calculations for Low-Z Systems"
10:30 a.m.	*Coffee Break*
11:00 a.m.	Gerhard Soff (TU Dresden) "Radiative Corrections in Highly Charged Ions"
11:20 a.m.	Peter Beiersdorfer (Lawrence Livermore National Laboratory) "Accurate QED Measurements at the LLNL EBIT"
11:40 a.m.	Vladimir Shabaev (St. Petersburg State University) "QED and Nuclear Effects in Highly Charged Ions"
12:00 p.m.	*Lunch Served (Asilomar)* *Crocker Dining Hall*

1:30 p.m. Thomas Kühl (GSI Darmstadt)
"Ground State Hyperfine Structure in H-like Heavy Ions"

1:50 p.m. Richard Mittleman (University of Washington)
"Eliminating the Systematics in the g-2 Electron Experiment"

2:10 p.m. Wolfgang Quint (GSI Darmstadt)
"The g-Factor of the Bound Electron in Hydrogen-like Ions:
A Precision Test of QED"

2:30 p.m. Alex Grossmann (University of Heidelberg)
"First Results from the New Muon (g-2) Experiment"

2:50 p.m. *Coffee Break*

SESSION #2: Special Topics (Dan Dubin, Chair)

3:15 p.m. Announcement: Proceedings
Dan Dubin (University of California, San Diego)

3:20 p.m. Alan Kostelecky (Indiana University)
"Theory of CPT Violation for Antihydrogen Studies"

3:40 p.m. Gerald Gabrielse (Harvard University)
"Antihydrogen Studies"

4:00 p.m. Michael Holzscheiter (Los Alamos National Laboratory)
"Antihydrogen at Rest for Tests of CPT and WEP"

4:20 p.m. Theodor Hänsch (Max-Planck-Institute for Quantenoptik)
"Laser Spectroscopy of Hydrogen and Antihydrogen"

4:50 p.m. Hans Miesner (Massachusetts Institute of Technology)
"Bose Einstein Condensation Review"

5:20 p.m. *Break for the day*

6:00 p.m. *Dinner Served (Asilomar)* *Crocker Dining Hall*

TUESDAY, September 1, 1998

7:30 a.m. *Breakfast Served (Asilomar)* *Crocker Dining Hall*

9:00 a.m. Program Begins Merrill Hall Auditorium

SESSION #3: Precision Mass Spectrometry (David Pritchard, Chair)

9:00 a.m. Conny Carlberg (Stockholm University)
"A Precision Determination of the Proton Mass Using Highly Charged Ions"

9:20 a.m. Marielle Chartier (NSCL / Michigan State University)
"Direct Mass Measurements by Use of a Cyclotron"

9:40 a.m. Marcus Steck (GSI Darmstadt)
"Cooling of Radioactive Isotopes for Schottky Mass Spectrometry"

10:00 a.m. David Lunney (CSNSM Orsay)
"MISTRAL - A Radio Frequency Mass Spectrometer for Very Short-lived Isotopes"

10:20 a.m. *Coffee Break*

10:50 a.m. Robert Van Dyck, Jr. (University of Washington)
"Precision Mass Spectroscopy"

11:20 a.m. Georg Bollen (CERN)
"Mass Measurements on Radioactive Isotopes with a Penning Trap Mass Spectrometer"

11:40 a.m. Simon Rainville (Massachusetts Institute of Technology)
"Two Ions in Two Traps: Towards $\Delta m/m = 10^{-12}$"

12:00 p.m. *Lunch Served (Asilomar)* *Crocker Dining Hall*

1:00 p.m. No program scheduled for this afternoon

Optional Kayak Boat Ride, Kayak Bay Cruise, or Whale Watching Tour

6:00 p.m. *Dinner Served (Asilomar)* *Crocker Dining Hall*

WEDNESDAY, September 2, 1998

7:30 a.m. *Breakfast Served (Asilomar)* *Crocker Dining Hall*

9:00 a.m. Program Begins Merrill Hall Auditorium

SESSION #4: Weak Interaction Studies (Stuart Freedman, Chair)

9:00 a.m. Robert Bluhm (Colby College)
"Testing CPT in Penning-Trap Experiments"

9:20 a.m. James Byrne (University of Sussex)
"Neutron Decay Study Using an Ion Trap"

9:40 a.m. David Vieira (Los Alamos National Laboratory)
"Weak Interaction Studies in a Laser Trap"

10:00 a.m. Luis Orozco (State University of New York, Stony Brook)
"Spectroscopy of Francium"

10:20 a.m. *Coffee Break*

10:50 a.m. Michael Schacht (University of Washington)
"A Parity Violation Experiment with a Single Trapped Ion"

11:10 a.m. John Behr (TRIUMF)
"Search for Scalar Contributions to the ^{38m}K Beta-Neutrino Correlation in a Magneto-Optic Trap"

11:40 a.m. Harvey Gould (Lawrence Berkeley National Laboratory)
"Laser Trapping and Cooling of Francium from a Radioactive Source"

12:00 p.m. *Lunch Served (Asilomar)* *Crocker Dining Hall*

SESSION #5: Storage Ring Physics (Ingmar Bergström, Chair)

1:30 p.m. Reinhold Schuch (Stockholm University)
"Recombination of Cold Electrons with Stored Ions"

1:50 p.m. Torkild Andersen (University of Aarhus)
"Negative Ion Spectroscopy with Stored Ions"

2:10 p.m. Preben Hvelplund (University of Aarhus)
"Clusters in Rings"

2:30 p.m. Andreas Wolf (Max-Planck-Institute for Kernphysik)
"Life-time Measurements in Storage Rings"

2:50 p.m. *Coffee Break*

3:20 p.m. Masanori Wakasugi (RIKEN Cyclotron Laboratory)
"Storage Rings at RIKEN Beam Factory"

3:40 p.m. Jacob (Yasha) Levin (Max-Planck Institute for Kernphysik)
"Molecular Structure Studies by Coulomb Explosion Imaging"

4:10 p.m. Matthias Weidemüller (Max-Planck Institute for Kernphysik)
"Laser Cooling in Storage Rings"

4:30 p.m. Daniel Zajfman (Weizmann Institute of Science)
"Storage of keV Ion Beams"

4:50 p.m. Alex Hamza (Lawrence Livermore National Laboratory)
"Surface Physics with Highly Charged Ions from Electron Beam Ion Traps"

5:10 p.m. *Break for the day*

6:30 p.m. *First bus departs from the West side of Asilomar's Administration Building for the Monterey Bay Aquarium*

7:00 p.m. *Reception and Aquarium visit*

7:45 p.m. *Dinner begins*
After Dinner Speakers:
Ingmar Bergström (Stockholm University) and
Charles Alcock (Lawrence Livermore National Laboratory)

9:30 p.m. *First bus departs the Aquarium for Asilomar*

THURSDAY, September 3, 1998

7:30 a.m. *Breakfast Served (Asilomar)* *Crocker Dining Hall*

9:00 a.m. Program Begins Merrill Hall Auditorium

SESSION #6: Studies of Low-Energy Trapped Ions (Herbert Walther, Chair)

9:00 a.m. David Church (Texas A&M University)
"RETRAP - A Trap for Highly Charged Ion Laser Spectroscopy"

9:30 a.m. Peter Toschek (University of Hamburg)
"Quantum Measurement and Non-Classical Vibration of an Ion in a Trap"

10:00 a.m. Nan Yu (Jet Propulsion Laboratory)
"Towards a Micromotion - Free rf Trap"

10:20 a.m. *Coffee Break*

10:50 a.m. Martin Kretzschmar (Johannes Gutenberg University)
"A Quantum Mechanical Model of Rabi Oscillations Between Two Interacting Harmonic Oscillator Modes"

SESSION #7: Plasma and Collective Behavior (Bret Beck, Chair)

11:10 a.m. Reinhold Blümel (University of Freiburg)
"Chaos in Ion Traps"

11:40 a.m. Travis Mitchell (National Institute of Standards and Technology)
"Crystalline Order and Modes in Strongly Coupled Plasmas"

12:10 p.m. *Lunch Served (Asilomar)* *Crocker Dining Hall*

1:30 p.m. Clifford Surko (University of California, San Diego)
"Positron Plasmas: Trapping and Applications"

1:50 p.m. Joachim Steiger (Lawrence Livermore National Laboratory)
"Highly Charged Ion Coulomb Clusters in RETRAP"

2:10 p.m. Fred Driscoll (University of California, San Diego)
"Collisional Transport in Non-Neutral Plasmas"

2:30 p.m. Francois Anderegg (University of California, San Diego)
"Steady-State Confinement of Non-Neutral Plasmas Using Trivelpiece-Gould Modes Excited by Rotating Wall"

2:50 p.m. *Coffee Break*

3:15 p.m. Jeffrey Hangst (University of Aarhus)
"Ion Crystals in a Linear Paul Trap"

3:35 p.m. Luigi Moi (University of Siena)
"White Light Laser Cooling"

3:55 p.m. Thomas O'Neil (University of California, San Diego)
"Thermodynamics of Trapped Non-neutral Plasmas"

4:25 p.m. *Break for the day*

6:00 p.m. *Beach-side Barbecue Dinner & Concert* *(Meadow Area at Asilomar)*

FRIDAY, September 4, 1998

7:30 a.m. *Breakfast Served (Asilomar)* *Crocker Dining Hall*

9:00 a.m. Program Begins Merrill Hall Auditorium

SESSION #8: Frequency Standards (Gunter Werth, Chair)

9:00 a.m. Warren Nagourney (University of Washington)
"Optical Frequency Standard Based Upon Single Indium Ion"

9:20 a.m. Jürgen Helmcke (PTB Braunschweig)
"Frequency Measurement of Visible Light"

9:40 a.m. John Prestage (Jet Propulsion Laboratory)
"Frequency Standards"

10:00 a.m. Brent Young (National Institute of Standards and Technology)
"Optical Frequency Standard Using Trapped Hg^+ Ions"

10:20 a.m. *Coffee Break*

10:50 a.m. Hugh Klein (National Physical Laboratory)
"Trapped Ions for Optical Frequency Standards"

11:10 a.m. Peter Mohr (National Institute of Standards and Technology)
"The Fundamental Constants as of 1998"

11:40 a.m. Lutz Schweikhard (Johannes-Gutenberg University)
"Clusters in Ion Cyclotron Resonance Traps"

12:00 p.m. *Lunch Served (Asilomar)* *Crocker Dining Hall*

SESSION #9: Coherent Quantum Control (David Wineland, Chair)

1:30 p.m. Herbert Walther (Max-Planck-Institute for Quantenoptik)
"Cavity Quantum Electrodynamics with Trapped Ions"

2:00 p.m. Hans Briegel (University of Innsbruck)
"Quantum Computing with Trapped Atoms and Ions (Including Applications in Quantum Communication)"

2:30 p.m. Michael Holzscheiter (Los Alamos National Laboratory)
"Prospect for Quantum Computation with Trapped Ions"

2:50 p.m. *Coffee Break*

3:20 p.m. Christopher Monroe (National Institute of Standards and Technology)
"Quantum Logic with Trapped Ions"

3:50 p.m. Jun Ye (California Institute of Technology)
"Measurements and Control of Single Atom Motions in the Quantum Regime"

4:10 p.m. Richard Thompson (Imperial College, London)
"Quantum Zeno Effect in Trapped Ions"

4:40 p.m. Concluding Remarks
Dieter Schneider (LLNL)

6:00 p.m. *Dinner Served (Asilomar)* *Crocker Dining Hall*

SATURDAY, September 5, 1998

7:30 a.m. *Breakfast Served* *Crocker Dining Hall*

Check-out time is 12:00 Noon today

12:00 p.m. *Lunch Served* *Crocker Dining Hall*
(for those not attending the EBIT tour)

Schedule for optional tour of the EBIT facility at LLNL
Times shown are approximate:

9:00 a.m. Bus departs from the West side of Asilomar's Administration Building

11:00 a.m. Arrive at LLNL's Westgate Badge Office and receive badges

12:30 p.m. Box lunch at the EBIT facility and tour

4:00 p.m. Bus departs LLNL for the Asilomar Conference Center

6:00 p.m. Bus arrives at the Asilomar Conference Center

B. Scientific Activities Centered Around EBIT

B-1 Visitors and Participating Guests in 1996

NAME	INSTITUTION	HOST
JANUARY		
Tsukiyo Tanaka	University of Nevada	Schneider
John Farley	University of Nevada	Schneider
Friedward Winterberg	University of Nevada	Schneider
Vincent Decaux	UC Berkeley	Beiersdorfer
Sheldon Datz	Oak Ridge National Laboratory	Schneider
Ali Belkacem	Lawrence Berkeley Laboratory	Schneider
Emanuel Kamber	Western Michigan University	Schneider
Alan Barnes	Vanderbilt University	Schneider
Kurt Becker	University of New York	Schneider
Michael Briere	Cherry Semiconductors	Schneider
FEBRUARY		
Vincent Decaux	UC Berkeley	Beiersdorfer
Steve Elliott	University of Washington	Beiersdorfer
Alan Barnes	Vanderbilt University	Schneider
MARCH		
Chander Bhalla	Kansas State University	Beiersdorfer
APRIL		
David DeWitt	Manne Siegbahn University	Schneider
Alan Barnes	Vanderbilt University	Schneider
Daniel Savin	UC Berkeley	Beiersdorfer
Vincent Decaux	UC Berkeley	Beiersdorfer
Martin Kretzschmar	University of Mainz	Schneider
Dan Pickard	Lawrence Berkeley Laboratory	Schneider
Don Williams	Lawrence Berkeley Laboratory	Schneider
Daniela Wutte	Lawrence Berkeley Laboratory	Schneider
Robert DuBois	University of Missouri-Rolla	Schneider

Mathew Bailey	University of Nevada	Schneider
Andrew Oxner	University of Nevada	Schneider
Ullrich Meyer	Institute für Kernphysik der Johann Wolfgang Goethe	Schneider
Klaus Ullmann-Pfleger	Institute für Kernphysik der Johann Wolfgang Goethe	Schneider

MAY

Horst Schmidt-Böcking	University of Frankfurt	Schneider
Reinhard Bruch	University of Nevada	Schneider
Dhanesh Chandra	University of Nevada	Schneider
Banmali Singh Rawat	University of Nevada	Schneider
Nelson Publicover	University of Nevada	Schneider
Norman Tolk	Vanderbilt University	Schneider
Leonard Feldmann	Vanderbilt University	Schneider
Markus Schmitt	Heidelberg University	Beiersdorfer
Shunsuke Ohtani	Institute for Laser Science University of Electron-Communications	Schneider
Rainer Radtke	Max-Planck-Institut für Plasmaphysik	Schneider
Ullrich Meyer	Institute für Kernphysik der Johann Wolfgang Goethe	Schneider
Jean Pierre Briand	University Pierre et Marie Curie	Schneider

JUNE

Stefan Borneis	Lambda Physik GmbH	Schneider
David Church	Texas A&M	Schneider
John Farley	University of Nevada	Schneider
James Selser	University of Nevada	Schneider
Serge Dreuil	University Pierre et Marie Curie	Schneider
Alan Barnes	Vanderbilt University	Schneider

JULY

John Gillaspy	NIST-Gaithersburg	Schneider/Schenkel
Norman Tolk	Vanderbilt University	Schneider

Edward Lever	University of California	Beck
John Reading	Texas A&M University	Schneider
Jean Pierre Briand	University Pierre et Marie Curie	Schneider
AUGUST		
Robert Jacobsen	Lawrence Berkeley Laboratory	Wenaus
Norman Tolk	Vanderbilt University	Schneider
Ewald Gruber	A.K.H. Wien	Schneider/Gruber
Serge Dreuil	University Pierre et Marie Curie	Schneider
Lutz Schweikhard	Johannes Gutenberg University	Beiersdorfer
SEPTEMBER		
Ullrich Meyer	Institute für Kernphysik der Johann Wolfgang Goethe	Schneider
Serge Dreuil	University Pierre et Marie Curie	Schneider
Jean Pierre Briand	University Pierre et Marie Curie	Schneider
Merlin Lopez	Nalorac Corporation	McDonald
Greggory Stefanelli	DOE EPSCoR	Beiersdorfer
OCTOBER		
Dale Nakano	Hewlett-Packard	Shi
Ronald Cicero	Stanford University	Schenkel
Eugene Clothiaux	Auburn University	Beiersdorfer
Jean Pierre Briand	University Pierre et Marie Curie	Schneider
Vincent LeRoux	University Pierre et Marie Curie	Schneider
Christoph Biedermann	Max-Planck-Institut für Plasmaphysik	Beiersdorfer
Verne Jacobs	Naval Research Laboratory	Beiersdorfer
Felicitas Kochs	University of Koeln	McDonald
NOVEMBER		
Augustine Smith	Morehouse College	Beiersdorfer

Eckhart Förster	Max-Planck-Gesellschaft für Föfderung der Wissenschaften	Beiersdorfer
Christoph Biedermann	Max-Planck-Institut für Plasmaphysik	Beiersdorfer
Ali Belkacem	Lawrence Berkeley Laboratory	Schneider
Paul Neill	University of Nevada	Beiersdorfer

B-1.1 Visitors and Participating Guests in 1997

NAME	INSTITUTION	HOST
JANUARY		
Mark Legros	Lawrence Berkeley Laboratory	Schneider
Robert DuBois	University of Missouri-Rolla	Schneider
Ron Olson	University of Missouri-Rolla	Schneider
James Kirchner	Coherent Laser	Gruber/Steiger
Reinhold Schuch	Stockholm University	Schneider
John Farley	University of Nevada	Schneider
Fred Meyer	Oak Ridge National Laboratory	Schneider
Carlos Reinhold-Larsson	Oak Ridge National Laboratory	Schneider
John Gillaspy	NIST-Gaithersburg	Schneider
Martin Stockli	Kansas State University	Schneider
John Tanis	Western Michigan University	Schneider
FEBRUARY		
Steve Elliott	University of Washington	Beiersdorfer
Heino Henke	Stanford Linear Accelerator	Schneider
Friedward Winterberg	University of Nevada	Schneider
Peter Kuerpick	Kansas State University	Schneider
Kurt Stiebing	University of Frankfurt	Schneider
Lothar Schmidt	University of Frankfurt	Schneider

MARCH

Tim Dinneen	Lawrence Berkeley Laboratory	Schneider
Norman Tolk	Vanderbilt University	Barnes
Eckhart Foerster	University of Jena, Germany	Beiersdorfer
Friedward Winterberg	University of Nevada	Schneider
Carl Vernon	University of San Diego	Beck
Philip Datte	University of San Diego	Beck
Shunsuke Ohtani	Institute for Laser Science University of Electron-Communications	Schneider
Nobuyuki Nakamura	Institute for Laser Science University of Electron-Communications	Schneider
Merle Lord	SpectroWest	Beck
Vincent LeRoux	University Pierre et Marie Curie	Schneider
Jean Briand	University Pierre et Marie Curie	Schneider
Phillip Gould	University of Connecticut	Schneider
Stephan Helms	Medtronic Inc.	McDonald

APRIL

Daniel Savin	Columbia University	Beiersdorfer
Raul Baragiola	University of Virginia	Barnes/Schneider
H. Schmidt-Böcking	University of Frankfurt	Schneider
Levent Erman	Coherent Laser Group	Gruber
Olaf Hartmut Herzog	Ruhr-Universität Bochum	Beiersdorfer
Manfred Bitter	Princton University	Beiersdorfer
Heinz-Jürgen Kluge	GSI-Darmstadt	Schneider

MAY

Shui-Yin Lo	American Tech. Group	Schneider
Reinhard Bruch	American Tech. Group	Schneider
Hugo Pomrehn	American Tech. Group	Schneider
Emanuel Kamber	Western Michigan University	Schneider

Andrew Puckett	Vanderbilt University	Barnes/Schneider
Michael Albert	Vanderbilt University	Barnes/Schneider
Norman Tolk	Vanderbilt University	Barnes/Schneider
Jonathan Gilligan	Vanderbilt University	Barnes/Schneider
Norman Tolk	Vanderbilt University	Barnes/Schneider
Jonathan Gilligan	Vanderbilt University	Barnes/Schneider

JUNE

Jean Pierre Briand	University Pierre et Marie Curie	Schneider
Nicolas Bechu	University Pierre et Marie Curie	Schneider
Jacques Merot	University Pierre et Marie Curie	Schneider
Guillaume Machicoane	University Pierre et Marie Curie	Schneider
Christophe Refaillac	University Pierre et Marie Curie	Schneider
Vincent LeRoux	University Pierre et Marie Curie	Schneider
Robert DuBois	University of Missouri-Rolla	Schneider
Ron Olson	University of Missouri-Rolla	Schneider
Robert DuBois	University of Missouri-Rolla	Schneider
Robert Polly	Institut für Experimental-physik	Schneider
Matthew Cook	University of Nevada	Schneider
John Tanis	Western Michigan University	Schneider
Henning LeBius	Manne Siegbahn Institute	Schneider

JULY

Joseph Martinez	DOE	Schneider
Edmund Taglauer	Max-Planck-Institute	Hamza
Berthold Senftinger	STAIB Instrumente GmbH	Hamza

AUGUST

Ron Cicero	Stanford University	Schenkel
Lutz Schweikhard	Johannes Gutenberg University	Beiersdorfer
H. Schmidt-Böcking	University of Frankfurt	Schneider

SEPTEMBER

Eugene Clothiaux	Auburn University	Beiersdorfer
Lisa Paulius	Western Michigan University	Schneider
Robert DuBois	University of Missouri-Rolla	Schneider
Ron Olson	University of Missouri-Rolla	Schneider

OCTOBER		
Elmar Träbert	Ruhr University	Beiersdorfer
Marty Kordesch	Lawrence Berkeley Laboratory	Hamza
NOVEMBER		
Thomas Stoehlker	GSI	Marrs
Denis Dauvergne	Institut de Physique Nuceure do Lyon	Schneider
Paul Neill	University of Nevada	Beiersdorfer
Reinhold Schuch	Manne Siegbahn Institute of Physics	Schneider
DECEMBER		
Sheldon Datz	Oak Ridge National Laboratory	Schneider
Robert DuBois	University of Missouri-Rolla	Schneider

B-2 LLNL EBIT Seminar Series in 1996 - 1997

Emanuel Kamber	"Translational Energy Spectroscopy Studies of Slow Multiply Charged Ions Following Capture"
Christiane Rühlicke	"Possible Fragmentation of Biomolecules with Highly Charged Ions"
John Reading	"Response Theory"
Peter Seelig	"Laser Spectroscopy of the Ground State Hyperfine Splitting of Highly Charged Ions"
Sheldon Datz	"Studies of Dissociative Recombination of Molecules (H_2D^+ and H_3^+) Relevant to Astrophysics"
Carlos Reinhold-Larsson	"Dynamics of Rydberg Atoms in Half Cycle Pulses"
Heino Henke	"Planar Millimeter Wave Structures for Electron Acceleration"
Peter Kuerpick	"Theory of Ion Surface Interactions"
Tim Dinneen	"Laser Trapping ^{221}Fr from a Radiactive Source"
Nobuyuki Nakamura	"Test Experiments on the Tokyo EBIT"
Phillip Gould	"Long Range Interactions Between Cold Atoms"
Uwe Thumm	"Interactions of Ions with Clusters (C_{60}) and Surfaces"
Raul Baragiola	"Ion Excitation of Plasmons"
Elmar Träbert	"Optical Measurements of Long Atomic Lifetimes at a Heavy-Ion Storage Ring"
Klaus Widmann	"High-Resolution Spectroscopic Diagnostics of very High-Temperature Plasmas in the Hard X-Ray Regime"
David Church	"Charge Exchange Studies with Highly Charged Ions"

C. Education

Graduate Education

The education of graduate students represents a major part of the EBIT program. During 1996 and 1997 a total of nine graduate students had been active in the program. The students came from different institutions, both national and international. The EBIT program also routinely involves undergraduate students. Twice a year students from the Undergraduate Summer Institute Research Program have a chance to actively participate in ongoing research for a two-week period. During 1996 and 1997, five undergraduates took advantage of this opportunity. The EBIT program has a continuing commitment to minority participation in its activities. A detailed description of our collaborative efforts with students and faculty from Historically Black Colleges and Universities continues.

Graduate Students at EBIT:

Greg Brown	Auburn University, Alabama Research on laboratory X-ray spectroscopy of L-shell transitions in Fe XVII for diagnostics of astrophysical plasmas towards a Ph.D. thesis.
Lukas Gruber	Technische Universität Graz, Austria Research on trapped highly charged ions towards a Ph.D. thesis.
Joe McDonald	Western Michigan University, Kalamazoo, Michigan Research in ion/surface interactions; completed his Ph.D. thesis in December of 1997.
Michael Newman	University of Connecticut Research on highly charged ion interactions with surfaces towards a Ph.D. thesis.
Christiane Rühlicke	University of Bielefeld, Germany Research on biomolecule fragmentation with highly charged ions towards a Ph.D. thesis.
Thomas Schenkel	University of Frankfurt, Germany Research in ion/surface interactions; completed his Ph.D. thesis in August of 1997.
George Weinberg	Texas A&M University, College Station, Texas Research on trapped highly charged ions; completed his Ph.D. thesis in June of 1996.
Klaus Widmann	University of Technology, Graz, Austria Research in atomic structure using EBIT towards a Ph.D. thesis.
Steven Utter	Auburn University, Alabama Research on EUV spectroscopy and atomic physics using EBIT towards a Ph.D. thesis.

D. Scientific Cooperations

U.S. Cooperations:

Auburn University, Auburn, AL
California Institute of Technology, Pasadena, CA
Columbia University, New York, NY
Kansas State University, Manhattan, KS
Lawrence Berkeley National Laboratory, Berkeley, CA
Morehouse College, Atlanta, GA
Naval Research Laboratory, Washington, DC
Princeton Plasma Physics Laboratory, NJ
Stanford University, Stanford, CA
Texas A&M University, College Station, TX
University of California-Berkeley, Berkeley, CA
University of Nevada-Las Vegas, Las Vegas, NV
University of Nevada-Reno, Reno, NV
University of Washington, Seattle, WA
Vanderbilt University, Brentwood, TN
Western Michigan University, Kalamazoo, MI

International Cooperations:

GSI, Darmstadt, Germany
Hahn-Meitner-Institut, Berlin, Germany
Institut für Allgemeine Physik, Wien, Austria
Institut für Kernphysik, Frankfurt, Germany
Johannes Kepler Universität, Linz, Austria
Johannes Gutenberg Universität, Mainz, Germany
Friedrich Schiller Universität Jena, Germany
Manne Siegbahn Institute, Stockholm, Sweden
Technische Universität Graz, Austria
University of Paris, France

E. Personnel

Associate Director for Physics & Space Technology: Richard J. Fortner
N Division Leader: Michael N. Kreisler
EBIT Program Leader: Dieter H. G. Schneider (schneider2@llnl.gov)

Scientific Staff Members:
- Alan Barnes (Term)
- Bret Beck (Term)
- Peter Beiersdorfer
- Roscoe Marrs
- Dieter Schneider
- Joachim Steiger (Term)

Post-doctorals:
- Matt Cook (UNLV)**
- Jose R. Crespo López-Urrutia**
- Vincent Decaux*
- Alexis Schach von Wittenau*
- Tsukiyo Tanaka (UNR)*

Students:
- Gregory Brown
- Lukas Gruber
- Joseph McDonald
- Christiane Rühlicke
- Thomas Schenkel
- Steven Utter
- Klaus Widmann

Technical Support Staff:
- Philip Dantonio
- Edward Magee
- Dan Nelson
- Kenneth Visbeck

Guest Scientists:
- David Church (Texas A&M University)
- John Farley (University of Nevada, Las Vegas)
- Eckhart Förster (Friedrich-Schiller Universität)
- Lutz Schweikhard (Johannes Gutenberg Universität)
- Augustine Smith (Morehouse College)
- Thomas Stoehlker (GSI Darmstadt)

Secretary:
- Candace Lewis (lewis24@llnl.gov)
- Telephone: (925) 422-8018
- Fax: (925) 422-5940

* *Position expired in 1996*
** *Position expired in 1997*